

# AN INVESTIGATION INTO THE MECHANISMS DRIVING SPONTANEOUS COUGH IN A PRECLINICAL MODEL OF IDIOPATHIC PULMONARY FIBROSIS

Jonathan Henry Alastair Miles

2021

A thesis submitted for the Degree of Doctor of Philosophy in the Faculty of Medicine,  
Imperial College London

Respiratory Pharmacology Group  
National Heart and Lung Institute  
Faculty of Medicine  
Imperial College London  
Sir Alexander Fleming Building  
Exhibition Road  
London  
SW7 2AZ

## Thesis Abstract

Idiopathic Pulmonary Fibrosis (IPF) is a terminal lung disease characterised by a progressive deposition of scar tissue within the lung interstitium. The disease is made more troubling for patients by being frequently accompanied by a chronic, sputumless cough, which has a severe impact on their quality of life. The pathophysiology behind cough in IPF remains poorly understood, and as such, it has proven refractory to treatment; the aim of this thesis was to elucidate the mechanisms behind this distressing symptom.

We sought to model IPF-associated chronic cough using a bleomycin-driven model of fibrosis in guinea pigs. After having characterised the inflammatory and fibrotic features of this model, we discovered, in a preclinical first, that bleomycin-treated guinea pigs cough spontaneously, much like IPF patients. We believe that this model more closely recapitulates the cough seen in patients than other provoked cough challenge models.

In search for the mediators that were driving cough within this preclinical model, we quantified the levels of different biomarkers in bronchoalveolar lavage fluid (BALF) that are reportedly elevated in the IPF lung: extracellular ATP, mast cell tryptase and 8-isoprostane (a biomarker for oxidative stress). We found evidence that all three of these were more highly present in the lungs of bleomycin-treated animals than the vehicle control group. Further to this, we measured these biomarkers in BALF donated by IPF patients at Royal Brompton Hospital and found that 8-isoprostane was significantly more concentrated in IPF BALF than in healthy volunteer BALF.

We then utilised a variety of *in vitro* and *in vivo* techniques to further investigate how these lung milieus might elicit cough. After showing that H<sub>2</sub>O<sub>2</sub>, a reactive oxygen species, was capable of generating oxidative stress in guinea pig vagal ganglia, we further determined that it caused vagus nerve depolarisation through the ion channel TRPA1. We also discovered that activating the PAR2 receptor, a target of mast cell tryptase, also caused airway sensory nerve activation through the ion channel TRPV4; TRPV4 activation has previously been shown to cause cough via the extracellular release of ATP.

Finally, we report on the efficacy of GSK2798745, a selective TRPV4 channel antagonist, that is capable of abrogating TRPV4-induced cough. In the near future, we intend to use a variety of pharmacological tools, including this one, in our novel *in vivo* model of fibrosis-induced spontaneous cough, with the end goal of finding an effective antitussive therapy for IPF patients.

## Acknowledgements

Firstly, I would like to thank my primary supervisors Dr Mark Birrell and Professor Maria Belvisi for giving me the opportunity to embark on this PhD in the first place, in their Respiratory Pharmacology group. Your expertise and guidance has been invaluable to me throughout the course of this project, and I am all the more grateful considering how precious your time is.

I would further like to thank the original postdocs of the lab: Dr Eric Dubuis, Dr Sara Bonvini and Dr Michael Wortley. Your assistance in helping me develop my model, and your patience and generosity as you taught me the functional techniques used in the lab is greatly appreciated.

Thanks also to my third supervisor Professor Toby Maher and Dr Philip Molyneux (as well as his lab), for their advice and assistance when it came to analysing patient bronchoalveolar lavage samples.

I would also like to thank: my beer buddies Dr James Pinkerton and Dimitrios Zervas (and Eric again too!) for your great company and assistance with my PhD; Dr John Adcock for your support, and entertaining theatrical endeavours; my fellow PhD students Pauline, Xue and Nadja, for all your help and suggestions over these last 4 years; Bilel for regularly going above and beyond the call of duty to aid me in my *in vivo* studies; and the rest of the Respiratory Pharmacology group for your help and regular encouragements.

My sincere thanks go out to the Medical Research Council and Chiesi Farmaceutici for funding this CASE studentship. A special mention must also go to Dr Silvia Pontis and Dr Marcello Trevisani of Chiesi for advising me on my *in vivo* model, and for allowing me to incorporate the use of their cutting-edge analytical techniques in my PhD, that would otherwise have not been possible.

I am also indebted to my family for their constant and unending support: especially my Mum and Dad - Alison and Alastair; my siblings - Gregory and Felicity; my Grandma - Patricia; and my Grandad - Ian.

Importantly, I would like to thank my partner Hannah, who has been with me throughout this PhD, and without whose companionship, love and support, none of this would have been possible.

Lastly, I would like to express my sincere gratitude to the patients suffering from idiopathic pulmonary fibrosis who donated bronchoalveolar lavage samples, and to the individuals who generously donated their lung tissue, all in the pursuit of medical research.

## Statement of Originality

The work contained in this thesis is my own work, except where otherwise indicated and referenced appropriately.

Throughout Chapter 3, all lung histology was prepared by Lorraine Lawrence. In Section 3.3.3.2, the experiments using vagus nerves deriving from bleomycin-treated animals were performed by Dr Sara Bonvini and Dr Michael Wortley, with my assistance. In Chapter 3, automated Visiopharm analysis of histology and immunohistochemical staining of histology, was performed by Dr Silvia Pontis, with my assistance, during a 2-week placement at Chiesi Farmaceutici, Parma, Italy. Differential cell counting of leukocytes within bronchoalveolar lavage (Section 3.3.6) was performed by Dr James Pinkerton.

In Chapter 4, bronchoalveolar lavage fluid was obtained from idiopathic pulmonary fibrosis patients and healthy volunteers by Dr Philip Molyneaux, Dr Peter Saunders and Dr Richard Hewitt.

In Chapter 6, the electrophysiological tracheal recording experiments, and the *in vivo* single fibre experiments, were performed by Dr Eric Dubuis and Dr John Adcock, respectively.

## Copyright Declaration

The copyright of this thesis rests with the author and is made available under a Creative Commons Attribution Non-Commercial No Derivatives licence. Researchers are free to copy, distribute or transmit the thesis on the condition that they attribute it, that they do not use it for commercial purposes and that they do not alter, transform or build upon it. For any reuse or redistribution, researchers must make clear to others the licence terms of this work.

Some of the work within this thesis has already been presented at the 2019 American Thoracic Society (ATS) International Conference and the 2020 European Respiratory Society (ERS) International Congress.

## Table of Contents

Thesis Abstract .....	2
Acknowledgements.....	3
Statement of Originality.....	4
Copyright Declaration .....	5
List of Figures .....	13
List of Tables.....	17
Abbreviations .....	18
1 Introduction .....	20
1.1 IPF .....	20
1.1.1 Introduction to IPF.....	20
1.1.2 Disease Classification.....	21
1.1.3 Diagnosis and clinical indications .....	22
1.1.4 Pathogenic risk factors .....	26
1.1.5 IPF Pathobiology.....	29
1.1.6 Oxidative stress in IPF.....	32
1.2 Modelling fibrosis and assessing anti-fibrotic therapies.....	33
1.2.1 Pre-clinical models of IPF.....	33
1.2.2 The bleomycin model .....	33
1.3 Cough.....	34
1.3.1 Introduction to cough.....	34
1.3.2 Physiology and prevalence of cough .....	35
1.3.3 Diseases featuring chronic cough, its burden on patients and current treatments.....	35
1.3.4 Cough in IPF.....	37
1.3.5 Introduction to airway sensory nerves.....	39
1.3.6 Sensory nerve subtypes.....	45
1.3.7 Previously proposed mechanisms for cough in IPF .....	48
1.4 Modelling cough and assessing antitussive therapies .....	49

1.4.1	Pre-clinical models of cough.....	49
1.4.2	Clinical assessment of cough .....	52
1.5	Ion channels and receptors implicated or hypothesised to be involved in cough or IPF....	55
1.5.1	P2X3.....	55
1.5.2	TRPV4 .....	57
1.5.3	TRPA1 .....	60
1.6	Thesis Plan .....	63
2	Methodology.....	64
2.1	Introduction .....	64
2.2	Animal Husbandry.....	64
2.3	Use of Knockout Mice .....	64
2.3.1	Procurement and breeding .....	64
2.3.2	Genotyping and PCR.....	64
2.4	Isolated Vagal Nerve Recordings .....	66
2.4.1	Tissue Dissection: Animals.....	66
2.4.2	Tissue Dissection: Human.....	67
2.4.3	Measurement of nerve depolarisation.....	68
2.4.4	Concentration Response and Antagonist Protocols .....	70
2.5	Electrophysiological tracheal recording of the Recurrent Laryngeal Nerve .....	71
2.5.1	Isolated perfused trachea RLN set-up .....	72
2.5.2	Interpretation of RLN recordings.....	75
2.5.3	Concentration response experiment protocols.....	75
2.5.4	Data Analysis .....	75
2.6	<i>In Vivo</i> Single Fibre Recordings .....	75
2.6.1	<i>In Vivo</i> Single Fibre Model Set-up and Surgery.....	76
2.6.2	Identification and characterisation of airway terminating single fibres.....	77
2.6.3	Concentration response experimental protocol for A $\delta$ -fibre.....	77
2.6.4	Aerosol-induced cough model.....	78



3	Developing an <i>in vivo</i> model of fibrosis-induced spontaneous cough .....	81
3.1	Rationale .....	81
3.1.1	Chapter Hypothesis .....	81
3.1.2	Aims .....	81
3.2	Methods.....	82
3.2.1	Recording guinea pigs through a CCTV system .....	82
3.2.2	Bleomycin dose response experiment .....	84
3.2.3	Bleomycin time course experiment.....	93
3.2.4	Measurement of mRNA levels to assess fibrosis-related gene expression .....	95
3.2.5	Quantifying Hydroxyproline in left cranial lobe.....	98
3.2.6	Statistics.....	99
3.3	Results.....	100
3.3.1	Capsaicin positive control cough response study.....	100
3.3.2	Bleomycin dose response study .....	101
3.3.3	Bleomycin time course study .....	112
3.3.4	Expression of fibrosis-related genes following bleomycin challenge .....	120
3.3.5	Hydroxyproline bioassay in left cranial lobe homogenate .....	121
3.3.6	Leukocytes in BALF .....	122
3.4	Discussion .....	123
4	Comparing biomarkers in IPF patient bronchoalveolar lavage fluid with samples produced from the bleomycin guinea pig fibrosis model which exhibits spontaneous cough .....	128
4.1	Rationale .....	128
4.1.1	Chapter Hypothesis: .....	129
4.1.2	Aims.....	129
4.2	Methods.....	129
4.2.1	Clinical PROFILE study.....	129
4.2.2	Pre-clinical Bleomycin Model Time Course Study with BAL collection.....	133
4.2.3	Mediator Assays .....	134

4.2.4	Tryptase.....	136
4.2.5	ATP.....	137
4.2.6	Statistical analysis.....	138
4.3	Results.....	138
4.3.1	8-Isoprostane.....	138
4.3.2	eATP.....	140
4.3.3	Tryptase.....	141
4.4	Discussion .....	143
5	Investigating a role for oxidative stress in airway sensory nerves .....	148
5.1	Rationale .....	148
5.1.1	Chapter Hypothesis .....	148
5.1.2	Aims.....	148
5.2	Methods.....	149
5.2.1	Neuronal isolation and imaging.....	149
5.2.2	Isolated Vagal Nerve Recordings .....	155
5.2.3	Data analysis and statistics.....	155
5.3	Results.....	157
5.3.1	Effect of H <sub>2</sub> O <sub>2</sub> on intracellular oxidative stress within vagal ganglia neurons .....	157
5.3.2	Effect of H <sub>2</sub> O <sub>2</sub> on intracellular calcium concentrations of vagal ganglia neurons .....	158
5.3.3	Effect of H <sub>2</sub> O <sub>2</sub> on depolarisation of isolated guinea pig vagus nerves.....	159
5.3.4	Selecting a TRPA1 inhibitor to take forward to inhibit H <sub>2</sub> O <sub>2</sub> -induced vagus nerve depolarisation .....	160
5.3.5	Effect of N-Acetylcysteine and a selective TRPA1 antagonist on H <sub>2</sub> O <sub>2</sub> -induced vagus nerve depolarisation .....	161
5.4	Discussion .....	163
6	Investigating a role for PAR2 in airway sensory nerves .....	167
6.1	Rationale .....	167
6.1.1	Chapter Hypotheses .....	167

6.1.2	Aims .....	167
6.2	Methods.....	168
6.2.1	Isolated Vagal Nerve Recordings .....	168
6.2.2	eTRec of the recurrent laryngeal nerve (RLN) .....	170
6.2.3	<i>In Vivo</i> Single Fibre Recording .....	170
6.3	Results.....	171
6.3.1	Effect of PAR2 agonists and antagonists on depolarisation of isolated vagus nerves..	171
6.3.2	Effect of PAR2 agonist 2-Furoyl-LIGRLO on RLN firing.....	177
6.3.3	Effect of PAR2 agonists on firing of airway terminating vagus nerve single fibres <i>in vivo</i> 178	
6.3.4	Determining a role for the TRPV4-ATP-P2X3 axis in PAR2-agonist induced vagus nerve depolarisation .....	179
6.4	Discussion .....	182
7	Characterising tools to be used in the fibrosis-induced spontaneous cough model .....	186
7.1	Rationale .....	186
7.1.1	Chapter Hypothesis .....	188
7.2	Methods.....	189
7.2.1	Isolated Vagal Nerve Recordings .....	189
7.2.2	TRPV4 agonist-induced cough .....	189
7.3	Results.....	191
7.3.1	Effect of selective TRPV4 antagonist GSK279 on TRPV4 agonist GSK101-induced vagus nerve depolarisation .....	191
7.3.2	Effect of TRPV4 antagonist GSK279 on the cough response to TRPV4 agonist GSK101 in naïve guinea pigs.....	193
7.4	Discussion .....	198
8	Conclusions and future work .....	202
8.1	Thesis Summary .....	202
8.2	Limitations of thesis.....	212
8.3	Thesis hypotheses.....	213

8.4	Future work .....	214
8.4.1	Increasing replicates, using more airway relevant techniques and power analyses....	214
8.4.2	Test novel antitussives in the <i>in vivo</i> model of fibrosis-induced spontaneous cough..	214
8.4.3	Optimise data acquisition in the <i>in vivo</i> model of fibrosis-induced spontaneous cough	215
8.4.4	Determine if aerosolised PAR2 agonists cause C-fibre activation, or elicit cough in guinea pigs or exaggerate the cough response.....	217
8.4.5	Correlation of BAL biomarkers .....	217
8.5	Concluding remarks .....	218
9	Bibliography .....	219
10	Appendix .....	249

## List of Figures

Figure 1-1 Lungs from a patient with IPF .....	21
Figure 1-2 A comparison between HRCT scans of a normal chest and UIP patterns .....	24
Figure 1-3 Histopathology showing fibrotic and non-fibrotic areas within a single lung biopsy .....	25
Figure 1-4 IPF pathobiology .....	31
Figure 1-5 Comparison between cough frequency in IPF and other lung diseases.....	38
Figure 1-6 The cough reflex.....	40
Figure 1-7 The phenomenology of cough .....	43
Figure 1-8 Brain regions involved in cough-related neural processing .....	44
Figure 1-9 The VitaloJAK™ cough monitor .....	54
Figure 1-10 TRPV4 agonism elicits cough in guinea pigs and can be inhibited by selective TRPV4 and P2X3 antagonists.....	58
Figure 1-12 The TRPV4-ATP-P2X3 axis: activation of airway afferents and cough.....	59
Figure 1-13 The PAR2 activation mechanism.....	60
Figure 1-14 The TRPA1 ion channel .....	62
Figure 2-1 Schematic of isolated vagus nerve recording system .....	70
Figure 2-2 Guinea pig airways with nerves attached. ....	72
Figure 2-3 eTRec Recording.....	74
Figure 2-4 a) The set-up of the in vivo single fibre technique.....	78
Figure 2-5 Aerosol-induced guinea pig cough model.....	80
Figure 3-1 Development of an in vivo CCTV monitoring system.....	83
Figure 3-2 Recording capsaicin-induced cough within guinea pig IVCs.....	84
Figure 3-3 Schematic of cage monitoring set up for spontaneous cough pilot study.....	88
Figure 3-4 Screenshot of CCTV playback software.....	88
Figure 3-5 Anatomical photograph of the guinea pig lung.....	90
Figure 3-6 Screenshots of the Visiopharm software package.....	92
Figure 3-7 CCTV quantification of guinea pig coughs to aerosolised capsaicin.....	100
Figure 3-8 Mean body weight over time of guinea pigs treated with different concentrations of bleomycin.....	101
Figure 3-9 Representative photographs of the lungs of guinea pigs incubated with different concentrations of bleomycin.....	102
Figure 3-10 Weights of guinea pig lungs after incubation with different doses of bleomycin. ....	103
Figure 3-11 Measuring right ventricular hypertrophy in bleomycin-treated guinea pigs.....	103

Figure 3-12 Representative micrographs of lungs taken from guinea pigs treated with different doses of bleomycin.....	105
Figure 3-13 Ashcroft scoring assessment of guinea pig lungs after incubation with different bleomycin concentrations.....	106
Figure 3-14 Automated Visiopharm analysis of the fibrosis within the lungs of guinea pigs treated with different concentrations of bleomycin. ....	107
Figure 3-15 Pilot study investigating guinea pig spontaneous coughs following intratracheal instillation of different concentrations of bleomycin, n=2.....	109
Figure 3-16 Guinea pig spontaneous coughs following intratracheal instillation of 0 USP/kg (saline vehicle) or 6 USP/kg of bleomycin. ....	110
Figure 3-17 Spontaneous coughing by guinea pigs treated with vehicle (saline) or bleomycin (6 USP/kg) over a 24-hour period.....	111
Figure 3-18 Guinea pig body weights throughout bleomycin time course study. ....	112
Figure 3-19 The effect of various tussive stimuli on vagus nerve depolarisation in bleomycin-treated guinea pigs. ....	113
Figure 3-20 Representative micrographs of lungs taken from guinea pigs in the bleomycin time course study.....	115
Figure 3-21 Ashcroft Score of guinea pig lungs from bleomycin time course study.....	116
Figure 3-22 Automated Visiopharm analysis of fibrosis from lungs from bleomycin time course ....	117
Figure 3-23 Immunohistochemical staining to identify fibroblastic foci in bleomycin-treated guinea pigs. ....	119
Figure 3-24 The expression of fibrosis-related genes in the parenchyma of guinea pigs in the bleomycin time course study. ....	120
Figure 3-25 Proportion of hydroxyproline in the lungs of guinea pigs incubated from the bleomycin time course study.....	121
Figure 3-26 Total and differential leukocytes in the BALF of guinea pigs from the bleomycin time course study.....	122
Figure 4-1 Timeline of the PROFILE study following IPF patient recruitment. ....	132
Figure 4-2 The metabolic formation of 8-isoprostane, a biomarker for lipid peroxidation. ....	134
Figure 4-3 Concentration of 8-isoprostane in guinea pig BALF from the bleomycin time course study. ....	139
Figure 4-4 Concentration of 8-isoprostane in IPF patient BALF and healthy controls. ....	139
Figure 4-5 Concentration of eATP in in guinea pig BALF from the bleomycin time course study.....	140
Figure 4-6 Concentration of eATP in BALF of IPF patients and healthy controls .....	141

Figure 4-7 Tryptase activity in the BALF of guinea pigs from the bleomycin time course study.....	142
Figure 4-8 Tryptase activity in BALF taken from patients diagnosed with IPF or healthy volunteers. .....	142
Figure 5-1 Anatomy of guinea pig vagal ganglia and its surrounding tissue. ....	150
Figure 5-2 Summary of the airway terminating-neuron isolation process .....	151
Figure 5-3 Imaging cellular oxidative stress with DHE. ....	152
Figure 5-4 The drug perfusion system for neuronal imaging experiments. ....	153
Figure 5-5 Imaging the resulting oxidative stress from a H <sub>2</sub> O <sub>2</sub> concentration response in guinea pig vagal ganglionic neurons.....	157
Figure 5-6 Changes in [Ca <sup>2+</sup> ] <sub>i</sub> in guinea pig vagal ganglia upon stimulation with H <sub>2</sub> O <sub>2</sub> . ....	158
Figure 5-7 A concentration response to the oxidant H <sub>2</sub> O <sub>2</sub> in the isolated vagus nerve model, using guinea pig tissue.....	159
Figure 5-8 Effect of J130 on acrolein induced vagus nerve depolarisation .....	160
Figure 5-9 Inhibition of H <sub>2</sub> O <sub>2</sub> -induced vagus nerve depolarisation by TRPA1-selective antagonist J130 .....	161
Figure 5-10 Inhibition of H <sub>2</sub> O <sub>2</sub> -induced vagus nerve depolarisation using NAC and J130. ....	162
Figure 6-1 Trace of vagus nerve depolarisations during a concentration response to a PAR2 agonist. .....	172
Figure 6-2 A selection of concentration responses to PAR2 agonists in guinea pig vagus nerves. ....	173
Figure 6-3 Confirming PAR2 knockout in gene edited mice.....	174
Figure 6-4 The effect of various PAR2 agonists and other protussive stimuli on vagus nerve depolarisation in PAR2 knockout (F2LR1 <sup>-/-</sup> ) mice. ....	175
Figure 6-5 Inhibition of PAR2 agonist-induced vagus nerve depolarisation with PAR2-selective antagonist P2Pal-18s.....	176
Figure 6-6 Measuring guinea pig recurrent laryngeal nerve (RLN) firing in response to PAR2 agonist 2- Furoyl-LIGLRO.....	177
Figure 6-7 In vivo Aδ-fibre firing in response to different concentrations of PAR2 agonist 2-Furoyl- LIGRLO in a guinea pig.....	178
Figure 6-8 Inhibition of PAR2 agonist-induced vagus nerve depolarisation with TRPV4 and P2X3 antagonists in guinea pigs.....	180
Figure 6-9 Inhibition of PAR2 agonist-induced vagus nerve depolarisation with a TRPV4 antagonist in donor human tissue. ....	181
Figure 7-1 Pharmacokinetic performance of GSK279 in a Phase 1 clinical trial .....	188

Figure 7-2 Effect of selective TRPV4 antagonists on TRPV4 agonist GSK101 (300nM) induced vagus nerve depolarisation. ....	192
Figure 7-3 The effect of TRPV4 selective antagonists on guinea pig coughs elicited by aerosolised TRPV4 agonist GSK101. ....	194
Figure 7-4 Total free plasma levels of GSK279 in guinea pigs treated with this compound in the second dose response study .....	195
Figure 7-5 A time course effect of selective TRPV4 antagonist GSK279 on GSK101-induced cough in guinea pigs. ....	196
Figure 7-6 Total free plasma levels of GSK279 in guinea pigs treated with this compound in the time course study .....	197
Figure 8-1 This thesis' first proposed mechanism for IPF-associated cough.....	211
Figure 8-2 The second proposed mechanism for IPF-associated cough .....	212
Figure 8-3 The effect of TRPV4 antagonist GSK279 on GSK101-induced cough in bleomycin-treated guinea pigs .....	215
Figure 8-4 Reengineering the VitaloJAK™ algorithm to optimise spontaneous cough quantification in guinea pigs .....	216



## List of Tables

Table 1-1 Criteria for classifying different high-resolution computed tomography patterns .....	23
Table 2-1 Primer sequences used to genotype F2RL1 <sup>-/-</sup> mice.....	65
Table 2-2 PCR protocol for F2RL1 <sup>-/-</sup> genotyping and size of product.....	65
Table 2-3 Criteria for acceptance of human lung tissue .....	67
Table 2-4 Tissue donor characteristics .....	68
Table 3-1 Modified Ashcroft Scale from Hubner et al., 2008.....	91
Table 3-2 The various protussive stimuli that the vagus nerves deriving from bleomycin-treated guinea pigs were exposed to, in the isolated vagus nerve model.....	93
Table 4-1 Patient criteria for participation within the PROFILE study.....	131
Table 5-1 The peak excitation and emission wavelengths of the superoxide-sensitive fluorescent dye DHE.....	151
Table 5-2 The peak excitation and emission wavelengths of the Ca <sup>2+</sup> indicator dye Fura-2.....	154
Table 7-1 The structure and potency of TRPV4 antagonists GSK219 compared with GSK279 .....	187
Table 10-1 Criteria for differential leukocyte counting in guinea pig BAL.....	249

## Abbreviations

<b>2-furoyl-LIGRLO</b>	2-furoyl-Leu-Ile-Gly-Arg-Leu-Orn-NH <sub>2</sub>
<b>6MWT</b>	Six Minute Walk Test
<b>4<math>\alpha</math>PDD</b>	4 $\alpha$ -phorbol 12,13-didecanoate
<b>AOD</b>	Assay-on-Demand
<b>ATP</b>	Adenosine Triphosphate
<b>AUC</b>	Area Under the Curve
<b>BAL</b>	Bronchoalveolar Lavage
<b>BALF</b>	Bronchoalveolar Lavage Fluid
<b>CAP</b>	Compound Action Potentials
<b>CCTV</b>	Closed-circuit Television
<b>CNS</b>	Central Nervous System
<b>CPG</b>	Central pattern generator
<b>DAPI</b>	4',6-diamidino-2-phenylindole
<b>DiI</b>	DiI <sub>C18</sub> (3) (1,1'-dioctadecyl-3,3,3',3'-tetramethyl-indocarbocyanine perchlorate)
<b>DHE</b>	Dihydroethidium
<b>DMSO</b>	Dimethyl Sulfoxide
<b>DNA</b>	Deoxyribose Nucleic Acid
<b>DVR</b>	Digital Video Recorder
<b>ECM</b>	Extracellular matrix
<b>ECS</b>	Extracellular Solution
<b>ED<sub>50</sub></b>	Median Effective Dose
<b>eTRec</b>	Electrophysiological Tracheal Recording
<b>FRET</b>	Förster resonance energy transfer
<b>Fura2-AM</b>	Fura2-acetoxymethyl
<b>FVC</b>	Forced Vital Capacity
<b>GSK101</b>	GSK1016790a
<b>GSK219</b>	GSK2193874
<b>GSK279</b>	GSK2798745
<b>H&amp;E</b>	Haematoxylin and eosin (stain)
<b>HBSS</b>	Hanks' Balanced Salt solution
<b>HRCT</b>	High resolution computerized tomography
<b>i.p.</b>	Intraperitoneal (administration)
<b>i.t.</b>	Intratracheal (instillation)
<b>i.v.</b>	Intravenous (administration)

<b>IC<sub>50</sub></b>	Half Maximal Inhibitory Concentration
<b>IIAM</b>	International Institute for the Advancement of Medicine
<b>IIP</b>	Idiopathic Interstitial Pneumonia
<b>J130</b>	Janssen 130
<b>KH</b>	Krebs–Henseleit (solution)
<b>ILD</b>	Interstitial Lung Disease
<b>IVC</b>	Individually Ventilated Cage
<b>IPF</b>	Idiopathic Pulmonary Fibrosis
<b>LCQ</b>	Leicester Cough Questionnaire
<b>mOsm</b>	milli-Osmole
<b>MUC5B</b>	Mucin 5B
<b>NAC</b>	N-Acetylcysteine
<b>NACWO</b>	Named Animal Care & Welfare Officer
<b>NTS</b>	Nucleus Tractus Solitarius
<b>P2Pal-18s</b>	palmitate-RSSAMDENSEKKRKSNIK-NH <sub>2</sub>
<b>PAR2</b>	Protease-activated Receptor 2
<b>PBS</b>	Phosphate-buffered saline
<b>PCR</b>	Polymerase Chain Reaction
<b>PGE<sub>2</sub></b>	Prostaglandin E2
<b>p.o.</b>	Per Os (Oral Administration)
<b>RARs</b>	Rapidly Adapting Receptors
<b>RLN</b>	Recurrent Laryngeal Nerve
<b>RNA</b>	Ribonucleic Acid
<b>ROS</b>	Reactive Oxygen Species
<b>S.E.M.</b>	Standard Error of the Mean
<b>SLIGKV</b>	Ser-Leu-Ile-Gly-Lys-Val-NH <sub>2</sub>
<b>SARs</b>	Slowly Adapting Receptor
<b>SLN</b>	Superior Laryngeal Nerve
<b>TRP</b>	Transient Receptor Potential
<b>UIP</b>	Usual Interstitial Pneumonia
<b>USP</b>	United State Pharmacopeia
<b>VGSCs</b>	Voltage gated sodium channels
<b>WT</b>	Wild Type

# 1 Introduction

## 1.1 IPF

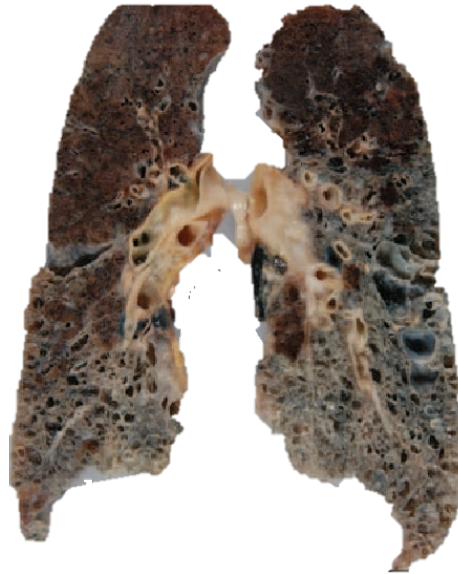
The current section introduces IPF, its diagnosis, risk factors and its pathobiology. A literature surrounding cough and how it manifests itself in IPF patients can be found in Section 1.3.

### 1.1.1 Introduction to IPF

Idiopathic Pulmonary Fibrosis (IPF) is a chronic and terminal interstitial lung disease characterised by a progressive build-up of scar tissue within the lung parenchyma that is of unknown cause (Raghu et al., 2018)(Figure 1-1). It is a debilitating respiratory disease invariably accompanied by worsening dyspnoea on exertion; other symptoms frequently accompanying the disease are bibasal inspiratory crackles on auscultation, digital clubbing, and pertinent to this thesis, a dry non-productive cough (Raghu et al., 2018, Key et al., 2010).

IPF is more common in men and typically affects patients beyond the age of 60 (Guenther et al., 2018). Estimations of the prevalence of IPF vary across studies, however a recent systemic review of the literature estimated that from the year 2000 onwards, the incidence range in Europe and North America was 3—9 cases per 100,000 per year; worryingly, the authors also noted that the incidence of the disease appears to be increasing worldwide (Hutchinson et al., 2015). IPF has a poor prognosis that is comparable to some of the most severe malignancies, and whilst there are recently approved anti-fibrotic therapies that can slow the progression of the disease (Lancaster et al., 2019), the median survival time of a patient following diagnosis is 3—5 years (Fernandez Perez et al., 2010, Nathan et al., 2011, Guenther et al., 2018).

Having a history of past cigarette smoking is the most widely accepted risk factor for IPF, increasing the risk of developing the disease by about twofold (Olson and Swigris, 2012, Bellou et al., 2017, Baumgartner et al., 1997). Other risk factors include gastro-oesophageal reflux disease (GERD), hepatitis C, viral infections (*e.g.* Epstein–Barr virus), occupational exposures (*e.g.* metal, wood or coal dust and silica), and a family history of interstitial lung disease (Raghu et al., 2006, Tobin et al., 1998, Blanc et al., 2019, Irving et al., 1993, Stewart et al., 1999, Kuwano et al., 1997, Borie et al., 2019).



*Figure 1-1 Lungs from a patient with IPF*

*A photograph of lungs (cut in the coronal plane) obtained at autopsy from a 78-year-old, female IPF patient. The image illustrates the scarring of the lower lung's parenchyma that is characteristic of the disease, as well as the large cystic airspaces, known as honeycombs. Adapted from Arakawa and Honma (2011)*

### 1.1.2 Disease Classification

IPF falls into a category of diseases known as the interstitial lung diseases (ILDs). These are diseases that affect the interstitium *i.e.* the alveoli and their surrounding tissue. ILDs are generally characterised clinically by exertional dyspnoea, abnormal gas transfer, bilateral pulmonary infiltrates and abnormal pulmonary physiology. Pathologically, ILDs are typically characterised by inflammatory and immune cell infiltration, which in turn is often accompanied by atypical extracellular matrix (ECM) deposition in the interstitium of the distal airways (Meyer et al., 2012).

The ILDs can be further subclassified according to whether or not their cause is known. ILDs can be secondary to: environmental and occupational diseases (*e.g.* asbestosis), multisystem diseases (*e.g.* sarcoidosis, or connective tissue diseases), adverse drug reactions (*e.g.* bleomycin-induced pulmonary toxicity) or rare lung diseases (*e.g.* pulmonary eosinophilia) (Bourke, 2006). Conversely, ILDs which have no known cause are classified as idiopathic interstitial pneumonias (IIPs); besides IPF, these include desquamative interstitial pneumonia, nonspecific interstitial pneumonia, respiratory bronchiolitis with interstitial lung disease, acute interstitial pneumonia, lymphoid interstitial pneumonia and cryptogenic organizing pneumonia (Meyer et al., 2012, Antoniou et al., 2014).

Although IPF is generally a sporadic condition, within IPF there also exists familial IPF. Familial IPF is defined as IPF that occurs within two or more members of the same family (Lee et al., 2005), and it is estimated to account for between 2 to 20% of all diagnosed IIP cases (Kropski et al., 2015a). This variation of the disease is due to the common inheritance of certain predisposing genetic factors (discussed in Section 1.1.4.2) and it has not been found to exhibit any different clinical, radiological or pathological features to sporadic (*i.e.* nonfamilial) IPF (Lee et al., 2005).

### 1.1.3 Diagnosis and clinical indications

#### 1.1.3.1 High-resolution computed tomography

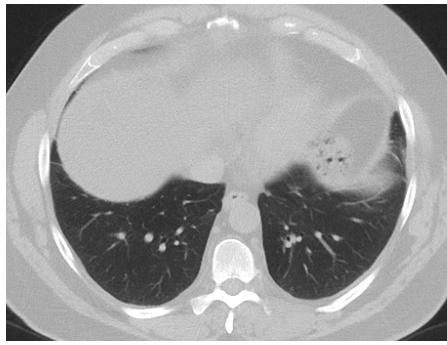
Crucial to diagnosing IPF is the use of high-resolution computed tomography (HRCT) to scan the chest (Raghu et al., 2018). HRCT combines x-rays and computer algorithms to generate multiple cross-sectional images through a patient's chest cavity, allowing a radiologist to identify whether the radiologic pattern of IPF is present (Lederer and Martinez, 2018). The pattern, known as usual interstitial pneumonia (UIP), is described in Table 1-1 and depicted in example HRCT scans in Figure 1-2 (Raghu et al., 2018), and is predominantly exhibited in the peripheral and in the lower lobes (Lederer and Martinez, 2018). It is important to note that a radiological pattern of UIP is not synonymous with IPF, although it is the most likely cause. Other diseases such as chronic hypersensitivity pneumonitis, drug toxicity, asbestosis and connective tissue disease are also associated with UIP (Wuyts et al., 2014). For this reason, it is important for clinicians to routinely ask questions of the patient relating to their lifestyle and employment history and to check for other clinical, serological or pathological indications; a history of workplace exposure to mould, dampness or birds for instance, is known to cause chronic hypersensitivity pneumonitis, which can be radiologically indistinguishable from IPF (Lederer and Martinez, 2018, Wuyts et al., 2014).

Table 1-1 Criteria for classifying different high-resolution computed tomography patterns

It is necessary for patients with a pattern that is not 'UIP' to undergo surgical lung biopsy to aid in diagnosis. Table adapted from Raghu et al. (2018). Despite the helpfulness of these sorts of guidelines, there is still only moderate inter-observer agreement, even between experienced radiologists, when it comes to diagnosing IPF (Walsh et al., 2016)

Radiological feature	UIP	Probable UIP	Indeterminate for UIP
<b>Honeycombing</b> (cystic airspaces with well-defined and thick walls)	✓	—	—
<b>Reticular Pattern</b> (interlacing shadows with a mesh or net like appearance)	(✓) Optional, as it is superseded by honeycombing	✓	✓ Sometimes subtle
<b>Subpleural and basal predominance</b> (abnormalities are under the pleural membrane and in the lower lung)	✓ Often heterogenous distribution	✓ Often heterogenous distribution	✓
<b>Peripheral traction bronchiectasis or bronchiolectasis</b> (Irreversible dilation of the bronchi or bronchioles, respectively, that can be a result of fibrosis)	(✓) Optional, as long as honeycombing is present	✓	—
<b>Mild ground glass opacities</b> (an area of the HRCT scan that appears lighter as a result of increased tissue density, usually due to air being replaced by fluid or fibrosis)	(✓) Optional	(✓) Optional	(✓) Optional
<b>Absent of features that are inconsistent with a UIP pattern</b> (e.g. extensive ground glass opacities, upper or mid-lung predominance, pleural effusions, consolidation, cysts, etc.)	✓	✓	✓

**a) Normal HRCT of chest**



**b) UIP pattern**



**c) Probable UIP pattern**



*Figure 1-2 A comparison between HRCT scans of a normal chest and UIP patterns*

*Axial chest high-resolution computed tomography (HRCT) images taken at the level of the lower lobes. a) HRCT scan of a normal chest for reference. Case courtesy of Assoc Prof Craig Hacking, Radiopaedia.org, rID: 40797. b) Usual interstitial pneumonia (UIP) pattern. The scan depicts subpleural honeycombing that is typical of a UIP pattern. c) Probable UIP pattern. This scan depicts traction bronchiectasis without clear evidence of subpleural honeycombing, there are however areas of ground glass opacification and reticulation. Whilst this patient is almost certainly suffering from IPF, a surgical lung biopsy would still be required to confirm the diagnosis. (b) and (c) adapted from Martinez et al. (2017)*

Only in the cases where a pattern of UIP cannot be definitively recognised (e.g. a scan pattern of probable UIP or indeterminate for UIP) do the ATS, ERS, JRS and ALAT joint guidelines recommend performing a diagnostic surgical lung biopsy (SLB) or bronchoalveolar lavage (BAL) (Raghu et al., 2018). Whilst BAL is widely considered to be safe for IPF patients, it is nonetheless an invasive procedure (Wells, 2010). The same cannot be said for SLB, which carries with it an increased risk of death that could outweigh the benefit of securing an IPF diagnosis, particularly if the patient already requires a high volume of oxygen or suffers from another condition that might make them higher risk, e.g. pulmonary hypertension (Lederer and Martinez, 2018).

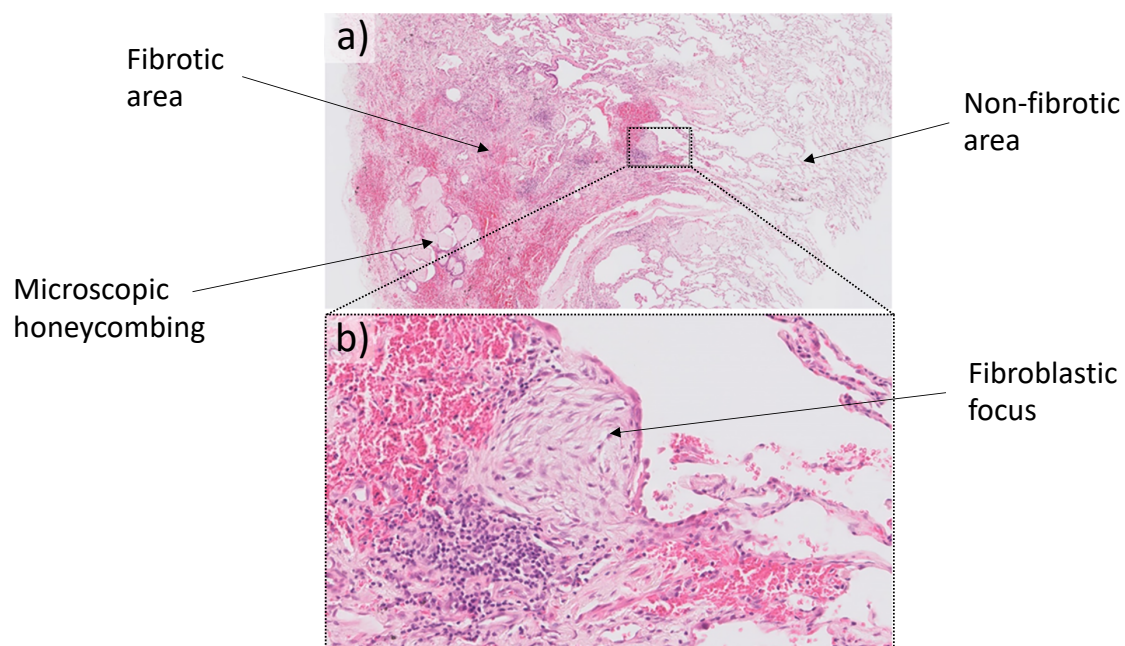
**1.1.3.2 Surgical lung biopsies and their histopathology**

When SLB is required because of an ambiguous HRCT pattern, it is advised by the ATS, ERS, JRS and ALAT joint guidelines that video-assisted thoroscopic surgery be used and that multiple biopsies are



taken, from two to three lobes, because the histologic pattern from different segments can be variable (Raghu et al., 2018).

The typical histopathological pattern of UIP (Figure 1-3) is one of “patchwork” fibrosis that disrupts the microscopic architecture of the alveoli, and results in honeycombing, however, this fibrosis still alternates with areas of the parenchyma that are relatively unaffected (Raghu et al., 2018, Snetselaar et al., 2017). Highly unique to the UIP histological pattern is the presence of so-called fibroblastic foci (Figure 1-3b): small areas that are densely packed with fibroblasts, myofibroblasts and the extracellular matrix (ECM) that they have excessively produced (Yamaguchi et al., 2017). These histopathological patterns have a predilection for the subpleural and paraseptal parenchyma and can be accompanied by mild inflammation in the form lymphocyte and plasma cell infiltration (Bjoraker et al., 1998). Much like the honeycombing seen in a UIP pattern radiologically, microscopic honeycombing is a regular feature in IPF histologically too (Nishimura et al., 1992, Raghu et al., 2018). As with their macroscopic counterparts, microscopic honeycombs are cystic airspaces that are bordered by bronchiolar epithelium and filled with mucus and inflammatory cells.



*Figure 1-3 Histopathology showing fibrotic and non-fibrotic areas within a single lung biopsy*

- a) Low magnification image of IPF lung tissue stained with haematoxylin and eosin (H&E) showing architectural distortion to alveoli in some areas, due to areas of dense fibrosis and microscopic honeycombing. This is juxtaposed by the areas of the parenchyma that are relatively unaffected by fibrosis, thereby illustrating the variability in architectural distortion that is possible within a single biopsy.*
- b) A magnification of the fibrotic boxed area from within image (a) showing a characteristic fibroblastic focus. Adapted from Snetselaar et al. (2017)*

### 1.1.3.3 Bronchoalveolar lavage and cellular analysis

As mentioned earlier, bronchoalveolar lavage (BAL) is only recommended by the ATS, ERS, JRS and ALAT joint guidelines in the event that a UIP HRCT pattern cannot be definitively confirmed in a patient with suspected interstitial lung disease (Raghu et al., 2018). BAL is especially useful if SLB is not suitable for a patient, this is due to BAL being a far lower risk procedure, even in patients that are critically unwell (Meyer et al., 2012, Wells, 2010, Hertz et al., 1991, Molyneaux et al., 2020).

BAL is typically a diagnostic method for the lower respiratory system in which a bronchoscope is passed into an appropriate airway of the lungs, via the mouth or nose, whereupon saline is instilled and subsequently retrieved again, using negative suction. Details for the exact methods BAL was performed to obtain the data in this thesis can be found in Section 4.2.1.1.

Performing a differential cell analysis of the leukocytes in BAL fluid can be a useful way of differentiating IPF from other ILDs (Raghu et al., 2018). For instance, whilst IPF patients typically have a higher eosinophil proportion than healthy individuals (2.39% to 7.5% versus  $\leq 1\%$ , respectively), a suspected ILD patient with a proportion of 50% would most likely be suffering from eosinophilic pneumonia rather than IPF (Lee et al., 2015, Raghu et al., 2018). Similarly, although IPF patients have a higher proportion of lymphocytes and CD4/CD8 ratio in their BAL than healthy individuals, it is still markedly lower than patients with sarcoidosis (Lee et al., 2015).

Like in this thesis, BAL can also be used for research purposes, as it also collects acellular components from the bronchioles (*e.g.* exozymes or cytokines) (Meloni et al., 2004, Bargagli et al., 2005). BAL is also a useful technique because it can easily be repeated in animal models of fibrosis, thereby allowing preclinical biomarkers to be compared with clinical ones. Whilst this thesis utilises BAL to measure and confirm the elevated levels of the alarmin ATP in IPF patient BAL, it remains possible, albeit unlikely, that the intrusive process of BAL itself could be instigating a release of such alarmins and thereby skewing the data of studies that attempt to measure them. Such a phenomenon has been reported as a result of ventilator use (Grazioli et al., 2019), however it has not to our knowledge been reported as a result of BAL.

### 1.1.4 Pathogenic risk factors

The prevailing theory behind the pathogenesis of IPF, is that recurrent microinjuries made to a senescent lung's epithelium, particularly when in the presence of certain predisposing genetic factors, can result in an aberrant wound healing process, involving the deposition of excess ECM by myofibroblasts within the interstitium (Lederer and Martinez, 2018, Barratt et al., 2018, Sgalla et al., 2018). These renegade myofibroblasts are thought to be encouraged to behave aberrantly by profibrotic mediators that have been secreted into the lung by alveolar cells that have endured

telomere shortening, proteostatic dysregulation, endoplasmic reticulum and oxidative stress, and mitochondrial dysfunction (Alder et al., 2008, Selman and Pardo, 2014).

#### 1.1.4.1 Environment

As mentioned in the introductory section, there are a variety of environmental risk factors that are thought to be implicated in the pathogenesis of IPF. Studies have shown that there is a strong association between exposure to cigarette smoke and metal dusts, and developing IPF (Taskar and Coultas, 2006). Other significant correlations have been described that connect IPF to working in agriculture or with livestock, as well workplace exposure to wood and stone dust, sand, and silica (Taskar and Coultas, 2008).

More confounding than the above, is the question of whether or not bacterial burdens are generally higher in the IPF lung and whether or not this is a causative factor in developing the disease. Whilst one study was unable to locate bacterial DNA in IPF patient lung explant tissue (Kitsios et al., 2018), others have identified plentiful colonies of *Haemophilus*, *Streptococcus*, *Neisseria*, *Veillonella* and *Staphylococcus* in IPF BAL (Han et al., 2014, Molyneaux et al., 2014), with the latter studies further asserting that bacterial burden is associated with a worse disease progression. Similarly, viruses such as Epstein-Barr virus have been suspected by some of having a role in IPF (Vergnon et al., 1984), but this has been contested by others (Molyneaux and Maher, 2013).

#### 1.1.4.2 Genetics and epigenetics

There exist a variety of genetic variations that confer a predisposition to developing IPF.

The gene variant with the strongest risk factor for developing IPF is a single nucleotide polymorphism (SNP) (rs35705950) in the promoter region of the gene encoding mucin 5B (*MUC5B*) (Kropski et al., 2015a). Mucins are high molecular weight glycoproteins that constitute a major component of airway mucus (Thornton et al., 2008), with mucin 5B playing an integral role in mucociliary clearance (Roy et al., 2014). This SNP, that was originally identified in a genome wide linkage study, was found to increase the risk for IPF by six to eight-fold (Seibold et al., 2011). Subsequent studies have verified this finding in multiple independent Caucasian IPF patient cohorts (Fingerlin et al., 2013, Borie et al., 2013, Noth et al., 2013, Peljto et al., 2012, Zhang et al., 2011), but have found it to be much rarer in east Asian IPF patient cohorts, which themselves appear to have alternative *MUC5B* polymorphisms that confer a predisposition to the disease (Peljto et al., 2015, Wei et al., 2014). Despite our understanding of mucin 5B's role in airway defence, the mechanism by which *MUC5B* polymorphisms mediate lung fibrosis are currently unknown (Kropski et al., 2015a).

Other gene variants that predispose one to IPF or accelerate its progression include: genes relating to intercellular adhesion such as *DSP*, *DPP9* and *CTTNA3* (Fingerlin et al., 2013); genes involved in profibrotic signalling pathways such as *AKAP13* (Allen et al., 2017); and genes involved in inflammation and immunity such as *TGFB1* and *TLR3* (Xaubet et al., 2003, O'Dwyer et al., 2013).

Less common gene variants that are more often seen in familial IPF than sporadic IPF, are in surfactant protein-related genes *e.g.* surfactant protein C (*SFTPC*) (Lawson et al., 2004, Markart et al., 2007, Ono et al., 2011). Mutant surfactant protein C precursor peptides are thought to fold incorrectly within the endoplasmic reticulum (ER), which leads to stress within that organelle and activation of the unfolded protein response (Bridges et al., 2003, Mulugeta et al., 2007, Mulugeta et al., 2005). Intriguingly, whilst mice with ER stress within their alveolar epithelium do not develop spontaneous pulmonary fibrosis, they do however appear to exhibit an exaggerated fibrotic response when administered with the profibrotic drug bleomycin (Lawson et al., 2011). The fact that ER stress and the unfolded protein response, which can be instigated by exposures to cigarette smoke and herpesviruses (Isler et al., 2005, Hengstermann and Muller, 2008, Zhao et al., 2011), is commonplace within the alveolar epithelium of IPF patients (Korfei et al., 2008, Lawson et al., 2008), could partly explain why such environmental insults are considered risk factors for developing the disease (Bellou et al., 2017, Lasithiotaki et al., 2011).

Besides genetic alterations linked to IPF, there is increasing evidence that epigenetic alterations also play a role in the disease's onset (Yang, 2012). For instance, expression of the microRNA cluster miR-17~92 that post-transcriptionally silences profibrotic genes, is reduced in IPF patient lung biopsies and fibroblasts, due to the clusters' promoter having undergone the epigenetic change of DNA hypermethylation (Dakhlallah et al., 2013). DNA methylation arrays performed in a subsequent study of 94 IPF patients and 67 control subjects, identified some 2,130 differentially methylated regions across the human genome, 738 of which were associated with significant changes in gene expression and included genetic variants already linked to IPF (*e.g.* *DSP*) (Yang et al., 2014).

#### 1.1.4.3 Senescence

Since IPF typically affects individuals over the age of 60 (Raghu et al., 2018), the disease is undoubtedly one of the aging lung, with senescence of the alveolar epithelium and fibroblasts thought to be a phenotype that promotes fibrosis (Selman and Pardo, 2014). Indeed, an *in vivo* study by Xu et al. (2009) found that mice bred to have accelerated senescence, developed a more severe pulmonary fibrosis following bleomycin challenge than their control, senescent-resistant counterparts. Similar findings were made in a later study that compared younger mice to naturally aged mice (Huang et al., 2015). This study also found evidence that myofibroblasts in older mice

shared a more apoptosis-resistant phenotype, supposedly due to higher expression of plasminogen activator inhibitor 1 (PAI-1). PAI-1 is believed to be a mediator of TGF- $\beta$ 1-induced alveolar senescence (Rana et al., 2020).

One of the key mechanisms of aging is the shortening of cell telomeres, which act as protective caps for a cell's chromosomes during each round of cell division (Jiang et al., 2007). In order to maintain genomic integrity, enzymes such as telomerase and non-coding RNAs such as telomerase RNA component are required to protect the telomeres during cell division. Rare mutations in these genes, such as *PARN*, *TERT*, *RTEL1* and *TERC*, accelerate senescence and have been linked to familial IPF (Armanios et al., 2007, Tsakiri et al., 2007).

### 1.1.5 IPF Pathobiology

As mentioned previously, key to the theory behind IPF pathogenesis is an abnormal healing process of the alveolar epithelium, in response to repetitive microinjuries.

Under normal circumstances, in a healthy lung, it is type I alveolar epithelial cells (AEC1s) that line the majority of the alveolar surface. Any damage to AEC1s (*e.g.* due to the inhalation of metal dusts), is promptly followed by the proliferation of type 2 alveolar epithelial cells (AEC2s), stem cells within the lung, which subsequently differentiate into the normal epithelium of AEC1s and re-establish alveolar integrity, to complete the healing process (Uhal, 1997, Desai et al., 2014). The IPF lung, however, has characteristically few AEC1s in fibrotic regions, with abnormal and hyperplastic AEC2s in their place instead, which are themselves typically adjacent to fibroblastic foci (Kallenberg et al., 1987, Kasper and Haroske, 1996, Kawanami et al., 1982). These AEC2s also show clear signs of senescence (discussed in Section 1.1.4.3) due to their telomeres being shortened, and they exhibit an impaired capacity for renewal (Alder et al., 2008, Kropski et al., 2015b, Liang et al., 2016).

Abnormal behaviour of the alveolar cells in response to injury in the IPF lung is thought to be due to the inappropriate activation of signalling pathways required for embryonic development, such as the Wnt and Sonic hedgehog pathways (Königshoff et al., 2009, Stewart et al., 2003). These activated alveolar epithelial cells also secrete a variety of fibrogenic growth factors *e.g.* transforming growth factor  $\beta$  (TGF- $\beta$ ) and platelet-derived growth factor (PDGF) (Fernandez and Eickelberg, 2012, Antoniadis et al., 1990). The accumulation of these fibrogenic growth factors within the lung drives the recruitment of myofibroblasts, a subpopulation of fibroblasts distinguished by their expression of alpha smooth muscle actin and their more contractile phenotype (Phan, 2008, McAnulty, 2007). As previously discussed (1.1.3.2), the myofibroblasts accumulate in areas referred to histopathologically as fibroblastic foci and they are generally accepted as the cellular perpetrators of the destruction and distortion to the IPF lung's architecture (Yamaguchi et al., 2017). The source of

the myofibroblasts that establish themselves in the lung has not been fully elucidated, however multiple progenitors and mechanisms have been proposed including: epithelial-mesenchymal transition, circulating fibrocytes, lung pericytes or resident mesenchymal cell proliferation (Hung et al., 2013, Rock et al., 2011). Once activated, the myofibroblasts secrete a range of ECM components including collagens (*e.g.* type I and type III), proteoglycans and fibronectin (McAnulty, 2007, Booth et al., 2012).

Rather problematically, multiple studies have suggested that the excessive and abnormal ECM deposited by the myofibroblasts that causes the parenchyma to become rigid, in turn, further promotes disease progression, through a positive feedback mechanism. This is evidenced *in vitro* by culturing fibroblasts on acellular ECM scaffolds with varying degrees of stiffness, whereupon they invariably increase their proliferation and activity (Liu et al., 2010, Booth et al., 2012, Parker et al., 2014). The mechanism by which abnormal ECM confers a more active and invasive fibroblast phenotype has not been fully elucidated, however it is believed to be through integrins (*e.g.*  $\alpha_6$ ), which are transmembrane receptors responsible for cell adhesion to ECM, that also form part of the cell's mechanotransduction machinery (Tschumperlin, 2015, Chen et al., 2016).

Another pathobiological feature that occurs in IPF is the so-called bronchiolisation of the alveoli, which is when cells resembling bronchiolar epithelium line the alveolar walls (Plantier et al., 2011). These proliferative bronchiolar lesions are associated with an increase in the expression of components from the developmental Wnt/ $\beta$ -catenin signalling pathway, which would go towards explaining why remodelling of the IPF lung is so profound (Chilosi et al., 2003).

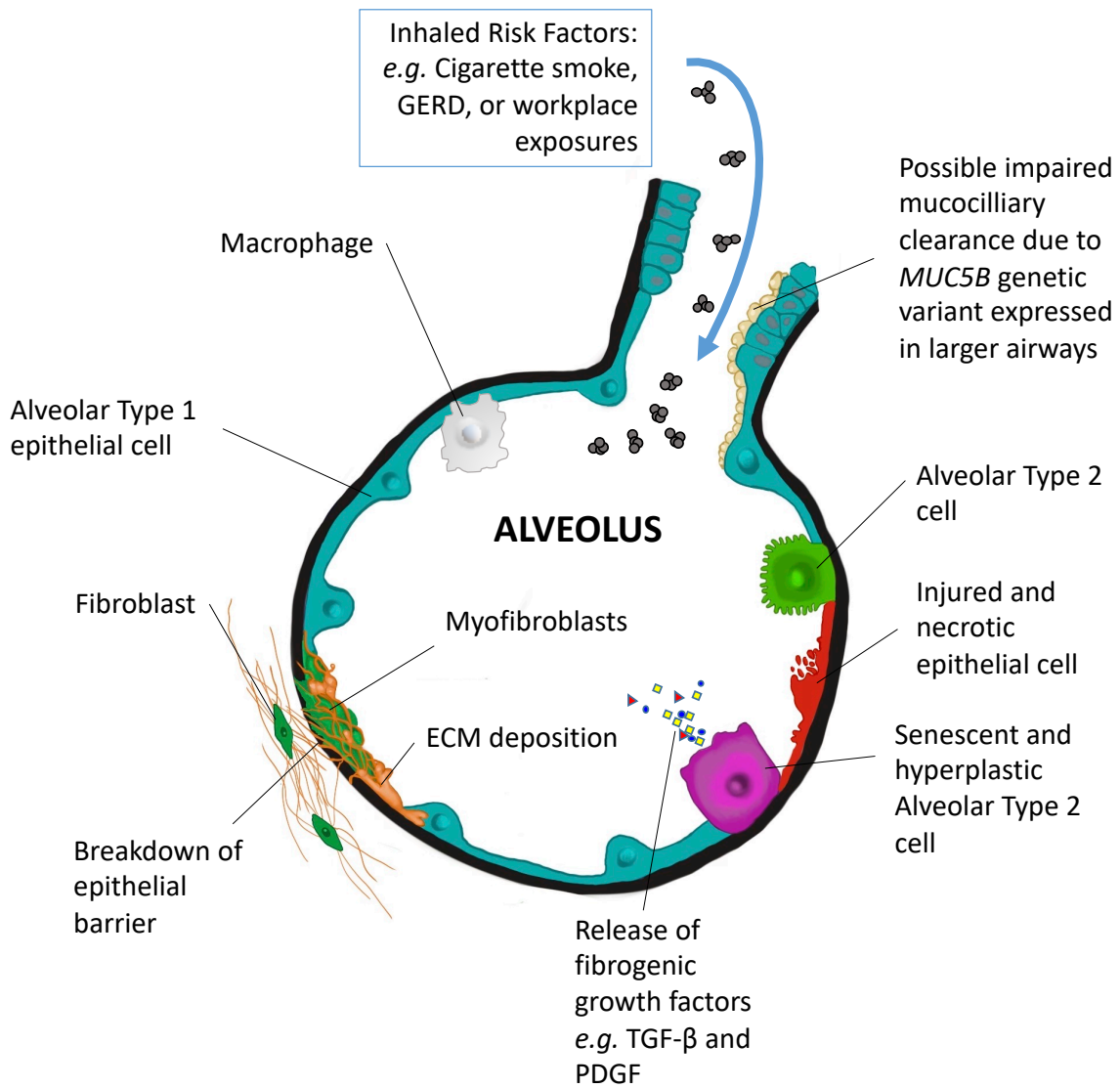


Figure 1-4 IPF pathobiology

A schematic to illustrate the pathobiological features of IPF and the current explanations as to how they cause the disease. Recurrent epithelial cell microinjuries made to a senescent lung are caused by inhaled environmental insults like cigarette smoke particles. Profibrotic mediators (e.g. platelet-derived growth factor) are released or activated by alveolar type 2 stem cells that themselves have become resistant to apoptosis and hyperplastic. These fibrogenic growth factors stimulate fibroblasts to proliferate, differentiate into myofibroblasts, and excessively deposit extracellular matrix into the lung parenchyma, that eventually destroys alveolar integrity. Original figure by author.

### 1.1.6 Oxidative stress in IPF

There is growing evidence that oxidative stress might also play an important role in the pathogenesis of IPF (Kliment and Oury, 2010, Daniil et al., 2008). Oxidative stress is often defined as an imbalance between the oxidants within a cell and a cell's antioxidant defences.

Studies have found neutrophilia and eosinophilia within the BALF of 70-90% and 40-60% of IPF patients, respectively (Schwartz et al., 1994). Besides via the release of proteases (*e.g.* tryptase), cytokines and growth factors, these inflammatory cells can also damage the lungs through the release of oxidative species (Bergeron et al., 2003, Waghray et al., 2005). Further to this, there is also evidence that alveolar inflammatory cells may release oxygen radicals in exaggerated quantities in IPF (Strausz et al., 1990). Not surprisingly, increases in these inflammatory cells have been associated with poorer prognoses for IPF patients in some clinical studies (Boomars et al., 1995, Kinder et al., 2008, Rudd et al., 1981).

As it is difficult to measure reduction-oxidation products and free radicals of oxygen directly in tissues, most clinical studies have instead measured the biochemical products of oxidative reactions (Fois et al., 2018); these biomarkers include oxidative changes to lipids, DNA, and proteins. Another alternative is to quantify the concentration of the antioxidants themselves, as a reduction in antioxidants is likely to signify an increased oxidative burden.

As mentioned previously, BAL is a useful technique for measuring the acellular components of the lung and it has proven extremely useful in measuring products of oxidative reactions in IPF. The presence of 8-isoprostane, a biomarker of lipid peroxidation by free radicals, has been reported to be present in increased concentration within the BAL of IPF patients (Montuschi et al., 1998). This biomarker has also been found to be elevated within the exhaled breath condensate from IPF patients, along with hydrogen peroxide (Psathakis et al., 2006). Exhaled ethane is another biomarker of lipid peroxidation, it has similarly been found to be present in higher concentrations in IPF patients and is associated with faster disease progression (Kanoj et al., 2005).

Protein carbonylation is a commonly used marker for protein peroxidation (Dalle-Donne et al., 2003). Carbonylated proteins are a commonly found feature within IPF BAL, especially proteins of lower molecular weight, where they have been negatively correlated with pulmonary function (Bargagli et al., 2007, Lenz et al., 1996, Rottoli et al., 2005).

The antioxidant capacity of the IPF lung also appears to be impaired. Glutathione, a tripeptide antioxidant that occurs ubiquitously throughout life on earth (Lienkamp et al., 2020), is not as present in the alveolar epithelial lining of IPF lungs as it is in healthy lungs (Cantin et al., 1987,



MacNee and Rahman, 1995). Similarly, extracellular superoxide dismutase, an enzyme that catalyses the dismutation of superoxide ( $O_2^-$ ) radicals, is significantly decreased in the fibrotic regions of lungs diagnosed with a UIP pattern (Kinnula et al., 2006).

## 1.2 Modelling fibrosis and assessing anti-fibrotic therapies

Various animal models of pulmonary fibrosis have been developed to probe the pathological mechanisms behind fibrogenesis and to assess the efficacy of candidate antifibrotic compounds. These models have been instrumental in the development of the only two antifibrotic therapies currently approved to treat IPF patients: nintedanib and pirfenidone (Chaudhary et al., 2007, Schaefer et al., 2011, Lederer and Martinez, 2018).

Whilst much focus has been on developing animal models that mimic the fibrotic hallmarks of IPF, no attempts to our knowledge have been made to develop models that recapitulate the chronic spontaneous cough symptom that is a common feature of IPF; this is what this PhD project set out to do.

### 1.2.1 Pre-clinical models of IPF

There exist a variety of different models that resemble idiopathic pulmonary fibrosis in some shape or form, these include: silica administration, asbestos exposure, age-related models (*e.g.* mice with accelerated senescence or aged mice), cytokine overexpression (*e.g.* TGF- $\beta$ ), and radiation exposure models (Tashiro et al., 2017). The bleomycin model remains the most ubiquitous and well characterised model of IPF (Peng et al., 2013, Tashiro et al., 2017). Mice and rats continue to be the most commonly used species for fibrosis models, although in the case of bleomycin models, the use of hamsters, dogs, sheep and even primates has also been described in the literature (Tashiro et al., 2017). To our knowledge, the only pulmonary fibrosis model guinea pigs have been described in is the bleomycin model.

### 1.2.2 The bleomycin model

Bleomycin's use as a model for IPF is discussed in detail later on (Section 3.2.2.1). In brief, it is a chemotherapeutic drug (Adamson and Bowden, 1974) used to treat squamous cell carcinomas, testicular cancer and malignant lymphomas (Bennett and Reich, 1979). The drug works by inducing strand breaks within DNA (Claussen and Long, 1999). Following the discovery that it could cause lung fibrosis in some cancer patients (Hay et al., 1991, Jules-Elysee and White, 1990), it was adopted as an *in vivo* model of IPF.

To our knowledge no research group has yet investigated whether guinea pigs with bleomycin-induced pulmonary fibrosis cough spontaneously in the manner of IPF patients, however cough reflex sensitivity in these animals has been assessed in two studies (see Section 1.4.1.5).

### 1.3 Cough

As mentioned at the beginning of the IPF section, a dry chronic cough is a symptom that affects approximately 80% of IPF patients (Ryerson et al., 2011, Crystal et al., 1976, Turner-Warwick et al., 1980). This next section will explore the burden of chronic cough before outlining the physiology behind the cough reflex and how it affects IPF patients.

#### 1.3.1 Introduction to cough

Cough is a vital reflex for expelling foreign objects, fluids, irritants and microbes from the airways (Fontana et al., 1999, Irwin et al., 1998, Widdicombe, 1995), a more frequent cough, however, usually indicates the presence of disease, with it being the most common reason for why a patient might visit a healthcare professional (Irwin, 2006b). As is exemplified by the ongoing COVID-19 pandemic, some viruses and bacteria have evolved to cause their host to cough in order to aid in their transmission (Wiersinga et al., 2020, Di Filippo et al., 2018). Indeed, in the majority of people, the primary cause of an acute cough is typically a viral upper respiratory tract infection, whilst the cause of most persistent coughs has historically been attributed to chronic bronchitis (Irwin et al., 1977).

Cough can occur pathologically too, however, and without a pathogenic underlying cause. In such circumstances, this excessive and unnecessary coughing can have a dramatic impact on an individual's quality of life and predispose them to depression (McGarvey et al., 2006, Brignall et al., 2008).

Coughing in response to airway irritation is a reflex pathway, the afferent limb of which utilises sensory nerve fibres that reside in the vagus nerve; a cranial nerve that innervates among other organs, the lungs and airways (Bonvini and Belvisi, 2017, Coleridge and Coleridge, 1984). The afferent limb of the cough reflex is initiated by ion channels that are expressed on these fibres at their free nerve endings. The family of ion channels most associated with cough is the Transient Receptor Potential (TRP) family, so called because of mutations in *Drosophilla* that conferred only a temporarily negative electroretinogram in response to light (unlike the longer lasting response in their wild type counterparts); the mutation also caused them to behave seemingly blind (Montell and Rubin, 1989). There is now a great deal of evidence that these channels (e.g. TRPA1 and TRPV1) can elicit the cough reflex in animals and in humans, when activated by a variety of different endogenous and exogenous stimuli (Birrell et al., 2009, Belvisi et al., 2017, Grace et al., 2012, Andre

et al., 2009). It would also be remiss not to mention the ATP-gated ion channel P2X3 at this stage, a pharmacological antagonist for which was shown to reduce objective cough frequency in patients (Abdulqawi et al., 2015), thereby implicating that purinergic receptor in cough, too. Much of the more recent research findings and clinical advances with regards to treating chronic cough have occurred by investigating the peripheral targets of the nervous system like those listed above, as opposed to targeting the cough reflex at the level of the central nervous system, which poses more problems through side effects such as respiratory depression and sedation (Belvisi and Geppetti, 2004).

### 1.3.2 Physiology and prevalence of cough

The cough reflex is a forced pulmonary event necessary for the clearance of foreign objects and secretions from within the larynx, trachea and bronchi, in order to prevent aspiration. The mechanics behind a cough follow three phases: (1) a large inhalation, (2) a powerful expiratory effort against a closed glottis, and lastly (3) the forced opening of the glottis accompanied by a rapid exhalation, thus producing the characteristic cough sound (Chung and Pavord, 2008). Coughs can occur individually or repetitively, in bouts, with the latter sometimes being referred to as a 'peal' (Smith et al., 2006b).

Acute coughs —like those which result from an upper respiratory tract infection— are defined as those that resolve themselves within 3 weeks of onset, meanwhile a cough is described as chronic if it has persisted for over 8 weeks; a cough that lasts for the intervening period is commonly referred to as a subacute cough (Chung and Pavord, 2008, Irwin et al., 1998). Chronic cough is the most frequent reason for visiting a general physician in the United States and in 2006 a cross-sectional study in Britain found that 12% of the population had a chronic cough, 7% of which said it was severe (Irwin et al., 1981, Ford et al., 2006).

### 1.3.3 Diseases featuring chronic cough, its burden on patients and current treatments

Besides IPF, chronic cough can also be a common symptom of other respiratory diseases. The inflammatory diseases asthma and chronic obstructive pulmonary disease (COPD) are often accompanied by chronic cough, and further, patients with these conditions are often diagnosed after presenting themselves to a physician because of this symptom (Irwin et al., 1998, Smith et al., 2006a, Polley et al., 2008, Vestbo et al., 2013). Chronic cough is also a common symptom of gastro oesophageal reflux disease (GERD), and furthermore, can present itself as a side effect to some medications *e.g.* ACE inhibitors (Fuller and Choudry, 1987, Irwin, 2006a, Choudry and Fuller, 1992). Similarly, postnasal drip has been documented as a cause of chronic cough (Irwin et al., 1990), however, others more recently have cast doubt as to whether this syndrome even exists, and

further, whether such patients actually suffer from rhinosinusitis or chronic idiopathic cough, or both (Morice, 2004).

Chronic cough can also occur 'idiopathically', where it affects mostly women in their fifth or sixth decade of life (Morice et al., 2014a). These patients often report feeling irritation in their throat or chest which drives what is for them an inescapable urge to cough (Hilton et al., 2015). Normally innocuous environmental stimuli such as perfumes or changes in temperature can trigger distressing bouts of uncontrollable coughing, as can ordinary bodily sensations from talking to eating (McGarvey et al., 2009); IPF patients who suffer from chronic cough have also described similar scenarios (Vigeland et al., 2017). This phenomenon of an overly sensitised cough reflex, that IPF patients frequently share (Swigris et al., 2005), is often referred to as 'Cough hypersensitivity syndrome' (Morice et al., 2014b).

Estimates as to the prevalence of chronic cough have found that it can affect up to 40% of the population whilst other studies have put it between 11 and 13% (Chamberlain et al., 2015, Cullinan, 1992, Janson et al., 2001, Morice et al., 2001).

The detrimental impact chronic cough has on a patient's quality of life cannot be overstated, with the cough persisting from months to years, and patients coughing hundreds or even thousands of times per day (Kelsall et al., 2009, Sunger et al., 2013, Yousaf et al., 2013). The physical consequences of chronic cough can include: syncope, vomiting, chest pains, hoarse voice, headache, incontinence, hernia, sleep deprivation, and lethargy (Brignall et al., 2008). The psychosocial impact of chronic cough on patients can sometimes be overlooked by physicians, however it is no less significant (French et al., 1998), with patients reporting relationship tensions, interrupted meals and telephone calls, and interference with work. Patients also often describe avoiding public spaces or social events; the onset of the COVID-19 pandemic has no doubt led chronic cough sufferers to become even more fearful of attending such places. Together these social impacts of the disease can cause deep frustration and embarrassment for patients, as well as depression and anxiety (Brignall et al., 2008).

There still remain no licensed treatments for chronic cough, treatments thus far instead have focused on acid suppression with proton pump inhibitors (PPIs), in case the underlying cause of cough is GERD-related. However, even in patients that are responsive to PPIs, they are largely ineffective in suppressing cough (Chang et al., 2011, Kahrilas et al., 2013). Failing this, centrally acting opiates like morphine sulphate could be administered, or gabapentinoids, however the clinical benefit of these medications for chronic cough patients is often limited and the adverse effects (*e.g.* constipation and suicidal thoughts, respectively) can be severe (Belvisi and Geppetti, 2004, Smith

and Woodcock, 2016). Unlike the pharmacotherapies above, there is also promising, albeit limited evidence that speech pathology management can reduce cough severity and improve patient quality of life; this was in the form of a treatment programme which consisted of 1) education, 2) strategies to reduce cough and laryngeal irritation and 3) psycho-educational counselling (Vertigan et al., 2006).

The most promise in terms of treatment for chronic cough patients currently lies with P2X3 antagonists *e.g.* Gefapixant, a P2X3 antagonist that was associated with a 75% reduction in objective cough frequency for chronic cough patients in a phase 2 clinical trial (Abdulqawi et al., 2015). This therapy is due to be filed soon by its developers, Merck & Co, with the world's medicine authorisation bodies following Phase 3 randomised clinical trials, this is, however, despite the drug reducing cough by a lesser extent (18.5% in one trial and 14.6% the another) compared to phase 2 trials; and between 15 and 20% of patients discontinuing the phase 3 trials due to taste-related adverse events (McGarvey et al., 2020, Merck, 2020).

There still remains a clinically unmet need for effective antitussive medications that lack dangerous or troublesome adverse effects.

#### 1.3.4 Cough in IPF

IPF affects patient wellbeing in a number of distressing ways besides the immediate symptoms of the disease, through worries about employment and finances, dependence on family and friends, sexual relations, social participation, mental and spiritual wellbeing, all of which can lead to sleep deprivation, exhaustion, anxiety and depression (Tzouveleakis et al., 2020, Swigris et al., 2005, Lee et al., 2017).

One of the most distressing and disabling symptoms of IPF is the chronic cough that frequently accompanies the disease, which is reported to affect between 73 and 86% of patients (Crystal et al., 1976, Turner-Warwick et al., 1980, Key et al., 2010). It is also often the first symptom to arise in patients and can sometimes precede the onset dyspnoea on exertion by several years (Vigeland et al., 2017).

In a survey conducted by Swigris et al. (2005) with 20 IPF patients to discuss how the disease affected their lives, participants described the cough as being “dry and non-productive”, “hacking” and “occurring when [they] talk for long periods”. Several participants also spoke of having a constant desire to cough but “never feeling relieved after [they] cough”.

The frequency of cough for IPF patients is higher than that seen in COPD and asthma patients, and rivals that of patients with chronic idiopathic cough, as Key et al. (2010) discovered when they

conducted the first study to objectively quantify IPF cough frequency (Figure 1-5). They found that patients coughed a median of 9.4 coughs per hour and that cough rate was much higher during daytime than at night-time (median of 14.6 vs 1.9, respectively), with patients rarely being awoken from their sleep to cough.

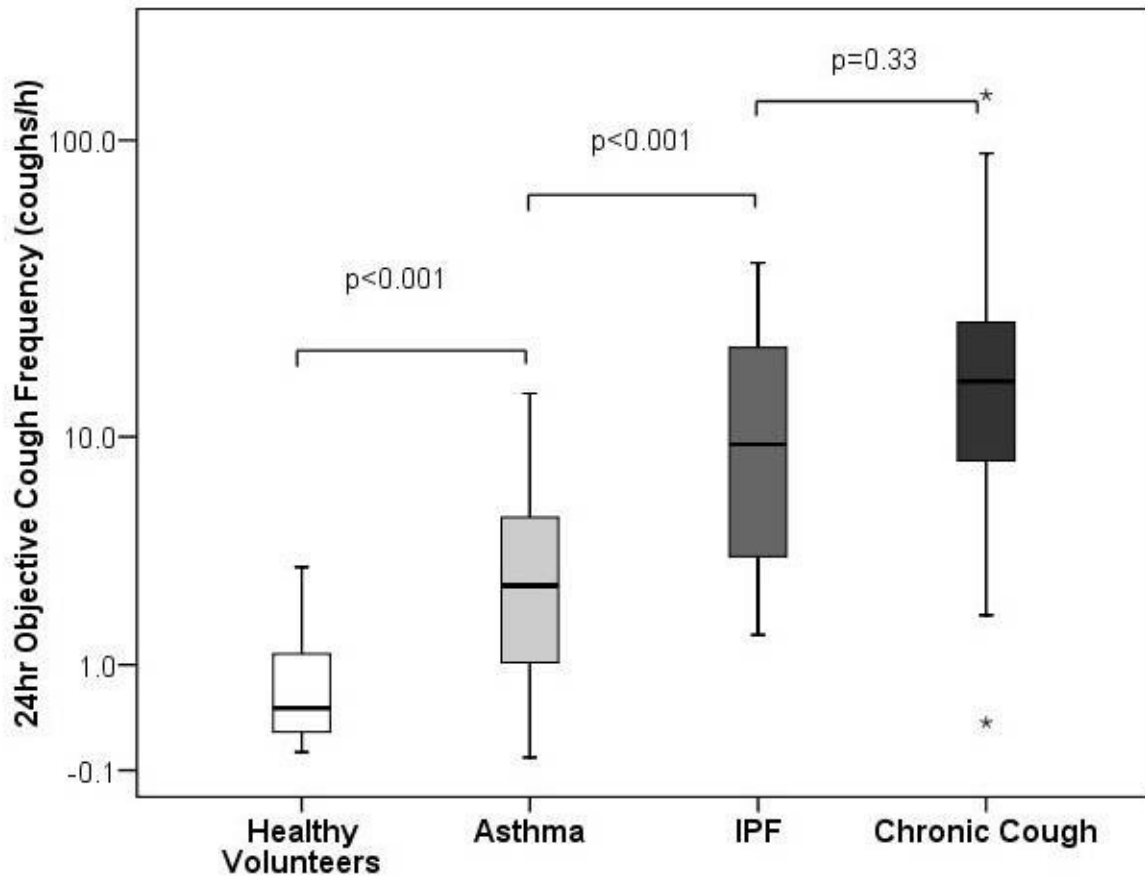


Figure 1-5 Comparison between cough frequency in IPF and other lung diseases

A comparison of median objective cough frequencies (coughs per hour) between healthy volunteers, asthma patients, IPF patients and chronic cough patients. Adapted from Key et al. (2010)

Cough in IPF patients can be exacerbated by various protussive comorbidities, such as post-nasal drip and GERD, yet despite this, it has still proven largely refractory to treatment, even when targeting these illnesses (Kilduff et al., 2014, Madison and Irwin, 2005).

Importantly, there is some evidence that cough is an independent predictor of disease prognosis in IPF patients. In a longitudinal study by Ryerson et al. (2011) that recruited 242 IPF patients, participants that reported coughing were more likely to have a lower forced vital capacity (FVC) and more likely to exhibit blood oxygen desaturation upon exertion. Using multivariate analysis, the authors also found that self-reported cough predicted disease progression, which the authors

defined as a “10% decline in FVC, 15% decline in DLCO, lung transplantation or death within 6 months of clinic visit”.

Standard antitussive medications provide no respite for the IPF sufferer, and often come with unwanted side-effects, such as respiratory depression in the case of opioids (Belvisi and Geppetti, 2004). There is no evidence to suggest that Nintedanib, one of the gold-standard IPF treatments used to slow disease progression, can reduce objective cough frequency in patients; there is limited evidence, however, that Pirfenidone can (Azuma et al., 2011, van Manen et al., 2017). The objective cough monitoring study with Pirfenidone should be interpreted somewhat cautiously though, firstly, due to it lacking any placebo control, and secondly, because it was conducted with a cough monitor that lacked FDA approval or CE marking (Azuma et al., 2011, van Manen et al., 2017). Objective cough frequency has recently been measured in a randomised controlled pilot study of IPF patients taking either placebo or the PPI omeprazole, where the drug showed an encouraging reduction (adjusted for baseline) of 39.1% (Dutta et al., 2019); this indicates the role GERD might play in some IPF patients’ chronic cough and highlights a possible mechanistic difference between chronic idiopathic cough.

### 1.3.5 Introduction to airway sensory nerves

Before delving into the different mechanisms that have been proposed as the aetiology for IPF-associated chronic cough, it is first necessary to explore the neurophysiology behind the cough reflex.

The sensory nerves that innervate the airways are capable of detecting physical and chemical changes to their environment and relaying this information to the central nervous system (CNS), this is then followed by reflex responses *e.g.* cough, bronchospasm and mucus hypersecretion (Belvisi, 2002, Brouns et al., 2012). *In vivo* and *in vitro* studies have elucidated that it is nerve fibres within the vagus nerve (the 10<sup>th</sup> cranial nerve) that carry the afferent limb of the cough reflex arc (Canning, 2006). Airway vagal afferent nerve fibres terminate peripherally in or just below the epithelium, and terminate centrally at the Nucleus Tractus Solitarius (NTS) in the brainstem (Belvisi, 2002). The cell bodies that these nerve fibres project from are found within the jugular or nodose ganglia, which are located beneath the ear bone. Airway sensory afferents can have different neurosensory properties (as will be detailed later) depending on which ganglion they emanate from. This is because the jugular and nodose ganglia have different embryological origins, with the former deriving from the neural crest and the latter from the epibranchial placode (Nasra and Belvisi, 2009). The vagus nerve runs parallel to the common carotid artery and internal jugular vein due to it also being housed within the carotid sheath. The nerve also gives rise to several branches including the superior

laryngeal nerve (SLN) and the recurrent laryngeal nerves which innervate the trachea and bronchi (Belvisi, 2003, Canning et al., 2004).

The reflex arc of cough is formed of three phases: in the first phase, endogenous or exogenous stimuli (*e.g.* the prostaglandin PGE<sub>2</sub> or aspirated food, respectively) activate airway sensory nerves and initiate an impulse; the second phase takes place in the CNS, which receives the nerve impulse and processes it through a complex neural network; and finally, the third phase utilises the efferent motor nerves which signal the effector muscles to contract (*e.g.* the abdominal muscles) (Pacheco, 2014).

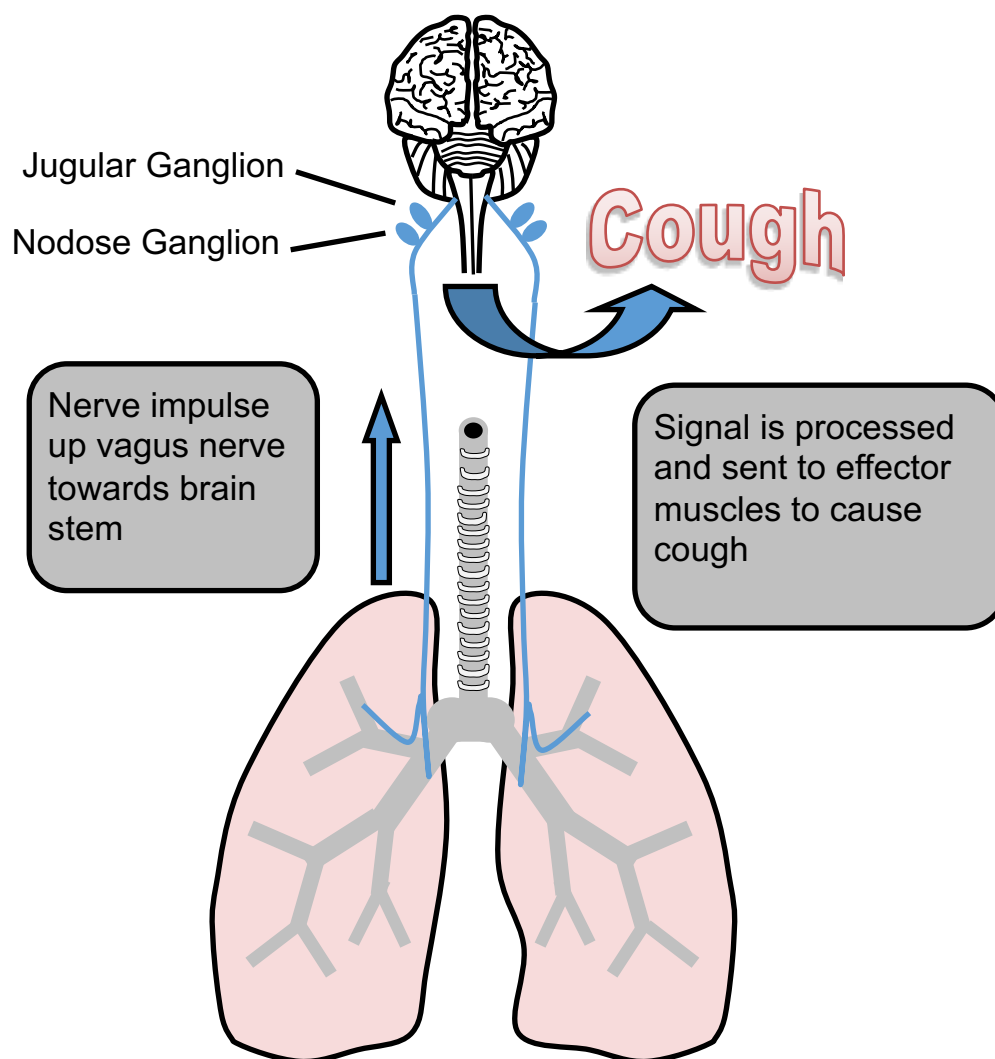


Figure 1-6 The cough reflex

*A schematic to illustrate the propagation of vagal nerve impulses that form the afferent arm of the cough reflex. Endogenous or environmental stimuli, such as PGE<sub>2</sub> or smoke, respectively, activate the airway sensory nerve termini. An action potential is carried up the vagus nerve, towards the central nervous system, and passes the cell bodies of the jugular or nodose ganglia, after which the signal terminates at the Nucleus Tractus Solitarius (NTS) within the brainstem. Once there the signal is processed and relayed to the effector muscles such as those in the abdominal wall and larynx to cause a cough. Original figure by author.*



The receptors present on an airway sensory nerve's surface can be activated by a multitude of different stimuli, including: mechanical irritation, inflammatory mediators and environmental stimuli; as well as changes in pH, temperature or osmolarity (Belvisi et al., 2011, Canning et al., 2006, Grace et al., 2012, Koskela et al., 2005, Lowry et al., 1988, Maher et al., 2009, McGarvey et al., 1998, Udem et al., 2004, Wong et al., 1999). When a sensory receptor is activated by one of the aforementioned stimuli, it causes an inward flow of current that depolarises the neuron, which if of sufficient magnitude (*i.e.* the threshold potential) triggers an action potential (Brouns et al., 2012). Action potentials occur when the membrane potential of a specific location along the neuronal axon rapidly rises and falls, this depolarisation causes adjacent locations along the axon to also depolarise. This nerve impulse propagates itself along the length of the axon without decrement.

Action potentials require the use of voltage gated sodium channels (VGSCs) which are embedded in the neuron's plasma membrane (Barnett and Larkman, 2007). The normal resting potential of a cell membrane sits at -70mV, but if an influx of Na<sup>+</sup> ions from a generator potential reaches the threshold potential (a value typically between -50 and -55mV, depending on several factors), this triggers the VGSCs to rapidly open, thereby allowing an influx of positively charged Na<sup>+</sup> ions, which further increases the membrane potential towards zero, and triggers more neighbouring VGSCs to open, and so on. This nerve impulse is propagated along the axon to the neuronal terminal at the CNS.

The opening of the VGSCs is followed by the opening of potassium ion channels, which allow for the exit of potassium ions from the cell. When the peak of the action potential is reached, the VGSCs close, but potassium continues to leave the cell. This efflux of potassium decreases the membrane potential and allows for repolarisation of the membrane. Importantly, action potentials remain the same size and magnitude as they propagate along the neuron, however, the frequency (firing rate) at which a neuron elicits these action potentials can greatly vary. The afferent pathway of the cough reflex requires a sustained high frequency of action potentials for initiation (Canning and Mori, 2011), which leads to the urge to cough that we are all familiar with.

Much is still unknown about how the brain processes the cough reflex (Fong et al., 2004). *In vivo* experiments measuring markers of neuronal activation (*e.g.* c-fos) following exposure to airway irritants; and functional brain imaging studies in which the regional brain responses of human subjects were monitored during exposure to airway irritants and coughing; have shown that cough neural pathways form a widely distributed and complex network within the brain, utilising many different regions (Figure 1-8) (Canning and Mori, 2010, Davenport and Vovk, 2009, Gestreau et al., 1997, Jakus et al., 2008, Poliacek et al., 2007). It is made more complicated still, by the

phenomenology of cough (Figure 1-7), as cough is a pulmonary event that can be voluntarily or involuntarily executed, and also one that can sometimes be suppressed when there is an 'urge to cough' (Ando et al., 2014). Processing of the basic, involuntary cough reflex only requires brainstem circuitry: the NTS and the pontomedullary respiratory central pattern generator (CPG), which is converted to that of a cough motor pattern (Mazzone et al., 2011). Neural processing of the urge to cough, voluntary coughing or inhibiting cough requires higher order (suprapontine) neural networks within the cerebral cortex (Pacheco, 2014). As mentioned previously, IPF patients cough far less during night-time, especially when they are asleep, thereby alluding to the influence cortical suppression plays on IPF associated cough (van Manen et al., 2016).

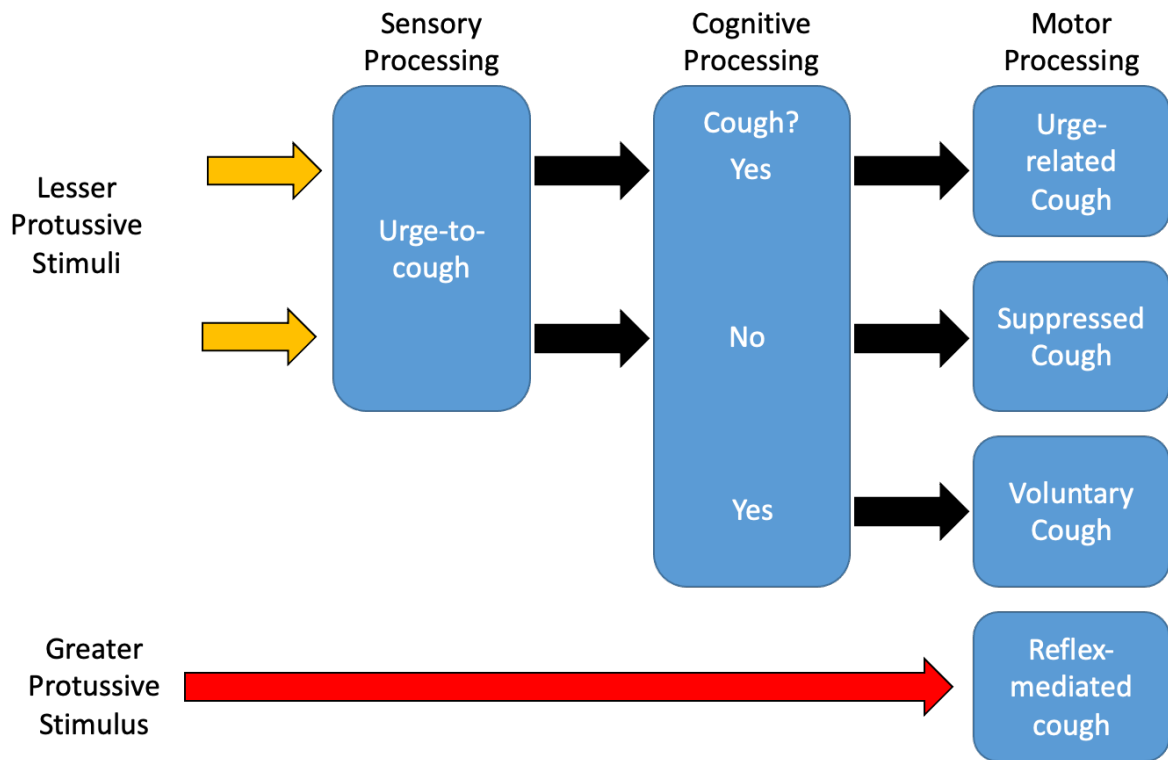
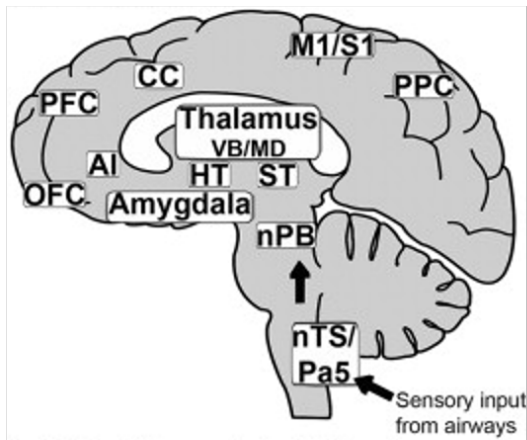


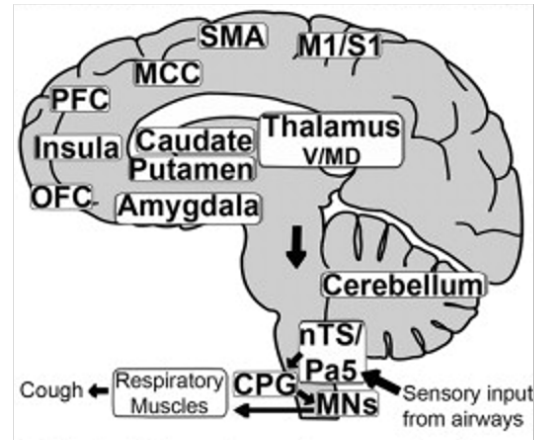
Figure 1-7 The phenomenology of cough

A schematic to represent the complex phenomenology of cough based on the model put forward by Ando et al. (2014). The model proposed is one that is based on evidence supporting a role for sensory, cognitive (behavioural) and motor processing steps in the brain which regulate coughing. Cough motor output could be down to 1 of 4 scenarios shown: 1) airway irritation results in an urge to cough which is followed through, 2) airway irritation results in an urge to cough but the cough is suppressed, 3) an individual chooses to cough in the absence of any urge to cough, and finally 4) the irritancy of the stimulus is so great as to bypass any need for sensory or cognitive processing, and thereby immediately elicits an involuntary reflex-mediated cough. Original figure by author.

### A) Airway sensory processing



### B) Reflex, urge and voluntary cough



### C) Inhibition of cough

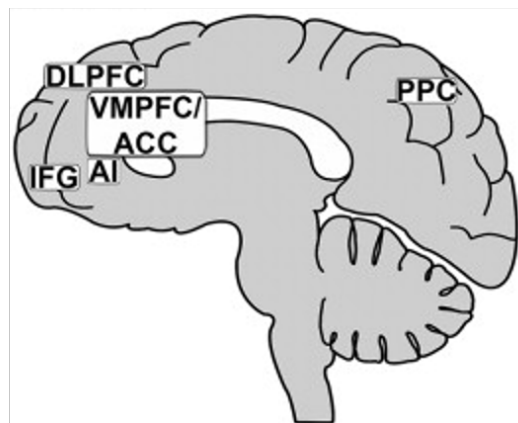


Figure 1-8 Brain regions involved in cough-related neural processing

A diagram to depict the brain regions involved in: (A) the processing of airway sensory inputs, (B) reflex-mediated, urge-related and voluntary coughing, and (C) the inhibition of cough from the urge-to-cough. Adapted from Ando et al. (2014).

All regions labelled have either been identified in animal models or human functional brain imaging studies.

Abbreviations (from brainstem to cortex): Nucleus Tractus Solitarius (NTS), paratrigeminal nucleus (Pa5), respiratory central pattern generator (CPG), respiratory motor neurons (MNs), parabrachial nucleus (nPB), hypothalamus (HT), subthalamic nuclei (ST), ventrobasal (VB) thalamus, mediodorsal (MD) thalamus, ventral (V) thalamus, dorsomedial (DM) thalamus, orbitofrontal cortex (OFC), anterior insula (AI), cingulate cortex (CC), mid-cingulate cortex (MCC), prefrontal cortex (PFC), sensorimotor cortex (M1/S1), posterior parietal cortex (PPC), supplementary motor area (SMA), inferior frontal gyrus (IFG), ventromedial prefrontal/anterior cingulate cortices (VMPFC/ACC) and dorsolateral prefrontal cortex (DLPFC).

Following CNS processing, comes the efferent limb of the reflex where the signal is finally sent to the inspiratory and expiratory motor neurons, via respiratory bulbospinal pre-motor neurons (I-augmenting and E-augmenting). This causes a large contraction of the abdominal and laryngeal muscles, and a powerful expulsion of air (Bongianni et al., 1998, Haji et al., 2008).

### 1.3.6 Sensory nerve subtypes

Before outlining the nerve fibres involved in the afferent limb of the cough reflex, it would be prudent to briefly explore the way all nerve fibres in the human body can be classified. The nerve fibres in the human body can be generally classified into three classes according to the system developed by Erlanger and Gasser: group A nerve fibres, B nerve fibres and C nerve fibres. Group A are heavily myelinated and therefore conduct the fastest, group B are moderately myelinated, and group C are unmyelinated, thereby giving them the slowest conduction velocity (Paintal, 1973, Gasser, 1941). The A group nerve fibres can be further divided into other subclasses according to the amount of myelination they have and their axon thickness: alpha ( $\alpha$ ), beta ( $\beta$ ), gamma ( $\gamma$ ), and delta ( $\delta$ ). A $\delta$ -fibres, which are highly involved in airway sensory innervation, have the thinnest myelin sheath and therefore have the slowest conduction velocity of the group A nerve fibres (3-30 metres per second); this is still faster however than the unmyelinated C fibres (0.5—2.0 metres per second), which are another group of nerve fibres heavily involved in airway sensing.

As discussed previously, airway sensory nerves can be activated by a wide range of different stimuli (Brouns et al., 2012), they can also be broadly categorised into either a mechanosensitive phenotype, or a chemosensitive phenotype; with the former responding to mechanical punctate stimuli (*e.g.* inhaled large particles), and the latter responding to exogenous chemical irritants and also endogenous inflammatory mediators (*e.g.* cigarette smoke or bradykinin, respectively) (Poliacek, 2020).

Most of the innervation of the airways is provided by the vagus nerve, however a subset of airway afferent nerves also originate from the dorsal root ganglion of the spinal cord as part of the sympathetic nervous system; it is unknown how involved these latter nerves are with airway reflexes (Undem et al., 1999).

It is generally believed that the vagal afferents innervating the airways can be divided into four types according to characteristics like their conduction velocity, thickness, adaptation index, whether they are myelinated or not, their physiochemical sensitivity and their embryological origin (Canning, 2006). It is important to note that the bulk of the experimental findings that led to these categorisations are derived from animal studies, so these categories may not necessarily be the same for humans. The mechanosensitive fibres are: the rapidly adapting receptors, and the slowly

adapting stretch receptors; both of which are A $\delta$ -fibres. The other two of the four nerve fibres, which are more chemosensitive, are C-fibres (which can be further divided according to whether they derive from the nodose or jugular ganglion) and A $\delta$ -nociceptors.

#### 1.3.6.1 *Rapidly Adapting Receptors*

Rapidly adapting receptors (RARs) are named because of their rapid adaptation *i.e.* they quickly cease firing following a maintained mechanical stimulus (Sant'Ambrogio and Widdicombe, 2001). Due to their myelination and relatively fast conduction velocity (>3 m/s) (Canning, 2006), they are classed as an A $\delta$ -fibre. They are sometimes referred to as irritant receptors, classical RARs or more simply as just A $\delta$ -fibres (Adcock et al., 2014, Adcock et al., 2003). These fibres innervate the airways throughout the respiratory tract, from the nose to the bronchi, although they are mostly present in the larger airways (Sant'Ambrogio and Widdicombe, 2001). RARs are polymodal as they are thought to respond to mechanical stimuli such as light touch and lung hyperinflation or deflation, and also chemical irritants such as citric acid (Adcock et al., 2003, Canning et al., 2006, Mortola et al., 1975, Riccio et al., 1996a, Sant'Ambrogio et al., 1978, Sant'Ambrogio and Widdicombe, 2001). It was originally thought that RARs were not activated by capsaicin or the endogenous inflammatory mediator bradykinin, but that they could however be indirectly activated by these stimuli from the subsequent mucus production and bronchoconstriction that comes as a result to their exposure (Widdicombe, 2003). Contrary to this, more recent evidence has shown that some RAR A $\delta$ -fibres can be activated by capsaicin (Adcock et al., 2014). RARs are thought to mostly project from the nodose ganglia and interestingly, have also been found to be capable of triggering the cough reflex in anaesthetised animals, further solidifying the theory that they play a crucial defensive role in clearing the lungs from foreign objects (Canning, 2006, Dicipinigaitis et al., 2014, Nasra and Belvisi, 2009, Riccio et al., 1996a).

#### 1.3.6.2 *Slowly Adapting Receptors*

Similar to RARs, slowly adapting receptors (SARs) are also fast conducting A $\delta$ -fibres, due to them being myelinated, and having conduction velocities of approximately 18 m/s (Canning et al., 2006). Their naming is due to them having a relatively slower adaptation to a maintained stimulus when compared to RARs. Unlike RARs, SARs are not thought to be involved in cough. Instead, SARs are thought to be involved with autonomic functions like tidal breathing (Schelegle and Green, 2001). They are of particular importance to the Hering-Breuer reflex, which is a reflex mechanism that has evolved to respond to and inhibit excessive stretching of the lung during inspiration, thereby preventing over-inflation. The nerve endings of SARs can be found within the smooth muscle of the airways (Bartlett et al., 1976).

#### 1.3.6.3 *A $\delta$ nociceptors*

A $\delta$  nociceptors are a subpopulation of nerve fibres that derive from the jugular ganglia and innervate the airways; their role in cough has not yet been fully determined (Canning et al., 2006, Riccio et al., 1996a). Despite being an A $\delta$ -fibre with a conduction velocity between 4-6m/s, A $\delta$  nociceptors are more pharmacologically similar to C-fibres. A $\delta$  nociceptors are sensitive to capsaicin and PGE<sub>2</sub>, due to their expression of TRPV1, and are less mechanosensitive than the other airway terminating A $\delta$ -fibres like RARs (Kajekar et al., 1999, Riccio et al., 1996a, Yu et al., 2005).

#### 1.3.6.4 *C-fibres*

C-fibres form the majority of the afferent nerve fibres that innervate the airways (Coleridge and Coleridge, 1984, Lee and Pisarri, 2001). These fibres have conduction velocities that are slower than A $\delta$ -fibres (0.5-2 m/s), due to their lack of myelination. C-fibres innervate the epithelium of the airways throughout the respiratory tract and can originate from both the jugular ganglia and nodose ganglia (Canning et al., 2006, Fox et al., 1993, Mazzone, 2004, Riccio et al., 1996a). Unlike RARs, stimulating C-fibres in anaesthetised guinea pigs does not trigger coughing, which could be interpreted that it is C-fibres that elicit the urge to cough (Mazzone, 2004).

C-fibres can be activated by a wide range of chemical stimuli due to their expression of members of the TRP family of ion channels. Bronchopulmonary C-fibres express TRPV1 and TRPA1, thereby enabling them to be activated by environmental tussive agents like capsaicin and allyl isothiocyanate, respectively, which elicits coughing; C-fibres can also be activated by endogenous inflammatory mediators like PGE<sub>2</sub> and bradykinin (Adcock et al., 2014, Birrell et al., 2009, Canning et al., 2004, Coleridge and Coleridge, 1984, Dicipinigitis and Alva, 2005, Dicipinigitis et al., 2014, Grace et al., 2012, Lalloo et al., 1995).

A key mechanism that sets C-fibres apart from RARs, is their ability to release neuropeptides like substance P from peripheral nerves lining the lungs via an axon reflex (Mazzone et al., 2003), these neuropeptides go on to then trigger local reflex responses like mucus secretion and bronchoconstriction; although this has only so far found to be the case in guinea pig and mouse airways, and has yet to be confirmed in humans. Some animal studies have also found Substance P to have a sensitising role in cough (Kohrogi et al., 1988, Moreaux et al., 2000). Interestingly, there is some evidence that Substance P is more highly present in higher concentration within IPF BAL and the plasma and sputum of patients with chronic cough (Takeyama et al., 1996, Otsuka et al., 2011), which could suggest C-fibres in these airways are under sustained activation. Exposure to substance P has also been shown to elicit cough in patients with IPF but not in healthy control subjects (Hope-Gill et al., 2003).

C-fibres can also be separated broadly into those that innervate the extrapulmonary airways (bronchial C-fibres) and those that innervate the lower airways (pulmonary C-fibres). Unlike bronchial C-fibres, pulmonary C-fibres have been shown to inhibit cough *in vivo* (Chou et al., 2008, Tatar et al., 1994, Widdicombe and Undem, 2002). They also do not appear to express Substance P or Calcitonin gene-related peptide (another neuropeptide) (Carr and Undem, 2003, Coleridge and Coleridge, 1984, Undem et al., 2004). Conversely, bronchial C-fibres do express the aforementioned neuropeptides and are thought to be involved in cough, because of the location that they innervate; their cell bodies appear to be mostly housed in the jugular ganglia (Coleridge and Coleridge, 1984, Undem and Kollarik, 2002).

### 1.3.7 Previously proposed mechanisms for cough in IPF

There remains no clear explanation or consensus amongst pulmonologists as to the pathogenesis behind IPF-associated chronic cough, but various mechanisms have been proposed which fall broadly into either mechanical, biochemical or neurosensory changes (van Manen et al., 2016). Elucidating the mechanism is also made more difficult by the frequent and varying comorbidities that IPF patients have (*e.g.* GERD).

One explanation for the aetiology of cough in IPF patients is the architectural distortion that the disease inflicts upon the lungs (Harrison, 2004). Surgical lung biopsies from IPF patients often feature peribronchiolar fibrosis or peribronchial inflammation, with airways often appearing narrowed in some places, yet dilated in others (bronchiectasis) (Crystal et al., 1976). It is theorised that this distortion subjects RARs to mechanical stress in the small airways, thereby stimulating coughing. Whilst this hypothesis explains why cough is more severe for patients with fibrotic lung disease, it does not explain why cough is often the first symptom IPF patients present themselves with to a physician (Vigeland et al., 2017), which is presumably before much of this distortion has taken place.

There is evidence that IPF patients have a heightened cough reflex sensitivity to some airway irritants, with IPF patients coughing more in response to capsaicin than healthy control subjects (Doherty et al., 2000, Hope-Gill et al., 2003); as outlined in the previous section, capsaicin is a stimulant more associated with the activation of C-fibres than A $\delta$ -fibres (like RARs), although nociceptors can be sensitive to capsaicin too. These studies should also be accompanied by the caveat that they were performed before the current international guidelines for diagnosing IPF cough existed (Raghu et al., 2011, Raghu et al., 2018). Why this heightened sensitivity exists, assuming it still affects some of the IPF patient population is still unknown, with some suggesting it could be due to the mechanical distortion described above and others suggesting that it could be



because the nerves that inhibit the cough reflex (*e.g.* pulmonary C-fibres) might be destroyed as the fibrotic process occurs (Jones et al., 2011).

IPF patient airway sensory nerves also appear to be more sensitive to mechanical stimulation. A study performed by Jones et al. (2011) found that applying percussive stimulation to the chest wall induced coughing in 85% of IPF subjects, whereas it only produced coughing in 17% of the healthy non-smoking control subjects they tested. This group percussed the chest wall at three different locations (the posterior lung base, upper anterior chest and manubrium sternum) and at three different frequencies (20 Hz, 40 Hz and 60 Hz). It has been theorised that this could be why IPF patients describe suffering bouts of unstoppable coughing when talking for long periods of time (*e.g.* on the phone), as the vibrations from the vocal folds and coughing transmit themselves down to mechanosensitive nerves (*e.g.* RARs), thereby perpetuating a cycle of cough and vibration (van Manen et al., 2016, Harrison, 2013).

Another hypothesis for the aetiology of IPF-associated chronic cough is the elevated presence of the neurotrophins nerve growth factor (NGF) and brain-derived neurotrophic factor (BDNF), in IPF patient sputum, when compared to healthy controls (Hope-Gill et al., 2003). Furthermore, immunohistochemical studies suggest that the source of these neurotrophins could be the fibroblastic foci or indeed interstitial cells of the IPF lung (Ricci et al., 2007). Neurotrophins are a family of protein growth factors that induce the development, function and survival of neurons and they are also thought to increase capsaicin sensitivity, which would thereby enhance the cough reflex to that stimulus (Sahay et al., 2017, Doherty et al., 2000, Harrison, 2004, Hope-Gill et al., 2003).

## 1.4 Modelling cough and assessing antitussive therapies

### 1.4.1 Pre-clinical models of cough

Although the cough reflex has been investigated in other animals such as dogs, cats, rabbits, mice and rats (Gardiner and Browne, 1984, Hanacek et al., 1984, Kamei et al., 1993, Tatar et al., 1994), it is widely agreed that the guinea pig is the most relevant model species for investigations into cough, due to them having similar airway neural architecture and demonstrating a similar sensitivity to different tussive stimuli (Belvisi and Hele, 2003, Canning et al., 2006, Karlsson and Fuller, 1999). For instance: citric acid, PGE<sub>2</sub>, as well as agonists of TRPV1 (*e.g.* capsaicin and resiniferatoxin); and TRPA1 (*e.g.* acrolein and cinnamaldehyde); all cause cough in both guinea pigs and human subjects (Costello et al., 1985, Laloo et al., 1995, Laude et al., 1993, Maher et al., 2009, Birrell et al., 2009).

Besides one vagus nerve experiment using knockout mice tissue (transgenic guinea pigs are seldom used in scientific research), all the *in vivo* and *ex vivo* work presented in this thesis used the guinea

pig. Detailed descriptions for each of these methods can be found in the relevant parts of the Methodology section (Chapter 2) or in the case of calcium and oxidative stress imaging, Chapter 5. They are briefly described below:

#### 1.4.1.1 *Neural isolation for oxidative stress or calcium imaging*

Harvesting vagal (jugular and nodose) ganglionic neurons from guinea pigs (or other species) can be a useful technique for single cell gene expression studies and patch clamp recordings, as well as for experiments that measure changes in intracellular calcium concentrations or oxidative stress (Dubuis et al., 2013, Nassenstein et al., 2008, Zhou et al., 2010).

By surgically removing the vagal ganglia, one can then use a mixture of digestive enzymes and precise dissection to free the neuronal cell bodies from any connective tissue. It is further possible to identify which neurons within these ganglia terminate in the airways, this can be accomplished by identifying the neurons that have been stained with a retrograde tracer dye, so long as this was administered to the animal intranasally 14 days prior to the dissection (Dubuis et al., 2013).

By loading the neurons with a calcium specific dye (*e.g.* Fura-2 AM) or a superoxide probe (*e.g.* dihydroethidium), it is possible to measure changes in intracellular calcium (*i.e.* activation) and oxidative stress levels, respectively, that come as a result of the neurons being exposed to different stimuli (Bindokas et al., 1996, Dubuis et al., 2013).

#### 1.4.1.2 *Isolated vagus nerve model*

As with vagal ganglionic neurons, vagus nerves can also be isolated from laboratory rodents and even humans. These nerves can then be fed through a grease-gap recording system which electrochemically isolates one side of the nerve trunk from the other. By attaching both ends of the nerve to silver-chloride electrodes and suffusing the nerve with a buffer on one side and a buffer mixed with a tussive agent, an antitussive agent or both, on the other, it is possible to measure compound membrane depolarisation as a measure for activation (Bonvini et al., 2016, Grace et al., 2012, Birrell et al., 2009, Belvisi et al., 2017).

#### 1.4.1.3 *Electrophysiological tracheal recording*

Electrophysiological tracheal recording (eTRec) is a more complicated *ex vivo* technique developed recently in this group by Dr. Dubuis, it is capable of measuring compound action potentials (CAP) of airway sensory nerve endings within the recurrent laryngeal nerve (RLN). The protocol for this technique is similar to one developed by Riccio et al. (1996b), which requires dissecting out the trachea from an animal but leaving the connected nerves that innervate the trachea attached. The trachea is then placed into a bath, suffused with a buffer, and cannulated, thereby allowing the

trachea itself to be perfused with a separate buffered solution that may or may not contain tussive or antitussive stimuli. Two electrodes are then required to measure CAP, a reference electrode is placed within the bath and a separate, suction electrode engulfs the RLN. This technique has the advantage of being able to measure nerve activity that is the result of activation of receptors on the nerve termini, rather than receptors expressed on the neuronal axon like in the isolated vagus nerve model.

#### 1.4.1.4 *In vivo single fibre recordings*

Through *in vivo* electrophysiology, it is possible to measure the rate of action potential firing by single airway specific nerve fibres in response to different protussive and antitussive stimuli (Canning et al., 2004). Using the *in vivo* single fibre technique outlined elsewhere (Bonvini et al., 2016, Adcock et al., 2003), and in this thesis (Section 2.6), it is possible to identify different types of nerve fibres (*e.g.* C-fibres or A $\delta$ -fibres) within an anaesthetised and neuromuscularly blocked whole animal, before ascertaining whether that airway terminating nerve fibre is activated or inhibited by a particular pharmacological agonist or antagonist, respectively.

#### 1.4.1.5 *Guinea pig conscious cough model*

A commonly used *in vivo* technique for assessing the cough reflex, is the guinea pig conscious cough model (Lewis et al., 2007). This technique requires the use of aerosolised cough challenge agents (*e.g.* citric acid or capsaicin), much like in the clinical cough challenge test. Guinea pigs are placed without restraint, into Perspex chambers and exposed to nebulised tussive agents, having often been treated prior with a pharmacological compound that is under investigation. This technique is useful due to guinea pigs having similar tussive responses to humans, but it is important to note that a compound that appears to inhibit a cough in a tussive challenge may not necessarily alleviate spontaneous coughing in chronic cough patients (Belvisi et al., 2017).

As mentioned before, no study has yet investigated whether guinea pigs with bleomycin-induced pulmonary fibrosis cough spontaneously like IPF patients, however two studies have assessed cough reflex sensitivity in these animals: Fernandez-Blanco et al. (2015) conducted a cough challenge with nebulised citric acid, capsaicin and allylisothiocyanate; whilst Guo et al. (2019) exposed them only to capsaicin. Both of these studies determined that pulmonary fibrotic guinea pigs had an exaggerated cough response to these stimuli when compared to non-fibrotic controls, with the former study emphasising the higher concentrations of neurotrophins in BAL as playing a role in this response and the latter study pointing to the enhanced expression of TRPV1 and TRPA1 ion channels in lung tissue.

## 1.4.2 Clinical assessment of cough

There exist a variety of different tools to assess cough clinically that can be broadly categorised into whether they are subjective or objective measures of cough. These tools can measure different aspects of the symptom and although most of these tools have been validated in chronic cough patients, experience and validation of these tools in IPF-related cough is limited (van Manen et al., 2016).

### 1.4.2.1 Subjective methods

Subjective measures of cough usually take the form of questionnaires, but visual assessment scales also exist.

The cough quality-of-life questionnaire contains 28 questions about cough and its effects on the patient, it has six domains: physical complaints, psychosocial issues, functional abilities, emotional well-being, extreme physical complaints, and personal safety fears (Lechtzin et al., 2013). The cough quality-of-life questionnaire is a comprehensive instrument for assessing chronic cough which has been validated for use in IPF patients.

Other subjective measures of cough are the Leicester Cough Questionnaire (LCQ) and the Visual Analogue Scale (VAS), both of which have been assessed in IPF and found to have good correlation with objective cough counts (Key et al., 2010, Jones et al., 2011). The LCQ is a 19-item self-administered questionnaire divided into three domains which assess the social, psychological and physical impact cough has on the patient (Birring et al., 2003). Unlike with the other subjective scoring systems, a lower LCQ score indicates a more severe cough.

Contrary to the other two subjective cough scoring measures that ask questions of the patient, the VAS instead requires the patient to mark a position between two end-points along a continuous line, with one end representing 0 (no cough) and the other end representing 100 (“the worst cough ever”) (Eccles et al., 1992).

### 1.4.2.2 Objective methods

One method of assessing cough in patients with chronic cough, is by conducting a cough challenge to test their cough reflex sensitivity. As with the pre-clinical method described above (1.4.1.5), this technique requires having the subject inhale nebulised tussive agents, which in the clinical case are most commonly citric acid or capsaicin (Morice et al., 2001). Helpfully, a standardised methodology was published by the European Respiratory Society so as to enable universal interpretation and comparison between different clinics (Morice et al., 2007). Cough challenge involves the subject

inhaling incrementally increasing doses of tussive agents. It is recommended that for each test, the concentrations of the tussive agent that produce 2 coughs ( $C_2$ ) and 5 coughs ( $C_5$ ) are recorded.

An advantage of this technique is that it has enabled clinicians to be able to examine how cough sensitivities vary among different respiratory diseases. One disadvantage, however, is that cough reflex sensitivity in patients with chronic cough and other respiratory conditions only weakly correlates with objective cough counts (Smith et al., 2006a, Birring et al., 2006, Decalmer et al., 2007), to our knowledge the correlation between objective cough counts and IPF patient cough sensitivity has not yet been evaluated. As a solution to this problem, it has been suggested that generating a non-linear dose response curve and quantifying the pharmacological metrics of  $E_{max}$  and  $ED_{50}$ , rather than  $C_2$  and  $C_5$ , could help distinguish different disease types from healthy controls and could enable better correlation with objective cough counts (Hilton et al., 2013, Smith et al., 2012).

Another disadvantage as mentioned previously and detailed more later, is that the success of a compound in inhibiting challenge-evoked cough does not necessarily ensure that it will inhibit spontaneous chronic cough (Belvisi et al., 2017).

Another objective method of assessing cough is ambulatory cough monitoring. This method requires the use of microphones and recording devices to facilitate the counting of cough frequencies. Objective cough frequency has now become the gold standard primary endpoint for assessing the efficacy of novel treatments for chronic cough (Hall et al., 2020), it has also been used to assess the infectiousness of tuberculosis and monitor the onset of exacerbations in COPD patients (Turner et al., 2018, Windmon et al., 2019).

A variety of different cough monitors have been trialled over the course of the last two decades that have achieved varying levels of success, whilst utilising a range of different quantification methods and technologies *e.g.* The Lifeshirt<sup>®</sup>, the Hull Automatic Cough Counter, Cayetano Cough Monitor and the Pulmotrack-CC<sup>™</sup> (Barry et al., 2006, Larson et al., 2012, Vigel et al., 2010, Coyle et al., 2005). Only two systems, however, have been widely adopted for use in cough research, they are the Leicester Cough Monitor (LCM) and the VitaloJAK<sup>™</sup> (Smith and Woodcock, 2008).

The LCM has been used to assess cough in patients suffering from: bronchiectasis, sarcoidosis and COPD (Cho et al., 2020, Spinou et al., 2017, Turner et al., 2018); it has also been used in clinical trials to assess medications in chronic cough patients (Ryan et al., 2012, Yousaf et al., 2010); and pertinent to this thesis, it was also used in the assessment of inhaled sodium cromoglycate for IPF patients (Birring et al., 2017)(discussed in Section 5.4). The monitor comprises a portable digital recording

device and a lapel microphone, the recorded audio data is analysed using an automated algorithm that detects coughs sounds and rejects other noises (Birring et al., 2008). Operator input is only required to calibrate the recording and takes approximately 5 minutes per 24-hour recording.

VitaloJAK™ analysis on the other hand is a semi-automated system, whereby an algorithm truncates a 24-hour audio recording by removing periods without sound (Barton et al., 2012). An experienced operator then listens back to a 1.5 hour condensed version of the original 24-hour recording.

VitaloJAK™ requires the use of a custom-designed recording device connected to two microphones, one lapel microphone, and one contact microphone attached to the subject's sternum. This design helps the observers eliminate background noise and discount coughs that might occur from other individuals. The VitaloJAK™ system has been used across a number of clinical studies that assessed cough in different respiratory diseases including: IPF, chronic cough, COPD, asthma and cystic fibrosis (Key et al., 2010, Marsden et al., 2016, Smith et al., 2006a, Smith et al., 2010, Smith et al., 2006c). The cough monitor was also used in randomised placebo controlled clinical trials in chronic cough patients like that of the P2X3 antagonist Gefapixant as well as the TRPV4 antagonist GSK2798745 (Abdulqawi et al., 2015, ClinicalTrials.gov, 2017, Smith et al., 2020b).

Both the VitaloJAK™ and the LCM are accurate tools with reported sensitivities of 99.92% and 91%, respectively (Hall et al., 2020); only the VitaloJAK™, however, currently has FDA approval and CE marking (Smith and Badri, 2019).

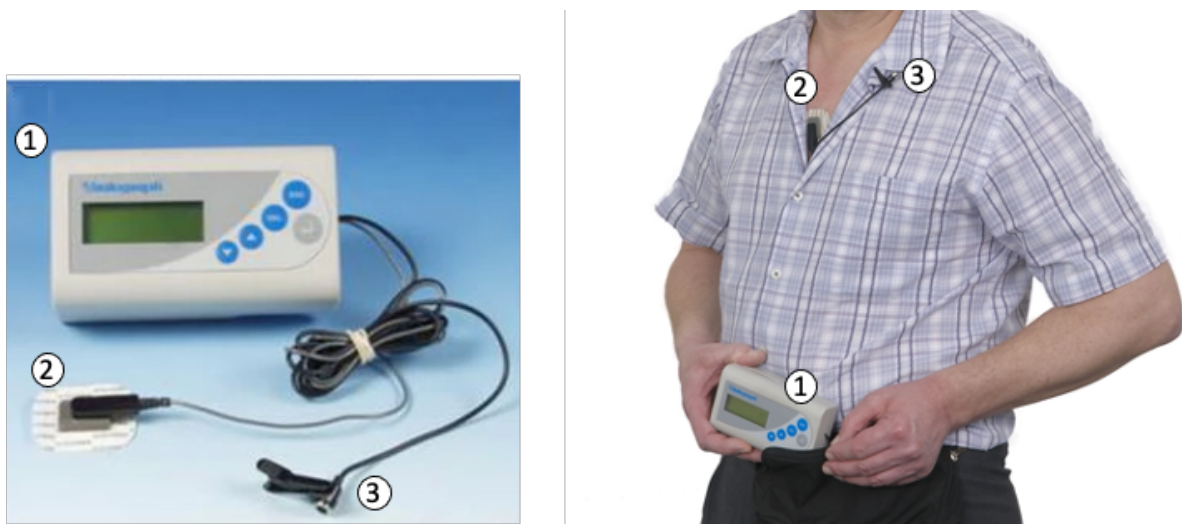


Figure 1-9 The VitaloJAK™ cough monitor

Labelled photographs of the VitaloJAK™, one of the most widely used 24-hour ambulatory cough monitors. **Left** – A VitaloJAK™ on display, and **Right** – a VitaloJAK™ whilst being worn. **1** – the VitaloJAK™'s digital recording device, **2** – The contact microphone that is adhered to the subject's sternum, and **3** – the lapel microphone, used to help differentiate sounds emanating from the subject and those emanating from the subject's environment. **Left** image adapted from Smith and Woodcock (2008) **Right** image adapted from Peake (2020)

## 1.5 Ion channels and receptors implicated or hypothesised to be involved in cough or IPF

This thesis will explore whether the purinergic receptor P2X3, or the Transient Receptor Potential (TRP) ion channels TRPV4 and TRPA1, could be involved with IPF-associated chronic cough. Transient Receptor Potential (TRP) channels have a well-established role in facilitating cough, with multiple studies proving that agonists for members of the ankyrin (TRPA) and vanilloid (TRPV) subfamilies elicit the reflex *e.g.* capsaicin and acrolein acting on TRPV1 and TRPA1, respectively (Birrell et al., 2009, Forsberg and Karlsson, 1986). TRPV4 and P2X3 have previously been linked together in a tussigenic signalling pathway: the TRPV4-ATP-P2X3 axis (Bonvini et al., 2016). Whether this pathway is active or not in IPF-associated cough or indeed chronic idiopathic cough, remains to be determined. Supposing that this mechanism could be involved in IPF cough, this thesis will also investigate whether PAR2, the G-protein coupled receptor, could be an upstream activator of this pathway. These receptors of interest are described in more detail in their relevant results chapters, however a brief description and summary of their involvement in cough or IPF can be found below.

### 1.5.1 P2X3

P2X3 is one member of the P2X purinoreceptor family. This group of cation-permeable ligand-gated ion channels open upon the binding of ATP, the molecule famous for being the molecular currency of energy transfer in all known forms of life. ATP, however, is also involved in the activation and regulation of sensory nerve excitability, with ATP triggering painful sensations in somatic tissues when administered exogenously, and visceral reflexes when delivered systemically or administered onto the mucosa of the bladder or airways (Basoglu et al., 2015, Basoglu et al., 2005, Haskell et al., 1996, Lee et al., 2012, Morice et al., 2019, Dicipinigaitis et al., 2020). Responses like these are all mediated through P2X purinoreceptors, particularly P2X2 and P2X3, whose expression is enriched in sensory nerves deriving from the dorsal root ganglia, vagal sensory ganglia and trigeminal ganglia (Kwong et al., 2008, Surprenant and North, 2009). Extracellular ATP has been shown to be present at higher concentrations in the lungs of IPF patients, as well as those of individuals suffering from asthma and COPD (Idzko et al., 2007, Lommatzsch et al., 2010, Riteau et al., 2010).

As mentioned previously, the P2X3 pharmacological antagonists are currently the most promising antitussive medication currently in development (Dicipinigaitis et al., 2020). In a proof-of-concept phase 2a clinical trial, P2X3 antagonist Gefapixant reduced cough frequency in patients with chronic idiopathic cough by an unprecedented 75% compared to placebo, this was however invariably accompanied by significant taste disruption that led to 25% of subjects withdrawing from the study (Abdulqawi et al., 2015).

The P2X3 receptor itself exists primarily as trimeric homomers, however they can form heteromers whereby one P2X2 subunit is included in the trimer (Fabbretti and Nistri, 2012). There is hope that by producing pharmacological antagonists that are more selective for the P2X3 homotrimer, rather than the P2X2/3 heterotrimer, that this would yield an antitussive with fewer taste-related adverse effects (Garceau and Chauret, 2019). Indeed, BLU-5937, a compound developed by BELLUS Health with a high selectivity for the P2X3 homomer, was well tolerated by healthy subjects in a Phase 1 clinical trial, and further demonstrated an improved taste safety profile (Garceau et al., 2019). Following this, a Phase 2 trial with BLU-5937 was then attempted that enrolled a total of 68 chronic cough patients; this trial was terminated after only 52 subjects had completed treatment, due to logistical complications arising from the COVID-19 pandemic (ClinicalTrials.gov, 2019). The results of this trial have not yet been published in full, but the top-line data from the company's press release showed that the placebo-adjusted reduction in awake cough frequency was less than in Gefapixant's Phase 2a trial, and further, that none of these reductions were statistically significant (although this could well be due to the early termination of the trial) (Abdulqawi et al., 2015, Matthews, 2020).

Other P2X3 receptor antagonists also designed to be much more selective for the P2X3 homotrimer than the P2X2/3 heterotrimer, are undergoing similar clinical testing by other pharmaceutical companies. These include Shionogi's S-600918, and Bayer's BAY 1902607, and while both of these compounds can also reduce 24-hour cough counts, they only reduced cough rates by between 30 and 40%, with the latter compound still being accompanied by taste-related adverse effects in many patients (Friedrich et al., 2020, Niimi et al., 2019).

One could interpret these results to mean that both the P2X2/3 heterotrimer and the P2X3 homotrimer are involved in chronic cough, which is why Gefapixant, a compound that antagonises both P2X receptors at nanomolar potency (Richards et al., 2019), likely had the highest antitussive efficacy (75%) (Abdulqawi et al., 2015) in its phase 2a trial, when compared to the above rival compounds. For the sake of simplicity, we will continue to mostly only refer to P2X3 throughout this thesis, but please note that the P2X2/3 heterotrimer is likely to also be involved in any of the same experiments involving agonists or antagonists for the P2X3 receptor.

Gefapixant was trialled in IPF patients (discussed in more detail in Section 4.4), and although it reduced awake cough frequency in patients by 25%, these findings, albeit only very slightly, failed to reach clinical significance ( $p=0.07$ ) (Martinez et al., 2019). The authors put this failure to reach the prespecified primary objective of reduction in awake cough frequency in IPF patients down to a randomisation error and a change in dosing regimen that reduced the statistical power of the study;



they further claimed post-hoc and responder analyses suggested Gefapixant had a therapeutic benefit to patients and therefore necessitated further research.

### 1.5.2 TRPV4

Transient Receptor Potential Vanilloid 4 (TRPV4) is a polymodal, calcium permeable receptor that was originally identified as an osmotic stress sensor (Liedtke et al., 2000); it has since been shown to also be activated by mechanical stretch and moderate heat (>24–27 °C) (Watanabe et al., 2002, Gao et al., 2003, Suzuki et al., 2003). Like other TRPV channels, TRPV4 features a cytosolic N terminus with 6 ankyrin repeats, which are 33 amino acid long motifs that mediate protein-protein interactions (Denker and Barber, 2002, Sedgwick and Smerdon, 1999). TRPV4 is expressed by many cell types within the lung, these include smooth muscle cells, macrophages and epithelial cells (Hamanaka et al., 2010, Lorenzo et al., 2008).

TRPV4 can be activated by synthetic small molecule ligands like GSK1016790a (GSK101) as well as phorbol esters (*e.g.* 4 $\alpha$ -phorbol 12,13-didecanoate) (Bonvini et al., 2016).

Importantly, it was discovered that exposure to TRPV4 agonists was capable of eliciting cough in guinea pigs (Bonvini et al., 2016). Further, this tussive response was shown to be mediated through P2X3 (and P2X2/3), as AF-353 (an antagonist for these purinergic receptors) blocked TRPV4-induced cough and TRPV4-mediated airway nerve activation (Figure 1-10) (Gever et al., 2010). Through *in vitro* calcium imaging and *in vivo* electrophysiological studies on airway terminating neurons and nerve fibres, respectively, it was further shown that TRPV4 agonists cause cough by activating only the nodose ganglia (not the jugular ganglia) and A $\delta$ -fibres (not C-fibres). The cells expressing TRPV4 and releasing ATP in this tussigenic mechanism are yet to be identified, however there is a distinct lack of expression of TRPV4 on guinea pig airway sensory neurons for them to be mediating this response (Bonvini et al., 2016). The authors of this study could not say for certain the mechanism by which ATP was released as part of this TRPV4-ATP-P2X3 axis, however TRPV4 agonist-induced vagus nerve depolarisation was virtually abolished in mice devoid of the gene for pannexin 1, a large transmembrane channel protein capable of transporting ATP as well as Ca<sup>2+</sup>, inositol triphosphate and other small molecules (Bonvini et al., 2016, Shestopalov and Panchin, 2008). A schematic to illustrate this protussive mechanism can be found in Figure 1-11.

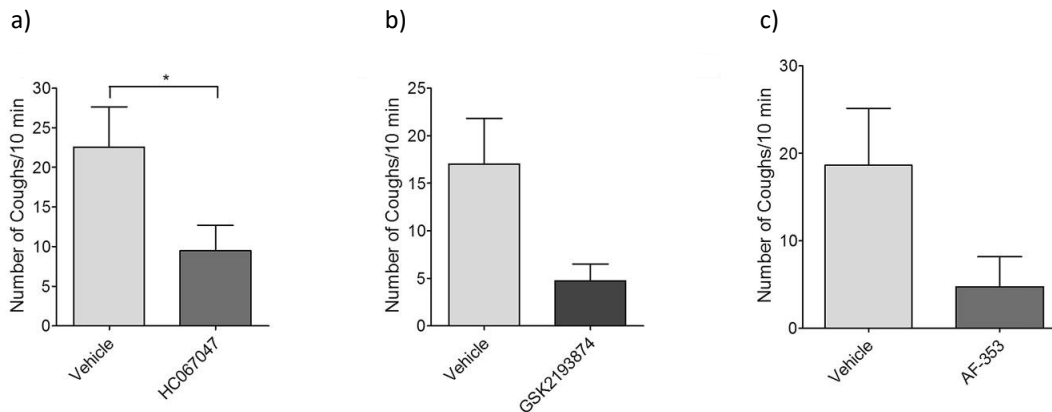


Figure 1-10 TRPV4 agonism elicits cough in guinea pigs and can be inhibited by selective TRPV4 and P2X3 antagonists

These histograms adapted from Bonvini et al. (2016) show the effect TRPV4 antagonists HC067047 (a) and GSK2193874 (b), and the P2X3 antagonist AF-353 (c), have on TRPV4 agonist GSK1016790A-induced coughing in guinea pigs. Data shown as mean  $\pm$  S.E.M.,  $8 \leq n \leq 12$ . \* indicates statistical significance ( $p < 0.05$ ), through using a Mann Whitney test where responses from the antagonist-treated group were compared to the vehicle control

TRPV4 has also been implicated in IPF. A study by Rahaman et al. (2014) made several important discoveries, among which were the findings that lung fibroblasts derived from IPF patients have increased TRPV4 activity, that bleomycin-induced lung fibrosis is attenuated in TRPV4 knockout mice, and that pharmacological inhibition or genetic disruption of TRPV4 inhibited TGF- $\beta$ -induced myofibroblast differentiation. To add to this, the team also showed that human myofibroblast TRPV4 channels could be activated if the myofibroblasts were plated onto matrices of increasing stiffness or stiff lung tissue sections, alone.

Considering TRPV4's ability to provoke cough in guinea pigs, its propensity to be activated by mechanical stress, and its apparent involvement in pulmonary fibrogenesis (Bonvini et al., 2016, Rahaman et al., 2014, Sharma et al., 2019), it stands to reason that this calcium channel might be implicated in IPF-associated cough. Whether this is the case remains to be seen, however some of the enthusiasm surrounding TRPV4 as a pharmacological target for cough has diminished since GSK terminated a phase 2 trial assessing a pharmacological antagonist for this channel in chronic cough patients. These results however do not necessarily rule out TRPV4 as a target specifically in IPF-associated cough (see Chapter 7).

## Unknown Accessory Cell

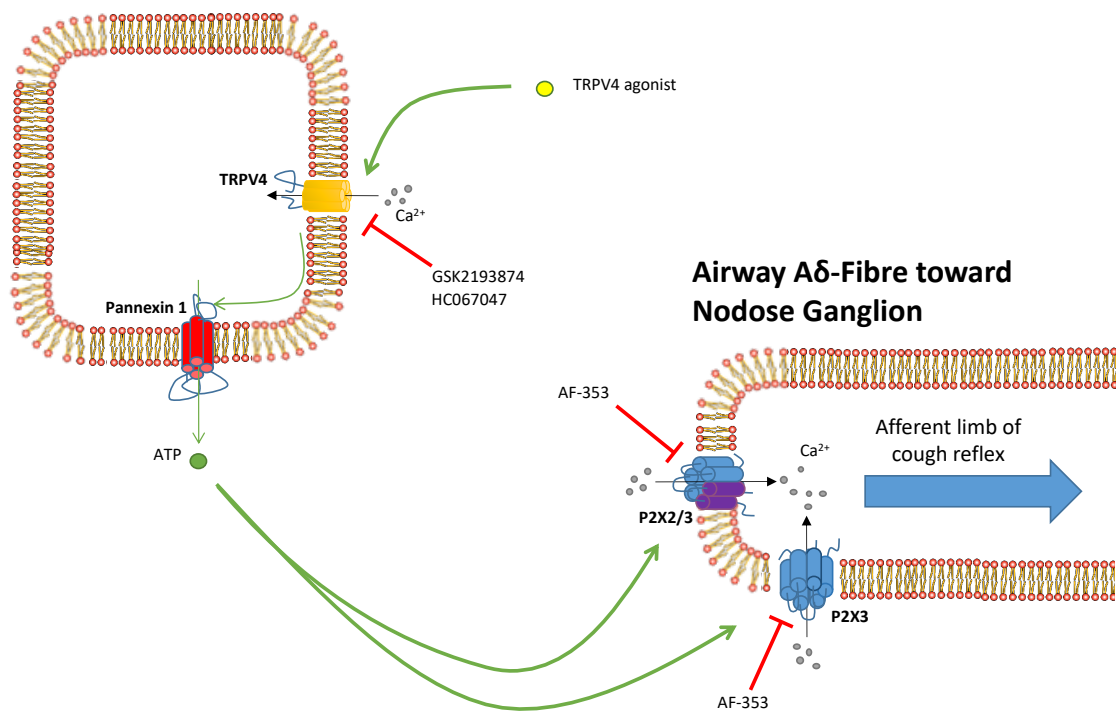


Figure 1-11 The TRPV4-ATP-P2X3 axis: activation of airway afferents and cough

A schematic to illustrate the mechanism by which TRPV4 agonists might evoke cough in guinea pigs, according to the results published by Bonvini et al. (2016). TRPV4 agonists (e.g. GSK1016790A) activate the TRPV4 channel that is expressed on a cell that resides in the airways; this can be inhibited by TRPV4 selective antagonists (e.g. GSK2193874 or HC067047). The influx of extracellular calcium causes pannexin 1 channels to open through an intracellular signalling cascade. The open pannexin 1 channels facilitate the release of ATP into the extracellular space of the lung lumen. This ATP then binds to and activates P2X3 present on airway sensory nerve termini, thereby causing an influx of calcium into these neurons; this step can be inhibited by an antagonist for P2X3 and P2X2/3 (e.g. AF-353). If of sufficient magnitude, the depolarisation at the airway sensory nerve ending will lead to the generation of an action potential, thus forming the afferent limb of the cough reflex. Original figure by author.

### 1.5.2.1 PAR2: an activator of TRPV4 and receptor involved in IPF pathogenesis?

If the TRPV4-ATP-P2X3 axis is an active signalling pathway causing IPF-associated cough and perhaps even idiopathic chronic cough too, it begs the question: what are the upstream activators of this signalling pathway?

One option could be Protease-activated receptor 2 (PAR2). PAR2 is expressed on nociceptive neurons (Steinhoff et al., 2000, Vergnolle et al., 2001) and has previously been shown to activate TRPV4 through an intracellular mechanism that may involve tyrosine kinases (Grace et al., 2014, Poole et al., 2013). PAR2 is a G-Protein coupled receptor that *in vivo* is activated through proteolytic cleavage of its amino terminus, thereby allowing the new amino terminus to act as a “tethered ligand”, which subsequently activates the receptor (Al-Ani et al., 2002) (Figure 1-12). One proteinase capable of facilitating this activation is tryptase (Molino et al., 1997), which has been shown to be

increased in the BALF of IPF patients and has been associated with poorer prognoses (Kawatani et al., 2007, Compton et al., 2001). Providing further evidence for the role of PAR2 in IPF, is the increased PAR2 expression in the IPF lung (Wygrecka et al., 2011), and the fact that this expression is associated with the ‘honeycombing’ of the lung architecture (Park et al., 2013).

PAR2 can be activated exogenously using small molecules (e.g. AC-55541) (Seitzberg et al., 2008) or small peptides that mimic the protein’s hidden tethered ligand (e.g. 2-Furoyl-LIGRLO) (Gatti et al., 2006).

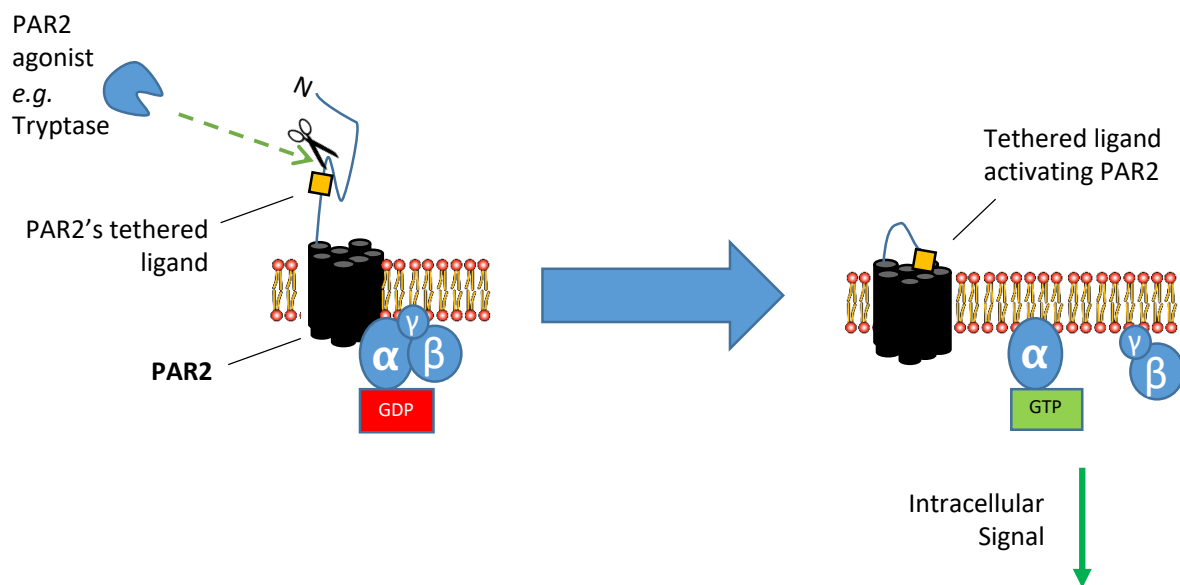


Figure 1-12 The PAR2 activation mechanism

A schematic to show the mechanism behind PAR2 activation. PAR2 is a 7-transmembrane receptor that is coupled to a G-protein. PAR2 is activated by a variety of endogenous and exogenous proteases (e.g. tryptase) (Guenther and Melzig, 2015). The agonist cleaves PAR2’s extracellular amino terminus between an arginine and serine residue, this reveals a newly exposed N-terminus which acts as a tethered ligand to PAR2. This ligand activates PAR2 by binding to one of its extracellular loops, which further activates its coupled G-protein, thereby propagating an intracellular signal (Heuberger and Schuepbach, 2019). Original figure by author.

### 1.5.3 TRPA1

Transient Receptor Potential Ankyrin 1 (TRPA1) is a  $\text{Ca}^{2+}$  permeant non-selective cation channel containing a 14-ankyrin repeat domain at its amino terminus; it is expressed on the majority of vagal nociceptive C-fibres in the airways (Grace and Belvisi, 2011). Since the discovery of TRPA1, the majority of studies investigating the channel have focused on its role in nociception, because of the huge diversity of compounds that can activate the receptor. These compounds include: inflammatory mediators such as bradykinin and prostaglandin (e.g.  $\text{PGE}_2$ ); environmental irritants present in air pollutants, burning vegetation and cigarette smoke like acrolein; organosulphur spices like allyl isothiocyanate, the compound responsible for the pungent taste of mustard, horseradish and wasabi (Bautista et al., 2006, Caterina, 2007).

The channel is now widely considered to be a protussive receptor in guinea pigs and humans, since it has been shown to evoke cough by activation with acrolein and cinemaldehyde (Andre et al., 2009, Birrell et al., 2009).

Unsurprisingly, the pharmaceutical industry took a keen interest in developing pharmacological antagonists for TRPA1. Glenmark Pharmaceuticals took a specific and potent TRPA1 antagonist forward to clinical trials in patients with chronic cough, after it showed a high efficacy at inhibiting citric acid-induced cough in guinea pigs (Mukhopadhyay et al., 2014). Although the results have not been fully published, the compound unfortunately showed no clinical efficacy at inhibiting cough in chronic cough patients (Morice, 2017). Much like the results from GSK's clinical trial that investigated the antitussive efficacy of a TRPV4 antagonist in chronic idiopathic cough patients, these results may appear discouraging, however, it is important to remember that neither of these studies proved target engagement with their respective compounds, and further, the results still do not necessarily rule out the targeting of these receptors in IPF-associated cough, which could work through a different mechanism (Chapter 5).

Indeed, a recent phase 2 clinical trial found that an inhaled formulation of sodium cromoglycate reduced daytime cough frequency in IPF patients (Birring et al., 2017). Interestingly, *in vitro* studies performed by this lab have found that cromoglycate is an agonist of G protein-coupled receptor 35 (GPR35), which inhibits airway nerve responses (e.g. cough and bronchoconstriction) mediated by TRPA1 (Maher et al., 2015). When viewing these two studies together, it is possible to envisage cromoglycate's antitussive mechanism in IPF patients being mediated through the inhibition of the TRPA1 channel. Adding further foundation to this hypothesis is the knowledge that TRPA1 can be activated by oxidants like H<sub>2</sub>O<sub>2</sub> in sensory neurons (Sawada et al., 2008, Andersson et al., 2008); oxidative stress is a well-known feature of the IPF lung and is thought by some to be involved in its pathogenesis (Section 1.1.6).

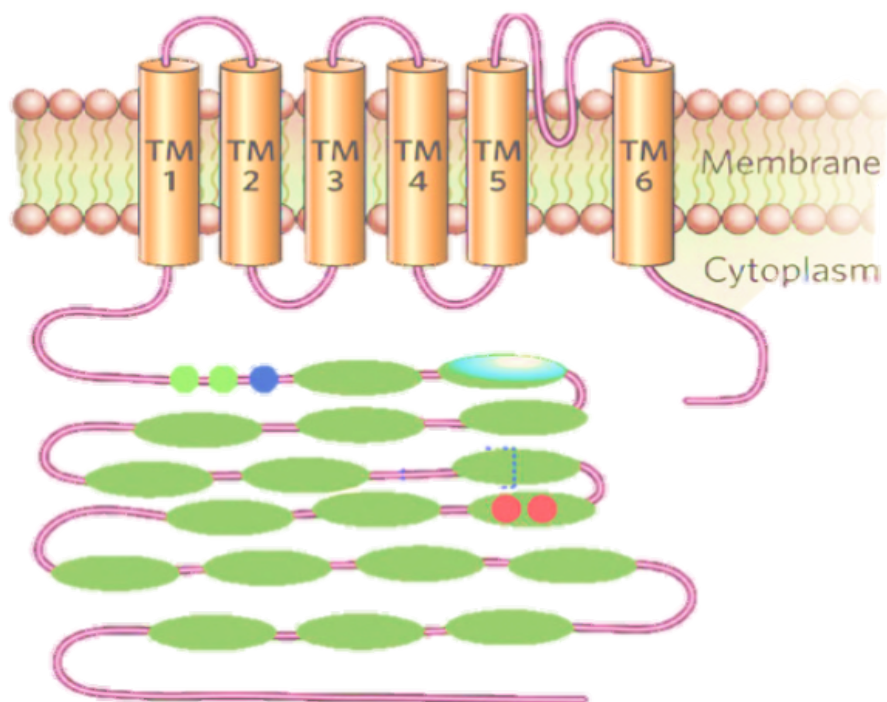


Figure 1-13 The TRPA1 ion channel

The secondary structure of one of the four identical subunits that make up the TRPA1 channel, adapted from Caterina (2007). As seen here each subunit has 6 alpha helical membrane spanning domains as well as a long cytoplasmic N-terminal domain. The green ovals represent ankyrin repeat domains whilst the smaller multi-coloured circles indicate cysteine residues required for covalent activation.

## 1.6 Thesis Plan

This thesis will aim to test the following hypotheses:

**Spontaneous cough in a guinea pig model of IPF is caused by:**

- 1) Oxidative stress which activates airway sensory nerves via the TRPA1 channel**
- and/or**
- 2) PAR2-induced activation of the TRPV4-ATP-P2X3 axis**

In order to test this hypothesis, this thesis will aim to:

- Establish and validate a first-of-its-kind model of spontaneous cough in pulmonary fibrotic guinea pigs (**Chapter 3**)
- Measure the presence of possible tussive-related biomarkers in this *in vivo* model and compare these with IPF patient samples and the literature (**Chapter 4**)
- Assess whether prospective tussive agents relating to the above biomarkers can cause airway sensory nerve activation
  - Oxidative stress via TRPA1 (**Chapters 5**)
  - PAR2 ligands via the TRPV4-ATP-P2X3 axis (**Chapter 6**)
- Characterise the efficacy of GSK2798745, a novel TRPV4 antagonist in preparation for it being tested in the *in vivo* model of fibrosis-induced spontaneous cough (**Chapter 7**)

These aims will be achieved by:

- Conducting a dose response to intratracheally instilled bleomycin in guinea pigs, before assessing them for spontaneous cough using a closed-circuit television (CCTV) system
- Quantifying different biomarkers in guinea pig BALF and comparing these biomarkers to BALF donated by patients and healthy volunteers at Royal Brompton Hospital
- Using intracellular oxidative stress and calcium imaging, and the *in vitro* isolated vagus nerve model to discern whether oxidative stress can activate airway sensory nerves through the TRPA1 channel
- Using the *in vitro* isolated vagus nerve model, eTRec and the *in vivo* single fibre model to see whether PAR2 ligands cause airway sensory nerve activation via the TRPV4-ATP-P2X3 axis
- Using naïve guinea pigs in a TRPV4 agonist-induced cough model to test the antitussive capabilities of the TRPV4 antagonist GSK2798745

## 2 Methodology

### 2.1 Introduction

This chapter describes the techniques used in this thesis. More precise details including statistical analysis can be found in the relevant results chapter. This chapter does not detail the development of the novel bleomycin-induced spontaneous cough model (Chapter 3), nor does it describe oxidative stress or calcium imaging of neurons (Chapter 5).

### 2.2 Animal Husbandry

Male Dunkin Hartley guinea pigs and male wild type (WT) C57Bl/6 mice were purchased from B&K (Hull, UK) and Envigo (Huntingdon, UK), respectively. Animals were housed in temperature controlled (21°C) rooms with food and water available *ad libitum* at least one week prior to commencement of experimentation. All animal work was carried out in accordance with the U.K. Home Office guidelines for animal welfare based on the Animals (Scientific Procedures) Act of 1986 and the ARRIVE guidelines (Kilkenny et al., 2010). Throughout any long-term study, the welfare of all animals was monitored frequently. All animals were euthanised with an intraperitoneal overdose of pentobarbitone (200 mg/kg, 1 ml/kg), which was administered by a trained individual.

Intraperitoneally administered barbiturate overdose is a technique listed within Schedule 1 of the 1986 Animals (Scientific Procedures) Act. Following pentobarbitone administration, death was confirmed by checking the loss of the righting, palpebral and pedal withdrawal reflexes, and finally by confirming a cessation of circulation by cutting the femoral artery.

### 2.3 Use of Knockout Mice

#### 2.3.1 Procurement and breeding

Homozygous breeding pairs of mice genetically modified to render the PAR2 gene inoperative (F2rl1<sup>-/-</sup>; Stock Number: 004993) were purchased from Jackson Laboratories (ME, US).

All mouse breeding was kept within the C57Bl/6 strain, the viable and fertile colonies were housed at Imperial College London. The WT mice were bred alongside their genetically modified counterparts so that they could be used as aged matched controls. Each generation of knockout mouse was genotyped to ensure the continuation of the gene's disruption.

#### 2.3.2 Genotyping and PCR

Following any experiment that compared the responses of PAR2 knockout mice to wild type mice, it was important to assay tissue samples derived from the animals to confirm their genotype. We used a commercially available kit to extract the animal's DNA ('Extracta DNA prep for PCR', Quanta Biosciences; MD, US). Following confirmation of death (Section 2.2) a 20mm portion from the tip of



the mouse's tail was removed, placed into 75 µl of the kit's extraction buffer and subsequently heated at 95°C for 30 minutes. Once the sample had cooled to room temperature, 75 µl of the kit's stabilisation buffer was added to the sample. After the concentration of DNA within the sample was quantified with a spectrophotometer (GeneQuant RNA/DNA quantifier; Amersham Pharmacia, UK), it was diluted to 10ng/ml with nuclease free water.

We used polymerase chain reaction (PCR) to amplify the DNA of interest between two primers (Table 2-1); all reagents were sourced from GoTaq® (Promega, UK) apart from the PCR primers which were purchased from Invitrogen (Thermo Fisher Scientific, UK). 5 µl of sample DNA (prepared at 10 ng/ml) was combined with: 5 µl Taq buffer, 1 µl dNTPs (10mM), 2 µl MgCl<sub>2</sub>, 0.2 µl GoTaq® polymerase, 8.8 µl nuclease free water, 1 µl mutant primer (10 pmol/µl), 1 µl WT forward primer (10 pmol/µl), and 1 µl WT reverse primer (10 pmol/µl). Samples were then heated to 95°C, following which they underwent 40 thermal cycles to amplify their PCR product (Table 2-2). After the thermal cycling was completed, the samples were held at 72°C for 10 minutes to allow all oligonucleotides that were still in the extension phase to reach their full length. Lastly, the samples were cooled to 4°C for 5 minutes.

*Table 2-1 Primer sequences used to genotype F2RL1<sup>-/-</sup> mice*

<b>Primer Type</b>	<b>Sequence (5' to 3')</b>
Mutant	GCC AGA GGC CAC TTG TGT AG
WT Forward	TCA AAG ACT GCT GGT GGT TG
WT Reverse	GGT CCA ACA GTA AGG CTG CT

*Table 2-2 PCR protocol for F2RL1<sup>-/-</sup> genotyping and size of product*

<b>PCR Conditions</b>				
<b>F2LR1</b>	<b>Denaturing</b>	<b>Annealing</b>	<b>Extension</b>	<b>Product Size</b>
	95°C	60°C	72°C	WT: 345 bp
	30 seconds	30 seconds	2 minutes	KO: 198 bp

The resulting PCR products and a 50-2000bp ladder (Hyperladder 50bp, Bioline Reagents, UK) were electrophoresed through a 2% agarose gel (80 V for 60 minutes) in TBE buffer containing a nucleic acid stain (SafeView; NBS Biologicals Ltd, Huntingdon, UK). The gel was visualised under UV light and photographed so that the size of the DNA fragments could be interpreted (Table 2-2).

## 2.4 Isolated Vagal Nerve Recordings

The isolated vagus nerve preparation presents a method of conducting a rudimentary pharmacological assessment into the effects of proposed tussive and antitussive compounds *in vitro*, that is relatively higher throughput than the other techniques used in this PhD (Patel et al., 2003). Tussive agents that cause cough in human and animal subjects, including exogenous stimuli such as capsaicin, acrolein and endogenous stimuli such as the prostanoid PGE<sub>2</sub>, bradykinin, all elicit depolarisation of isolated vagus nerves from humans, guinea pigs, mice and rats (Bonvini et al., 2016, Grace et al., 2012, Birrell et al., 2009, Belvisi et al., 2017). The technique can further elucidate protussive mechanisms without the use of pharmacological intervention when using the vagal tissue derived from knockout mice. Another advantage due to the *in vitro* nature of the technique, means that the assessment of a drug's action is not obscured by any pharmacokinetic issues, neither is it susceptible to any respiratory complications, such as bronchoconstriction or mucus production, that make interpretation of data from *in vivo* cough models more difficult. Despite this, data should still be interpreted somewhat cautiously, as any pharmacological agent is being applied to the collective axons which make up the vagus nerve trunk. Firstly, this means any resulting depolarisation is a summation of the changes in membrane potential of all the axons within that trunk and not just sensory neurons that innervate the airways. Secondly, although there is expression of receptors along the neuronal axon, these same receptors may be expressed at different levels or behave differently when activated in the peripheral endings *in situ* in the intact animal.

### 2.4.1 Tissue Dissection: Animals

Male Dunkin Hartley guinea pigs (250-350g), WT (C57Bl/6) or genetically modified mice (PAR2<sup>-/-</sup>) (18-20g) were euthanized through overdose of pentobarbitone i.p. (200 mg/kg) and death was confirmed (see 2.2).

A vertical inline incision was made from the abdomen towards the neck. Any muscle or glandular tissue obscuring the vagal nerves was removed, followed by the rib cage. The vagal nerves were then removed by cutting caudally to the point where the vagus nerves leave the inferior vagal ganglia and separate from the hypoglossal nerves, and by cutting superior to the cardiac plexus. Next, the vagal tissue was placed into modified Krebs–Henseleit (KH) solution (in mM: NaCl 118; KCl 5.9; MgSO<sub>4</sub> 1.2; CaCl<sub>2</sub> 2.5; NaH<sub>2</sub>PO<sub>4</sub> 1.2; NaHCO<sub>3</sub> 25.5 and glucose 5.6; pH 7.4) and bubbled with 95% O<sub>2</sub> / 5% CO<sub>2</sub>. Any remaining connective tissue was removed, and in the case of the guinea pig, the nerve was further desheathed and cut into 10-15 mm long pieces; particular care was taken to not damage the nerve trunk through any excessive pulling or crushing.

### 2.4.2 Tissue Dissection: Human

Human tissue that was unsuitable for transplantation was purchased from the *International Institute for the Advancement of Medicine* (IIAM; New Jersey, US). *En bloc* lungs with the trachea and vagus nerves attached, were harvested from deceased donors and couriered to the lab, on ice in University of Wisconsin transplant solution, within 36 hours of aortic cross clamping. Upon arrival, the tissue was immediately placed within bubbled KH solution (see previous section). In human nerves, the epineurium that envelops the nerve fascicles is more difficult to remove, thus necessitating the use of a dissecting microscope to precisely tease it apart. As with guinea pig and mice vagal nerves, the dissected human nerves were cut into 10 – 15 mm sections and remained in bubbled KH solution until they were mounted into the recording system. Due to the relative scarcity of human tissue compared to animal tissue, only key experiments were repeated.

The criteria for accepting donor human lung tissue can be found in Table 2-3, whilst a summary of the donor characteristics is shown in Table 2-4.

*Table 2-3 Criteria for acceptance of human lung tissue*

	Conditions for acceptance
Donor Age	> 18 years
Downtime	None
Time on ventilator	≤ 14 days
Warm Ischemia Time (Hours)	< 2
Cold Ischemia Time (Hours)	< 36
Serotypes	Serotypes must be negative except for: <ul style="list-style-type: none"> <li>• CMV</li> <li>• EBV</li> <li>• HBsAb (with confirmed vaccination)</li> </ul>
Cannot have any of the following:	Cancer (past or present). Gram stain (+) (i.e. (+) cocci). Jail time (past or present). MRSA in any culture. Bacterial & Viral Meningitis. H1N1.
Chest X-Ray cannot reveal:	Aspiration, Pneumonia, infiltrates, contusions, pneumothoraces

Table 2-4 Tissue donor characteristics

Patient <i>n</i> =3	Age (years) <i>Average =</i> <i>64</i>	Sex	Smoking Status	Diseases ( <b><i>Respiratory</i></b> )	Relevant thesis chapter(s) tissue was used in
1	56	Male	Non smoker	Hypertension	5
2	70	Female	Smoker	-	5
3	65	Female	Unknown	Schizophrenia, GERD, hypertension, <b><i>COPD</i></b> , depression, anaemia	6 & 7

### 2.4.3 Measurement of nerve depolarisation

A desheathed nerve trunk section was removed from the KH solution and loaded into a ‘grease-gap’ recording chamber (Figure 2-1), as previously described (Birrell et al., 2002, Bonvini et al., 2016, Grace et al., 2012, Maher et al., 2009). Briefly, the nerve was pulled through a narrow channel ( $\varnothing$  2 mm, *l* 10 mm) that resided in a custom designed Perspex block, each end of the nerve was then electrochemically isolated from the opposite end, by slowly injecting the middle of the channel with petroleum jelly, thus forming a ‘grease-gap’. On one side of the grease-gap, the nerve was constantly suffused with 37°C bubbled KH solution, at a rate of 2 ml/min; the opposite side of the nerve remained in still, warm KH solution and was used as a reference. A borosilicate glass capillary (Ext.  $\varnothing$ . 2mm, Int  $\varnothing$  1.16mm, Clark glass capillaries, GC200-15, Warner Instruments, UK) was inserted into a Ag/AgCl-pellet half-cell electrode (Mere 2 flexible electrodes; WPI, UK), and carefully filled with KH solution to avoid air bubbles. Two such electrodes were positioned, one on each side of the grease-gap, so that their glass tip made gentle but direct contact with the nerve. Both electrodes were connected to the same differential amplifier (DAM 50; WPI, UK) which amplified the DC potential signal (x10 gain, low pass filter 1KHz, high pass filter 1hz). This amplified signal was relayed to a computer in real time, using a USB-coupled data acquisition system (Lab-Trax 4/16; WPI, UK, 10KHz sampling rate), where it was recorded in LabScribe (iWorx Systems, Inc.; New Hampshire, US). During any experiment, simultaneous recordings were made for up to 4 different nerves, each in a separate chamber with separate suffusion apparatus.

The activation of vagus nerves in response to stimuli was assessed by measuring a difference of electric potential between the reference electrode and the test electrode. Each electrode measures the summation of charges on the surface of each axon located under the electrode (which can change if some axons undergo depolarisation). By comparing the different electrical potential of the

nerve sections either side of the 'grease-gap', i.e. a potential difference ( $\Delta V$ ), we can assess the activation of the vagus nerve by different drugs. For instance, when a drug capable of activating neurons is applied to one side of the grease-gap, this will lead to an influx of positively charged ions into those neurons within the nerve *i.e.* it depolarises them, thus causing an electrical potential difference between the electrodes on either end of the vagal nerve trunk, which is then amplified by the differential amplifier. These generated potential differences that are detected in the model may be any depolarisation of the vagal nerve trunk including generator potentials and action potentials, which are the result of calcium and sodium channels opening, respectively. It is important to note that a drug capable of depolarising a vagus nerve in this model, may not necessarily generate an action potential, but it will however cause a potential difference, nonetheless.

In our isolated nerve recording model, when vagus nerve trunk axons are activated by a drug, the  $\text{Na}^+$  and  $\text{Ca}^{2+}$  ions present in the KH solution move down the electrochemical gradient and into the cells, this leaves the chloride ( $\text{Cl}^-$ ) ions free to associate with the oppositely charged silver ions ( $\text{Ag}^+$ ) on the surface of the electrode pellet. These interactions pump charge between the electrode ( $\text{Ag}_{(s)}$ ) and its electrolyte ( $\text{Ag}^+_{(aq)} + \text{Cl}^-_{(aq)}$ ). As the drug has only been applied to the side of the system with the 'recording' electrode, the grease gap prevents any action of the agonist on the other side of the nerve thereby maintaining the original ion concentrations at the side of the 'reference' electrode; the resulting potential difference in electric charge can then be amplified and recorded onto the computer. When the drug is washed off with KH solution, potassium channels in the nerve cells open, thus releasing potassium ions into the extracellular space and repolarising the cell. The potassium ( $\text{K}^+$ ) ions associate with the free  $\text{Cl}^-$  ions and therefore shift the equilibrium of the electrode, which restores the original potential difference.

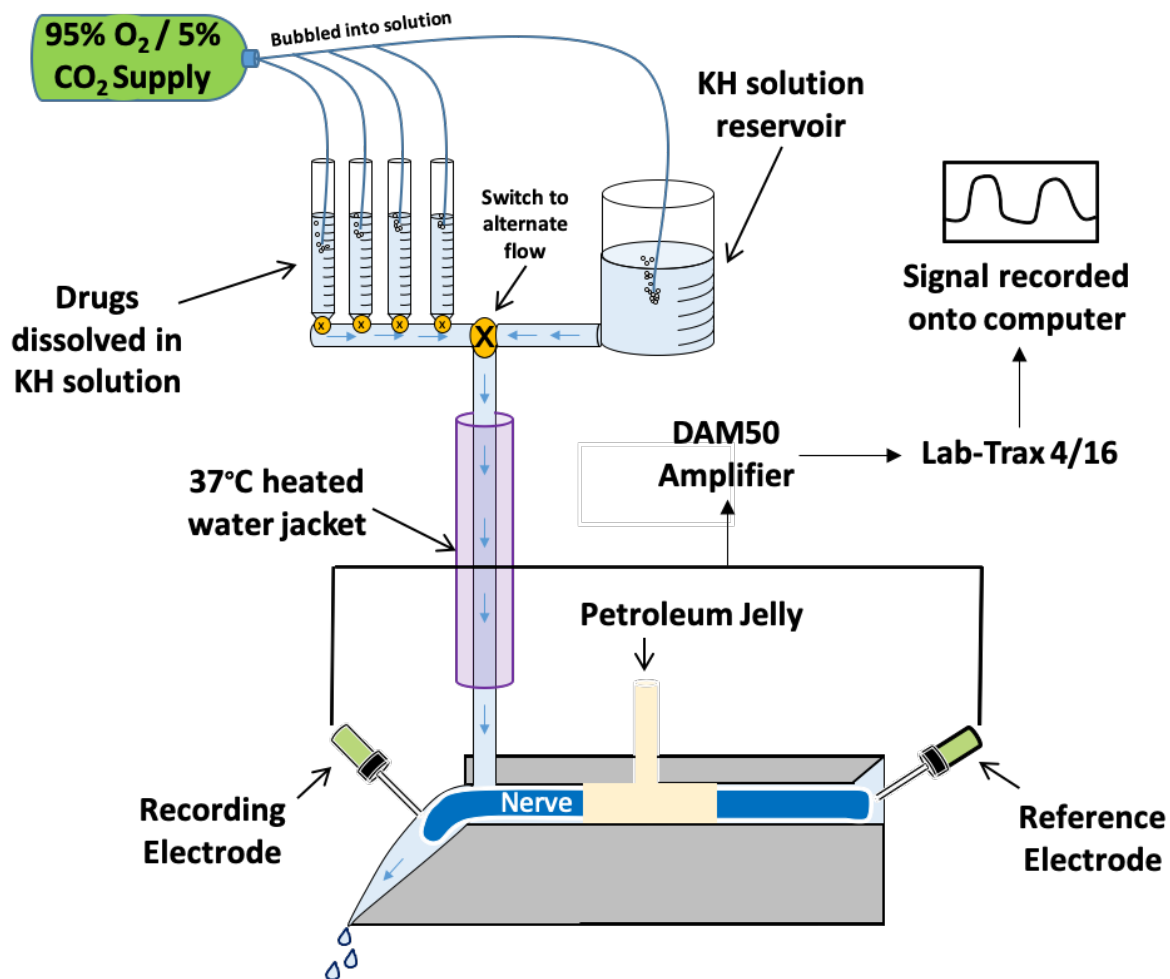


Figure 2-1 Schematic of isolated vagus nerve recording system

A piece of vagus nerve trunk is inserted into a Perspex chamber, petroleum jelly is then inserted into the centre of this chamber so that it surrounds a segment of the middle of the nerve trunk; this grease gap prevents the drugs applied to one side of the nerve from making contact with the opposite side of the nerve. Two Ag/AgCl-pellet half-cell electrodes are allowed to make contact with the vagus nerve, one on each side of the grease gap. KH solution, bubbled with compressed air and heated to 37°C, suffuses one side of the nerve at a rate of 2 ml/min; drugs can be dissolved in this solution to stimulate the nerve.

#### 2.4.4 Concentration Response and Antagonist Protocols

In order to determine if a compound was capable of depolarising the vagus nerve, which therefore might indicate a protussive effect, the nerve was exposed to non-cumulative concentrations of the compound, as well as a vehicle control. Unless otherwise indicated, compounds were usually stored at -20°C in stock aliquots at a 1000-fold concentration, using dimethyl sulfoxide (DMSO; Sigma-Aldrich, UK) as a vehicle. Aliquots were thawed to room temperature on the day of the experiment and then diluted down to a working concentration in KH solution. The nerve was stimulated with the drug for 2 minutes, following which, the compound was washed off with KH solution until the signal returned to baseline. This was repeated for all the concentrations of the compound that were to be

tested, including the vehicle. To ensure nerve viability, the nerve was usually stimulated with a known protussive compound before and after each concentration response experiment; this was usually capsaicin (1  $\mu$ M). As the nerve survives for only a limited time in the recording system, each nerve was subjected to a maximum of 6 stimulations; previous work conducted by this lab has found that vagus nerves usually remain viable in this preparation for that number of moderate stimulations. After completion of the experiment, the nerve recording was exported from LabScribe to Clampfit 10.7 (Molecular Devices, LLC.; San Jose, CA, US). There, the microfluctuations of the baseline of the recording was manually compensated, and the peak amplitude of each response was measured (in mV). After characterising a compound's effect, a submaximal concentration was taken forward for future antagonist experiments.

We employed a classical pharmacological approach to investigate the inhibitory effect of antagonists on agonist-induced vagus nerve depolarisation. As above, the nerve was suffused with the stimulant for two minutes, this was then washed off with KH solution and the signal was allowed to return to baseline. This was repeated one or two times to ensure that the agonist-induced depolarisation was reproducible. Next, the nerve was suffused or 'blocked' with the antagonist for 10 minutes, this was followed immediately by suffusing the nerve with a mixture of agonist and antagonist for 2 minutes. The duration of time used for these agonist and antagonist exposures have previously been determined by the group to be sufficient to pharmacologically stimulate and block vagus nerves in this preparation, respectively, and further, strictly abiding by such times during every experiment ensures that results are comparable. Comparing the magnitude of depolarisation generated by the agonist alone, with that of the depolarisation from the agonist in the presence of the antagonist, enables one to see whether the antagonist is having any inhibitory effect; this was presented as % inhibition using the following equation:

$$\% \text{ inhibition} = 100 \left( \frac{\text{Agonist mean depolarisation} - \text{Agonist depolarisation in presence of antagonist}}{\text{Agonist mean depolarisation}} \right)$$

Finally, after a period of 6 to 8 minutes, the nerve was stimulated with the agonist a final time, for two minutes, to ensure it was still viable and that the antagonist had been washed off. Only one concentration of antagonist was tested per piece of nerve.

## 2.5 Electrophysiological tracheal recording of the Recurrent Laryngeal Nerve

As mentioned previously, one of the main limitations of the isolated vagus nerve recording technique is that the nerve activity measured is the result of activation of receptors expressed along the neuronal axon, rather than receptors on the nerve endings themselves. An *ex vivo* technique recently developed by our lab is the measurement of compound action potentials (CAP) of airway

sensory nerve endings within the recurrent laryngeal nerve (RLN), that result from stimulating the nerve endings located within tracheal wall. This technique has been coined eTRec, which stands for: electrophysiological tracheal recording.

### 2.5.1 Isolated perfused trachea RLN set-up

Male Dunkin Hartley guinea pigs (350 – 400 g) were euthanised through an intraperitoneal overdose of pentobarbitone (Section 2.2). The skin, ribcage and any cervical muscles or glands that obscured the upper airways were removed. The larynx, trachea, lungs and the nerves that innervated them, from the vagal ganglia down to the superior mediastinum, were removed *en bloc*. Any connective tissue was removed whilst taking care to ensure that all nervous connections remained intact. Similar to a technique described by Riccio *et al* from 1996, the remaining tissues in the preparation were: the trachea, the primary bronchi, and the left and right vagus nerves (including the left nodose ganglion). Importantly, vagus nerves' innervations of the airways were left intact, including: the left superior and inferior branches of the laryngeal nerve, and the left and right recurrent laryngeal nerves (Figure 2-2). The tissues were placed inside a custom-made Perspex bath and immersed in bubbled KH solution (as in Section 2.4.1) to maintain oxygenation and a pH of 7.4.

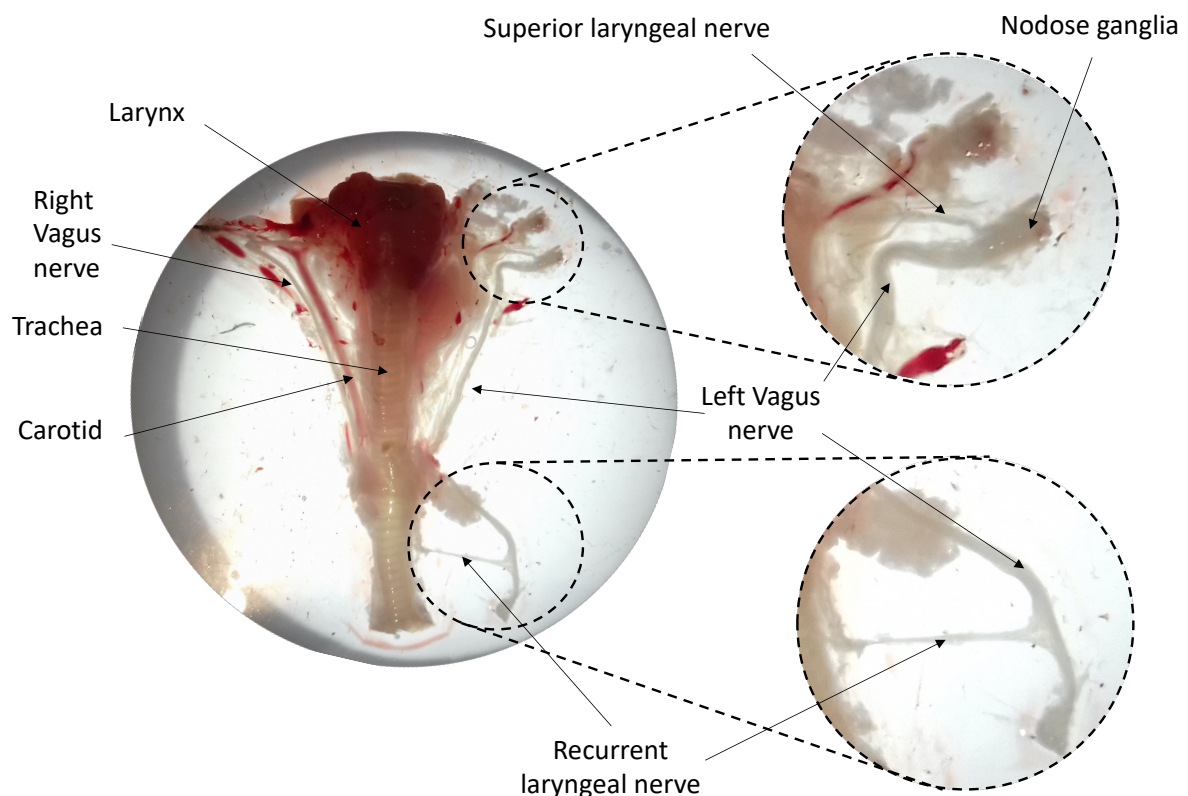


Figure 2-2 Guinea pig airways with nerves attached.

A picture of guinea pig tracheal and nervous tissue after dissection and cleaning has taken place, and prior to eTRec. Tissue dissected by Dr Dubuis; photographed and annotated by author.

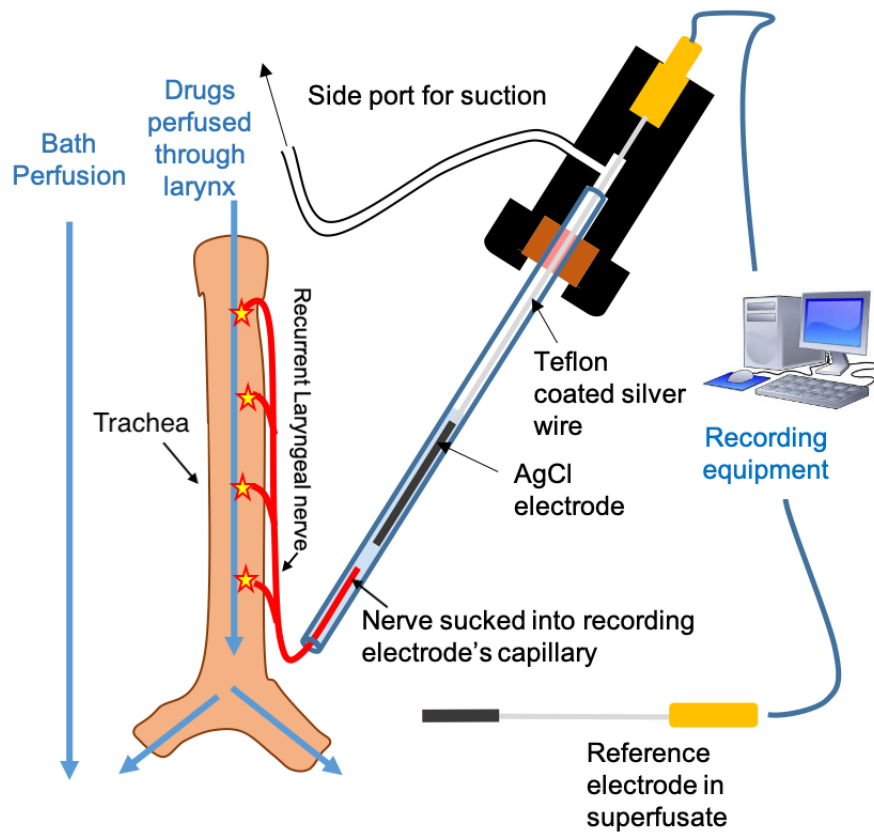


The left RLN was then cut near the point at which it branches from the vagus nerve and drawn into a suction recording electrode pulled from a borosilicate glass capillary (2 mm Ext.  $\emptyset$ , 1.73 mm Int.  $\emptyset$ ; Clark glass capillary, Warner Instruments), that had been filled prior with KH solution; the other (reference) electrode was submerged in the bath. Both electrodes contained a Ag/AgCl filament sensor and were positioned using a precision made holder with a side suction port (QSW-M20P, Warner Instruments) and connected to a recording headstage (NL100AK Neurolog headstage, Digitimer; FL, USA).

The larynx and bronchi were cannulated, thus allowing the airways to be perfused, and thereby preventing this perfusate from coming into contact with the suffusate of the bath. KH solution or drugs (that were dissolved in KH solution) were perfused through the airways (in through the larynx and out through the bronchi) at a rate of 2 ml per minute and collected in a waste trap. Separately, the tissue within the bath was suffused at a rate of 5-6 ml per minute. Both the perfusate and suffusate were maintained at 37°C using an automated heating controller (TC-344B, Warner Instruments, UK).

The potential difference ( $\mu\text{V}$ ) between the two electrodes was recorded by connecting them to a pre-amp headstage (NL104A – AC Preamplifier, Digitimer; FL, USA). The signal was amplified (NL106 – AC/DC Amplifier, Digitimer), filtered (NL125 – Band-Pass Filter, Digitimer set to 500Hz High Pass and 2000Hz low pass) and had mains electrical 50 Hz interference removed using a noise eliminator (Humbug, Digitimer; FL, USA). Finally, the output was converted to a digital signal and analysed with Spike 2 software (Cambridge Electronic Design Limited; Cambridge, England).

a)



b)

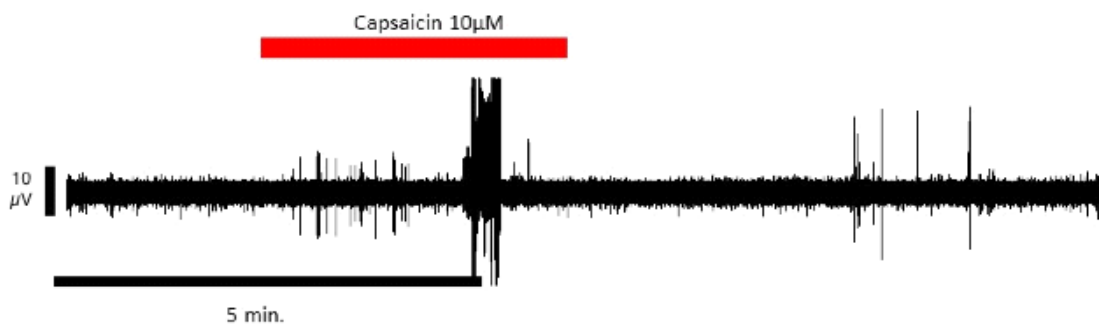


Figure 2-3 eTRec Recording.

a) a schematic to demonstrate the set-up of the eTRec system as it records the axon firing of the Left Recurrent Laryngeal Nerve (RLN). b) An example neurogram showing the rate of firing of an RLN when the trachea is perfused with capsaicin.

### 2.5.2 Interpretation of RLN recordings

eTRec allows one to measure the ability of drugs to cause compound action potential firing by activating nerve endings of the RLN (a distal branch of the vagus nerve) from within the trachea. The technique also uses KH solution and the same type of electrodes as the isolated vagus system, so the electrochemical principles remain much the same (Section 2.4.3), however, unlike the vagus system where the recording electrode is making contact with the outside of the vagus nerve, in eTRec, the recording electrode is making contact with a cross section of RLN. Another key difference in eTRec's favour is that as the drugs used to activate the nerve are perfused through the trachea, any resulting nerve firing can only have originated from airway sensory afferent nerve endings that innervate the trachea; this being the case, one can have more confidence in a drug's protussive abilities than one might have with the vagus technique alone.

### 2.5.3 Concentration response experiment protocols

Due to this being a technique that arrived relatively recently within our lab and because of the onset of Covid-19, only concentration responses were performed (*i.e.* no antagonist experiments). The nature of these eTRec concentration response experiments on the RLN was much the same as the isolated vagus nerve technique (Section 2.4.4), except that the drug incubation times were longer, to account for the added time it would take the compounds to cause depolarisation in an *ex vivo* set up, unlike in the isolated vagus technique where nerves are more exposed due to desheathing and the small size of the chamber.

### 2.5.4 Data Analysis

To determine the effect of a drug, data was generated by subtracting the max firing rate of the RLN during baseline for a particular time, from the max firing rate of the RLN whilst the trachea was perfused with a drug for the same amount of time (*i.e.*  $\Delta$  impulse. $\text{sec}^{-1}$ ).

## 2.6 *In Vivo* Single Fibre Recordings

The single fibre technique enables the experimenter to see the affect a compound has on the firing rate of an individual airway sensory afferent nerve fibre within an anaesthetised animal. The technique requires the cutting of both the left and right vagus nerves at the central end to stop the generation of centrally-mediated reflex bronchoconstriction. The left vagus nerve is then teased down to measure impulses from individual fibres. As a result of this, any impulses that are measured can only have originated at the sensory field and cannot be the result of a reflex arc. As these experiments were performed in living (albeit anaesthetised) guinea pigs, this is the most physiologically relevant technique for assessing the protussive activity of a compound, besides an *in vivo* cough model.

### 2.6.1 *In Vivo* Single Fibre Model Set-up and Surgery

Male Dunkin Hartley guinea pigs (400-750g) were anaesthetised through an i.p. administration of urethane (1.5g/kg), with additional anaesthetic being supplied if and when required. The animal was also paralysed with the neuromuscular blocker vecuronium bromide by administering 0.1 mg/kg i.v. initially, then 0.05 mg/kg every 20 minutes thereafter. The level of anaesthesia was constantly monitored throughout the procedure.

Guinea pigs were prepared as outlined by Adcock *et al.*, 2003. Briefly, the animal was intubated with a cannula, and the pH and oxygen saturation of the animal's blood was maintained at physiological levels through the use of a rodent ventilator (Ugo Basile; Gemonio, Italy). The ventilation rate was kept to 50-60 breaths per minute with a tidal volume of 10 ml/kg. An Aerogen nebuliser (DSI; Minnesota, US) was connected to the ventilator in order to deliver aerosolised compounds into the airways. Both the right jugular vein and right carotid artery were cannulated for the systemic administration of drugs and to measure systemic arterial blood pressure, respectively. Heart rate and blood pressure were continuously monitored using a transducer (Gould P2X3L, MEMSCAP SP 844; Crolles, France), whilst temperature was monitored with a rectal thermometer and maintained at 37°C using a heated blanket and control unit (Harvard Apparatus; Massachusetts, US). Although the data is not presented in this report, tracheal pressure was also recorded throughout the experiment, using an air pressure transducer (SenSymb647, MEMSCAP SP 844; Crolles, France) attached to the side arm of the tracheal cannula.

Both of the guinea pig's cervical vagal nerves were severed at the central end and were dissected free from the carotid artery, sympathetic and aortic nerves, however, only the left vagus nerve was used for recording, which was additionally cleared of all surrounding tissue and fascia. The decision to record from the left vagus nerve, instead of the right vagus nerve, was purely down to operator preference, as this side is easier to access for a right-handed individual. The skin and muscle surrounding either side of the cervical incision were tied to a metal ring, the centre of which was filled with mineral oil to create a non-conductive well. Bipolar Teflon coated platinum electrodes, with exposed tips, were used to record action potentials. Using a binocular microscope, thin filaments were teased away from the vagus nerve and placed onto the recording electrode, until a single active unit of no more than 2 or 3 fibres, was obtained; the reference electrode was then placed onto the nerve fascia. The nerve fibres recorded within a single unit were not necessarily of the same class, however, providing that the fibre of interest had large enough action potentials to discriminate it from the other fibres within the bundle, then it was possible to isolate its firing electronically using Spike 2 data acquisition software. Both electrodes were connected to a preamplifier headstage (NL100k Digitimer), the signal was then amplified (NL104 Digitimer), filtered

(NL125 Digitimer), and passed through a 'Humbug' to remove 50-60hz mains electrical noise (Digitimer). All signals (including arterial blood pressure, tracheal pressure and heart rate) were recorded using Spike 2 data acquisition software, which is capable of pulse train counting over selected periods of time. The input signal was also monitored in real time using a digital storage oscilloscope (DPO 2012, Tektronix; OR, USA) and fed through an audio amplifier to a loudspeaker. Finally, at the end of the experiment, guinea pigs were euthanised through an overdose of pentobarbitone (see Section 2.2).

### 2.6.2 Identification and characterisation of airway terminating single fibres

Using a set of criteria previously outlined by Adcock et al. (2003) using rabbits, but that also applies to other rodents and humans, it was possible to identify which family of sensory nerve endings the nerve fibre making contact with the electrode belonged to: SARs, RARs or chemosensitive C-fibres (Section 1.3.6). These tests included: measuring the fibre's conduction velocity, ascertaining if the fibre had any patterns of spontaneous discharge, checking if the fibre responded to hyperinflation or deflation of the airways, calculating the fibre's adaptation index, and seeing if the fibre responded to inhaled citric acid or capsaicin (Adcock et al., 2003). A fibre that lacked spontaneous activity, a response to hyperinflation and deflation but however did respond to aerosolised capsaicin, was assumed to be a C-fibre. Conversely, if a fibre had a set pattern of spontaneous activity, responded to hyperinflation, deflation and to citric acid aerosol, it was categorised as an A $\delta$ -fibre (RAR).

After the experiment was completed, the conduction velocity of the fibre was measured as a final means of verification, as non-myelinated C-fibres are slower than myelinated A $\delta$ -fibres. Conduction velocities were measured by stimulating the vagus nerve close to the thorax with bipolar silver electrodes using a suprathreshold voltage at 0.5 ms, 1 Hz (Grass S44 stimulator). The stimulus and its resulting action potential were recorded as a single sweep on the Spike software, and the distance and time interval between the stimulating electrode and recording electrode was used to calculate the fibre's conduction velocity.

### 2.6.3 Concentration response experimental protocol for A $\delta$ -fibre

The protocol below was followed in order to ascertain whether a compound was capable of causing airway single fibres to discharge; the exact timings of the doses and recordings are laid out in the relevant chapter (Section 6.2.3). Due to time restrictions and the onset of Covid-19, only A $\delta$ -fibres were tested as these are known to be involved in the TRPV4-ATP-P2X3 axis (Bonvini et al., 2016), and therefore we speculated that these may facilitate responses to PAR2 agonists as well. Probing C-fibres for PAR2-induced impulses is something we plan to do in the future (Section 8.4)

Following the identification of an airway A $\delta$  single fibre, a baseline recording was made for 2 minutes. First, an aerosol of capsaicin was administered into the lungs for 20 seconds, to determine whether the A $\delta$ -fibre was capsaicin sensitive. During this time, any changes in nerve impulse rate, intratracheal pressure or systemic arterial blood pressure were monitored. Following this, any readout signals were allowed to return to baseline for between 10 and 20 minutes. This process was repeated with a 1 minute administration of citric acid (0.3M), and repeated again for the vehicle and each of the different concentrations of the compound of interest, each time allowing the signals to return to baseline. Lastly, a final dose of citric acid was administered to ensure that the fibre was still responsive.

Data was presented in neurograms, with firing rate (impulses s<sup>-1</sup>) in the y axis.

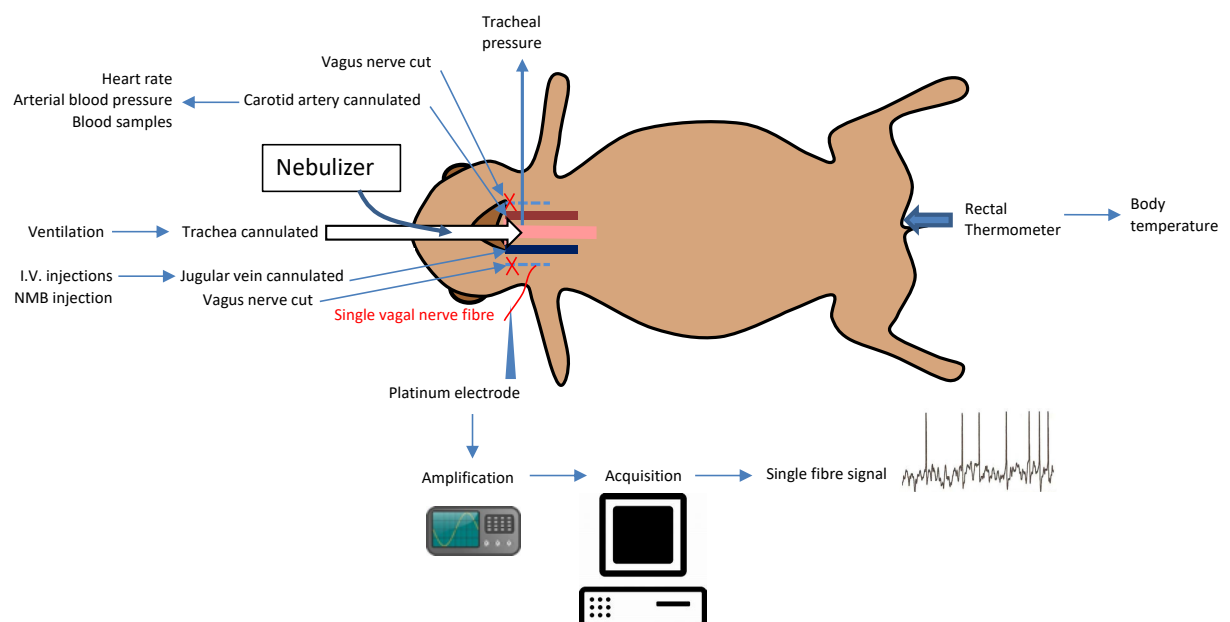


Figure 2-4 a) The set-up of the *in vivo* single fibre technique.

*A platinum electrode makes contact with a single fibre that has been teased out of the left Vagus nerve. Using a nebuliser, compounds of interest are then aerosolised, these are then insufflated into the animal's airways with a ventilator. An example trace (bottom right) can be seen showing the action potentials in the single fibre that result from a protussive agonist being administered to the lungs.*

#### 2.6.4 Aerosol-induced cough model

To assess the tussive and antitussive capability of compounds *in vivo*, we deployed a conscious, unrestrained, naïve guinea pig cough model. For reasons that can only be theorised from an evolutionary perspective, guinea pigs (unlike mice and rats) are the smallest rodents that have a cough response similar to our own (Maher et al., 2009). Therefore, should a compound cause cough or inhibit an irritant-induced cough in this guinea pig model, it stands to reason that it should have the same effect in humans. Nevertheless, an antitussive compound that appears effective at inhibiting a provoked cough in guinea pig or human subjects will not necessarily prove effective in

combating a chronic cough. A notable example of this was the failure of XEN-D0501, a novel TRPV1 antagonist that despite being highly efficacious at inhibiting capsaicin-induced cough in guinea pigs and chronic cough patients, was not capable of reducing the latter's spontaneous awake cough frequency (Belvisi et al., 2017).

Dunkin Hartley guinea pigs (250-300g) were placed into transparent Perspex plethysmography chambers (DSI; Minnesota, US) (Figure 2-5). Eight chambers (that were run concurrently) were each connected to an Aerogen nebuliser (DSI), thereby allowing 8 animals to be exposed to a tussive challenge aerosol at once. Coughs were quantified as previously described (Birrell et al., 2009, Maher et al., 2009, Bonvini et al., 2016) by using a combination of the following: a pressure transducer connected to a computer showed the airflow inside the chamber in real time (Figure 2-5), therefore any large inhalations and exhalations performed by the animal could be assumed to be a cough; a microphone was also placed inside the chamber so that coughs could be identified aurally; and finally, the animals were filmed (Bird Box Camera, Spy Camera CCTV; Bristol, UK) within the chamber so that the characteristic changes in posture and abdominal contractions that accompany a cough, could be identified retrospectively. The coughs were always counted by at least two trained observers that were blinded to the treatment, thus eliminating the risk of confirmation bias.

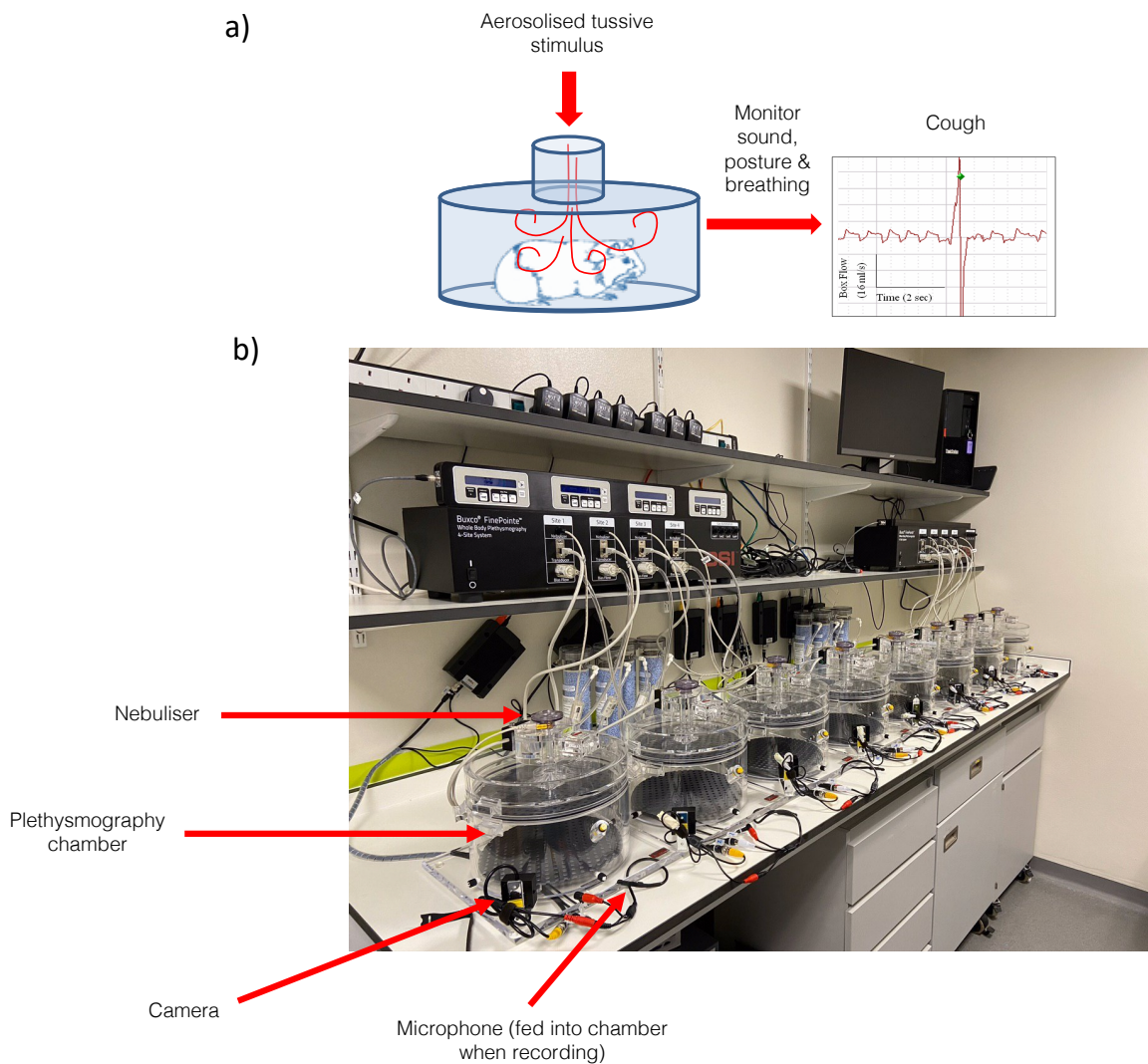


Figure 2-5 Aerosol-induced guinea pig cough model.

*a) a schematic to illustrate the induced cough model and the way by which data is acquired. b) a photograph of the cough system showing the central nebuliser units, the connected plethysmography chambers, cameras and microphones*

For antagonist studies, the guinea pigs were dosed with the antagonist compound at a specific time prior to being challenged with the aerosolised tussive agent. Following administration of the antagonist compound, the animals were monitored for signs of adverse effects. Finally, after the experiment was completed, the animals were euthanised with an overdose of pentobarbitone (Section 2.2).



## 3 Developing an *in vivo* model of fibrosis-induced spontaneous cough

### 3.1 Rationale

Idiopathic Pulmonary Fibrosis (IPF) is a respiratory disease with a high level of morbidity and mortality. As well as shortness of breath, patients often suffer from chronic, unproductive cough (Hope-Gill et al., 2003). Chronic cough is a distressing symptom which dramatically impacts the quality of life in patients with IPF (Key et al., 2010). There is therefore an urgent need to understand what drives this symptom and to seek out appropriate avenues for therapeutic intervention. Typically, cough is modelled by exposing guinea pigs or humans to inhaled tussive, challenge agents (Bonvini et al., 2015). Recent findings have shown, however, that just because a therapy is capable of altering a chronic cough patient's cough reflex sensitivity to an inhaled challenge agent, it does not necessarily mean that the same therapy will reduce their spontaneous cough frequency. A notable example of this discrepancy was with XEN-DE501, a TRPV1 antagonist that was capable of reducing guinea pig and chronic cough patient sensitivity to capsaicin-induced cough, yet had no effect on patient objective cough frequency (Belvisi et al., 2017).

The aim of this chapter was to determine if we could detect spontaneous cough in a bleomycin-driven guinea pig model of lung fibrosis. Having a model that more closely recapitulates the cough seen in patients than the current cough challenge models will hopefully allow for a greater understanding of disease pathophysiology and a more appropriate platform to test novel antitussive therapeutics.

#### 3.1.1 Chapter Hypothesis

Guinea pigs that develop pulmonary fibrosis through intratracheal bleomycin instillation go on to develop a spontaneous cough akin to IPF patients

#### 3.1.2 Aims

- Develop a CCTV monitoring system that allows for the assessment of cough in guinea pigs. Test this system on capsaicin-induced cough to determine if it is capable of recording cough in a way that can be interpreted through retrospective manual observation
- Develop and characterise a model of fibrosis by measuring the following in bleomycin-treated guinea pigs through a dose response and time course response:
  - The weight of the animals' lungs to detect hypertrophy of the organ
  - Assess the severity of fibrosis histologically using:

- A modified version of the Ashcroft score, a semi quantitative fibrosis scoring system (Hubner et al., 2008)
- An objective, automated quantification imaging app running within Visiopharm® Software
- Immunohistochemical staining for alpha smooth muscle actin ( $\alpha$ -SMA), a marker of myofibroblast formation (Nagamoto et al., 2000)
- The concentration of hydroxyproline in the lung, a biomarker for collagen deposition (Srivastava et al., 2016)
- The expression in the lung of genes relating to fibrosis and extracellular matrix production
- The total leukocytes in the bronchoalveolar lavage as a marker for inflammation
- Complete an initial dose response at n=2 to bleomycin and assess these animals for spontaneous cough through retrospective observation of ‘dusk’ and ‘dawn’ periods (the time at which the animals are most active) over a 3-week incubation period
- Take forward a submaximal dose and assess this dose for spontaneous cough at n=6 for ‘dusk’ and ‘dawn’ periods
- Investigate whether vagus nerve tissue show an altered sensory nerve phenotype when exposed to different protussive stimuli

## 3.2 Methods

### 3.2.1 Recording guinea pigs through a CCTV system

In order to be able to record guinea pigs within their individually ventilated cages (IVCs) so that spontaneous cough could be assessed, a Closed-Circuit Television (CCTV) monitoring system was developed. We used ‘Bird box’ cameras (Spy Camera CCTV, UK) because of their wide-angle lenses, compact design and inbuilt infrared night vision, which allowed filming to keep the entire cage in frame and also take place during the 12-hour dark period of the animals’ 24-hour lighting cycle.

To ensure guinea pig coughs were as audible as possible, an inline audio microphone with loop through power was fed through the IVC’s microbiological filter and attached to the top of the IVC’s interior with Blu Tak.

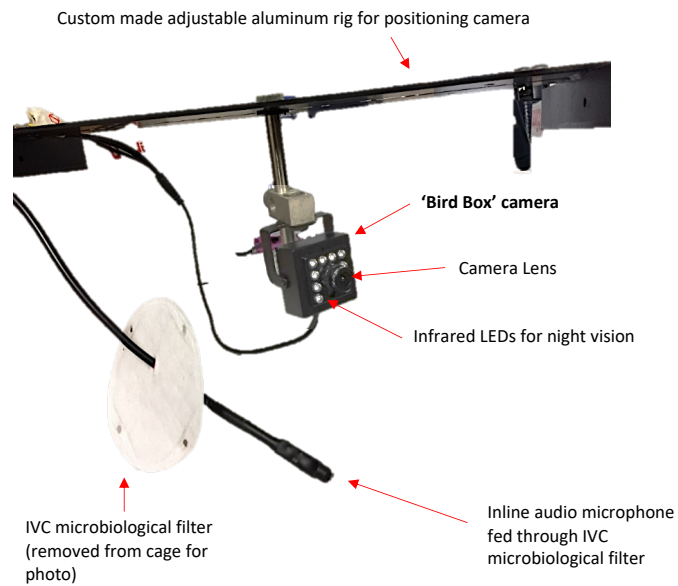


Figure 3-1 Development of an *in vivo* CCTV monitoring system.

**Top** – A diagram to show the camera and microphone equipment used for observing the animals. **Bottom** – Original test footage of guinea pigs within an IVC.

### 3.2.1.1 Validating CCTV cough surveillance system with aerosolised capsaicin

To ensure our monitoring system enabled guinea pig coughs to be observed, we aerosolised capsaicin into the IVC as a positive control. Due to their highly social nature, it is important for guinea pigs to be housed in groups of at least two (Fenske, 1992, Sachser and Lick, 1991), and as such, all CCTV observational experiments (including this one) implemented this welfare requirement. In order to tell them apart, two male Dunkin-Hartley guinea pigs (300-400g) had their fur labelled with a black marker pen; this was done by marking the fur of one animals' neck and marking the fur of the other animal's rear. By labelling the animals in this way, it allowed trained observers to precisely tally which coughs belonged to which guinea pig, thereby facilitating the collection of more precise data. Throughout the experiment the two animals were constantly filmed with the CCTV

system, so that their coughs could be counted. Lab personnel made a note of the time at the beginning and end of each experimental phase. The animals first underwent an initial 20-minute baseline recording. Next, using a nebuliser pump, the animals were then exposed to nebulised vehicle (1% ethanol + 1% Tween80 in saline) for 5 minutes. The aerosol entered the IVC through the hole normally occupied by the water pouch's mouthpiece. Once this was complete, the nebuliser was turned off, and the animals continued to be recorded for a further 15 minutes. After this, capsaicin (60  $\mu$ M) was then nebulised into the IVC for 5 minutes. Once the 5 minutes was up, the nebuliser was switched off and the animals continued to be monitored for a further 15 minutes. Finally, the animals were euthanised as previously described (Section 2.2). The footage was later watched back and the capsaicin-induced coughs were quantified.

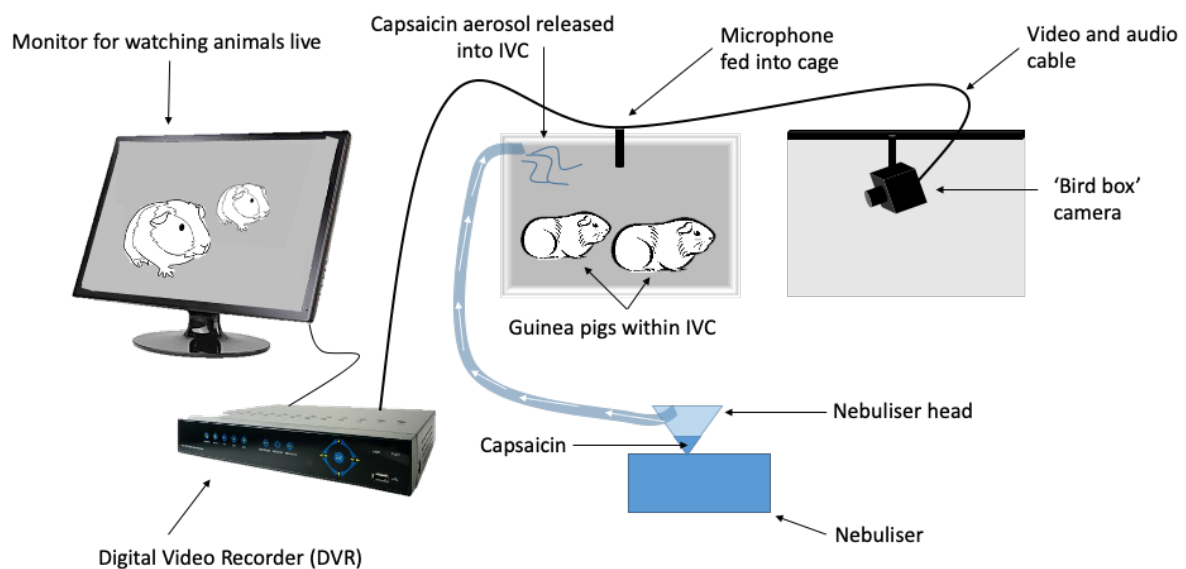


Figure 3-2 Recording capsaicin-induced cough within guinea pig IVCs.

*A schematic to illustrate the CCTV system and nebuliser system where footage of capsaicin-induced cough was recorded as a positive control, thereby ensuring the camera and microphone set-up could be used for assessing bleomycin-treated guinea pigs for spontaneous cough*

### 3.2.2 Bleomycin dose response experiment

This section describes the work undertaken to evaluate what doses of bleomycin caused lung fibrosis in guinea pigs and whether any of these doses were also capable of causing spontaneous cough. The animals were incubated with bleomycin for a total of 3 weeks before termination; the animals were also weighed daily and assessed for distress throughout the study.

#### 3.2.2.1 Bleomycin and its nomenclature

Bleomycin is a chemotherapeutic, antibiotic, peptide produced by *Streptomyces verticillatus* (Adamson and Bowden, 1974), that is used to treat squamous cell carcinomas, testicular cancer and malignant lymphomas (Bennett and Reich, 1979). Its mechanism of action is through the induction of

single and double stranded DNA breaks, thereby interrupting the cell cycle of relentlessly dividing tumour cells. Bleomycin is thought to be able to perform this by chelating metal ions, and in doing so, forming a pseudoenzyme with oxygen, which is capable of producing DNA-cleaving superoxide and hydroxyl radicals (Claussen and Long, 1999). Due to it having the unfortunate adverse effect of instigating lung fibrosis in some patients (Hay et al., 1991, Jules-Elysee and White, 1990), it was adopted as an *in vivo* model of IPF. These adverse effects from bleomycin chemotherapy are believed to be isolated to the lung because of the organ's relative lack of expression of bleomycin hydrolase, a bleomycin inactivating enzyme (Jona et al., 2016, Onuma et al., 1974). Despite being unable to replicate the slow, irreversible disease progression seen in IPF patients, the bleomycin-induced fibrosis model still mirrors many of the specific molecular changes of the disease, *e.g.* expression of the pro-fibrotic cytokine transforming growth factor beta (TGF- $\beta$ ) (Higashiyama et al., 2007).

Bleomycin has historically been measured in milligram-potency, where 1 mg-potency corresponded to 1 unit in the United State Pharmacopeia (USP), which was also equivalent to 1 mg of bleomycin by weight (Stefanou, 2001). Due to improvements in the purifying process, 1 USP unit of bleomycin now weighs less than 1 mg, but the exact weight of 1 USP unit varies by manufacturer. Despite this ambiguity, studies are still regularly published with bleomycin referred to by its weight. To add further confusion, the British Pharmacopoeia and European Pharmacopoeia measure bleomycin in 'International Units' (IU), which is equivalent to 1/1000<sup>th</sup> of 1 USP. Unsurprisingly this has led to cancer patients being prescribed an incorrect dose (Stefanou, 2001), as well as some *in vivo* studies incorrectly labelling their bleomycin units as IU, instead of USP or *vice versa*. For instance, a study published in Clinical Science in 2015 by Fernández-Blanco *et al* mistakenly referred to intratracheally dosing guinea pigs with 8 IU/kg bleomycin, a dose that would have had little, if at all any, effect on the animal. To avoid confusion, throughout this chapter we have opted to use USP units to describe the bleomycin doses that were intratracheally instilled.

### 3.2.2.2 Selection of doses for bleomycin dose response

The dose response experiment was begun by intratracheally instilling bleomycin (Baxter Oncology GmbH, Germany) into the lungs of guinea pigs (Section 3.2.2.3), using the doses 0 (Saline vehicle), 2, 4, 6, & 8 USP/kg. Due to concern regarding bleomycin's cytotoxicity, the doses instilled did not exceed that which had already been found to be tolerable and effective in the literature (Cisneros-Lira et al., 2003, Brozmanova et al., 2004).

An initial pilot dose response study was performed at n=2, when all doses were to be tolerable, a further 4 animals were added to each dose group, bringing the study to n=6.

### 3.2.2.3 *Bleomycin intratracheal instillation*

Throughout each fibrosis study, and in accordance with Chiesi, our industrial collaborators, we utilised a double dosing regimen, whereby bleomycin was intratracheally dosed twice, three days apart, this was to help mimic the progressiveness of the fibrosis in IPF patients. To instil compounds accurately into the lungs, we used a rigid endoscope (Karl Storz Endoscopy, UK) that prior to being inserted into the animal's trachea, had been fed through a cannula (Vygon, UK).

Male Dunkin Hartley guinea pigs (220 - 320g) were anaesthetised by being exposed to 4% isoflurane at a rate of 4 litres/min, for between 3 and 4 minutes. Once the animal was sufficiently anaesthetised, it was suspended by its teeth on a surgical table using elastic bands at an angle of 60°. Following this, forceps were used to gently push the tongue towards the bottom of the animal's mouth whilst cotton wool buds were used to wipe away masticated food from within the animal's throat that might obscure the view of the endoscope. Next, the endoscope (with the catheter already having been slid onto it) was inserted into the animal's mouth, and by using the eyepiece, the operator moved the tip of the endoscope through the folds of the soft palate until they reached the glottis, whereupon they gently applied pressure until the endoscope was through the glottis and inside the trachea. The catheter was then slid off the endoscope and into the trachea and the endoscope was promptly withdrawn from the animal's throat, thereby leaving the animal intubated. Finally, bleomycin dissolved in medical saline (or saline alone in the case of vehicle groups) was then intratracheally instilled at a volume of 1ml/kg, the animal's chest was gently massaged to aid its distribution, the catheter was removed, and the animal was left to recover from its anaesthesia under watchful supervision. Throughout the rest of the day, the welfare of the animal was checked at regular intervals.

### 3.2.2.4 *Spontaneous cough monitoring*

Guinea pigs were housed in pairs within IVCs, with each animal's cage-mate being another animal on the same treatment. Animals were fed *ad libitum* and lived through 12:12 hour light/dark cycles, with the daylight phase taking place from 07:00 until 19:00. The bird box cameras (3.2.1) recorded the animals for 24 hours a day, 7 days a week. To aid us in telling the animals apart within a cage, we coloured a small part of the animals' fur in with a permanent marker pen.

Each day, footage recorded onto the CCTV Digital Video Recorder (DVR; Gamut, UK) was backed-up onto a portable hard drive. Later, this footage was watched back on a separate computer using the DVR's accompanying software, with up to 8 cages being watched simultaneously using a dual screen set up. Coughs were manually confirmed by listening out for its high pitched and highly characteristic sound (the result of the abdominal muscles forcing air through a closed glottis) and

then further confirmed by observing the animals' typically stretched out posture and explosive contraction of the abdominal muscles. Once a cough was confirmed, the time and date were noted, and a short video clip of the event was exported for any further auditing.

Quantifying coughs through retrospective manual observation was a highly time-consuming process; because of this, the guinea pigs from the three-week dose response were not all monitored for 24 hours a day. Instead, all animals within the  $n=2$  pilot study were initially monitored for approximately 4 hours a day, 2 hours at what equated to the animals' dawn within their 12/12 light dark cycle and 2 hours at the animals' dusk period. This was on the advice of the facility's veterinarian that guinea pigs are crepuscular animals in order to avoid predation (Terril et al., 1998); incidentally, IPF patients tend to cough much less at night time (Key et al., 2010). Next, a submaximal dose and the vehicle dose were brought to  $n$  of 6 for each dusk and dawn period of the three-week experiment. Finally, to make the data more comparable to the 24-hour ambulatory cough recordings of patients made by our collaborators at the University of Manchester, we picked two separate days for which the submaximal dosing groups' cough rates were highest, and performed a 24 hour assessment on these days.

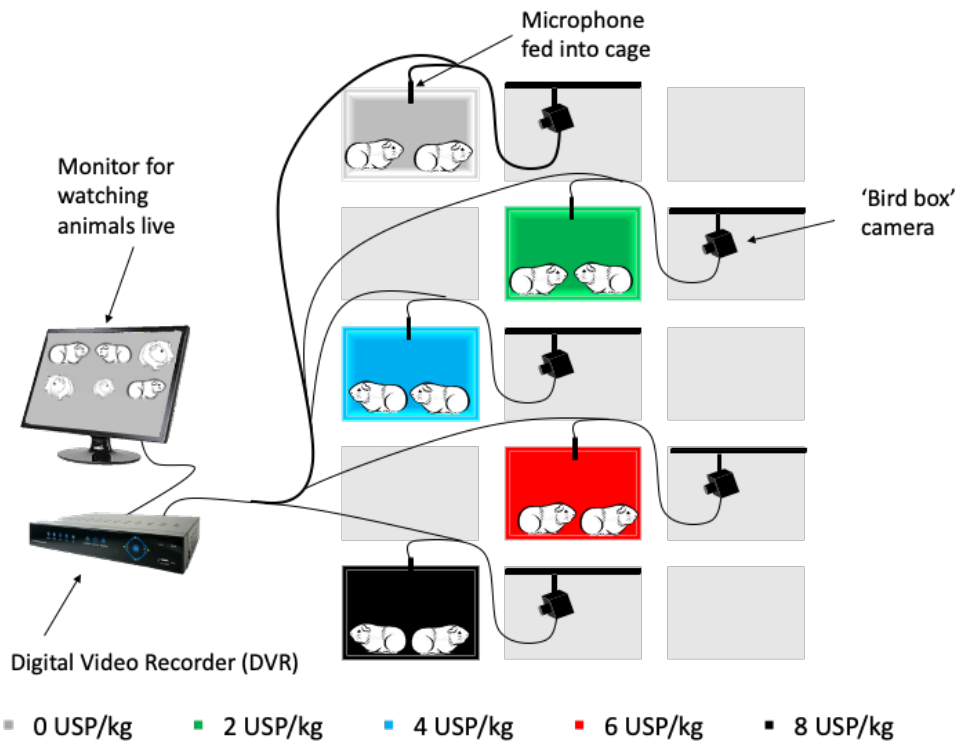


Figure 3-3 Schematic of cage monitoring set up for spontaneous cough pilot study.

Each pair of animals were intratracheally instilled with a different dose of bleomycin (Cage colours correspond to the doses beneath). Throughout the study, each cage was recorded with night-vision enabled CCTV using bird box cameras.



Figure 3-4 Screenshot of CCTV playback software.

Pictured is a screenshot showing a recording from the vehicle-treated group. Notice the animal on the right's posterior has been marked to distinguish it from the other animal.



### 3.2.2.5 Dissection, macroscopic assessment and storage of heart and lungs

After the animals had been incubated with bleomycin for 3 weeks, the animals were euthanised through an overdose of pentobarbitone (see Section 2.2), the animals' vagal tissue was then removed (as described in Section 2.4.1) to assess for changes in neurophenotype (see Section 3.2.2.9). After cutting the trachea beneath the larynx, the heart and lungs were then removed together, washed with saline, and photographed. The lungs were weighed *en bloc* as an initial marker for fibrosis. To assess right ventricle hypertrophy, a marker of pulmonary burden, the heart was first weighed without its atria, leaving the left and right ventricles and the septum intact, before removing right ventricle and weighing it separately. This data was presented as:

$$\frac{\text{Right Ventricle Weight}}{\text{Left Ventricle+Septum Weight}}$$

The left lobes of the lung were cut into pieces and flash frozen in liquid nitrogen, before being stored at 80°C for future gene expression and collagen assessment.

### 3.2.2.6 Histology preparation

After inserting a cannula into the trachea, the right side of the lung was inflated with 10% buffered neutral formalin, this was achieved by ligaturing the left primary bronchus and connecting the intubated trachea to a gravity assisted formalin-dispensing system. After inflation, the trachea was ligatured and the lungs were stored in 10% buffered neutral formalin for between 24 and 48 hours at room temperature. After this time was up, the lungs were transferred to 70% ethanol, where they remained for up to one month and at 4°C.

Later, the right caudal lobe (Figure 3-5) was removed from the remaining fixed lung tissue, placed within an embedding cassette and delivered to the onsite histologist (Stan, 2015). Once there, it was processed through a graded series of alcohols and xylene, prior to paraffin embedding. Finally, the paraffin-embedded tissue was sliced into 4µm sections in an orientation as to maximise surface area.

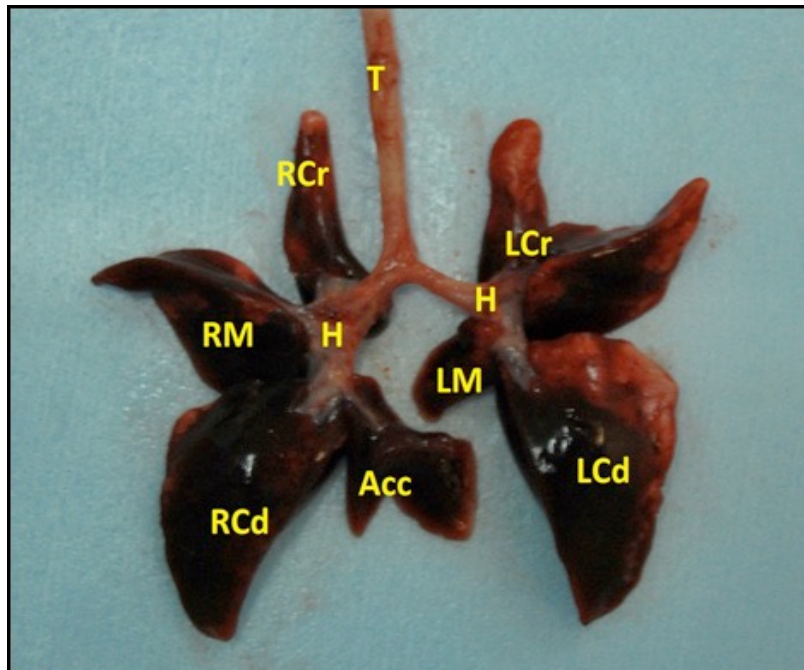


Figure 3-5 Anatomical photograph of the guinea pig lung.

A photograph to illustrate the different lobes within a guinea pig's lungs. T-trachea; RCr-right cranial lung lobe; RM-right medial lung lobe; RCd-right caudal lung lobe; Acc-accessory lobe; H-hilus. Adapted from Stan, F. G. 2015.

#### 3.2.2.7 Ashcroft assessment of fibrosis

One way by which we assessed fibrosis was through using a modified version of Ashcroft et al's scoring system (Ashcroft et al., 1988, Hubner et al., 2008). This semi-quantitative scoring system grades the lung by assessing fibrotic changes to the microscopic, alveolar architecture (Table 3-1).

4  $\mu$ M thick coronal sections of the right caudal lung lobe were stained with H&E or Sirius Red. Three blinded assessors were asked to grade different pictures of the lung, captured from a microscope at 10x and 20x magnification, their scores for each animal were then compiled and averaged to generate a mean Ashcroft score.

Table 3-1 Modified Ashcroft Scale from Hubner et al., 2008

Grade of Fibrosis	Modified Scale
0	<b>Alveolar Septa:</b> No fibrotic burden at the most flimsy small fibres in some alveolar walls <b>Lung Structure:</b> Normal Lung
1	<b>Alveolar Septa:</b> Isolated gentle fibrotic changes (septum $\leq 3x$ thicker than normal) <b>Lung Structure:</b> Alveoli partly enlarged and rarefied, but no fibrotic masses
2	<b>Alveolar Septa:</b> Clearly fibrotic changes (septum $>3x$ thicker than normal) with knot-like formation but not connected to each other <b>Lung Structure:</b> Alveoli partly enlarged and rarefied, but no fibrotic masses
3	<b>Alveolar Septa:</b> Contiguous fibrotic walls (septum $>3x$ thicker than normal) predominantly in whole microscopic field <b>Lung structure:</b> Alveoli partly enlarged and rarefied, but no fibrotic masses
4	<b>Alveolar Septa:</b> Variable <b>Lung Structure:</b> Single fibrotic masses ( $\leq 10\%$ of microscopic field).
5	<b>Alveolar Septa:</b> Variable <b>Lung Structure:</b> Confluent fibrotic masses ( $>10\%$ and $\leq 50\%$ of microscopic field). Lung structure severely damaged but still preserved
6	<b>Alveolar Septa:</b> Variable, mostly not existent <b>Lung Structure:</b> Large contiguous fibrotic masses ( $>50\%$ of microscopic field). Lung architecture mostly not preserved
7	<b>Alveolar Septa:</b> Non-existent <b>Lung Structure:</b> Alveoli nearly obliterated with fibrous masses but still up to five air bubbles
8	<b>Alveolar Septa:</b> Non-existent <b>Lung Structure:</b> Microscopic field with complete obliteration with fibrotic masses

### 3.2.2.8 *Visiopharm App automated analysis of fibrosis*

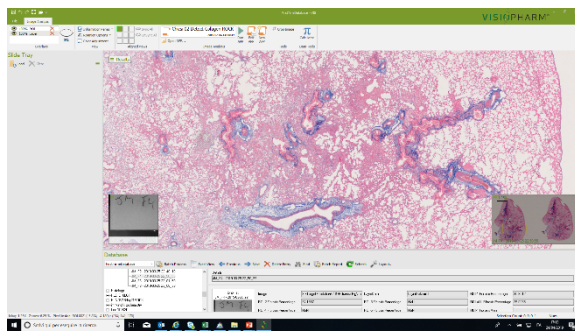
Whilst it is relatively easy to assess lung sections using the Ashcroft score, it has two main disadvantages: firstly, its subjectivity, sometimes leading to large variations between assessors' scores; and secondly, its lack of scope, it would be time consuming to assess the entire lobe section using the scoring system, so instead, the assessors view multiple representative microscope fields to create their score. For these reasons, it is beneficial to use an objective and automated form of

assessment, capable of assessing the entire section, hence why Visiopharm (Hørsholm, Denmark), a histopathology image analysis software package, was used.

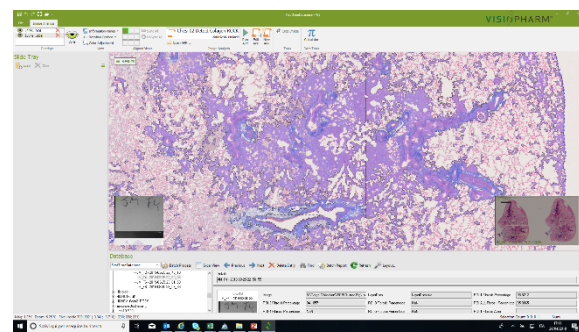
4  $\mu\text{M}$  thick coronal sections of the right caudal lung lobe were stained with Heidenhain's Azan trichrome stain, a variation of Mallory's trichrome stain, where azocarmine G (rather than acid fuchsin) is used, followed by a solution containing PTA, orange G and aniline blue. This method stains cell nuclei dark red, the cytoplasm a variety of colours and collagen blue (Heidenhain, 1915).

Images of the slides were then captured on a high-throughput scanner and imported into Visiopharm. Using this software it was possible to write "Apps". Chiesi (the industrial partner of this PhD project), had created and validated two such apps that could quantify the fibrosis. One was an App that quantified the proportion of slide tissue that was fibrotic, the other was an app that quantified the proportion of slide tissue that was collagen.

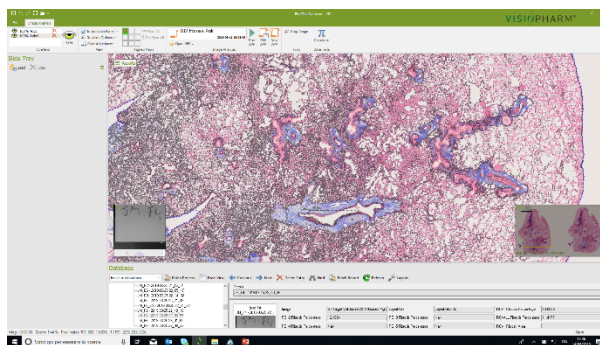
a)



b)



c)



*Figure 3-6 Screenshots of the Visiopharm software package.*

***Figure 3-6a)** A screenshot of Visiopharm software showing a magnified section of guinea pig lung being viewed. **Figure 3-6b)** A screenshot of the app as it identifies fibrotic tissue within the same microscopic field as (a) (highlighted in violet). **Figure 3-6c)** A screenshot of the app as it identifies collagen within the same microscopic field as (a) (highlighted in grey)*

### 3.2.2.9 Assessment for altered sensory nerve phenotype using in vitro isolated vagus nerve model

To check for an altered sensory nerve phenotype, the vagus nerves of the animals intratracheally instilled with saline vehicle and bleomycin were exposed to a variety of proven or hypothesised

protussive stimuli (Table 3-2). Both the animal's vagal nerves were isolated from vagal tissue and cut into two pieces, then kept in KH solution until required. Vagus nerves were assayed using the O<sub>2</sub>/CO<sub>2</sub> gassed, grease-gap recording system as previously described (Section 2.4).

*Table 3-2 The various protussive stimuli that the vagus nerves deriving from bleomycin-treated guinea pigs were exposed to, in the isolated vagus nerve model*

<b>Protussive Stimulus</b>	<b>Protussive Protein Target(s)</b>	<b>Reference</b>
<b>Acrolein</b>	TRPA1	Birrell et al. (2009)
<b>alpha,beta-methylene-ATP</b>	P2X3	Bonvini et al. (2016)
<b>Capsaicin</b>	TRPV1	Belvisi et al. (2017)
<b>Prostaglandin E<sub>2</sub></b>	EP <sub>3</sub>	Maher et al. (2009)
<b>GSK1016790A</b>	TRPV4	Bonvini et al. (2016)
<b>-80mOsm, +300mOsm</b>	TRPV4	Bonvini et al. (2016)
<b>Substance P</b>	Neurokinin-1 (NK1)	Smith et al. (2020a)
<b>2-Furoyl-LIGRLO</b>	PAR2	Gatti et al. (2006)
<b>Citric Acid</b>	TRPV1, acid sensing ion channels (ASICs), TRPA1	Rai et al. (2018)

The pieces were perfused with the following tussive stimuli, in the order written:

Piece 1: CIM0216 (1uM), 0mOsm, -80mOsm, Acrolein (300uM)

Piece 2: Substance P (1uM), +300mOsm, Vehicle (water), alpha,beta-methylene-ATP (100uM)

Piece 3: 2-Furoyl-LIGRLO (10nM), SLIGKV (100nM), Vehicle, Capsaicin (1uM)

Piece 4: Prostaglandin E<sub>2</sub> (10uM), AC55541 (1uM), GSK1016790A (300nM), Citric Acid (30mM)

### 3.2.3 Bleomycin time course experiment

The physiological response to bleomycin *in vivo* models is known to be formed of two phases: an inflammatory phase and a fibrotic phase (Moeller et al., 2008). To determine when these phases occurred in the guinea pigs and to further characterise the model with the aim of eventually introducing antitussive therapeutics into it, a time course response experiment to bleomycin was undertaken. The animals were intratracheally dosed with either saline vehicle or the submaximal concentration selected from the previous study. The guinea pigs were incubated with bleomycin for 1, 2, 3 or 4 weeks and weighed daily, following which they were euthanised (Section 2.2).

### *3.2.3.1 Bronchoalveolar lavage, surgery and organ storage*

Once death had been confirmed, a tracheostomy was performed, thereby allowing for the insertion of a cannula. 4ml of 4°C RPMI medium was then injected into the lungs and retained inside for 20 seconds before being withdrawn, this was then repeated with another 4ml of fresh RPMI medium. The bronchoalveolar lavage fluid (BALF) was then promptly placed into ice before being processed for future analyses (3.2.3.4).

### *3.2.3.2 Histology preparation, staining and assessment*

After inserting a cannula into the trachea, the lung was inflated with formalin as described previously (3.2.2.6), however this time the lungs were kept within the animal's body, as this study did not require that they be weighed.

Fibrosis assessment through Ashcroft scoring and automated analysis with Visiopharm software was then completed (previously outlined in sections 3.2.2.7 and 3.2.2.8, respectively)

### *3.2.3.3 Immunohistochemical staining for alpha smooth muscle actin*

In order to be able to visualise myofibroblasts, the cells responsible for extracellular matrix deposition in IPF and in the bleomycin model, we immunostained for alpha smooth muscle actin ( $\alpha$ -SMA).  $\alpha$ -SMA is a distinctive biomarker for myofibroblasts (Nagamoto et al., 2000), but it is also highly involved in the contractile apparatus of smooth muscle (Skalli et al., 1986).

Paraffinised sections were first deparaffinized by being placed in xylene twice for 5 minutes in between being rinsed with distilled water. The sections were then hydrated by being immersed within 100% ethanol for 3 minutes in between being rinsed with distilled water. Finally, the sections were hydrated once more by being placed in 95% ethanol for 1 minute, before being rinsed with distilled water.

The tissue sections were then pre-treated with 70% HCl (v/v in distilled water), twice for 5 minutes, in between being rinsed with distilled water.

Next, the sections were rinsed in PBS-Tween 20 twice, for 2 minutes each time. To block non-specific binding, the sections were then incubated with 5% normal donkey serum in 0.1 % Triton-X PBS. To bind the primary antibody, the sections were incubated overnight at 4°C with 'rabbit polyclonal anti-alpha smooth muscle actin' (ab5694; Abcam, UK), diluted 1:200 in the blocking solution above.

Unbound primary antibody was then washed off by rinsing the lung section in PBS-Tween 20 for 10 minutes, 3 times. The second antibody was then bound by incubating the section in 'Donkey anti-Rabbit IgG (H+L) Highly Cross-Adsorbed Secondary Antibody, Alexa Fluor Plus 555' (A32794; Thermo

Fisher Scientific, UK) in PBS for 1 hour. After this, unbound secondary antibody was washed off by being rinsed with PBS for 10 minutes, 3 times.

Lastly, the sections were mounted with 'ProLong™ Gold Antifade Mountant with DAPI' (P36931; Thermo Fisher Scientific, UK) covered with a cover slip, and stored in the dark at 4°C until use.

#### 3.2.3.4 Processing BALF and quantifying inflammatory cell counts

To determine inflammatory status, 800µL of neat BALF was collected and centrifuged (800xg, 10 mins, 4°C). Supernatant was collected and stored (-80°C), and cell pellet was resuspended (200µL, RPMI), total leukocytes were attained using a Sysmex XP-300 automated cell counter (Sysmex Ltd, Milton Keynes, UK).

For differential cell counting, cytopsin slides were prepared using 100µL of neat BALF, centrifuged (700rpm, 5 mins, RT, low acceleration; Cytospin 2, Shandon, Runcorn, UK). The slides were then stained with Wright-Giemsa. The quantity of macrophages, lymphocytes, eosinophils and heterophils (the guinea pig equivalent of neutrophils)(Godlewski et al., 1999) in each slide was then assessed. A table with the criteria for differential cell counting using guinea pig BAL can be found in the appendix (Table 10-1).

### 3.2.4 Measurement of mRNA levels to assess fibrosis-related gene expression

#### 3.2.4.1 RNA Extraction and Purification from Lung Parenchyma

In order to investigate changes in gene expression from within the fibrotic lung, it was first necessary to extract its RNA. To do this, we used the *RNeasy Mini Kit* (Qiagen, UK), a commercially available kit that utilises the guanidine-isothiocyanate lysis technique, a method that was first established in 1986 by Chomczynski and Sacchi.

To begin with, frozen lung tissue fragments from the left cranial lobe of the guinea pig were removed from a -80 °C freezer and pulverised into a fine powder using a pestle and mortar, in the presence of liquid nitrogen. Approximately 30 mg of frozen pulverised lung powder was then decanted into an autoclaved 2 ml microcentrifuge tube. 600 µl of the kit's lysis buffer (*Buffer RLT Plus*) was added to the lung powder, which was then vortexed until the tissue had lysed and dissolved. If the tissue did not dissolve readily, a hypodermic needle and syringe was also used to fully dissociate the tissue. The lysate was then centrifuged at maximum speed for 3 minutes following which the supernatant was carefully removed and placed inside the kit's *gDNA Eliminator spin column*, which itself was placed on top of a 2 ml collection tube. Next, to remove DNA from the sample, the column was centrifuged for 30 seconds at  $\geq 8000 \times g$ . A volume of 600 µl of 70% ethanol was added to the flow-through and mixed by pipetting. A volume of 700 µl of the sample was then

transferred to the *RNeasy spin column*, this was centrifuged for 15 seconds at  $\geq 8000 \times g$ , following which the flow-through was discarded. Next, 700  $\mu\text{l}$  *Buffer RW1* was added to the *RNeasy spin column*, which was again centrifuged for 15 seconds at  $\geq 8000 \times g$ , following which the flow-through was discarded. This step was repeated, but 500  $\mu\text{l}$  *Buffer RPE* was used instead of 700  $\mu\text{l}$  *Buffer RW1*. This was then repeated using 500  $\mu\text{l}$  *Buffer RPE* again, however this time, it was centrifuged for 2 minutes instead of 15 seconds. Lastly, the *RNeasy spin column* was placed within a new 1.5 ml collection tube and 50  $\mu\text{l}$  of RNase-free water (provided by the kit) was pipetted directly onto the column's membrane; it was then centrifuged for a final 1 minute at  $\geq 8000 \times g$  to elute the RNA.

#### 3.2.4.2 RNA measurement and cDNA Synthesis

Prior to reverse transcription, the RNA extract quantity and quality had to first be measured, this was performed by utilising a *NanoDrop Spectrophotometer* (Thermo Fisher Scientific, UK), and an *RNA ScreenTape* and *TapeStation* system (Agilent, US), respectively. *TapeStation* is an automated electrophoresis system that generates an RNA integrity number equivalent (RIN<sup>e</sup>) between 1 and 10; the higher the RIN<sup>e</sup> the more intact the RNA. We ensured all RNA samples had a RIN<sup>e</sup> of  $>7$  prior to reverse transcription. Once the concentration of each of the RNA samples had been quality checked and quantified, it was then diluted to 100 ng/ $\mu\text{l}$  in RNase free water.

In order to reverse transcribe the RNA samples into cDNA, we used *TaqMan Reverse Transcription Reagents* (Thermo Fisher Scientific, UK). For each reaction, 5  $\mu\text{l}$  of RNA sample was combined with the following reagents provided by the kit, inside an autoclaved 500  $\mu\text{l}$  micro centrifuge tube: 11  $\mu\text{l}$   $\text{MgCl}_2$  solution, 10  $\mu\text{l}$  dNTP Mixture, 2.5  $\mu\text{l}$  Random Hexamers, 1  $\mu\text{l}$  RNase Inhibitor, 1.25  $\mu\text{l}$  MultiScribe™ Reverse Transcriptase and 14.25  $\mu\text{l}$  RNase free  $\text{H}_2\text{O}$ . RNA samples were next incubated in a thermal cycler (model 480; Perkin Elmer, US) where they were exposed to the following: 25°C for 10 minutes, 48°C for 30 minutes and 95°C for 2 minutes. The resulting cDNA transcripts had a concentration of approximately 10 ng/ $\mu\text{l}$ , and were promptly diluted down to 2.5 ng/ $\mu\text{l}$  using RNase free water and stored at -80°C for future TaqMan real-time Polymerase Chain Reaction (PCR).

#### 3.2.4.3 TaqMan real-time PCR

TaqMan real-time PCR allows for quantitation of gene expression because it measures PCR amplification as it occurs, during the exponential growth phase. The principle behind real-time PCR is much the same as ordinary PCR, however in addition to the two PCR primers, there is a TaqMan probe; the combination of primers and the TaqMan probe is often referred to as an Assay On Demand (AOD). This probe is a sequence specific oligonucleotide that has a fluorophore or "reporter" molecule covalently attached to the 5'-end, and a quencher molecule at the 3'-end. Upon excitation by the cycler's light source, the fluorescence emitted by the fluorophore would ordinarily be



quenched by the quencher molecule, via Förster resonance energy transfer (FRET), due to their proximity. However, as the Taq polymerase extends the annealed primer, its 5' to 3' exonuclease activity enables it to degrade the annealed probe. Once degraded, the fluorophore loses its proximity to the quenching molecule, thereby enabling it to fluoresce unimpeded. This means that the fluorescence detected by the cycler is directly proportional to the amount of DNA template present in the PCR.

There are a variety of different fluorophores and quenchers available for a TaqMan probe. Any AOD for a specific gene of interest was synthesised to contain Fluorescein amidites (FAM) as the reporter and a Non Fluorescent Quencher (NFQ). We also quantified the cDNA of 18s rRNA to use as a positive control and as a means to normalise the expression data of our target gene (see Analysis of Real Time PCR). As part of the ribosome, 18s is a highly and consistently expressed gene in all eukaryotic cells. Our 18s probes used FAM™ as the fluorophore and TAMRA™ as the quencher.

The cDNA transcripts were removed from the -80°C freezer and thawed slowly on ice. For each individual reaction, 3 µl of cDNA sample was combined with the following reagents inside the well of a 96-Well Skirted PCR Plate (all plates and reagents were obtained from Thermo Fisher Scientific, UK): 12.5 µl TaqMan™ Universal PCR Master Mix (this contained the Taq DNA polymerase), 1.25 µl AOD reagent (contains target gene specific primers and probe) and 18S internal control assay (contains specific primers and probe for 18S ribosomal RNA's cDNA transcript).

The plate was amplified using a *StepOnePlus* Real-Time PCR System Thermal Cycling Block (Applied Biosystems, United Kingdom) by executing the following cycles: cycle at 50°C for 2 minutes, 1 cycle at 95°C for 10 minutes, 40 cycles at 95°C for 15 seconds and finally the sample is kept for 1 minute at 60°C.

#### 3.2.4.4 Procuring an 'Assay on Demand' (AOD)

It is particularly ironic that despite the frequency of the idiom "guinea pig", commonly used to denote someone or something that is being used as the subject of an experiment, there remains a distinct lack of research regarding the guinea pig's (*Cavia Porcellus*) transcriptome when compared to other more commonly used lab animals *e.g.* the rat and the mouse. As a result of this, much of the mRNA transcripts listed for the guinea pig on the National Centre for Biotechnology Information's (NCBI's) Nucleotide Database are predicted, *i.e.* the corresponding genes have not been experimentally proven to be expressed yet.

Using the NCBI's nucleotide database we found the predicted sequences for the transcripts of our genes of interest and sent them to Thermo Fisher Scientific, so that they could design our AOD for

TaqMan real-time PCR. For reasons of corporate competitiveness, Thermo Fisher Scientific do not reveal where along the mRNA transcript the primers or the TaqMan probe correspond to, however any AOD made to order by Thermo Fisher Scientific is accompanied by a unique assay ID, and these will be made available to the reader on request. Due to the highly conserved sequence of 18s rRNA throughout all eukaryotes, real time PCR assays for 18s are relatively much more reliable.

#### 3.2.4.5 *Fibrosis related genes*

Four genes relating to fibrosis were chosen for expression quantification within the parenchyma of bleomycin or vehicle treated guinea pigs. Three of these genes encode structural proteins integral to the extracellular matrix (Frantz et al., 2010), they were: collagen type I alpha 1 (*COL1A1*), collagen type III alpha 1 (*COL3A1*) and fibronectin (*FN1X*). The other gene whose expression was quantified was alpha smooth muscle actin (*ACTA2*), a gene which is also highly expressed by myofibroblasts (Nagamoto et al., 2000).

#### 3.2.4.6 *Analysis of real time PCR*

Samples were analysed using the StepOne™ Software (Thermo Fisher Scientific, UK), the amount of target gene was normalised to the amount of 18s in the same cycle. Following guidelines from Thermo Fisher, a manually set threshold of fluorescence was set above the background signal noise, during the geometric (linear) phase of amplification; the number of cycles required for the fluorescence to rise above this threshold is known as the Threshold Cycle ( $C_t$ ). As  $C_t$  values are inversely proportional to the initial copy number of template cDNA, a lower  $C_t$  indicates a higher expression of target in the sample. Each sample's  $C_t$  for 18s was subtracted from the  $C_t$  of the target gene ( $\Delta C_t$ ). To account for the exponential amplification, the data was transformed to  $2^{-\Delta C_t}$ , and was multiplied by a factor of  $10^6$  for interpretability. Normalising expression data to 18s increases the reliability of comparing the expression of a particular target gene between samples, by accounting for any variations in the processes of mRNA extraction, reverse transcription or dilution.

#### 3.2.5 *Quantifying Hydroxyproline in left cranial lobe*

Hydroxyproline is a non-proteinogenic amino acid formed through the post-translational hydroxylation of proline. Its use in mammalian tissue is largely restricted to collagen, where it serves in a crucial, structural role by stabilizing its helical structure (Ramachandran et al., 1973).

A commercially available assay kit (MAK008; Sigma-Aldrich, UK) was used to assess hydroxyproline within the left cranial lung lobe of bleomycin treated guinea pigs. Briefly, the frozen left cranial lobes were removed from a  $-80\text{ }^\circ\text{C}$  freezer and pulverised into a fine powder using a pestle and mortar, in the presence of liquid nitrogen. 10 mg of tissue was added to 100  $\mu\text{l}$  of water and transferred to a

pressure-tight polypropylene vial with a PTFE-lined cap. Next the samples were hydrolysed by adding 100  $\mu$ l of concentrated hydrochloric acid (HCl, 12 M), and incubating them overnight at 100°C.

100  $\mu$ l of the kit's 'Chloramine T/Oxidation Buffer' was added to each sample and each standard's well, and incubated at room temperature for 5 minutes. Next, 100  $\mu$ l of the kit's 'Diluted DMAB Reagent' was added to each sample well and standard well, before being incubated for 90 minutes at 60°C. Finally, the absorbance of the plate was read at 560nm.

Data was then presented as mean hydroxyproline ( $\mu$ g) per mg of protein (protein concentration had been assayed prior using a standard Bradford assay (Bio-Rad, UK)).

### 3.2.6 Statistics

All data are presented as mean  $\pm$  SEM. Unless stated otherwise, the typical statistical test used to check for significance when comparing results from doses of bleomycin to vehicle was the Kruskal-Wallis test with Dunn's post-test. Unless stated otherwise, when comparing a single dose's results with vehicle, a nonparametric Mann Whitney test was used.

### 3.3 Results

#### 3.3.1 Capsaicin positive control cough response study

To determine whether the CCTV system was capable of recording cough adequately enough so that it could be retrospectively quantified, two guinea pigs were filmed after being exposed to nebulised capsaicin whilst within their IVC.

After analysing the footage, a total of 14 coughs were counted during and after capsaicin nebulisation, 10 coughs from guinea pig 1 (GP1) and 4 coughs from guinea pig 2 (GP2) (Figure 3-7). These coughs can be viewed within the supplementary PowerPoint file (Slides 2 & 3). The animals did not cough during the baseline recording or during the nebulisation of vehicle.

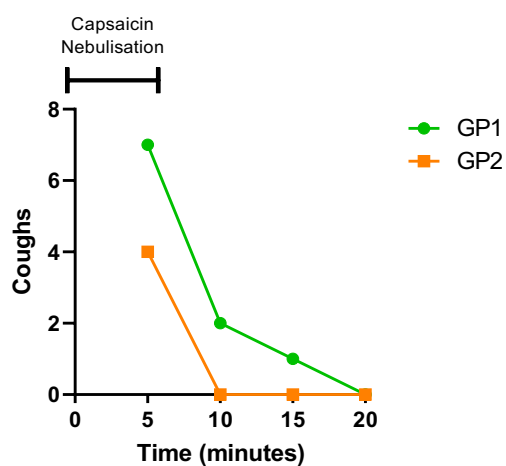


Figure 3-7 CCTV quantification of guinea pig coughs to aerosolised capsaicin.

*2 guinea pigs (GP1 & GP2) were filmed within their IVCs as a positive control in preparation for detecting cough in the bleomycin study. Coughs were counted over a total of 20 minutes from guinea pigs exposed to a 5-minute nebulisation of capsaicin.*

### 3.3.2 Bleomycin dose response study

#### 3.3.2.1 Animals weights throughout experiment and welfare

Nearly all of the animals completed the bleomycin dose response study without any issues. Only 2 of the 30 animals appeared to suffer any form of discomfort. One animal treated with 4 USP/kg was terminated early through pentobarbitone i.p. on the basis of it appearing more distressed following its second i.t. instillation, and another animal on the highest dose appeared more lethargic than the others, however the Named Animal Care & Welfare Officer (NACWO) did not deem this in excess of the 'moderate' category for this procedure. The rest of the animals appeared healthy and continued to gain weight throughout the study (Figure 3-8); a trend can be seen that shows the animals on the higher doses of bleomycin were slower to gain weight.

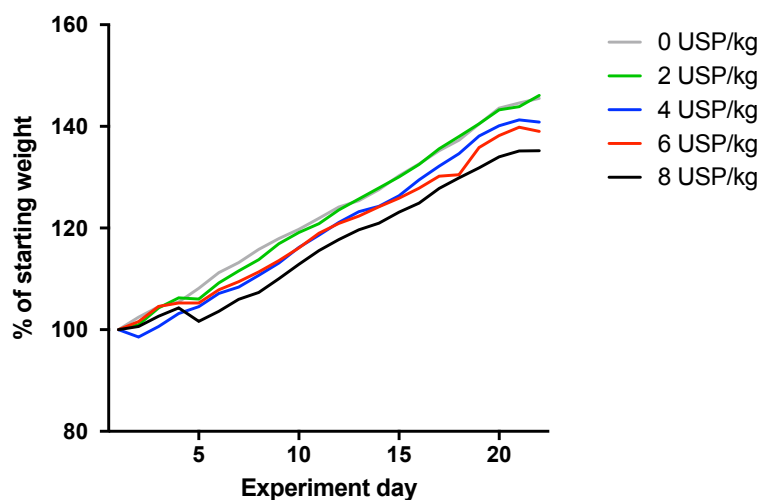


Figure 3-8 Mean body weight over time of guinea pigs treated with different concentrations of bleomycin.

The animals were intratracheally instilled with different concentrations of bleomycin and weighed daily for up to 3 weeks. Data shown as mean over time,  $5 \leq n \leq 6$ .

### 3.3.2.2 Lung weight and macroscopic appearance

The lungs of the animals treated with vehicle had a pink parenchyma and more malleable lobes, as the doses of bleomycin increased however, the parenchyma of the lungs became whiter and the lobes became more rigid, hypertrophic and misshapen (Figure 3-9). Some lungs on the higher doses also appeared to have haemorrhaging.

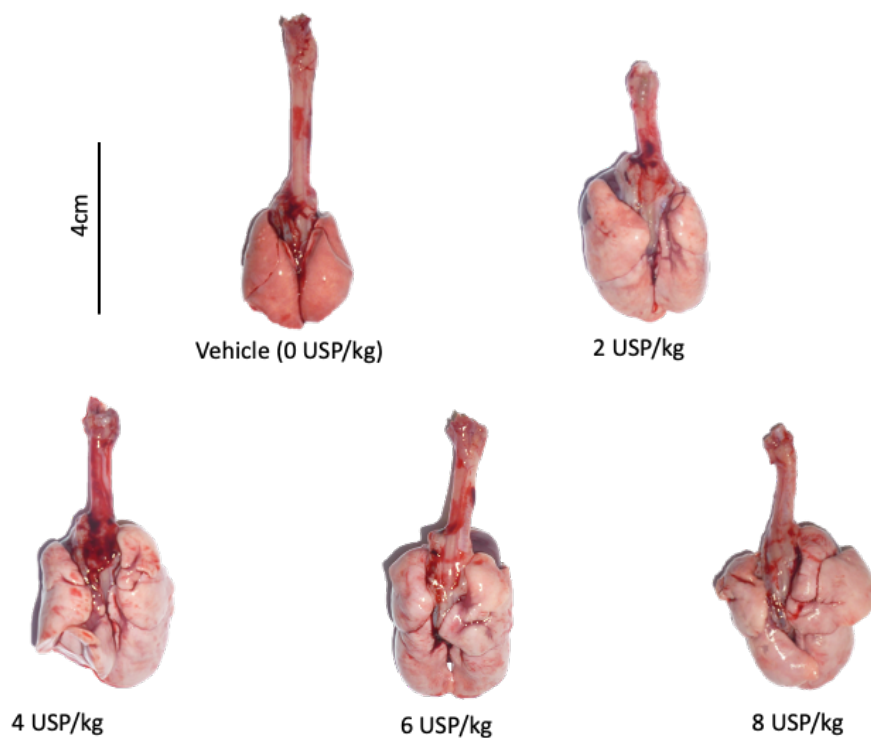


Figure 3-9 Representative photographs of the lungs of guinea pigs incubated with different concentrations of bleomycin.

Animals were incubated with vehicle or different concentration of bleomycin for 3 weeks. As the dose increases, the pinkish parenchyma of the lung becomes whiter due to the higher amount of inflammation and scar tissue (i.e. fibrosis), with the structure of the lobes eventually becoming more rigid and misshapen.

The weights of the animals' lungs increased with the dose of bleomycin they received (Figure 3-10). Doses 6 and 8 USP/kg led to the animals' lungs weighing significantly more than the vehicle treated group's lungs:  $5.96g \pm 0.139$  and  $6.13g \pm 0.317$  versus  $4.28g \pm 0.163$ , respectively.

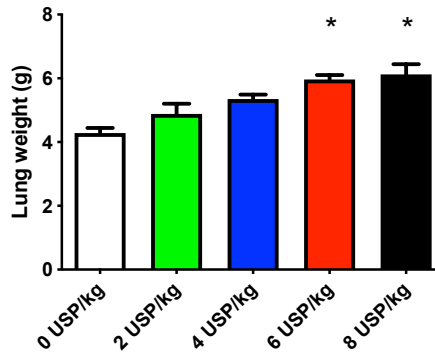


Figure 3-10 Weights of guinea pig lungs after incubation with different doses of bleomycin.

Animals were intratracheally instilled with different concentrations of bleomycin and culled 3 weeks later, before having their lungs weighed. Data shown as mean  $\pm$  S.E.M.,  $5 \leq n \leq 6$ . \* indicates statistical significance ( $p < 0.05$ ) measured by performing Kruskal-Wallis test with Dunn's post-test comparing weight to vehicle

### 3.3.2.3 Heart hypertrophy

To determine if intratracheal administration of bleomycin caused right ventricular hypertrophy in guinea pigs, the weight ratio of the right ventricle to left ventricle plus septum was assessed. A trend towards right ventricular hypertrophy was noted, however no changes were significant.

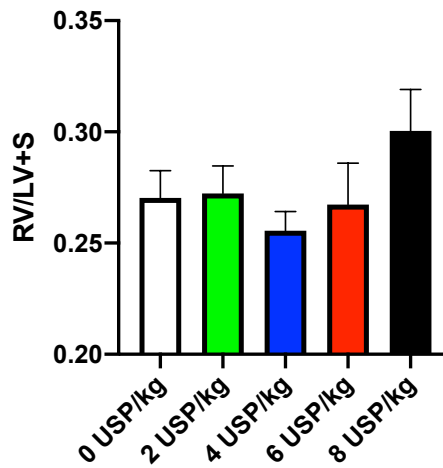


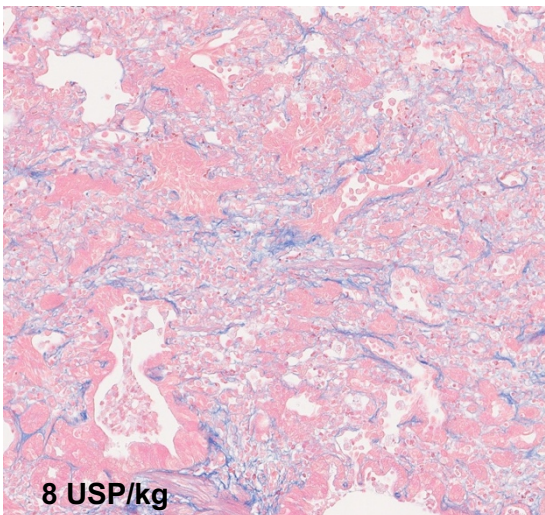
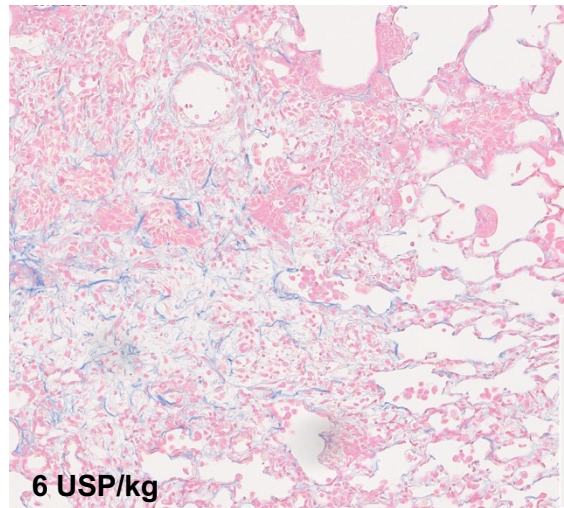
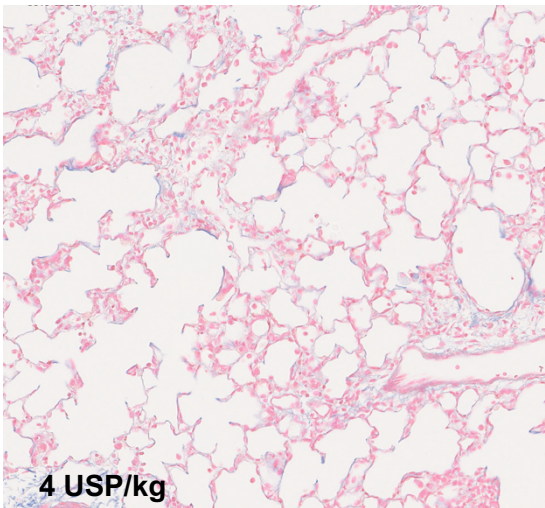
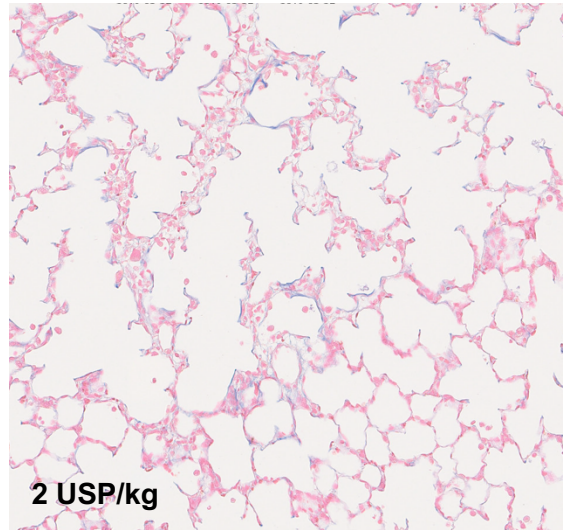
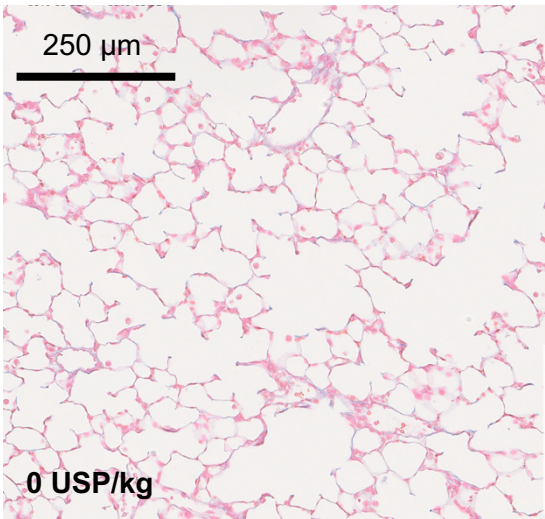
Figure 3-11 Measuring right ventricular hypertrophy in bleomycin-treated guinea pigs.

The weight ratio of the right ventricle to left ventricle plus septum, in guinea pigs treated with different doses of bleomycin. Data shown as mean  $\pm$  S.E.M.,  $5 \leq n \leq 6$ .

#### 3.3.2.4 *Histological assessment*

When viewed under a microscope, the vehicle group's alveolar septa were thin and there was a complete absence of any fibrotic burden (Figure 3-12). As the doses increased to 2 and 4 USP/kg, the alveolar septa became thicker in some places and the alveoli also became more rarefied, with the latter dose also beginning to gain small fibrotic masses. As the doses increased further, the fibrotic masses took over a higher proportion of the microscope field and the alveolar architecture as a result, was severely distorted, and in some places, non-existent. The excess collagen, deposited by the myofibroblasts, is stained blue due to the Azan Mallory stain, and is most prominent in the 2 highest doses: 6 USP/kg and 8 USP/kg.





*Figure 3-12 Representative micrographs of lungs taken from guinea pigs treated with different doses of bleomycin.*

*Images are of 4 $\mu$ m slices from the right caudal lobe stained with Azan Mallory, with 10x magnification. Azan Mallory stains cell nuclei dark red, the cytoplasm a variety of colours and collagen blue.*

### 3.3.2.4.1 Ashcroft Score

The severity of the fibrosis caused by bleomycin instillation was assessed using a modified version of the Ashcroft score, a semi-quantitative scoring system. Intratracheal bleomycin instillation caused a dose dependent increase in Ashcroft score. Doses 6 and 8 USP/kg led to the animals' Ashcroft score being significantly higher than the vehicle treated group's score:  $4.17 \pm 0.295$  and  $4.56 \pm 0.428$  versus  $1.28 \pm 0.163$ , respectively.

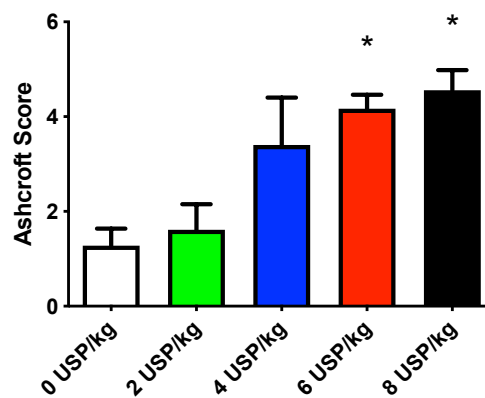


Figure 3-13 Ashcroft scoring assessment of guinea pig lungs after incubation with different bleomycin concentrations.

Guinea pigs were intratracheally instilled with different concentrations of bleomycin before being terminated 3 weeks later.  $4\mu\text{m}$  lung slices of the right caudal lung lobe stained with H&E were scored by three blinded assessors. Data shown as mean  $\pm$  S.E.M.,  $5 \leq n \leq 6$ . \* indicates statistical significance ( $p < 0.05$ ) measured by performing Kruskal-Wallis test with Dunn's post-test comparing Ashcroft score to vehicle.

### 3.3.2.4.2 Automated Assessment

Two apps constructed within the Visiopharm software package were used to objectively and quantitatively assess fibrosis within Azan Mallory-stained lung slices from bleomycin treated guinea pigs; one app measured the proportion of the lung lobe slice that appeared fibrotic (Figure 3-14a), the other measured the proportion of the lobe that was occupied by collagen (stained blue by Azan) (Figure 3-14b). The % area of the lung slices affected by fibrosis increased dose dependently; a similar but more subtle trend could also be seen in the % area occupied by collagen. The highest dose caused a significant increase in the proportion of the lung slice occupied by fibrosis relative to vehicle:  $31.7\% \pm 5.11$  versus  $7.64\% \pm 0.793$ , respectively.

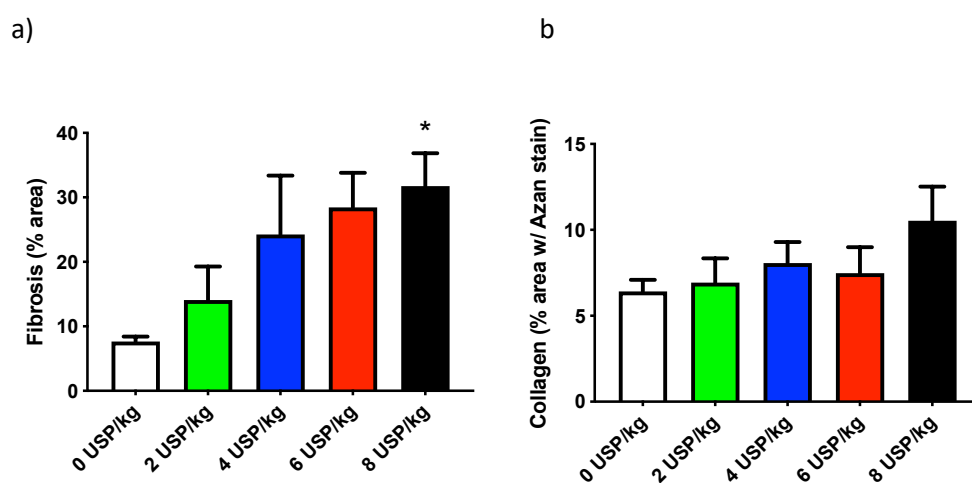


Figure 3-14 Automated Visiopharm analysis of the fibrosis within the lungs of guinea pigs treated with different concentrations of bleomycin.

a) the % area of the lung lobe slice occupied by fibrosis. b) the % area of the lung lobe slice stained by Azan i.e. occupied by collagen.  $4\mu\text{m}$  lung slices of the right caudal lung lobe stained with Azan Mallory. Data shown as mean  $\pm$  S.E.M.,  $4 \leq n \leq 6$ . \* indicates statistical significance ( $p < 0.05$ ) measured by performing Kruskal-Wallis test with Dunn's post-test comparing % area to vehicle.

### 3.3.2.5 *Spontaneous cough assessment*

#### 3.3.2.5.1 *Pilot investigation into fibrosis-induced spontaneous cough*

A pilot study of  $n$  of 2, was initially conducted to gauge the effect bleomycin had on guinea pigs and what dose, if any, caused the animals to have a spontaneous cough. As each IVC contained 2 animals treated with the same dose of bleomycin, footage of each IVC was watched back after the study was completed; for three days prior to the first bleomycin instillation and up until termination, approximately 4 hours of footage was watched from each day.

Bleomycin caused a dose dependent increase in spontaneous cough (Figure 3-15a). No coughs were detected in the vehicle group during the pilot study, whilst animals instilled with doses 2, 4, 6 and 8 USP/kg coughed an average total of 14, 18, 95 and 105 times, respectively. Coughs did not typically present as solitary events but instead formed part of consecutive 'peals' of coughs (see supplementary PowerPoint slides 4&5), this was especially the case for the animals treated with the higher doses 6 USP/kg and 8 USP/kg, whose cough rate peaked in the second week (Figure 3-15b). Total coughs were similar within dosing pairs when assessing the study in its entirety (Figure 3-15a), however, daily cough rates were highly variable within groups, particularly in the groups treated with the two highest doses (Figure 3-15f,g); this is likely due to the limited amount of footage that was reviewed from each day (approximately 4 hours).

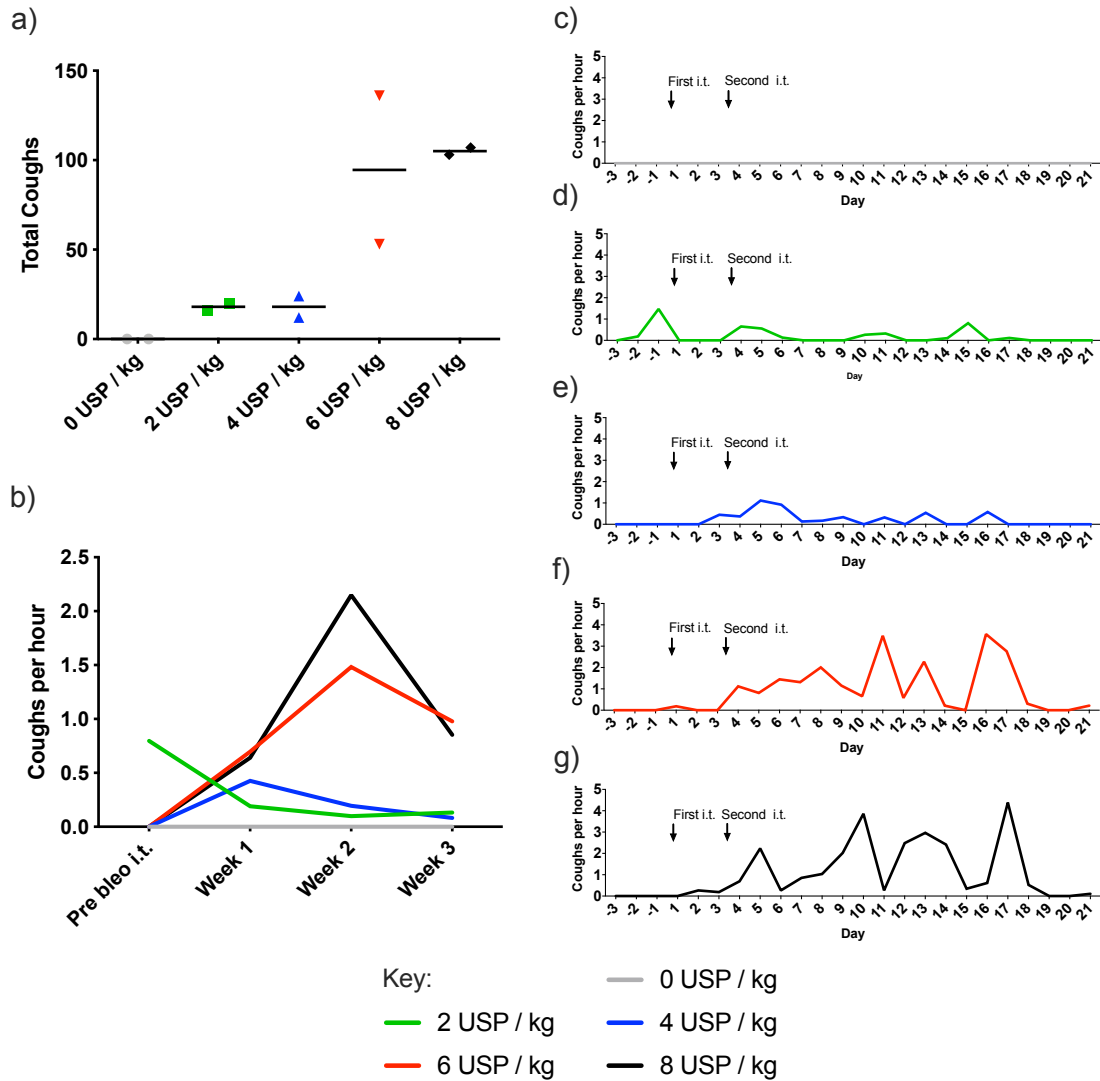


Figure 3-15 Pilot study investigating guinea pig spontaneous coughs following intratracheal instillation of different concentrations of bleomycin, n=2.

a) Total coughs recorded after first bleomycin i.t. Data shown as mean with individual values. b) Average hourly cough rate in each week for each bleomycin dose. Data shown as mean for each week. c)- g) Average hourly cough rate on each day for guinea pigs treated with 0 USP/kg (vehicle)(c), 2 USP/kg (d), 4 USP/kg (e), 6 USP/kg (f) or 8 USP/kg (g). Data shown as mean for each day. Animals were filmed 24/7 but footage of each animal was only watched back for four hours a day for the duration of the 3-week study.

### 3.3.2.5.2 Full investigation into fibrosis-induced spontaneous cough

To achieve more statistically powerful data, 6 USP/kg was selected as a submaximal dose of bleomycin to investigate more thoroughly. An extra 4 and 5 animals were observed in the same way as the pilot study, bringing the total animals to  $n$  of 6 for 6 USP/kg and 7 for the vehicle group (the extra animal was due to an administrative error by the animal facility), respectively.

Guinea pigs intratracheally instilled with bleomycin coughed significantly more than guinea pigs treated with vehicle during the time for which they were observed (Figure 3-16a):  $74.0 \pm 18.12$  coughs versus  $2.1 \pm 1.82$  coughs, respectively. Cough rates were highest for the 6 USP/kg dose group on day 8 ( $2.48 \pm 1.10$  coughs per hour).

As with the previous analysis (Figure 3-15), the inter-day variability for cough rates remained high for the bleomycin treated group (Figure 3-16b), with animals coughing more than 2 times per hour on some days (e.g. days 4 and 8) and under 0.5 coughs per hour on other days (e.g. days 10 and 14). One explanation for this is the limited amount of footage that was being reviewed from each day (approximately 4 hours rather than the full 24).

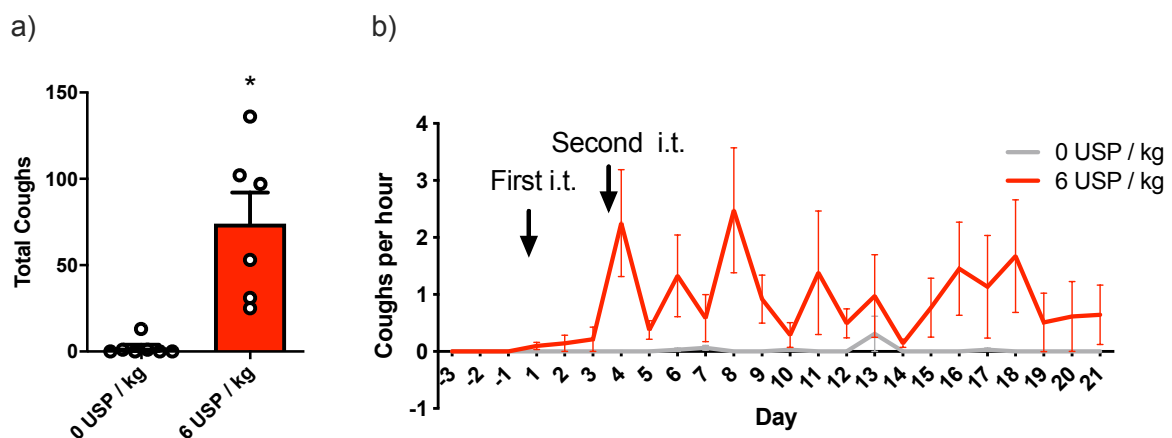


Figure 3-16 Guinea pig spontaneous coughs following intratracheal instillation of 0 USP/kg (saline vehicle) or 6 USP/kg of bleomycin.

Data shown as mean  $\pm$  S.E.M.,  $6 \leq n \leq 7$ . a) Total coughs recorded after first bleomycin i.t. b) Average hourly cough rate on each day. Animals were filmed 24/7 but footage of each animal was only watched back for four hours a day for the duration of the 3-week study. \* indicates statistical significance ( $p < 0.05$ ) measured by performing a nonparametric Mann Whitney test comparing total coughs to vehicle.

### 3.3.2.5.3 24-hour cough assessment

To make the cough data from this model more comparable to that produced in patient 24-hour ambulatory cough recordings, 2 days that were found to have a high cough rate from the approximately 4 hours observed, were watched back in their entirety: day 8 and day 16.

Guinea pigs treated with bleomycin coughed significantly more than vehicle treated animals on day 8 ( $22.8 \pm 5.63$  versus  $0.6 \pm 0.43$ ) and day 16 ( $22.8 \pm 7.77$  versus  $0.1 \pm 0.14$ ) (Figure 3-17a). Cough rates peaked between 06:00 and 09:00 on day 8 for bleomycin treated animals and between 06:00 and 12:00 on day 16.

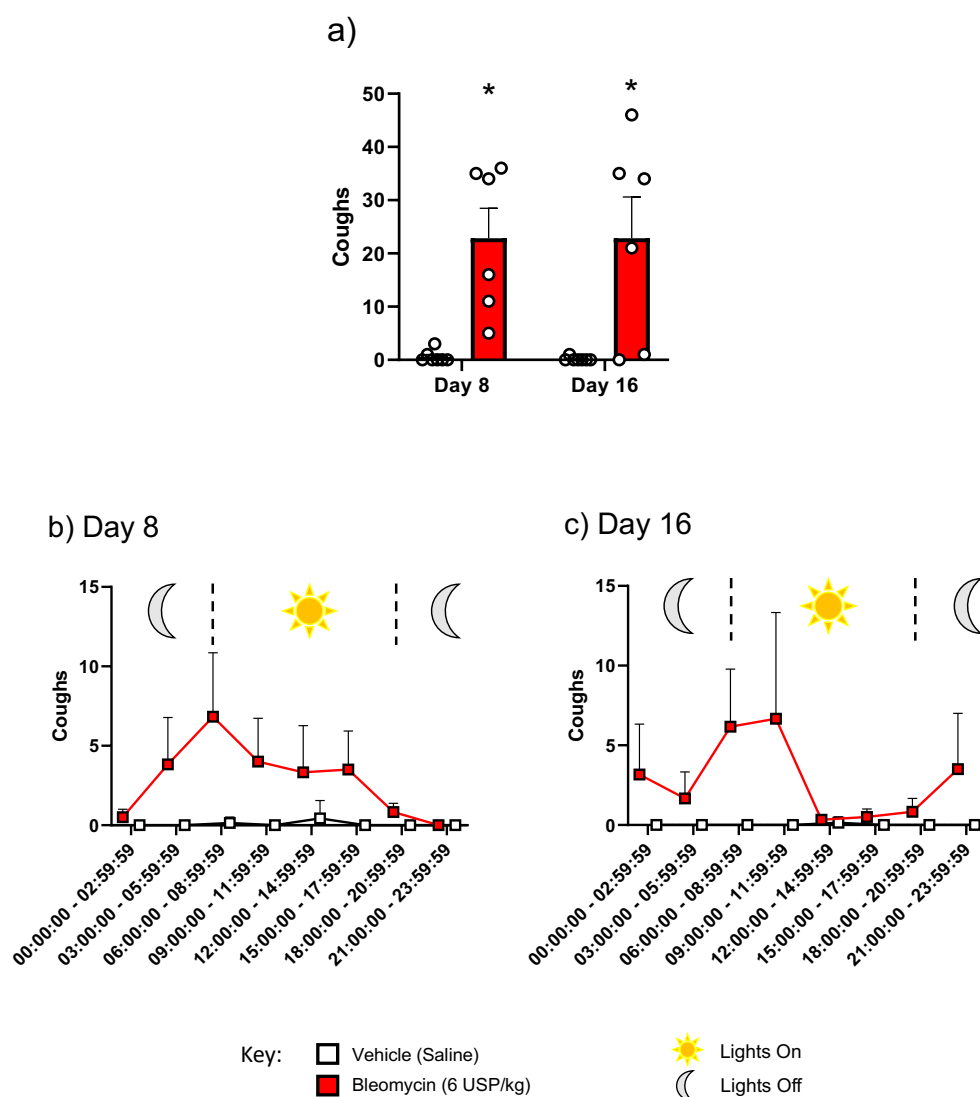


Figure 3-17 Spontaneous coughing by guinea pigs treated with vehicle (saline) or bleomycin (6 USP/kg) over a 24-hour period.

**a)** Total spontaneous coughs in 24 hours on Day 8 after the first intratracheal administration and Day 16. **b & c)** Total coughs over 24 hours in 3-hour segments on day 8 (b) and 16 (c). Lights were turned on gradually at 07:00 and turned off at 19:00; illustrated by vertical dashed lines between the moon and sun glyphs. Data shown as mean  $\pm$  S.E.M.,  $6 \leq n \leq 7$ . \* indicates statistical significance ( $p < 0.05$ ) measured by performing a nonparametric Mann Whitney test comparing coughs to vehicle.

### 3.3.3 Bleomycin time course study

To further characterise the guinea pig bleomycin model, a time course study was undertaken where guinea pigs were incubated with vehicle or bleomycin for 1, 2, 3, or 4 weeks.

#### 3.3.3.1 Animal weights

Bleomycin guinea pigs continued to gain weight at the same rate as vehicle treated guinea pigs after an initial pause in growth following i.t. instillations (Figure 3-18).

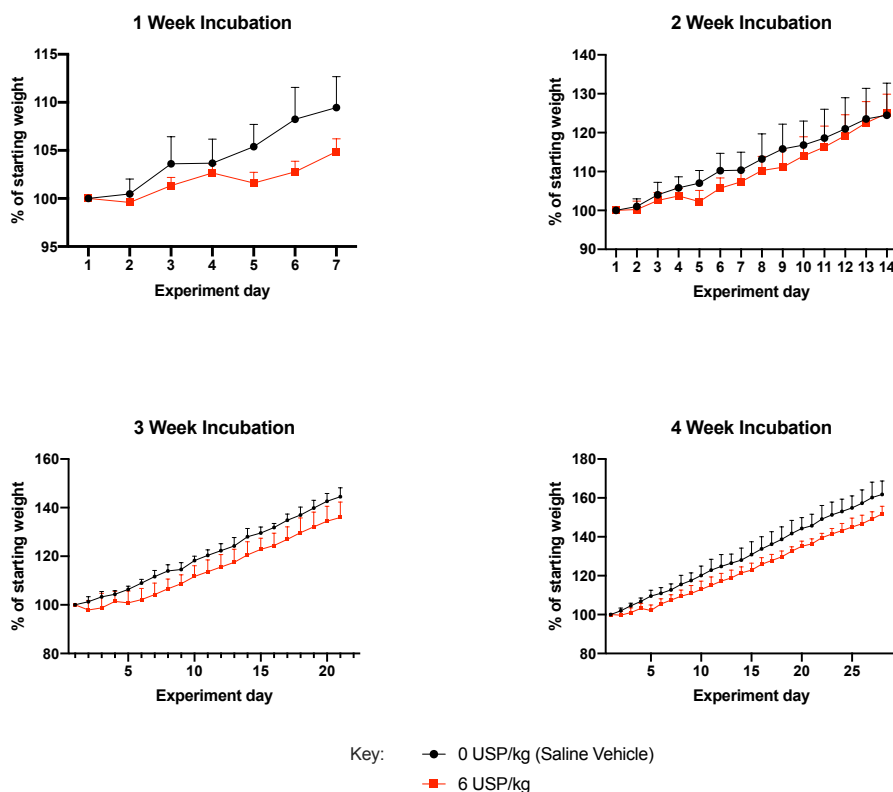


Figure 3-18 Guinea pig body weights throughout bleomycin time course study.

Data shown as mean  $\pm$  S.E.M.,  $5 \leq n \leq 6$ . Like with the dose response study, animals were intratracheally instilled with either vehicle or bleomycin on days 1 and 4.

#### 3.3.3.2 In vitro isolated vagus nerve model

To check for an altered sensory nerve phenotype, vagus nerves derived from animals treated with bleomycin were exposed to a range of protussive stimuli.

No significant differences were seen in the response of vagus nerves to protussive stimuli (3.2.2.9) from bleomycin treated animals and vehicle treated animals.



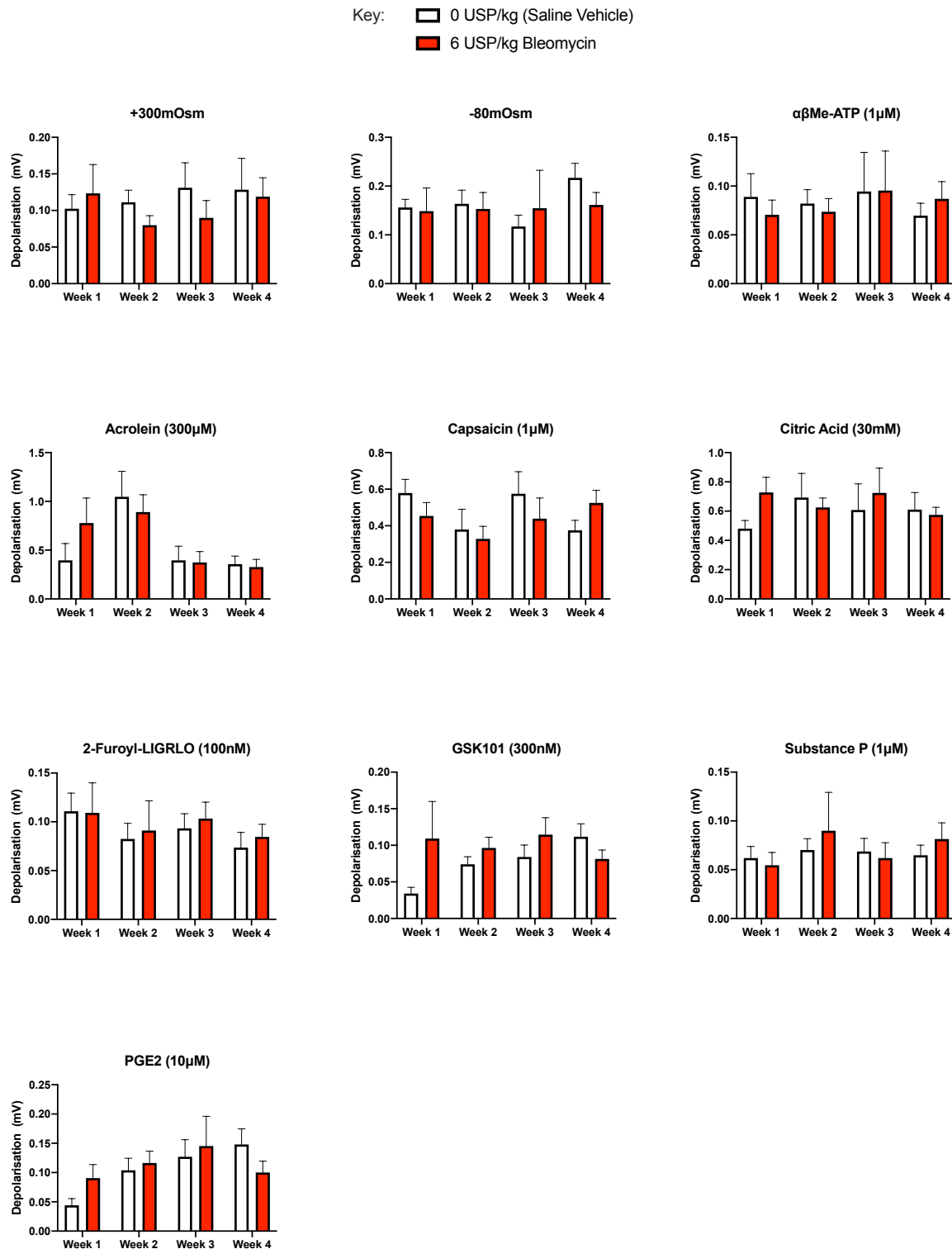


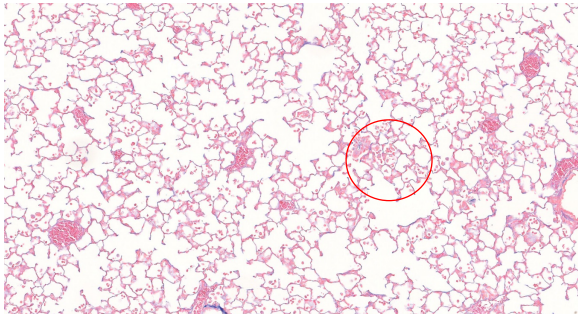
Figure 3-19 The effect of various tussive stimuli on vagus nerve depolarisation in bleomycin-treated guinea pigs.

Responses to a range of tussive agents were measured in saline and bleomycin-treated guinea pigs using the isolated vagus nerve model, 1, 2, 3 or 4 weeks after the first intratracheal instillation. Guinea pig nerves were exposed to each of the above stimuli for 2 minutes, before being washed off with KH solution. For the targeted protussive receptor for each of these stimuli, please see Section 3.2.2.9. Data shown as mean  $\pm$  S.E.M.,  $5 \leq n \leq 6$ .

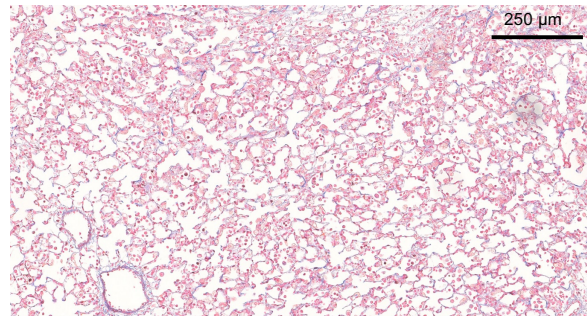
### 3.3.3.3 *Histological assessment*

On inspection of histology collected from animals treated with vehicle, some inflammatory cell infiltration could be seen after 1 week (Figure 3-20; red circle), however this did not appear to be as extensive as that seen in bleomycin treated animals after 1 week. Following 2 weeks of bleomycin incubation, fibroblastic foci appear (Figure 3-20; black arrows), some of which seemed to already be surrounded by deposited collagen (stained blue due to Azan); at this point lung architecture is severely disrupted. After 3 weeks of incubation, some alveoli appear freer from inflammatory cells, but are more rarefied, however the presence of fibrotic masses remain. Finally, after 4 weeks of bleomycin incubation, collagen deposition appears most intense. Vehicle treated guinea pigs' lung architecture remained unchanged throughout the study.

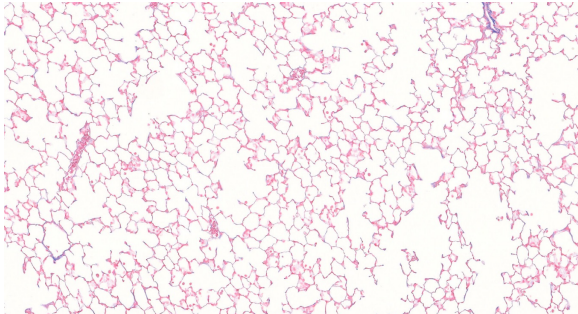
Saline 1 week



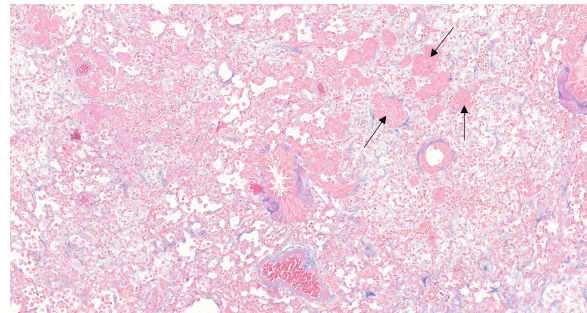
Bleomycin 1 week



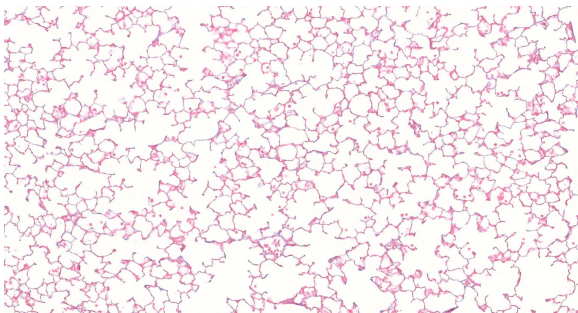
Saline 2 weeks



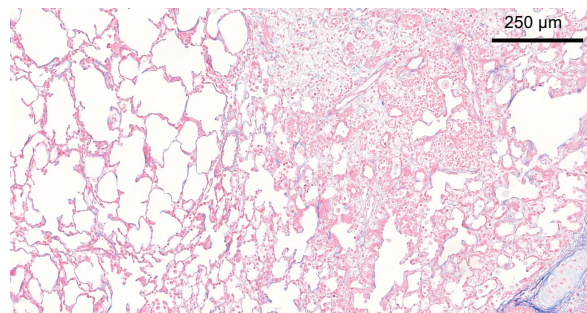
Bleomycin 2 weeks



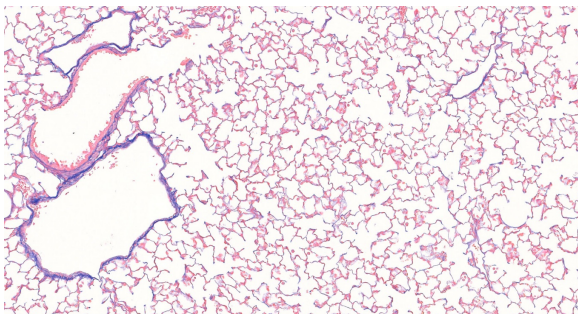
Saline 3 weeks



Bleomycin 3 weeks



Saline 4 weeks



Bleomycin 4 weeks

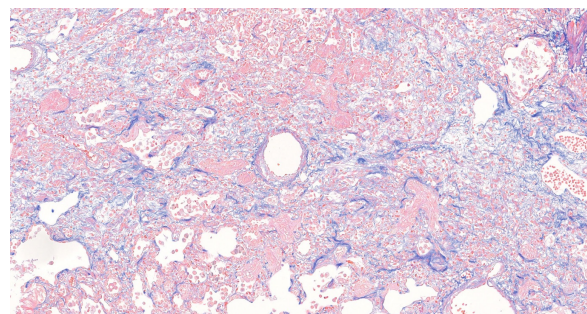


Figure 3-20 Representative micrographs of lungs taken from guinea pigs in the bleomycin time course study

Images are of 4 $\mu$ m slices from the right caudal lobe stained with Azan Mallory, with 10x magnification. Azan Mallory stains cell nuclei dark red, the cytoplasm a variety of colours, and collagen blue. Some inflammatory cell infiltration is present following i.t. in the vehicle group (red circle), whilst in the bleomycin treated group a high amount of inflammatory cell infiltration can be seen. Fibroblastic foci appear in second week for bleomycin treated animals (black arrows), inflammation then reduces by the third week, followed by more collagen deposition after 4 weeks.

### 3.3.3.3.1 Ashcroft Score

A blinded Ashcroft assessment was undertaken to determine the severity of fibrosis in bleomycin treated guinea pigs over time, compared to vehicle treated guinea pigs.

At each week, bleomycin treated animals had a significantly higher Ashcroft score than their vehicle-treated counterparts (Figure 3-21). Ashcroft score peaked after 2 weeks of bleomycin incubation ( $4.7 \pm 0.18$ ).

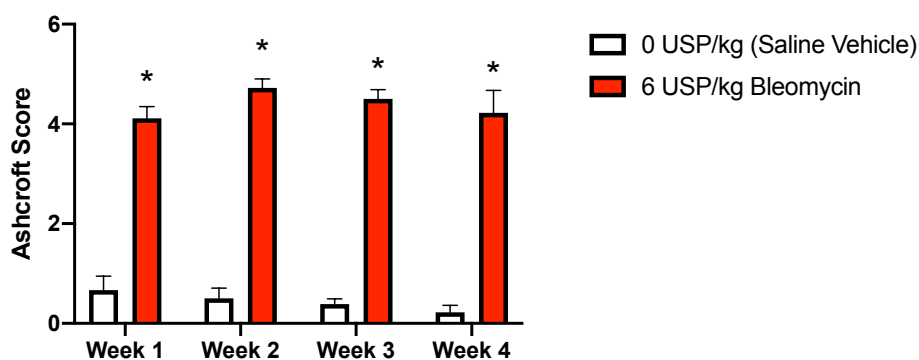


Figure 3-21 Ashcroft Score of guinea pig lungs from bleomycin time course study.

Animals were intratracheally instilled with vehicle or bleomycin and euthanised after 1, 2, 3 or 4 weeks.  $4\mu\text{m}$  lung slices of the right caudal lung lobe stained with H&E were scored by three blinded assessors. Data shown as mean  $\pm$  S.E.M.,  $5 \leq n \leq 6$ . \* indicates statistical significance ( $p < 0.05$ ) measured by performing Mann-Whitney test comparing Ashcroft score of bleomycin treated group to vehicle group for that week.

### 3.3.3.3.2 Automated analysis

Two apps constructed within the Visiopharm software package were used to objectively and quantitatively assess fibrosis within Azan Mallory-stained lung slices from bleomycin treated guinea pigs; one app measured the proportion of the lung lobe slice that appeared fibrotic (Figure 3-22a), the other measured the proportion of the lobe that was occupied by collagen (stained blue by Azan)(Figure 3-22b).

At each week, bleomycin treated animals had a significantly higher proportion of fibrosis and collagen in slides of the right caudal lobe than their vehicle-treated counterparts. Fibrotic area peaked after 2 weeks of bleomycin incubation ( $41.5 \pm 3.40\%$ ), whereas collagenous area was highest after 4 weeks of bleomycin incubation ( $13.1 \pm 1.40\%$ ).

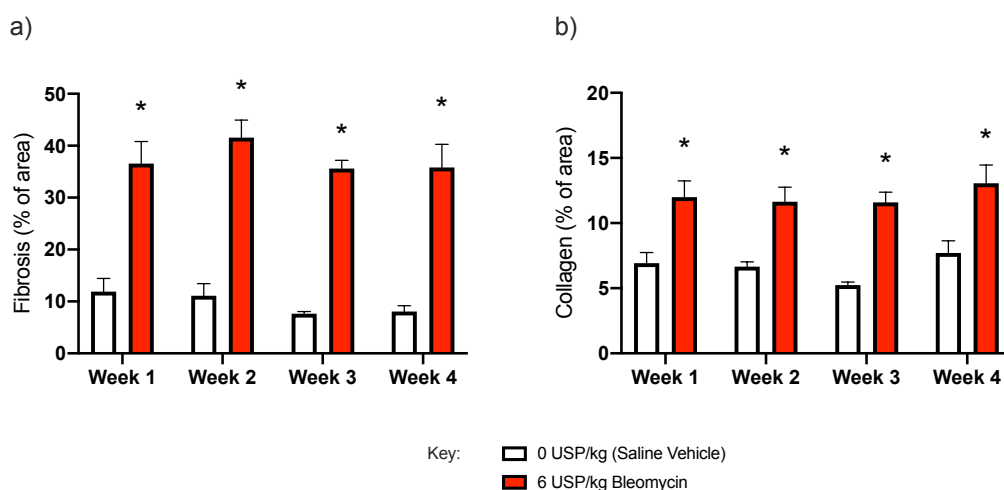


Figure 3-22 Automated Visiopharm analysis of fibrosis from lungs from bleomycin time course

Animals were intratracheally instilled with bleomycin or vehicle and culled after 1, 2, 3 or 4 weeks. a) the % area of the lung lobe slice occupied by fibrosis. b) the % area of the lung lobe slice stained by Azan i.e. occupied by collagen.  $4\mu\text{m}$  lung slices of the right caudal lung lobe stained with Azan Mallory. Data shown as mean  $\pm$  S.E.M.,  $5 \leq n \leq 6$ . \* indicates statistical significance ( $p < 0.05$ ) measured by performing Mann-Whitney test comparing % area of bleomycin treated group to vehicle group for that week.

#### 3.3.3.4 *Immunohistochemical analysis*

$\alpha$ -SMA immunofluorescence was seen to be expressed by the smooth muscle cells of bronchioli and terminal bronchioli (Figure 3-23a,b; white arrows) and in associated vessels (green arrows) for both vehicle and bleomycin treated animals.

Expression was low or absent in the alveoli of normal lung. In bleomycin-treated guinea pigs however,  $\alpha$ -SMA immunofluorescence was also observed in focal fibrotic parenchymal regions (white arrowheads). DAPI staining also exposes the increased cellular density of these regions (Figure 3-23c) and the loss of normal lung architecture, indicating the presence of myofibroblasts and airway remodelling.

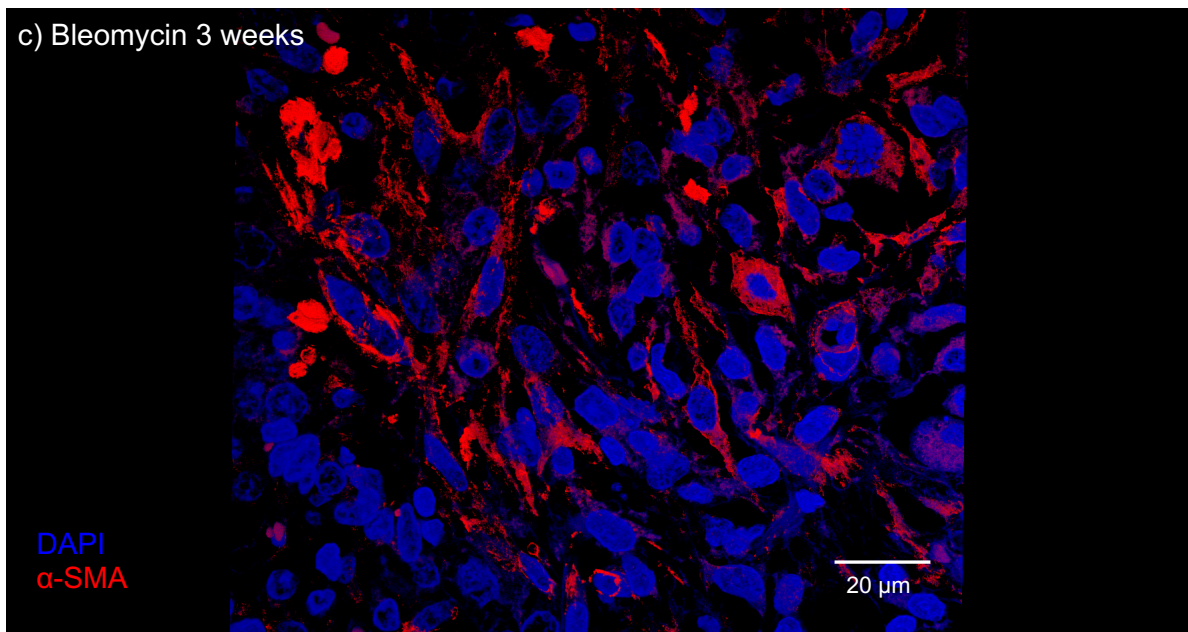
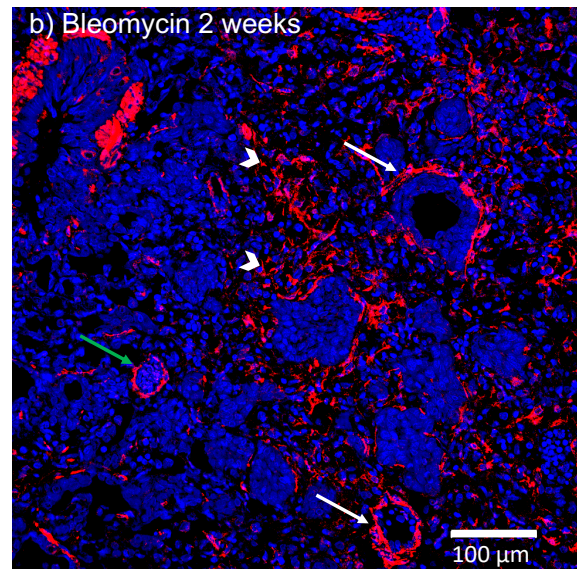
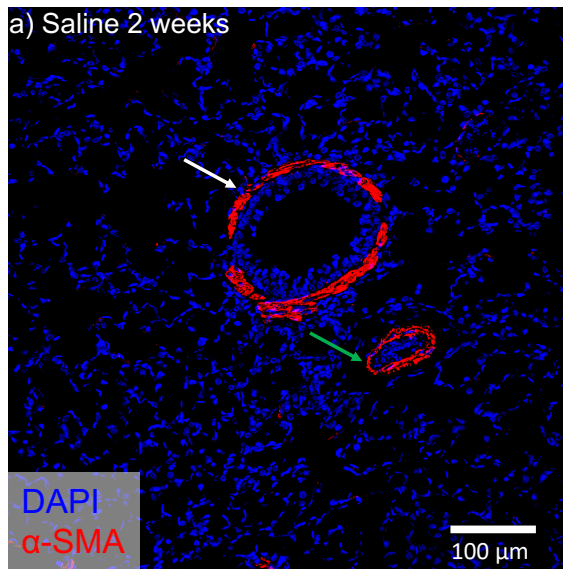


Figure 3-23 Immunohistochemical staining to identify fibroblastic foci in bleomycin-treated guinea pigs.

Representative immunohistochemical stains for  $\alpha$ -SMA (in red) within lung sections from guinea pigs incubated with saline vehicle (a) or bleomycin (b) for 2 weeks, DAPI stain = blue. c) Further magnified image of a 3D reconstruction (z-projection of 20 pictures) of a myofibroblast cluster, within a bleomycin treated-guinea pig's parenchyma.

### 3.3.4 Expression of fibrosis-related genes following bleomycin challenge

To further characterise this guinea pig bleomycin-driven fibrosis model, the expression of genes within the lung that were relevant to fibrosis was quantified over the time course study: collagen type I and type III, alpha smooth muscle actin ( $\alpha$ -SMA) and fibronectin (Figure 3-24).

No genes relating to fibrosis were significantly increased by 1 week following the first bleomycin instillation, however, from the second week onwards, expression of Type I Collagen (*COL1A1*) and  $\alpha$ -SMA (*ACTA2*) were significantly increased when compared to vehicle treated animals. From week 3 onwards, all 4 of the fibrosis-related genes assessed were expressed significantly more in bleomycin treated animals than in vehicle treated animals.

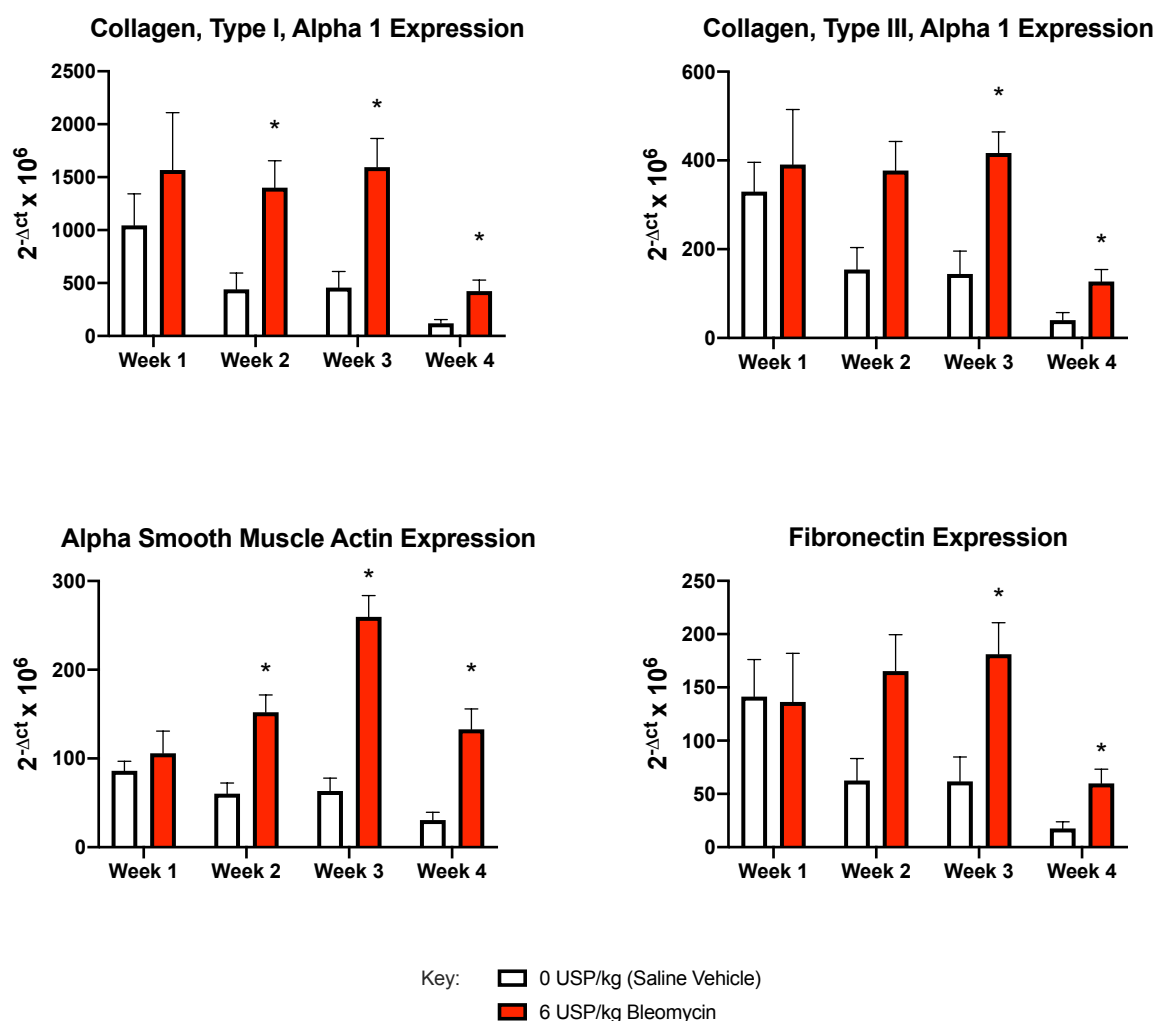


Figure 3-24 The expression of fibrosis-related genes in the parenchyma of guinea pigs in the bleomycin time course study.

Guinea pigs were intratracheally instilled with bleomycin or saline vehicle and culled after 1, 2, 3 or 4 weeks. The genes for the following proteins were quantified within the animals' left cranial lung lobe: collagen type I and type III, alpha smooth muscle actin ( $\alpha$ -SMA) and fibronectin. The housekeeping gene eukaryotic 18s was used to normalise data. Expression data was acquired through real time quantitative PCR and is presented as mean  $\pm$  S.E.M.,  $5 \leq n \leq 6$ . \* indicates statistical significance ( $p < 0.05$ ) measured by performing nonparametric Mann-Whitney test comparing expression in bleomycin-treated animals with vehicle-treated animals from that week.



### 3.3.5 Hydroxyproline bioassay in left cranial lobe homogenate

Hydroxyproline, a biomarker for collagen production and therefore ECM deposition, was quantified within the left cranial lung lobes of guinea pigs incubated with vehicle or bleomycin for 1, 2, 3 or 4 weeks.

Despite week 4 showing a slight increase in hydroxyproline for bleomycin treated animals, and week 1 showing the opposite, no statistically significant differences were seen.

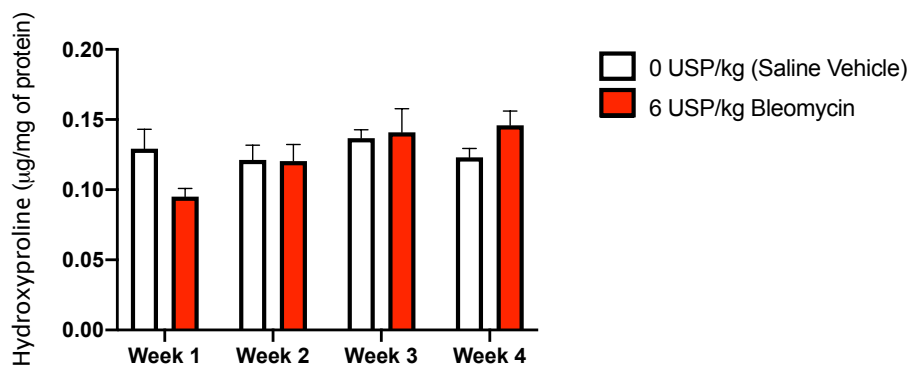


Figure 3-25 Proportion of hydroxyproline in the lungs of guinea pigs incubated from the bleomycin time course study.

The proportion of hydroxyproline ( $\mu\text{g}$ ) per mg of protein within the left cranial lung lobe of guinea pigs incubated with saline or bleomycin for 1, 2, 3 or 4 weeks. Data shown as mean  $\pm$  S.E.M.,  $5 \leq n \leq 6$ .

### 3.3.6 Leukocytes in BALF

Total and differential white blood cells were quantified in bronchoalveolar lavage fluid (BALF) as a way of assessing inflammation within the lungs of guinea pigs treated with bleomycin. Due to the relatively high level of inflammatory cell infiltration in the vehicle group, the increase in leukocytes in the BALF of bleomycin treated guinea pigs is not significant at week 1. From week 2 onwards however, leukocyte quantity in bleomycin-treated guinea pigs is significantly increased compared to vehicle treated guinea pigs. Additionally, the increased leukocyte quantity in the lungs after 1 week of bleomycin incubation has significantly reduced by week 3 and week 4.

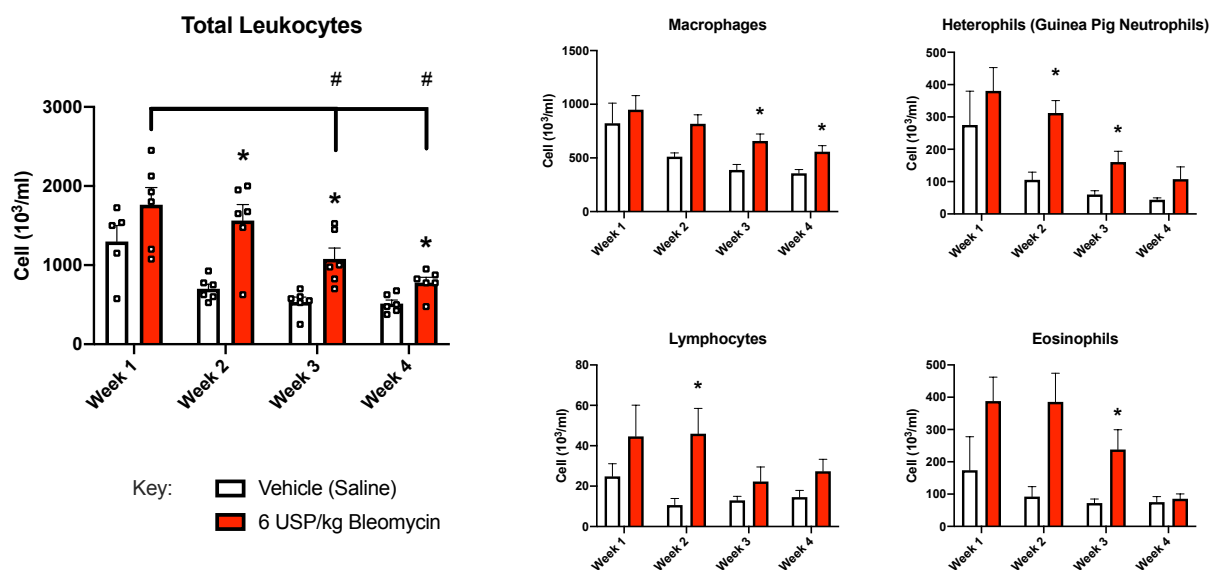


Figure 3-26 Total and differential leukocytes in the BALF of guinea pigs from the bleomycin time course study.

Leukocytes include: macrophages, heterophils (guinea pig equivalent of neutrophils), lymphocytes and eosinophils. Guinea pigs incubated with vehicle or bleomycin for 1, 2, 3 or 4 weeks. Data shown as mean  $\pm$  S.E.M.,  $5 \leq n \leq 6$ . \* indicates statistical significance ( $p < 0.05$ ) measured by performing nonparametric Mann-Whitney test comparing cell count in bleomycin-treated animal BALF to vehicle-treated BALF for that week. # indicates statistical significance ( $p < 0.05$ ) measured by performing nonparametric Mann-Whitney test comparing cell count between groups incubated with bleomycin for a different number of weeks.

### 3.4 Discussion

The aim of this chapter was to develop a bleomycin-driven model of pulmonary fibrosis, and further, to assess whether these animals had a spontaneous, chronic cough, like IPF patients. Target engagement for novel antitussive therapeutics is evaluated clinically and pre-clinically by exposing human volunteers or guinea pigs, respectively, to inhaled tussive challenge agents such as capsaicin or citric acid (Bonvini et al., 2015). Chronic cough sufferers (and IPF patients) are known to be more sensitive to capsaicin-induced cough than healthy control subjects, so unsurprisingly, it was believed that TRPV1 (the receptor for capsaicin-mediated airway nerve responses) was a causal factor in this enhanced tussive response (Belvisi et al., 2016, Choudry and Fuller, 1992, Hope-Gill et al., 2003). The recent failure of TRPV1 antagonist XEN-DE501 to reduce spontaneous awake cough frequency in refractory chronic cough patients, despite its efficacy at inhibiting capsaicin-induced cough in these patients and guinea pigs, has led to questions about the suitability of provoked cough models (Belvisi et al., 2017). We sought to develop a pre-clinical model of spontaneous cough with the hope that it would provide a more reliable way of predicting an antitussive medication's effectiveness in the future.

IPF is a chronic lung disease characterised by progressive scarring of the lungs, with 70-85% of patients also frequently suffering from a dry, chronic cough that worsens upon exertion (Vigeland et al., 2017). This cough, that is highly distressing and disabling for patients, is usually refractory to treatment, meaning there is a clinically unmet need to improve these patients' quality of life (Key et al., 2010, Swigris et al., 2005). As intratracheal bleomycin instillation, is the most commonly used and well characterised pre-clinical model of IPF (Peng et al., 2013, Tashiro et al., 2017), we postulated that guinea pigs with bleomycin-induced pulmonary fibrosis might also cough spontaneously in the manner of IPF patients. Indeed, recent *in vivo* studies have found that guinea pigs with bleomycin-induced fibrosis have an enhanced cough response to capsaicin (as well as other protussive stimuli) (Fernandez-Blanco et al., 2015, Guo et al., 2019), similarly, IPF patients also have a heightened cough sensitivity to capsaicin (Hope-Gill et al., 2003).

Before we could determine whether bleomycin-treated animals coughed spontaneously, we first had to develop a system capable of recording guinea pig coughs *in situ*, so that the footage could be watched back by a trained observer and coughs could be quantified. Following a CCTV recording of guinea pigs exposed to nebulised capsaicin whilst inside an IVC, we determined that our CCTV system was indeed capable of recording the cage to a high enough quality, visually and aurally, that future spontaneous coughs elicited following bleomycin challenge would be detectable (Figure 3-7).

Even though the vast majority of *in vivo* studies using the bleomycin model of pulmonary fibrosis are with mice and rats as the model species, it was necessary for this chapter to use guinea pigs in this instance, since they are the smallest rodents that have a cough response similar to our own (Maher et al., 2009). This relative lack of study for guinea pigs made choosing a tolerable range of bleomycin doses for a dose response study more difficult, however, we opted to not exceed 8 USP/kg, a dose that was found to be tolerated and effective in the literature (Cisneros-Lira et al., 2003).

There is some debate within the pulmonary fibrosis research community as to the best variation of the bleomycin model: *i.e.* whether or not it should be dosed systemically or intratracheally; and whether or not it should be dosed through single or multiple challenges (Schaefer et al., 2011). It can be argued however, that a multiple intratracheal dosing regimen with a lower dose of bleomycin has the most relevance to IPF, because it helps to mimic the onslaught of repetitive alveolar microinjuries, aberrant wound healing and progressive scarring, that are characteristic of the disease (Degryse et al., 2010, Baily et al., 2019). Whilst some bleomycin models exceed more than 4, sometimes 8 intratracheal instillations for mice and rats, one must take into consideration the stress that repeated intratracheal dosing can have on an animal, especially that on a juvenile guinea pig, which are particularly vulnerable to airway inflammation (Regal et al., 2006); because of this, we opted for a double dosing regimen, like that of the industrial funders of this PhD (Pitozzi et al., 2018). As can be seen from the weight gain diagram (Figure 3-10), all bleomycin doses and the route and regimen by which they were administered, were mostly well tolerated.

When viewed macroscopically, lungs derived from animals treated with any dose of bleomycin appeared markedly different from lungs removed from animals treated with vehicle (Figure 3-9). The parenchyma of bleomycin treated animal lungs appeared far whiter, likely due to a combination of reduced blood flow from inflammation and the deposition of scar tissue. When assessing the lung fibrosis quantitatively however (*e.g.* weight, Ashcroft score, etc), there were much more distinct gradations between the different doses of bleomycin. Although not significant, there also appeared to be a dose dependent trend towards heart hypertrophy; right sided heart failure is recognised as a late stage feature of IPF (ATS and ERS, 2002), due to the increased pulmonary burden on the heart.

Further to this, we believe we have validated two new objective and automated methods of assessing fibrosis using apps developed within the Visiopharm software package, as like Ashcroft score, the % area measured featuring fibrosis or that contained collagen also increased dose dependently. One drawback with the app that determines the % area of the lobe occupied by collagen is that it currently does not yet have the functionality to assess the intensity of the blue azan stain, *i.e.* it cannot tell the difference between the degree of collagen deposition between two

areas both fully occupied by different amounts of collagen; enabling it to do this will no doubt further increase the usefulness of this technique. These two automated methods will likely prove beneficial in future iterations of this model, because it is a less labour-intensive and more objective method than Ashcroft scoring.

Most importantly, we discovered that guinea pigs treated with bleomycin intratracheally, did indeed cough spontaneously, much like IPF patients, and further, these spontaneous coughs increased dose dependently. To our knowledge, there are only 3 other examples of spontaneous cough being assessed as part of a guinea pig model of disease in the literature. When this research was first conducted, there was only one: *Hirata et al. (2003)* detected spontaneous coughs in guinea pigs orally administered with the Angiotensin-converting-enzyme inhibitor elapril. Since then, besides this study (Miles et al., 2019), spontaneous cough has also been measured in guinea pigs infected with *Mycobacterium tuberculosis* (Ruhl et al., 2020), and in guinea pigs exposed to traffic-related air pollution whilst caged inside of a tunnel in southern China (Fang et al., 2019). Unlike the spontaneous model outlined in this chapter, where we relied solely on video footage to quantify spontaneous coughing, the studies above differed from ours by also utilising some form of airflow wave-form analysis. This more precise method may explain the higher coughing rates detected in vehicle treated animals from these studies compared to the vehicle group from this chapter. Besides animal welfare, our reason for not using any form of plethysmography to count cough was because putting the animals inside a whole-body plethysmography chamber for up to 24 hours might discourage natural, relaxed behaviour, which could then lead to the animals stifling their cough. Using whole body plethysmography is something we will consider for future experiments, not least to see if cough quantification can be more automated and less laborious. Another criticism that could be made at this chapter is the fact that coughs were not quantified in a blinded fashion. This was because in the knowledge of bleomycin's cytotoxicity, as the model was being developed, it was important for observers to quickly and easily determine what dose a guinea pig had been treated with, so that any signs of distress could more easily be detected. Now that 6 USP/kg has been determined to be tolerable, any future therapeutic cough study will involve observers being blinded to treatment, thereby avoiding accusations of confirmation bias.

Despite determining that the highest cough rates take place between 06:00 and 12:00 on both 8 days and 16 days after initial bleomycin instillation, the variability was still high. Therefore, to generate enough statistical power in a future antitussive therapeutic study, it is likely the animals will still have to be assessed for spontaneous cough over two entire days, with the first day being a pre-treatment baseline, thereby enabling the use of a paired statistical test.

Part of our intention to assess cough over 24-hour periods was in order to determine whether fibrotic guinea pigs, like IPF patients, would also cough more frequently during the day than at night time (Key et al., 2010). Having completed this work, it is now apparent that it may not be strictly fair to draw comparisons between “daytime” cough rates in this *in vivo* model, and daytime cough rates in IPF patients, since the animals often slept during the day and were also active at night. Contrary to humans, guinea pigs do not appear to show a preference for diurnality or nocturnality, and in further contrast to humans, they tend to follow a polyphasic sleep pattern rather than a monophasic one (Tobler, 1995, Tobler et al., 1993). Therefore, in order to differentiate coughs according to whether or not they took place during periods of wakefulness or rest, it may be worthwhile quantifying spontaneous coughs in parallel to measuring animal activity; as opposed to stratifying coughs according to whether the lights in the animals’ room were switched on or off.

We also utilised the *in vitro* isolated vagus nerve model in order to determine if the vagus nerves of pulmonary fibrotic guinea pigs had an altered sensory nerve phenotype. Cigarette smoke exposure for instance, has been found to cause phenotypic switching in airway sensory nerves, where vagus nerves derived from deceased donors that smoked or cigarette smoke-exposed guinea pigs, have a heightened response to capsaicin, but a reduced response to the prostaglandin PGE<sub>2</sub> (Belvisi et al., 2016). However, we did not find any statistically significant changes to suggest that the airway sensory nerves of the bleomycin-treated guinea pigs had an altered phenotype. By ruling this out, it is therefore more likely that some kind of endogenous mediator is instead responsible for the spontaneous coughs in this model, and by extension, IPF patients; investigations into what this mediator could be is the theme of the next chapter.

We further characterised our model of bleomycin driven pulmonary fibrosis by conducting a time course experiment, as knowing when the inflammatory period of our model ends, and the fibrotic period begins (Moeller et al., 2008), will be useful knowledge for future antitussive therapeutic studies. After only 1 week of bleomycin incubation, Ashcroft score, % fibrotic area and % area occupied by collagen were all significantly increased compared to vehicle. Conversely, there were no significant increases in any of the fibrosis-related genes until after the 2 weeks of incubation. Similarly, fibroblastic foci, did not appear until after the second week of bleomycin incubation either. However, leukocyte counts within the BALF were at their highest after one week of bleomycin incubation, before steadily decreasing. This suggests, firstly, that these histological assessment methods may not be well adapted to differentiating between inflammatory changes in lung architecture and fibrotic changes in lung architecture; and secondly, that the change between the inflammatory phase and the fibrotic phase is not in distinct stages, but instead, more of a gradual and overlapping transition.

The inflammatory cell infiltration in the BALF was relatively high in vehicle treated animals after 1 week of incubation, similarly, the expression of some ECM-related genes was also high for this group. This is most likely explained by the tissue damage and resulting healing that takes place after two intratracheal instillations and exemplifies why repeated dosing through this route could be problematic.

The leading criticisms of the bleomycin model of fibrosis are that, by most accounts, it resolves over time (Moore et al., 2013), and that it also fails to recapitulate the more important characteristic features of Usual Interstitial Pneumonia (UIP), in particular: the presence of fibroblastic foci (Degryse and Lawson, 2011). Whilst we did not incubate bleomycin to a point at which we could see the pulmonary fibrosis resolve, we have no reason to doubt that it would also resolve eventually in our model. Importantly however, we do believe that fibroblastic foci have been recreated in our model as observing Azan Mallory, as well as DAPI and  $\alpha$ -SMA immunostained micrographs after two weeks of bleomycin incubation, one can clearly see areas densely packed with myofibroblasts that are surrounded by extracellular matrix. This is further supported by the gene expression data, where after the second week of bleomycin incubation, there is a significant upregulation of the gene for  $\alpha$ -SMA (*ACTA2*).

The lack of any significant increase in hydroxyproline was disappointing, especially since this is one of the most commonly used endpoints in *in vivo* pulmonary fibrosis studies (Bigatto et al., 2019). Besides increasing *n* numbers, a future study could measure hydroxyproline in an entire lung lobe instead of relative to protein content, which might better emphasise any signal. Despite this concern, we are still in no doubt as to the success of the model due to the overwhelming evidence of pulmonary fibrosis listed above.

In summary, we outlined the development of a CCTV system for observing guinea pig spontaneous coughs less intrusively, whilst they remain within their IVCs. We have shown histologically that intratracheally instilled bleomycin causes dose dependent pulmonary fibrosis in our model. Most importantly, and in support of this chapter's hypothesis, we have shown for the first time that guinea pigs treated with bleomycin also cough spontaneously, much like IPF patients. Further to this, we have shown that inflammatory cell infiltration begins immediately but reduces over time, whilst fibroblastic foci and significant increases in fibrosis-related gene expression are present following two weeks of bleomycin incubation.

We believe that this model more closely recapitulates cough seen in patients than the standard provoked cough challenge models, and that this will allow for a greater understanding of IPF pathophysiology, thereby providing a better way to evaluate future antitussive therapeutics.

## 4 Comparing biomarkers in IPF patient bronchoalveolar lavage fluid with samples produced from the bleomycin guinea pig fibrosis model which exhibits spontaneous cough

### 4.1 Rationale

The aims of this PhD are to elucidate the pathological mechanisms behind IPF-associated chronic cough, a deeply distressing symptom for many patients, which if better understood could aid in the search for a therapy.

As previously discussed, work conducted by this lab has shown that ATP is capable of causing airway nerve activation and cough (Bonvini et al., 2016); and pertinent to this thesis, extracellular ATP (eATP) concentrations have been shown to be elevated in IPF patient bronchoalveolar lavage (BAL), when compared to healthy volunteers (Riteau et al., 2010). Evidence for eATP's involvement in chronic cough is further emboldened by the antitussive efficacy of AF219 (Gefapixant), a pharmacological antagonist for the ATP-gated purinergic receptor P2X3, that reduced cough frequency in patients with chronic idiopathic cough by 75% (Abdulqawi et al., 2015). A phase 2 clinical trial by Martinez et al. (2019) attempted to see whether Gefapixant could repeat its success in IPF patients, unfortunately however, the statistical power of the study was diminished due to a randomisation error and a change in dosing regimen part way through, thus rendering the study inconclusive. It is still not known definitively whether pharmacologically inhibiting P2X3, the protussive target of eATP, could reduce cough frequency in IPF patients, however, determining whether eATP is increased in the lungs of IPF patients and pulmonary fibrotic guinea pigs that cough, could indicate whether or not it is involved.

Previous studies have also shown that tryptase (a PAR2 activating protease) (Molino et al., 1997), is more evident in the lungs of IPF patients, than in the lungs of healthy controls (Walls et al., 1991, Compton et al., 2001, Kawatani et al., 2007). PAR2 is expressed on nociceptive neurons (Steinhoff et al., 2000, Vergnolle et al., 2001) and has previously been shown to activate TRPV4 through an intracellular mechanism that may involve tyrosine kinases (Grace et al., 2014, Poole et al., 2013). As TRPV4 activation is capable of causing cough in guinea pigs and activating human airway sensory nerves (Bonvini et al., 2016), it therefore raises the possibility that PAR2 agonists could be an upstream actor of IPF-associated cough, particularly as there is evidence that TRPV4 activation and TRPV4-mediated ATP release might be involved in IPF pathogenesis itself (Rahaman et al., 2014, Rahman et al., 2018). Whether or not PAR2 agonists can activate airway sensory nerves is explored in Chapter 6.



Also elevated in the BAL of IPF patients are biomarkers for oxidative stress (Fois et al., 2018), e.g. 8-isoprostane (Montuschi et al., 1998). Reactive Oxygen Species (ROS) like H<sub>2</sub>O<sub>2</sub> are capable of activating sensory neurons through agonism of the TRPA1 channel (Sawada et al., 2008, Andersson et al., 2008), which itself is widely considered to be a protussive receptor in guinea pigs and humans (Andre et al., 2009, Birrell et al., 2009). It therefore remains possible that ROS in the IPF lung could be causing patients to cough; whether or not oxidative stress can activate airway sensory nerves is explored in Chapter 5.

Being in the privileged position of having access to bronchoalveolar lavage fluid (BALF) samples obtained from IPF patients involved in the PROFILE (Prospective Observation of Fibrosis in the Lung Clinical Endpoints) study at Royal Brompton Hospital (Section 4.2.1), we sought to repeat the findings of the clinical studies above by measuring these same biomarkers. Further to this, we sought to also measure these biomarkers in the bronchoalveolar lavage fluid (BALF) of guinea pigs from our *in vivo* model of fibrosis-induced spontaneous cough.

#### 4.1.1 Chapter Hypothesis:

eATP, tryptase and oxidative stress biomarker 8-isoprostane are increased in the BALF of IPF patients and bleomycin-treated guinea pigs when compared to healthy controls and vehicle-treated guinea pigs, respectively.

#### 4.1.2 Aims

- Measure eATP in bleomycin-treated guinea pig and IPF patient BALF using the ATPlite Luminescence Assay System
- Measure 8-isoprostane (biomarker of lipid peroxidation) in BALF of bleomycin-treated guinea pigs and IPF patients using a competitive ELISA kit
- Measure PAR2 agonist tryptase in BALF of IPF patients and bleomycin-treated guinea pigs by assessing the cleavage of substrate tosyl-gly-pro-lys-pNA through tryptase enzymatic activity

## 4.2 Methods

### 4.2.1 Clinical PROFILE study

Launched in 2010, the Prospective Observation of Fibrosis in the Lung Clinical Endpoints (PROFILE) study was a UK-based, multicentre, prospective cohort study of patients recently diagnosed with IPF (Maher, 2013). From the point of diagnosis, the enrolled subjects all underwent clinical assessment and blood sample collection, at seven pre-specified time-points, for 3 years (Figure 4-1).

The PROFILE study's stated aims were:

*“1) to prospectively validate a panel of previously published biomarkers in patients with well-characterised IPF; 2) to undertake open platform omic-based analysis of biological samples with a view to applying computational biology methodology to deliver a comprehensive disease fingerprint; and 3) to prospectively evaluate longitudinal disease behaviour in patients with IPF with a view to developing composite biological and clinical end-points for subsequent use in intervention studies”*  
(Maher, 2013)

Patients were recruited between the Royal Brompton Hospital in London, Queens Medical Centre in Nottingham and district general hospitals around the Nottingham area, although the BAL used in this study was only from patients recruited at Royal Brompton Hospital.

Diagnosis of IPF was based on the joint guidelines issued by the American Thoracic Society (ATS), European Respiratory Society (ERS), the Japanese Respiratory Society (JRS), and the Latin American Thoracic Association (ALAT) (Raghu et al., 2011). Criteria for inclusion can be found in Table 4-1.

Before being consented for the study, all patients received a copy of the patient information sheet and were given adequate time to consider whether they wanted to partake in the research. Prior to involvement, all patients provided informed written consent and study specific procedures were undertaken as per Good Clinical Practice guidelines (Dixon, 1998). The PROFILE study was approved by the Royal Free Hospital Research Ethics Committee (Ref: 10/H0720/12). In addition to profile BAL, we also collected BAL from healthy volunteers to act as a healthy a control (Research Ethics Committee Ref: 15/LO/1399)

Procurement of BAL for this PhD required spare BAL being available from Royal Brompton hospital and lab personnel also being free to collect it.

Table 4-1 Patient criteria for participation within the PROFILE study

PROFILE Patient Inclusion Criteria	PROFILE Patient Exclusion Criteria
<ul style="list-style-type: none"> <li>• Above the age of 18</li> <li>• Received diagnosis of IPF based on joint guidelines (Raghu et al., 2011)</li> </ul>	<ul style="list-style-type: none"> <li>• Was diagnosed within 6 months of entry to the study</li> <li>• Presence of co-existent conditions associated with the development of interstitial lung disease (ILD)</li> <li>• Positive auto-immune profile suggestive of a possible connective tissue disease. Participation in clinical trials of novel medications for fibrotic lung disease.</li> <li>• Diagnosis of a co-existent life limiting condition (defined as a predicted life expectancy under one year).</li> </ul>



Figure 4-1 Timeline of the PROFILE study following IPF patient recruitment.

PROFILE (Prospective Observation of Fibrosis in the Lung Clinical Endpoints) study conducted at Royal Brompton hospital. Diagnosis of IPF was based on the 2011 joint guidelines (Raghu, 2011). Bronchoalveolar lavage (BAL) was performed as an initial baseline at recruitment and 3 months following recruitment (highlighted in yellow). Other acronyms: High-resolution computed tomography (HRCT) of chest, 6 Minute Walk Test (6MWT).

#### 4.2.1.1 *PROFILE Study BAL collection*

Fibreoptic bronchoscopy with BAL was performed through the oropharyngeal route, according to the ATS guidelines (Meyer et al., 2012) at Royal Brompton Hospital, described previously by Molyneaux et al. (2014). The donation of any BALF towards research depended on there being adequate volume for microbiological and cytological assessment; these took priority as they were required for clinical diagnosis of IPF.

Patients were sedated with midazolam, fitted with a mouthguard and then orally intubated for bronchoscopy. 240 ml of buffered saline with 0.005% sodium bicarbonate was divided into 4 x 60 ml syringes. A 60 ml syringe full was slowly instilled into a segment of the right middle lung lobe before being aspirated completely, this process was then repeated for each syringe. The samples were then stored in 200 ml falcon tubes on ice before being spun at 1900rpm for ten minutes at 4°C. The supernatant was then stored at -80°C, whilst the pellet (airway cells) was discarded.

#### 4.2.2 *Pre-clinical Bleomycin Model Time Course Study with BAL collection*

As outlined in Chapter 3, we conducted a time course experiment for our bleomycin-driven guinea pig model of IPF that also caused the animals to cough spontaneously. Guinea pigs were intratracheally instilled with 6 USP/kg of bleomycin or saline vehicle, and terminated 1, 2, 3 or 4 weeks later. Guinea pig BALF was collected (as described in Section 3.2.3.1), processed and stored (as described in Section 3.2.3.4).

## 4.2.3 Mediator Assays

### 4.2.3.1 8-isoprostane

To detect evidence of oxidative stress in the lungs of bleomycin-treated guinea pigs or IPF patients, we sought to quantify the concentration of 8-isoprostane (also known as 8-iso-PGF<sub>2α</sub>) in their BALF. 8-isoprostane is a prostaglandin isomer formed through the free radical catalysed metabolism of arachidonic acid, which is itself derived from the cell membrane's phospholipids, as such it is widely used as a biomarker for antioxidant deficiency and oxidative stress (Figure 4-2)(Montuschi et al., 1998, Catalán et al., 2018).

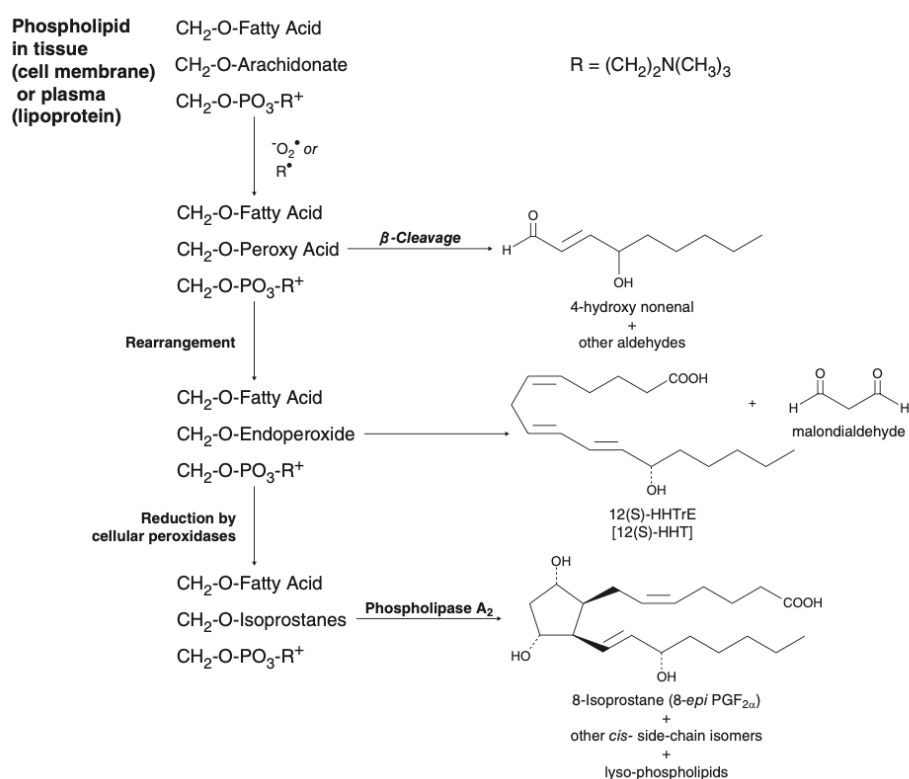


Figure 4-2 The metabolic formation of 8-isoprostane, a biomarker for lipid peroxidation.

8-isoprostanes are metabolised through free radical catalysis of arachidonic acid, a molecule derived from the phospholipids of the cell membrane. Adapted from the accompanying booklet to Cayman's 8-isoprostane ELISA kit (516351; Cayman Chemical, USA).

#### 4.2.3.1.1 8-Isoprostane ELISA

To determine the concentration of 8-Isoprostane in BALF we used a commercially available Acetylcholinesterase (AChE) competitive enzyme-linked immunosorbent assay (ELISA) kit (Item No. 516351; Cayman Chemical, USA). In short, the assay works by using an 8-isoprostane-AChE conjugate (henceforth referred to as 8-isoprostane tracer) that competes with the free 8-isoprostane in the sample being quantified, to bind to rabbit antiserum binding sites. The rabbit antiserum-8-

isoprostane (either free or tracer) complex then binds to mouse anti-rabbit IgG that is itself adhered to the well of the plate. After washing off any unbound reagent, Ellman's reagent, a solution containing acetylthiocholine and 5,5'-dithio-*bis*-(2-nitrobenzoic acid) is added to the well. The AChE (derived from the electric eel due to its high catalytic turnover) catalyses the hydrolysis of acetylthiocholine into thiocoline, which then in turn produces 5-thio-2-nitrobenzoic acid, which has a strong absorbance at 412 nm.

The kit was followed according to the manufacturer's instructions. Bronchoalveolar Lavage Fluid (BALF) samples from the guinea pigs that were part of the bleomycin time course response experiment (Chapter 3), or BALF samples from IPF patients in the PROFILE study were thawed on ice.

50 µl of the of the kit's ELISA buffer was combined with 50 µl of the BALF buffer and added to designated non-specific binding (NSB) wells of the assay plate whilst 50 µl of BALF buffer was added to the designated maximum binding ( $B_0$ ) wells. As mentioned previously, the BALF buffer used for *in vivo* experiments was RPMI media and for IPF patients in the clinic it was a solution combined of the following: 0.275 ml of Sodium Bicarbonate (8.4% w/v) added to 500 ml of 0.9% Sodium Chloride (0.9% w/v).

Next, 50 µl from each of the 8-isoprostane ELISA standards was added to its designated well. The final concentrations of these 8-isoprostane standards ranged from between 0.8 and 500 pg/ml, having been serially diluted with the relevant BALF buffer.

Following this, 50 µl of each BALF sample was added to the relevant well; each sample was tested in duplicate. After the samples were added, 50 µl of the kit's AChE Tracer was added to all of the wells except the total activity (TA) and the blank wells. Similarly, 50 µl of the kits ELISA Antiserum was added to each well except the TA, NSB and the blank wells. The plate was then incubated overnight for 18 hours at 4°C.

The next day, the plate's wells were emptied of all reagents before being rinsed 5 times with the kit's wash buffer. The kit's Ellman's reagent was reconstituted and a volume of 200 µl of it was immediately added to each well. The plate was then covered in plastic film, agitated by an orbital shaker with an opaque lid, and allowed to develop in the dark for between 90-120 minutes.

Finally, the plate was read at a wavelength between 405-420 nm, once the absorbance of the  $B_0$  wells was between 0.3-1.0 arbitrary units (A.U.).

The data was prepared according to the instructions that accompanied the kit so that the 'Sample or Standard Bound/Maximum' ( $B/B_0$ ) could be calculated for all the wells. Using Prism software

(GraphPad; CA, US), a standard curve was created by using linear (y) and log (x) axes and performing a 4-parameter logistic fit.

#### 4.2.4 Tryptase

As we will discuss later on in this thesis, trypsin is the major PAR2 cleaving enzyme in the body (Nystedt et al., 1994), but PAR2 can also be activated by tryptase and non-endogenous agonists of PAR2, which can lead to airway sensory nerve activation in both guinea pigs and humans (see Chapter 6). As previously discussed, tryptase has been shown to be increased in the BALF of IPF patients and has been associated with poorer prognoses (Kawatani et al., 2007, Compton et al., 2001, Walls et al., 1991). We sought to determine whether the presence of tryptase in the lungs is increased for the bleomycin-treated guinea pigs of this thesis and IPF patients recruited in the PROFILE study.

Degranulation is a key method by which leukocytes enact their proinflammatory effects. Granules from leukocytes (*e.g.* basophils, neutrophils, eosinophils, *etc*) contain a range of proinflammatory mediators including, but not limited to: histamine, heparin, cytokines, chemokines and proteases (Hallgren et al., 2001). Tryptase however, is almost exclusively derived from mast cells, where it makes up the major component of their granules and also forms up to 20% of the cell's protein in mast cells derived from colon, skin and lung tissue (He et al., 1998, He and Xie, 2004, Schwartz and Bradford, 1986).

##### 4.2.4.1 Tryptase Activity Assay

To measure tryptase, we used a commercially available mast cell degranulation assay kit that included a means for assaying tryptase activity (IMM001; Merck, Germany). Induction of mast cell degranulation was not necessary however, since the BALF derived from both humans and guinea pigs had been centrifuged, thereby removing all mast cells; this assay was therefore only measuring tryptase that had already been released into the lung.

In short, the assay is based on the spectrophotometric detection of the chromophore *p*-nitroaniline (*p*NA). BAL samples are incubated with tosyl-gly-pro-lys-*p*NA, a tryptase substrate, the tryptase present within the sample then proteolytically cleaves *p*NA. The free *p*NA can then be quantified using a microtiter plate reader set at 405 nm.

The kit was followed according to the manufacturer's instructions. Briefly, bronchoalveolar Lavage Fluid (BALF) samples from the guinea pigs that were part of the bleomycin time course response experiment (Chapter 3), or BALF samples from IPF patients in the PROFILE study were thawed on ice.



Next, 180 µl of each sample was added to a 96-well microtiter plate. The colourimetric reaction was then initiated by adding 20 µl of the tryptase substrate (tosyl-gly-pro-lys-pNA) to each well. The plate was then incubated in the dark and gently agitated in a plate reader for 120 minutes, as this is when the enzymatic reaction begins to plateau. Finally, the absorbance was read at 405 nm.

#### 4.2.5 ATP

As discussed previously (Chapter 6), various studies have found that excess levels of extracellular ATP (eATP) are present within the lungs of patients with a range of different chronic respiratory diseases, including: IPF, asthma and COPD (Baxter et al., 2014, Idzko et al., 2007, Riteau et al., 2010). It is thought that eATP may represent a danger signal to alert the immune system to tissue damage or cellular stress (Riteau et al., 2010). As evidenced by Bonvini et al. (2016), ATP can elicit cough in guinea pigs through activation of the purinergic receptor P2X3, similarly, Abdulqawi et al. (2015) found that pharmacologically inhibiting P2X3 significantly reduced the daytime cough rate of refractory chronic cough patients. We sought to investigate whether ATP was elevated in the BALF of bleomycin guinea pigs and IPF patients from the PROFILE study as this could be contributing to their cough.

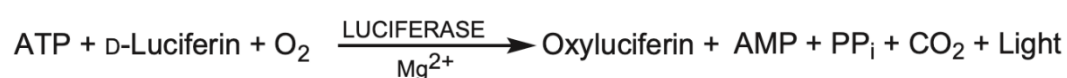
Whilst this thesis utilises BAL to measure and confirm the elevated levels of the alarmin ATP in IPF patient BAL, it remains possible, albeit unlikely, that the intrusive process of BAL itself could be instigating a release of such alarmins and thereby skewing the data of studies that attempt to measure them. Such a phenomenon has been reported as a result of ventilator use (Grazioli et al., 2019), however it has not to our knowledge been reported as a result of BAL.

##### 4.2.5.1 ATP Assay

To measure ATP, we used a commercially available ATP detection assay that utilised the ATP-dependent, bioluminescent reaction where the molecule D-luciferin is catalysed into oxyluciferin by the firefly (*Photinus pyralis*) enzyme luciferase (ATPlite Luminescence Assay System; PerkinElmer, MA, US)(Equation 4-1). The intensity of the bioluminescence detected by the luminescence reader is therefore directly proportional to the concentration of ATP in the sample being tested.

*Equation 4-1 The bioluminescent reaction catalysed by firefly (Photinus pyralis) luciferase.*

*This reaction is utilised in this chapter to measure ATP concentrations in Guinea Pig and IPF patient BALF. Adapted from the accompanying booklet to PerkinElmer's 'ATPLite' ATP detection assay (PerkinElmer, MA, US).*



The protocol for the ATP detection assay was slightly altered from the kit's manual since it was not necessary to use the accompanying cell lysis solution, as the BAL from both bleomycin-treated guinea pigs and humans had been spun down prior to ATP measurement. Briefly, bronchoalveolar Lavage Fluid (BALF) samples from the guinea pigs that were part of the bleomycin time course response experiment (Chapter 3), or BALF samples from IPF patients in the PROFILE study were thawed on ice. Next, ATP standard solutions were serially diluted in nuclease free water, so that they had a final concentration ranging between 100 pM and 100  $\mu$ M. 10  $\mu$ l of each standard was added to the relevant wells of the plate, whilst 10  $\mu$ l of nuclease free water was added to each of (what were shortly to become) the sample wells. Next 100  $\mu$ l of BALF buffer was added to the standard wells; as mentioned previously, the BALF buffer used for *in vivo* experiments was RPMI media and for IPF patients in the clinic it was a solution combined of the following: 0.275 ml of Sodium Bicarbonate (8.4% w/v) added to 500 ml of 0.9% Sodium Chloride (0.9% w/v). After this, 100  $\mu$ l of BALF sample was added to each of the sample wells. To initiate the bioluminescent reaction, 50  $\mu$ l of the kit's substrate solution was added to all of the wells. The plate was then incubated in the dark, at room temperature, for 10 minutes, the first 5 minutes of which it was agitated by an orbital shaker set to 700 rpm. Finally, the plate was placed within a plate reader capable of quantifying luminescence, and the light emerging out of each of the plate's wells was measured.

The ATP concentrations were then interpolated from the standard curve linearly by plotting Log[concentration] in the x axis and Log[bioluminescence] (A.U.) in the y axis.

#### 4.2.6 Statistical analysis

All data are presented as mean  $\pm$  S.E.M. Non-parametric Mann-Whitney tests were used to determine significance between the levels of different biomarkers in BALF, due to there being too few replicates to test for normal distribution.

### 4.3 Results

#### 4.3.1 8-Isoprostane

##### 4.3.1.1 8-isoprostane in bleomycin-treated guinea pig BALF

To see if oxidative stress was higher in the lungs of guinea pigs with bleomycin-induced pulmonary fibrosis, 8-isoprostane concentration (a biomarker for lipid peroxidation) was quantified in their BALF. 8-isoprostane concentration was significantly higher in bleomycin-treated guinea pigs than in vehicle-treated guinea pigs following 1 week (22.6 $\pm$ 2.49 vs. 11.4 $\pm$ 1.07 pg/ml), 2 weeks (33.1 $\pm$ 8.80 vs. 12.0 $\pm$ 1.20 pg/ml), and 4 weeks (15.9 $\pm$ 4.33 vs. 7.0 $\pm$ 1.20 pg/ml) of intratracheal incubation. The highest mean concentration of 8-isoprostane was after 3 weeks of bleomycin incubation, however this was not significantly more than vehicle (50.0 $\pm$ 24.13 vs. 5.6 $\pm$ 1.03 pg/ml).

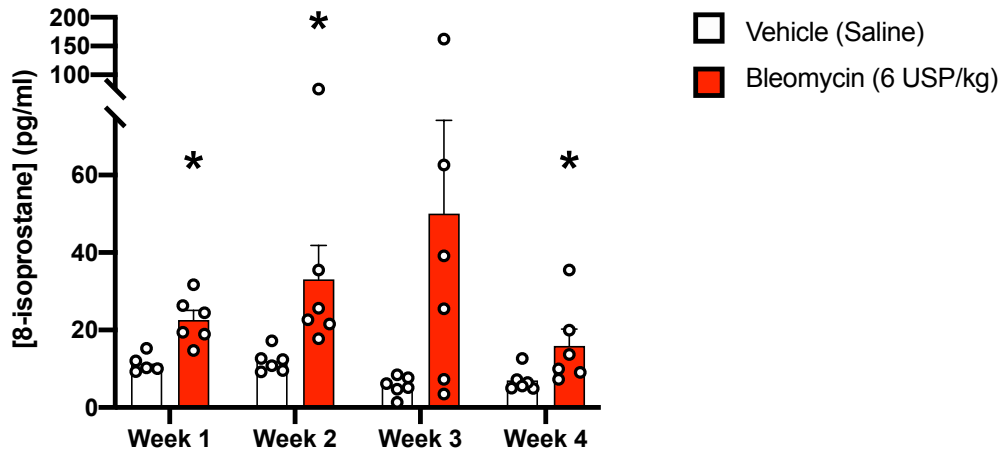


Figure 4-3 Concentration of 8-isoprostane in guinea pig BALF from the bleomycin time course study.

8-isoprostane — a biomarker of lipid peroxidation — was measured in the BALF of guinea pigs intratracheally incubated with bleomycin or saline vehicle for 1, 2, 3, or 4 weeks. Data shown as mean  $\pm$  S.E.M.,  $5 \leq n \leq 6$ . \* indicates statistical significance ( $p < 0.05$ ) measured by performing nonparametric Mann-Whitney test comparing [8-isoprostane] in bleomycin-treated animal BALF to vehicle-treated BALF for that week.

#### 4.3.1.2 8-isoprostane in IPF patient BALF

To see if oxidative stress was higher in the lungs of IPF patients than healthy controls, 8-isoprostane concentration (a biomarker for lipid peroxidation) was quantified in their BALF. 8-isoprostane concentration was significantly higher in IPF patients than in healthy controls ( $2.1 \pm 0.58$  versus  $0.5 \pm 0.46$  pg/ml, respectively).

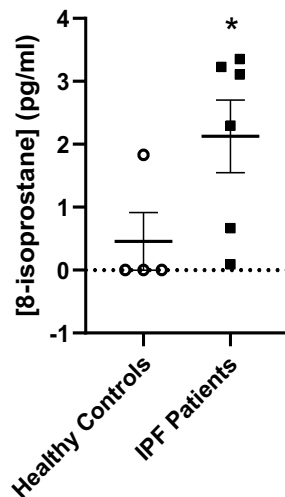


Figure 4-4 Concentration of 8-isoprostane in IPF patient BALF and healthy controls.

8-isoprostane — a biomarker of lipid peroxidation — was measured in BALF taken from patients diagnosed with IPF or from healthy volunteers. Data shown as individual values, with mean  $\pm$  S.E.M.,  $4 \leq n \leq 6$ . \* indicates statistical significance ( $p < 0.05$ ) measured by performing nonparametric Mann-Whitney test comparing [8-isoprostane] in IPF patients to healthy controls.

### 4.3.2 eATP

#### 4.3.2.1 eATP in bleomycin-treated guinea pig BALF

eATP concentration was assessed in the BALF of guinea pigs to see if levels were increased in animals with bleomycin-induced fibrosis. eATP concentration peaked after 1 week of incubation for the bleomycin animals ( $446 \pm 55.6$  pM), however this was not statistically significant ( $p=0.0628$ ) compared to vehicle ( $176 \pm 89.1$  pM). In fact, there were no statistically significant differences in BALF [eATP] between vehicle-treated animals and bleomycin-treated animals after any of the incubation times. One value in week 3 that was more than 2 standard deviations away from the mean was excluded from the bleomycin treated group; this was following an outlier identification test using Prism's inbuilt ROUT (robust regression followed by outlier identification) method (Motulsky and Brown, 2006).

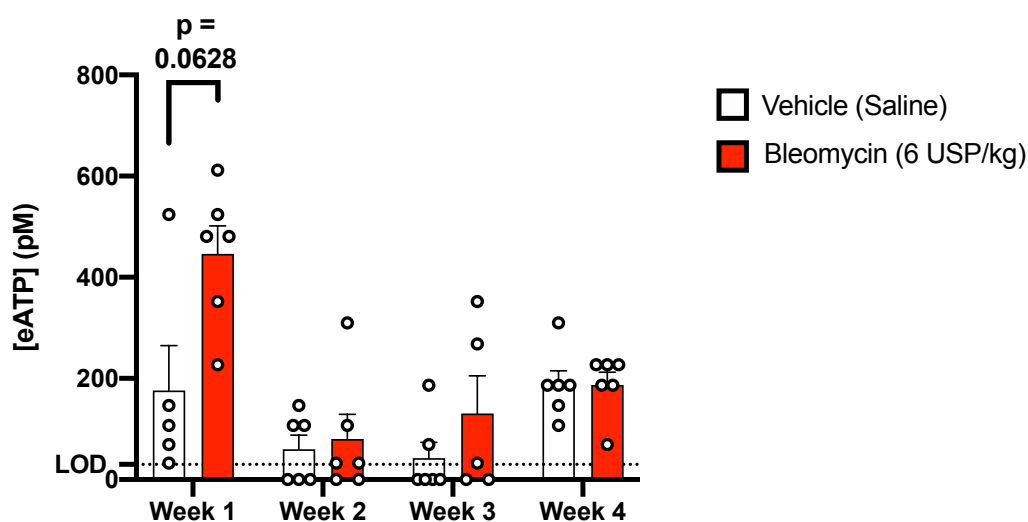


Figure 4-5 Concentration of eATP in in guinea pig BALF from the bleomycin time course study.

Extracellular ATP (eATP) was measured in the BALF of guinea pigs intratracheally incubated with saline vehicle or bleomycin for 1, 2, 3 or 4 weeks. Data shown as individual values, with mean  $\pm$  S.E.M.,  $4 \leq n \leq 6$ . No statistically significant differences ( $p < 0.05$ ) were seen between vehicle and bleomycin-treated animals by means of a nonparametric Mann-Whitney test, however after 1 week of bleomycin incubation  $p = 0.0628$  compared to vehicle-treated animals. LOD (Limit of Detection) for this particular ATP assay was 30pM.

#### 4.3.2.2 eATP in IPF patient BALF

To see if eATP was higher in the lungs of IPF patients than healthy controls, it was assayed in their BALF. In the few patient samples that were tested, there appeared to be no differences between [eATP] in IPF patient BALF ( $2.41 \pm 0.733$  nM) or in healthy control BALF ( $2.27 \pm 0.59$  nM).

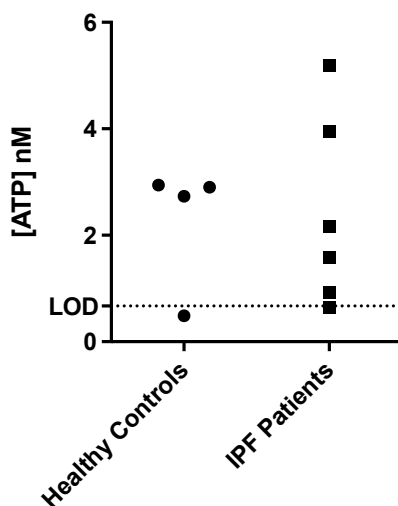


Figure 4-6 Concentration of eATP in BALF of IPF patients and healthy controls

Extracellular ATP (eATP) was measured in the BALF donated by IPF patients and healthy volunteers. Data shown as individual values,  $4 \leq n \leq 6$ . LOD (Limit of Detection) for this particular ATP assay it was 670pM.

#### 4.3.3 Tryptase

##### 4.3.3.1 Tryptase activity in bleomycin-treated guinea pig BALF

Tryptase activity (quantified by measuring quantity of cleaved tryptase substrate) was assessed in the BALF of guinea pigs to see if levels were increased in animals with bleomycin-induced fibrosis. Guinea pigs intratracheally instilled with bleomycin had significantly more tryptase activity than vehicle-treated animals following 1 week ( $0.17 \pm 0.017$  vs.  $0.08 \pm 0.001$  A.U), 2 weeks ( $0.16 \pm 0.015$  vs.  $0.08 \pm 0.01$  A.U.), 3 weeks ( $0.15 \pm 0.023$  vs.  $0.08 \pm 0.012$  A.U) and 4 weeks ( $0.17 \pm 0.013$  vs  $0.07 \pm 0.004$  A.U.) of incubation.

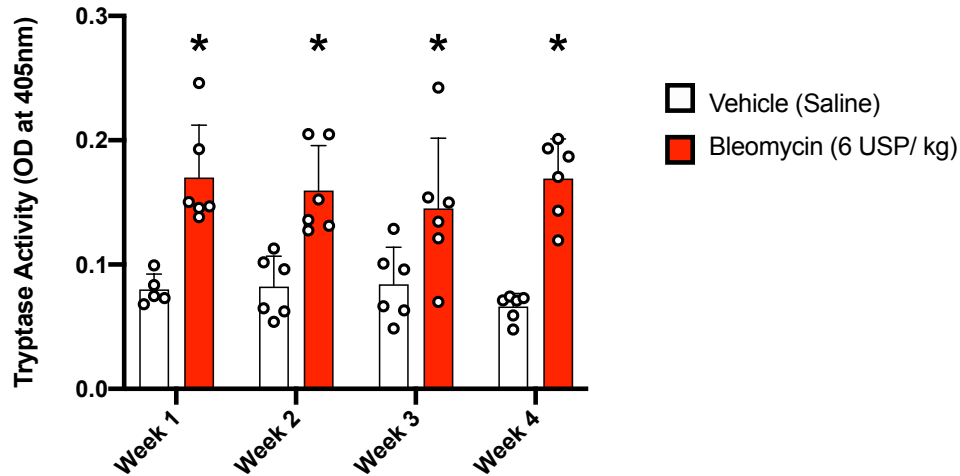


Figure 4-7 Tryptase activity in the BALF of guinea pigs from the bleomycin time course study.

Guinea pigs were intratracheally incubated with either vehicle or bleomycin for 1, 2, 3 or 4 weeks. Optical density (OD) at 405 nm was measured in A.U. in each BALF sample after 120 min incubation with the tryptase substrate tosyl-gly-pro-lys-pNA. Data shown as mean A.U.  $\pm$  S.E.M.,  $5 \leq n \leq 6$ . \* indicates statistical significance ( $p < 0.05$ ) measured by performing nonparametric Mann-Whitney test comparing OD in bleomycin-treated animal BALF to vehicle-treated BALF for that week.

#### 4.3.3.2 Tryptase activity in IPF patient BALF

To see if tryptase levels were higher in the lungs of IPF patients than in healthy controls, tryptase activity (quantified by measuring quantity of cleaved tryptase substrate) was quantified in their BALF. Tryptase activity was not significantly higher in IPF patients than in healthy controls ( $0.057 \pm 0.031$  versus  $0.026 \pm 0.004$  A.U., respectively), although 1 IPF patient seemed to have a value that far exceeded the rest of the patients in the cohort (0.305 A.U.).

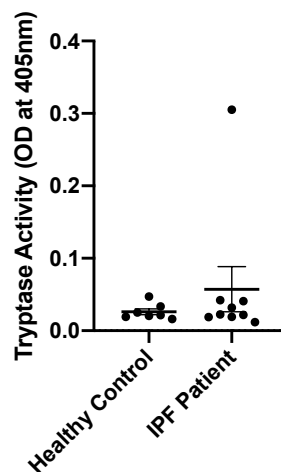


Figure 4-8 Tryptase activity in BALF taken from patients diagnosed with IPF or healthy volunteers.

Optical density (OD) at 405 nm was measured in A.U. in each BALF sample after 120 min incubation with the tryptase substrate tosyl-gly-pro-lys-pNA. Data shown as individual values, with mean A.U.  $\pm$  S.E.M.,  $7 \leq n \leq 9$ . \* indicates statistical significance ( $p < 0.05$ ) measured by performing nonparametric Mann-Whitney test comparing [8-isoprostane] in IPF patients to healthy controls.

## 4.4 Discussion

The aims of this chapter were: firstly, to replicate findings from other research centres that BALF from IPF patients has elevated levels of eATP (Riteau et al., 2010, Müller et al., 2017), mast cell tryptase (Walls et al., 1991) and oxidative stress (in the form of 8-isoprostane) (Krauss et al., 2019, Montuschi et al., 1998) when compared to healthy controls; and secondly, to also measure the presence of these biomarkers within BALF of guinea pigs from the *in vivo* model of fibrosis-induced spontaneous cough (outlined in Chapter 3), and to see if levels were increased compared to animals without fibrosis. As we will see in the next chapters, PAR2 agonists and ROS activate airway sensory nerves, whilst ATP is also capable of this and has been further shown to elicit cough (Bonvini et al., 2016, Abdulqawi et al., 2015). Therefore, if any of these biomarkers were found to be increased in both IPF patients, and in our model, then it would designate it as a worthwhile target for future antitussive therapeutic investigation.

Firstly, 8-isoprostane was measured in the BALF of guinea pigs from the bleomycin time course response experiment (Section 3.2.3). As discussed previously (Section 4.2.3.1), 8-isoprostane is widely used as a biomarker for lipid peroxidation. 8-isoprostane concentration was found to be significantly higher in the BALF of pulmonary fibrotic guinea pigs following 1, 2 and 4 weeks of bleomycin incubation. This is not necessarily surprising, at least for the first week, when considering the evidence (see Section 3.2.2.1) that bleomycin does in fact exert its inflammatory and fibrotic effects through the direct production of Reactive Oxygen Species (ROS) (Claussen and Long, 1999). However, there is also more recent evidence that bleomycin indirectly causes the production of extracellular ROS too (Allawzi et al., 2019), which perhaps better explains the higher levels of oxidative stress, particularly in the later weeks of the *in vivo* study. Key to this evidence is the finding that mice unable to express the p47<sup>phox</sup> subunit of the NADPH oxidase complex are protected from bleomycin-induced fibrosis (Manoury et al., 2005). Although dormant under normal circumstances, NADPH oxidase is an extracellular space-facing, membrane bound enzyme complex, expressed by neutrophils, that when activated, catalyses the production of superoxide radicals to kill bacteria *i.e.* respiratory bursts (Thomas, 2017). Similarly, myeloperoxidase, another bactericidal enzyme that is highly expressed by the macrophages and neutrophils recruited to the lung, produce ROS (specifically HOCl<sup>-</sup>) (Bos et al., 1978, Xu et al., 2016). The radicals generated by these oxidative bursts augment the alveolar epithelial damage caused by bleomycin and further perpetuate inflammation (Leach et al., 2013, Moore et al., 2001). The robustness of the fibrotic response from the bleomycin model demonstrated in this thesis is therefore not unexpected when observing the high level of macrophage and heterophil (the guinea pig equivalent of a neutrophil) recruitment to the lungs (Figure 3-26).

Similar to what has been described elsewhere (Montuschi et al., 1998), 8-isoprostane was significantly increased in the BALF of IPF patients compared to healthy controls (Figure 4-4). 8-isoprostane has also been found by others to be elevated in the exhaled breath concentrate (EBC)(Chow et al., 2012, Psathakis et al., 2006), serum (Malli et al., 2013) and urine (following exercise)(Jackson et al., 2010) of IPF patients. Oxidative stress is well documented in IPF (Kinnula et al., 2005, Kliment and Oury, 2010) and is suspected to play a critical role in the pathogenesis of the disease through: the promotion of inflammation via increased production of cytokines and growth factors; which leads to the fragmentation of the ECM, myofibroblast differentiation, aberrant epithelialisation; and consequently, DNA damage, P53 activation and eventually, apoptosis of alveolar epithelial cells (Fois et al., 2018). Despite the antioxidant NAC proving able to attenuate bleomycin-induced fibrosis in mice and rat models (Berend, 1985, Hagiwara et al., 2000, Shahzeidi et al., 1991), NAC (discussed in more detail in Section 5.4) has generated contradictory and often unsatisfactory results in IPF patients (Rogliani et al., 2016); this has raised questions about the reliability of the bleomycin model, and whether oxidative stress is actually a consequence of IPF, rather than a cause (Otoupalova et al., 2020).

With regards to the source or (more likely) sources of the oxidative stress in the IPF lung, there is unsurprisingly a larger list of suspects compared to bleomycin-induced fibrosis. As with the bleomycin model, much of the ROS generation in the IPF lung could be generated by the NADPH oxidase complex, and not only by immune cells; interestingly, NOX4 a subunit of the complex is highly expressed in the fibroblastic foci of IPF patients (Amara et al., 2010). Some also point to cigarette smoke as a contributing source; being the single largest risk factor of developing IPF (Baumgartner et al., 1997), coupled with the evidence that it causes oxidative injury to the lung epithelium (Kosmider et al., 2011), this is indeed a possibility. There is also evidence that implicates mitochondrial-generated ROS (including H<sub>2</sub>O<sub>2</sub>) from epithelial cells, fibroblasts and alveolar macrophages in the pathogenesis of IPF (He et al., 2011); mitochondrial dysfunction is also a hallmark of IPF (Zank et al., 2018). Similarly, peroxisomes, another source of cellular ROS, have been shown to have impaired function in IPF lung tissue (Oruqaj et al., 2015). It would also be remiss to not mention cellular senescence. IPF is widely considered to be a disease of the aging lung (Schafer et al., 2017) and senescent cells have a reduced antioxidant capacity (Zhang et al., 2015) thereby allowing the sources of oxidative stress listed above to inflict more alveolar damage.

[eATP] was measured in the BALF of guinea pigs from the bleomycin time-course study, but there was no statistically significant difference in the eATP concentration between vehicle and bleomycin-treated animals. After 1 week of bleomycin incubation however, eATP concentration peaked and was over twice as concentrated in the lungs of bleomycin-treated animals when compared to



vehicle-treated animals; this difference was close to being significant ( $p=0.0628$ ). We are aware of only two other studies that have measured [eATP] in the BALF of a pre-clinical model of IPF, both of which were bleomycin-driven murine models (Müller *et al.*, 2017, Riteau *et al.*, 2010). Rather than investigating eATP in a tussive capacity, these studies instead investigated whether eATP mediated fibrosis; with Riteau *et al.* and Müller *et al.* concluding that eATP drives fibrosis by engaging the purinergic receptors P2X7 and P2Y2, respectively. Each of these studies found [eATP] was significantly increased in bleomycin-treated mouse BALF when compared to vehicle-treated controls, with Riteau *et al.* confirming an acute increase 4 hours post bleomycin i.t. and Müller *et al.* confirming a longer term increase that (like in this chapter) peaks 7 days following bleomycin i.t..

Unlike in this chapter, both Riteau *et al.* and Müller *et al.* detected significantly elevated eATP levels in the BALF of IPF patients when compared to healthy controls. We suppose that this could be due to two main reasons: firstly, the relatively low sample number of IPF patients and healthy controls used in this chapter; and secondly, the lack of enough provision to avoid ATP catabolism. eATP is hydrolysed very quickly in biological samples by extracellular ATP/ADPases (Kaczmarek *et al.*, 1996, Picher *et al.*, 2003). Riteau *et al.* used a Hanks' balanced salt solution when sampling BALF that omitted calcium and magnesium, and also contained EDTA, to help slow the breakdown of ATP by ATPases, whilst Müller *et al.* used fresh BALF where possible. Whilst it would be prudent to implement these methods in any future study of [ATP] in BALF, we further intend to look at breakdown products of ATP (ADP, AMP, *etc*) as a proxy-biomarker using techniques such as mass spectrometry, in the hope that this might improve the reliability of [ATP] quantification in the future. Despite our inability to demonstrate an elevated [ATP] within IPF BALF, we are still under the assumption that it exists.

As to the source of this eATP, it is well documented that under conditions of cellular stress, there exist a variety of lytic and non-lytic mechanisms by which a multitude of airway cells (*e.g.* platelets, structural and inflammatory cells) release ATP, in what has been referred to as a 'danger signal' (Bours *et al.*, 2006, Burnstock, 2006, Cicko *et al.*, 2018, Ferrari *et al.*, 1997).

As mentioned previously, much of the excitement surrounding purinergic signalling with regards to cough, was the finding that Gefapixant (AF-219), an oral P2X3 antagonist, was capable of reducing cough frequency in chronic idiopathic cough patients by an unprecedented 75% (Abdulqawi *et al.*, 2015). Hoping to repeat this success with IPF-associated chronic cough, the medication was also assessed within IPF patients in a phase 2 clinical trial (Martinez *et al.*, 2019). Whilst being generally well tolerated in patients, Gefapixant was only able to inhibit awake cough frequency by 25%, following 14 days of treatment, and more disappointingly, this reduction of cough rate was not

statistically significant ( $p=0.07$ ); the authors blamed this insignificant reduction on a randomisation error that took place mid study. Despite this, Gefapixant achieved a reduction in cough rate greater than 30% in 50% of patients, whereas only 26% of patients administered with placebo had the same % reduction. Notwithstanding the failure of this study to achieve its primary endpoint, the authors remain hopeful that a redesigned study with a change in dosing regimen could yield a significant result. Assuming that the true inhibitory capacity of Gefapixant is not far higher than 25%, it is not unreasonable to suppose that there is at least one other mediator driving IPF-associated cough besides ATP, *e.g.* oxidative stress.

Tryptase activity was quantified in the BALF of bleomycin-treated guinea pigs. Following intratracheal instillation, tryptase activity was significantly increased in the BALF of guinea pigs treated with bleomycin for the entirety of the study (Figure 4-7). Evidence implicating mast cell tryptase in fibrosis is plentiful, as it is a potent mitogen for fibroblasts, whilst also stimulating them to produce more collagen and increase their chemotactic activity (Cairns and Walls, 1997, Gruber et al., 1997, Ruoss et al., 1991). It was more recently discovered through research that included the use of bleomycin models, that the pro-fibrotic effect proteases like tryptase have on fibroblasts is mediated through PAR2 (Bagher et al., 2018, Lin et al., 2015a). As the PAR2 antagonist P2pal-18s has been shown to significantly reduce bleomycin-induced fibrosis through prophylactic and therapeutic administration in mice (Bagher et al., 2018, Lin et al., 2015a), it will be interesting to see whether it can also reduce cough rate therapeutically in the *in vivo* model of fibrosis-induced spontaneous cough developed as part of this thesis; especially in light of the evidence (shown later in Chapter 6) that PAR2 activation causes airway nerve impulses and that it can potentiate cough sensitivity in guinea pigs (Gatti et al., 2006).

Lastly, tryptase activity was assessed in the BALF of IPF patients and healthy controls. The quantity of mast cells within the IPF lung has previously found to be increased, and the cells themselves supposedly release more tryptase than mast cells within a normal human lung (Hunt et al., 1992). Although there was an increase in the mean tryptase activity for IPF patients (Figure 4-8), this was not statistically significant. Curiously, however, one patient had a much higher rate of tryptase activity than the other patients, raising the possibility of there being a patient subgroup with this phenotype. Indeed, Kawatani et al. (2007) were only able to detect an activated form of tryptase in 14 of the 32 IPF patients they collected BALF from; these 14 patients also had a poorer prognosis than the tryptase-negative patients.

The onset of the COVID-19 pandemic has understandably put great strain on Royal Brompton Hospital, the specialist lung medical centre associated with Imperial College's National Heart and

Lung Institute, where this PhD was undertaken. It had been our intention to correlate levels of the biomarkers measured in this chapter, with lung function parameters, cough-related quality of life questionnaire scores, and objective cough measurements, within an expanded IPF BAL sample set. Work towards this objective is currently ongoing (see Section 8.4.5), but we hope that through stratifying the patient data by these different parameters it will reveal new statistically significant insights into how these biomarkers relate to patient disease progression and cough severity.

In summary: oxidative stress biomarker 8-isoprostane was significantly elevated in the BALF of both bleomycin-treated guinea pigs and IPF patients, which supports our hypothesis for this biomarker; eATP concentration, however, was only elevated in bleomycin-treated guinea pigs and only in week 1 ( $p=0.0628$ ); and whilst tryptase activity was significantly upregulated in bleomycin-treated animals at all 4 weeks, the increase in its activity was not significant in IPF patients. Besides the 8-isoprostane findings, our results do not fully support this chapter's hypothesis that all three biomarkers are increased in the IPF lung, nonetheless, when considering the limitations of this chapter, (namely, the limited patient samples and the inefficient method of measuring eATP), we also believe that it would not be wise to reject the hypothesis outright for tryptase and eATP at this stage, before more human samples can be tested for both biomarkers, and more reliable eATP measurements can be taken. Oxidative stress and TRPA1 —the neuronal receptor that mediates oxidative stress-induced airway nerve activation (see next chapter)— are no doubt worthy targets to pharmacologically probe in this thesis' *in vivo* model of fibrosis-induced spontaneous cough and perhaps within IPF patients themselves. Similarly, mechanisms that inhibit the cellular release of ATP and tryptase, or prevent them from activating their downstream receptors, also appear worth investigating further in our model in pursuit of an efficacious antitussive medication for IPF-associated chronic cough.

## 5 Investigating a role for oxidative stress in airway sensory nerves

### 5.1 Rationale

There is a growing body of evidence that oxidative stress plays a pivotal role in the pathogenesis of IPF (Kinnula et al., 2005, Kliment and Oury, 2010), as well as a range of other lung diseases including asthma and COPD (Anderson and Macnee, 2009, Riedl and Nel, 2008). Oxidative stress is an imbalance between the body's production of oxidants and antioxidants, which leads to tissue damage and cellular dysfunction. Activities that are associated risk factors for developing IPF such as smoking cigarettes, are known to not only generate the production of reactive oxygen species (ROS) (e.g. H<sub>2</sub>O<sub>2</sub>), but are also associated with fibrotic interstitial lung reactions (Kinnula et al., 2005).

Given the above evidence implicating oxidative stress in IPF, and the fact that IPF patients frequently suffer from a chronic cough, we sought to explore whether ROS could be contributing to this symptom by seeing if they were capable of activating the airway sensory nerves that facilitate cough.

Further to this, we used pharmacological tools to discern whether such an activation was mediated through TRPA1, a non-selective cation channel known to be activated by the ROS H<sub>2</sub>O<sub>2</sub> in other sensory neurons (Sawada et al., 2008, Andersson et al., 2008).

A recent phase 2 clinical trial found that an inhaled formulation of sodium cromoglycate reduced daytime cough frequency in IPF patients (Birring et al., 2017). Interestingly, *in vitro* studies performed by this lab have found that cromoglycate is an agonist of G protein-coupled receptor 35 (GPR35), which inhibits TRPA1 driven activation of airway sensory nerves and initiation of airway reflexes (e.g. cough and bronchospasm) (Maher et al., 2015). The clinical effect of cromoglycate, when considered alongside the *in vitro* data showing a blockade of TRPA1-driven sensory nerve activation, suggests TRPA1 could possibly have a role in IPF-associated chronic cough.

With this knowledge in mind, we sought to investigate a role for TRPA1 in oxidant-induced airway nerve activation.

#### 5.1.1 Chapter Hypothesis

ROS such as H<sub>2</sub>O<sub>2</sub> can activate airway sensory nerves through the TRPA1 ion channel

#### 5.1.2 Aims

- Using dihydroethidium, the oxidative stress sensitive dye, show that H<sub>2</sub>O<sub>2</sub> causes intracellular oxidative stress in airway terminating neurons.

- To evaluate the effect of H<sub>2</sub>O<sub>2</sub> on airway sensory nerves *in vitro*. The oxidant will be assessed using calcium imaging of guinea pig airway specific ganglia and vagal nerve depolarisation in isolated guinea pig tissue.
- Determine a role for TRPA1 in H<sub>2</sub>O<sub>2</sub>-induced airway nerve activation by attempting to inhibit these responses with Janssen 130 (J130), a selective TRPA1 antagonist (Berthelot Didier et al., 2010), and N-Acetylcysteine, an antioxidant (Samuni et al., 2013), as a positive control.

## 5.2 Methods

### 5.2.1 Neuronal isolation and imaging

#### 5.2.1.1 *Labelling and identifying airway terminating neurons through retrograde tracking*

In order to make sure that a neuron being imaged did indeed innervate the airways, it had to have been labelled prior with 1,1'-dioctadecyl-3,3,3',3'-tetramethyl-indocarbocyanine perchlorate (Dil), a retrograde tracer dye. The dye works by infiltrating the sensory nerve endings' membrane and then being moved towards the cell body (soma), through retrograde transport (Undem et al., 2003).

Briefly, 12-14 days prior to a neuronal imaging experiment, male Dunkin Hartley guinea pigs were administered with 1 ml/kg of 0.25 mg/ml Dil through intranasal dosing; previous work conducted by this lab had found this to be an efficient route of administration towards the airways, with minimal amounts of Dil being deposited in the stomach and staining the dorsal root ganglia that innervate the abdomen. Administering the dye 12-14 days prior to the imaging experiment ensured that the dye had been axonally transported from the sensory nerve ending of the trachea, to the cell body inside the vagal ganglia. The Dil was dissolved in ethanol and diluted on the day of the administration within 0.9% saline to give a 2% V/V concentration.

To ensure Dil staining does not affect neuronal function, previous experiments have been conducted by this group to assess vagus nerve depolarisation and vagal ganglia neuronal calcium uptake in Dil-stained animals, in response to various tussive stimuli. No obvious differences were seen in these animals when compared to non-stained animals.

Prior to the administration of any drugs in a neuron imaging experiment, airway specific cells were identified by their Dil staining, which produces a fluorescent emission ( $\lambda_{Em}$ ) of 570 nm when excited at 520 nm ( $\lambda_{Ex}$ ).

#### 5.2.1.2 *Ganglia dissection and dissociation*

Guinea pigs were euthanised as described in Section 2.2. The vagal ganglia consists of the nodose and jugular ganglia, and they are located between the ear bone and the mastoid bone; they were removed using the method described previously (Dubuis et al., 2013). Briefly, the skin from the

animal's head and neck was removed and any muscle tissue covering the skull was also cleared. Next, the top of the skull was removed to reveal the brain which was then also extracted.

After this, the ear bone was removed to reveal the vagal ganglia, which are covered in a semi-transparent membrane and stuck to the occipital bone. This membrane was carefully shredded and the ganglia were then removed by cutting them free from surrounding connective tissue and the rest of the vagus nerve, they were then placed into ice cold sterile Hanks Balanced Salt Solution (HBSS: containing 5.33M KCl, 0.441mM KH<sub>2</sub>PO<sub>4</sub>, 138mM NaCl, 0.3mM Na<sub>2</sub>HPO<sub>4</sub>-7H, 5.6mM glucose, 5mM HEPES and pH 7.4; Gibco/Invitrogen).

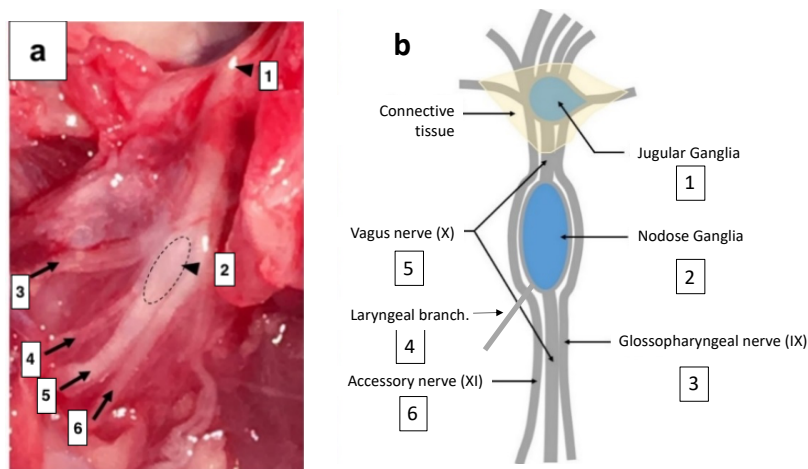


Figure 5-1 Anatomy of guinea pig vagal ganglia and its surrounding tissue.

a) a photograph of a guinea pig's vagal ganglia and its surrounding tissue: 1 – jugular ganglia; 2 – nodose ganglia; 3 – Glossopharyngeal nerve (IX); 4 – laryngeal branch; 5 – vagal nerve (X); 6 – Accessory nerve (XI). b) A schematic to better illustrate the neighbouring photograph. Diagram by Dr Eric Dubuis and displayed here with his permission

Using a microscope, the ganglia were further cleared of large obstructive connective tissue and then underwent a two-step enzymatic digestion process. Firstly, the ganglia were incubated in an activated papain solution for 30 minutes at 37°C; this solution consisted of 20 units/ml Papain (Sigma, UK) within HBSS, that was supplemented with 400mg/L L-Cysteine, 1ml/L EDTA 0.5M stock solution and 1.5ml/L CaCl<sub>2</sub> 1M stock solution. In the second step, the ganglia were incubated for 40 minutes in a solution containing Type IV collagenase (Worthington, USA, 2mg/ml) and Dispase II (Roche, UK, 2.4mg/ml), at 37°C in sterile HBSS. After this enzymatic digestion had taken place, the ganglia were then washed and centrifuged, having their supernatant removed and the pellet resuspended in sterile HBSS. The cells were then dissociated by triturating them with a heat-smoothed glass Pasteur pipette coated with L15 medium. To eliminate unwanted cell types and retain the larger neuronal cell bodies, the cell suspension was then centrifuged through a higher density L15 medium containing 20% v/v Percoll<sup>®</sup>, which is itself a suspension of colloidal silica particles. Following this centrifugation, the Percoll<sup>®</sup> was washed off with L15 medium, and after a

final centrifugation, the cells were resuspended for the last time in F12 medium (containing 1% FBS, 1% Penicillin and 100,000u/ml streptomycin). The cells were then left to adhere to Poly-D-Lysine and laminin (22.5µg/ml) coated fluorodishes, for 2 hours. Lastly, the dishes were flooded with 2ml of complete F12 medium and incubated at 37°C for 16 hours prior to the imaging experiment.

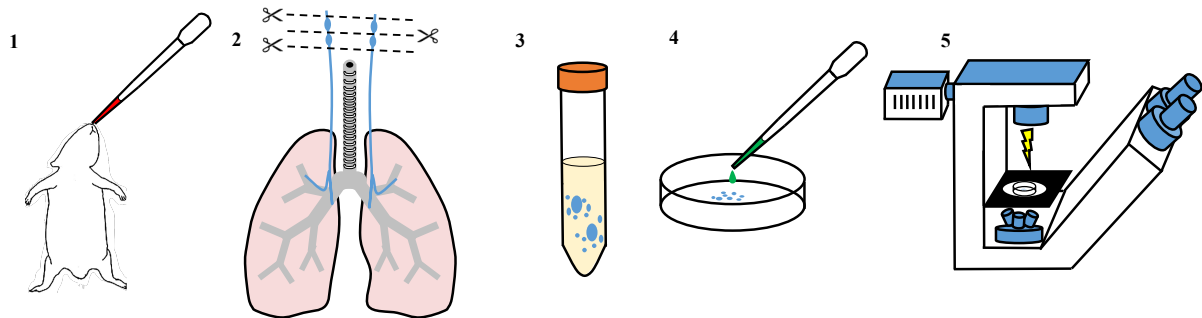


Figure 5-2 Summary of the airway terminating-neuron isolation process

**1)** Guinea pigs were dosed intranasally with the retrograde tracer dye Dil. Thereby ensuring that neurons that projected fibres towards the airways could be identified. **2)** Animals were culled by an overdose of pentobarbitone (dose, i.p.). Vagal ganglia were removed and dissected free of connective tissue. **3)** Ganglia cells were then isolated through enzymatic digestion. **4)** Neurons were then plated into a poly-D-lysine/laminin coated FluoroDish™. Prior to imaging, cells were loaded with Fura-2 AM or DHE, for calcium imaging and oxidative stress imaging experiments, respectively. **5)** Neurons that were stained with Dil were selected for imaging. Original figure by author.

### 5.2.1.3 Oxidative stress Imaging with dihydroethidium

To show that the oxidant H<sub>2</sub>O<sub>2</sub> caused intracellular oxidative stress within vagal ganglia neurons, the neurons were loaded with Dihydroethidium (DHE; Life technologies), a superoxide-sensitive fluorescent dye (Bindokas et al., 1996). Briefly, after being incubated for 16 hours following isolation (5.2.1.2), neurons were washed three times with Extracellular Solution (ECS - in mM: NaCl 136; KCl 5.4; NaH<sub>2</sub>PO<sub>4</sub> 0.33; MgCl<sub>2</sub> 1; CaCl<sub>2</sub> 2.5; Glucose 10; HEPES 10).

Next, the neurons were loaded with DHE (6µM in ECS) and incubated for 30 minutes at 37°C in the dark. The peak excitation and emission wavelengths for DHE are listed below (Table 5-1)

Table 5-1 The peak excitation and emission wavelengths of the superoxide-sensitive fluorescent dye DHE

Dye	λ <sub>Ex</sub> (nm)	λ <sub>Em</sub> (nm)
DHE	365	480
Oxidised DHE	515	580

λ<sub>Ex</sub> : Peak excitation wavelength. λ<sub>Em</sub>: Peak emission wavelength

DHE has peak excitation wavelengths (λ<sub>Ex</sub>) of 365nm (near UV blue) and 515nm (green), and peak emission wavelengths of 480 (light blue) and 580 (bright red). DHE exhibits light blue fluorescence from within the cytosol, until it becomes oxidised, whereupon it intercalates with the cell's nuclear

DNA and fluoresces bright red (Figure 5-3). To detect these changes, a mercury arc lamp was used with 2 sets of filters. The first set detected the non-oxidised DHE using excitation/emission at 365/30nm (deep blue) and 485/20nm (light blue), respectively, with a beam splitter set to 400nm. The second set detected oxidised DHE using excitation/emission at 520/21nm (green) and 581/20nm (bright red), respectively, with a beam splitter set to 550nm. The images were captured using a Hamamatsu cooled CCD camera and HClmage software (Hamamatsu, Japan).

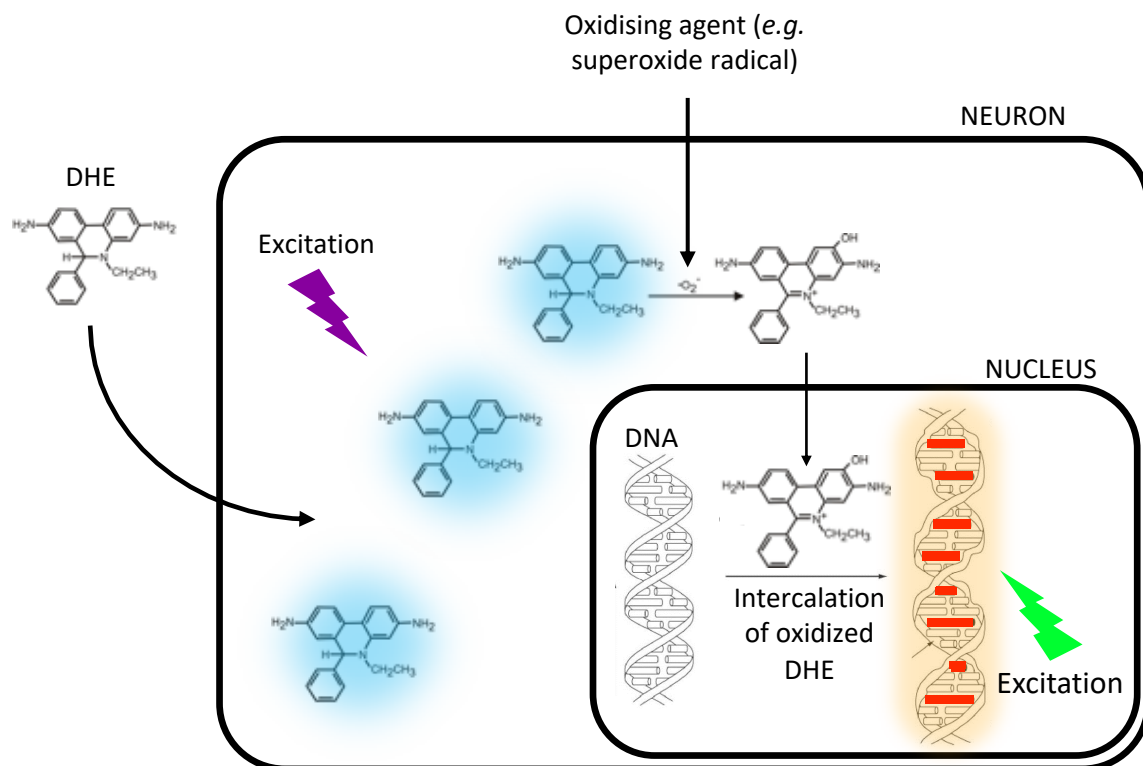


Figure 5-3 Imaging cellular oxidative stress with DHE.

*A schematic to illustrate the way by which cellular oxidative stress can be visualised with dihydroethidium (DHE). DHE permeates the cell and exhibits light blue fluorescence from within the cytosol. When DHE becomes oxidised due to oxidants within the cell, it translocates to the cell's nucleus, intercalates with the nuclear DNA, and exhibits red fluorescence upon excitation. Figure by Dr Dubuis and displayed here with his permission.*

After the 30-minute incubation with DHE had elapsed, any remaining extracellular DHE was removed by washing the neurons 3 times, at 5-minute intervals, with ECS. The fluorodish was then placed onto the microscope's stage, which itself was housed within a Perspex incubation chamber and maintained at 37°C.

All drug solutions were maintained at 37°C prior to being applied to the cells. In order to apply drugs to the cells, a perfusion system was used that allowed a complete bath change within seconds (Figure 5-4); this same system was also used in the calcium imaging experiments.



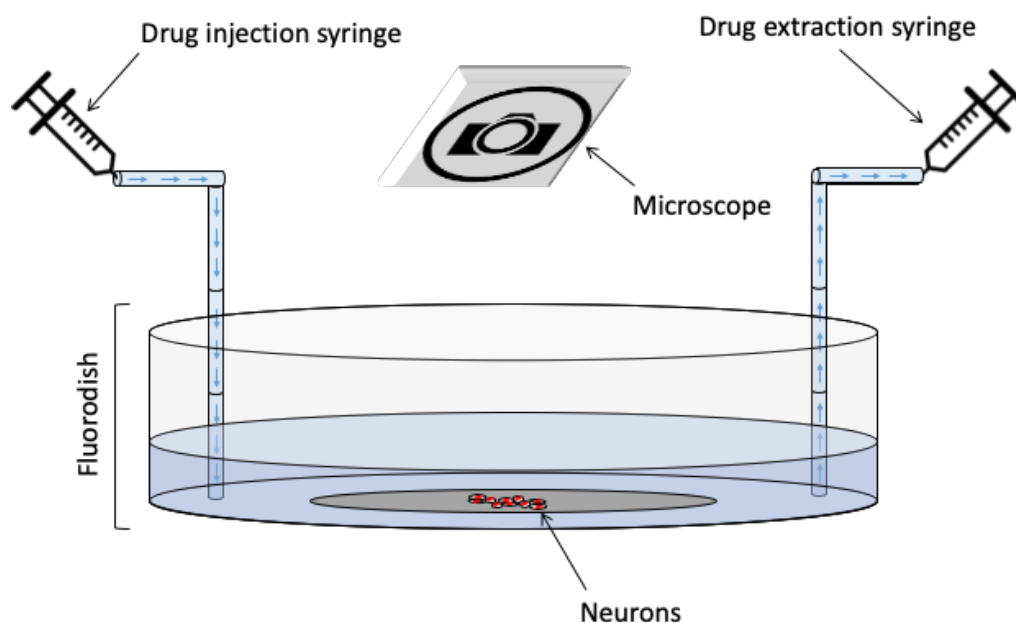


Figure 5-4 The drug perfusion system for neuronal imaging experiments.

*A schematic to illustrate the solution-changing perfusion system for neuronal imaging experiments. Perfusion tubes are placed within the bath at the edges of the fluorodish and allow for a full extraction of the bath apart from a remaining 200µl that immerses the cells in an inner well (grey circle), thereby preventing them from drying out. Original figure by author.*

The measurement of oxidative stress was undertaken by exposing the neurons to noncumulative concentrations of H<sub>2</sub>O<sub>2</sub>, ranging from 100nM to 10µM; each application was administered using volume of 2.5ml and lasted 3 minutes. Throughout the exposure to each concentration of H<sub>2</sub>O<sub>2</sub>, images were recorded at a rate of 0.1 frames per second (fps); however, when the cells were being exposed to vehicle or drugs for a long period of time, an image was recorded every 60 seconds (0.0167fps), this was to reduce photobleaching of the dye. The resting state was recording over 2 minutes prior to each application, to compare the change in oxidative stress immediately prior to and after administration of the compound. Following each application, the cells were then washed with ECS until the signal stabilised, with a minimum of 6 changes of the bath volume.

#### 5.2.1.4 Calcium Imaging

Calcium imaging is a useful technique, as it enables one to see if a stimulant is capable of causing an influx of calcium into airway terminating neurons, which is indicative of activation and thereby suggests that the compound might have a protussive effect.

Fura2-AM (Molecular Probes/Invitrogen), the membrane permeable Ca<sup>2+</sup> indicator dye, was used to measure changes in intracellular Ca<sup>2+</sup> levels ([Ca<sup>2+</sup>]<sub>i</sub>) within vagal neurons when treated with the oxidant H<sub>2</sub>O<sub>2</sub>. The acetoxymethyl (AM) moiety is attached to the Fura2 molecule through an ester bond and is necessary for it to permeate a cell membrane. Fura2-AM was dissolved in DMSO and

combined with an equal volume of PowerLoad™ (Thermo Fisher Scientific, UK), a formulation of surfactant polyols that helps disperse water insoluble molecules such as Fura2-AM, thereby further helping it permeate the cell. The Fura2-AM/PowerLoad solution was then diluted 1/100 (v/v) in ECS giving a final concentration of 12µM for Fura2-AM in the loading solution. Prior to loading, the neurons were washed three times with ECS to remove the F12 culture medium they had been incubated with after their isolation (Section 5.2.1.2). The cells were then incubated with the Fura2-AM/PowerLoad/ECS solution for 40 minutes, in the dark, at room temperature. After this, the fluorodish was washed with ECS twice to remove any remaining extracellular Fura2-AM that had not penetrated the cells. The cells were then further left in the dark for 30 minutes; this time allowed for the neurons' cellular esterases to remove the AM group from Fura2 molecule, thereby trapping the dye within the cell.

The fluorodish was then placed on the microscope's stage which resided within a chamber maintained at 37°C. The microscope used was an inverted epifluorescence microscope (Zeiss) equipped with a mercury arc lamp and a set of excitation filters at 335/7 nm (near UV) and 387/11 nm (deep blue), a 529/24 nm (green) emission filter and a 500 nm beam splitter. As with the oxidative stress imaging in the previous section, the images were also captured using a Hamamatsu cooled CCD camera and HClmage software (Hamamatsu, Japan). The peak excitation wavelengths for Fura-2 are listed below (Table 5-2).

*Table 5-2 The peak excitation and emission wavelengths of the Ca<sup>2+</sup> indicator dye Fura-2*

Dye	$\lambda_{Ex}$ (nm)	$\lambda_{Em}$ (nm)
Fura-2 Ca <sup>2+</sup> free	380	512
Fura-2 Ca <sup>2+</sup> bound	340	510

$\lambda_{Ex}$ : Peak excitation wavelength.  $\lambda_{Em}$ : Peak emission wavelength

All solutions were maintained at 37°C and applied using the perfusion system described in the previous section (Figure 5-4). At the beginning and end of each calcium imaging experiment, a solution containing a concentration of 50mM of potassium chloride, henceforth referred to as K<sub>50</sub>, (in mM: 50mM KCl, 91.4mM NaCl, 1mM MgCl<sub>2</sub>, 2.5mM CaCl<sub>2</sub>, 0.3M NaH<sub>2</sub>PO<sub>4</sub>, 10mM glucose 1mM HEPES at pH 7.4), was applied to the cells for 15 seconds. The high concentration of potassium in the K<sub>50</sub> depolarises the membrane and induces a rapid influx of calcium into the neurons via voltage gated calcium channels. After the 15 seconds had elapsed, this response was washed off with ECS until the calcium signal returned to baseline. The K<sub>50</sub> serves as a way of normalising neuron responses from different dishes, as well as a means of ensuring neuron viability at the beginning and

by then end of the experiment. After the first  $K_{50}$  had washed off,  $H_2O_2$  (10mM) was applied to the neurons for 3 minutes and washed with ECS until the signal returns to baseline.

### 5.2.2 Isolated Vagal Nerve Recordings

The effect of the oxidant  $H_2O_2$  was assessed on the isolated vagus nerve model outlined in the methods chapter (Section 2.4).

To determine whether  $H_2O_2$  was capable of causing vagus nerve depolarisation, a concentration response experiment (technique described in Section 2.4.4) was performed on guinea pig vagus nerves using noncumulative concentration of  $H_2O_2$  ranging between  $1\mu M$  and 1M.

After this had been completed, a submaximal concentration of  $H_2O_2$  (10mM) was taken forward for antagonist experiments, using the same techniques described in Section 2.4.4. As a positive control, the antioxidant N-Acetylcysteine (NAC; 1mM) was tested against  $H_2O_2$ -induced vagus nerve depolarisation. Additionally, to determine whether TRPA1 mediated  $H_2O_2$ -induced vagus nerve depolarisation, Janssen 130 (J130;  $10\mu M$ ), a selective TRPA1 antagonist (Berthelot Didier et al., 2010), was also used. A concentration of  $10\mu M$  was chosen for J130 because this concentration had already been proven by our lab to be capable of inhibiting TRPA1-driven stimuli without cross-reacting with other classical pro-tussive targets (*e.g.* TRPV1) (Robinson et al., 2018). Prior to attempting to inhibit  $H_2O_2$ -induced vagus nerve depolarisation with J130, we attempted to block nerve depolarisation induced by acrolein, a TRPA1 agonist (Birrell et al., 2009), to prove its efficacy.

### 5.2.3 Data analysis and statistics

In oxidative stress and calcium imaging experiments, regions of interest were drawn around each of the neurons that were exhibiting Dil staining within the microscope's field (5.2.1.1); this was so that their fluorescence intensity could be measured over time using Fiji analysis software (Version 1.51n). To measure a neuron's fluorescence, the intensity of the background of the microscope's field was averaged and subtracted from each neuron, the fluorescence ratio over time for DHE (F580/F480) or Fura2 (F340/F380) was then calculated.

For calcium imaging, the responses to  $H_2O_2$  were calculated as area under curve (in order to account for the time taken for the cells to extrude the calcium from their cytoplasm) and expressed as a percentage of the  $K_{50}$  response's area under curve. Statistical significance was measured by comparing neuronal responses (in % $K_{50}$ ) to vehicle and  $H_2O_2$ , with a paired t-test. The data is presented as mean  $\pm$  SEM, with statistical significance set at  $p < 0.05$ .

For oxidative stress imaging experiments, the baseline was adjusted linearly in order to compensate for photobleaching of the DHE dye. Responses to  $H_2O_2$  were then calculated as peak magnitude,

compared to baseline recorded prior administration of the compound, and presented as change in ratio intensity ( $\Delta F_{580}/F_{480}$ ). Statistical significance was measured for the oxidative stress imaging of  $H_2O_2$  concentration response by comparing  $H_2O_2$  responses to that of vehicle using a Kruskal-Wallis multiple comparison test followed by Dunn's multiple comparison test.

Throughout the data, 'GP' denotes the number of guinea pigs used and 'n' denotes the number of neurons measured.

## 5.3 Results

### 5.3.1 Effect of H<sub>2</sub>O<sub>2</sub> on intracellular oxidative stress within vagal ganglia neurons

The effect of H<sub>2</sub>O<sub>2</sub> on the intracellular levels of oxidative stress in vagal ganglia neurons was measured using DHE. H<sub>2</sub>O<sub>2</sub> (0.1-10mM) produced concentration dependent intracellular oxidative stress within vagal ganglia neurons (Figure 5-5); and at the concentrations 1mM and 10mM, was able to generate significant increases in DHE fluorescence compared to vehicle (ECS).

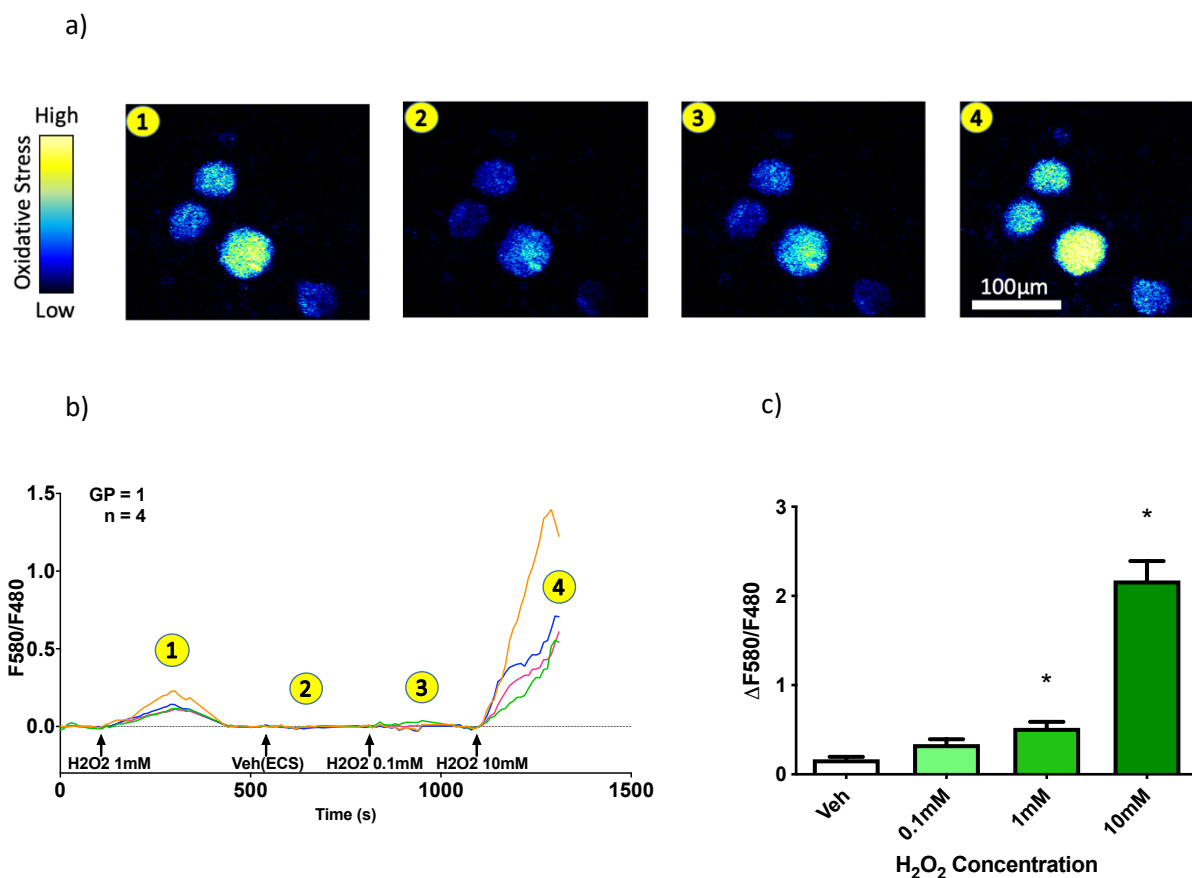


Figure 5-5 Imaging the resulting oxidative stress from a H<sub>2</sub>O<sub>2</sub> concentration response in guinea pig vagal ganglionic neurons.

a) Oxidative stress intensity images (acquired using DHE dye) captured from the same vagal ganglia neurons exposed to the following: 1 – 1mM H<sub>2</sub>O<sub>2</sub>, 2 – Vehicle ECS, 3 – 0.1mM H<sub>2</sub>O<sub>2</sub>, and 4 – 10mM H<sub>2</sub>O<sub>2</sub>. b) An example trace showing oxidative stress dye DHE fluorescence (F580/F480), over time, from the vagal ganglia neurons in the corresponding photographs from (a), when exposed to different concentrations of H<sub>2</sub>O<sub>2</sub>. c) A histogram showing the change in oxidative stress intensity (signal – baseline) with DHE dye (F580/F480) when guinea pig vagal ganglia neurons were exposed to different concentrations of H<sub>2</sub>O<sub>2</sub>. Data shown as mean ± S.E.M. of GP=4, n=32. \* indicates statistical significance ( $p < 0.05$ ) of response compared to vehicle, analysed with Kruskal-Wallis multiple comparison test following by Dunn's multiple comparison test.

### 5.3.2 Effect of H<sub>2</sub>O<sub>2</sub> on intracellular calcium concentrations of vagal ganglia neurons

A functional effect for H<sub>2</sub>O<sub>2</sub> on the intracellular calcium concentrations ([Ca<sup>2+</sup>]<sub>i</sub>) of vagal ganglia neurons was assessed, using the concentration that caused the highest amount of oxidative stress. 10mM H<sub>2</sub>O<sub>2</sub> caused a significant increase in [Ca<sup>2+</sup>]<sub>i</sub> compared to vehicle (978%±120 of the K<sub>50</sub> A.U.C versus 12.92%±2.4)(Figure 5-6).

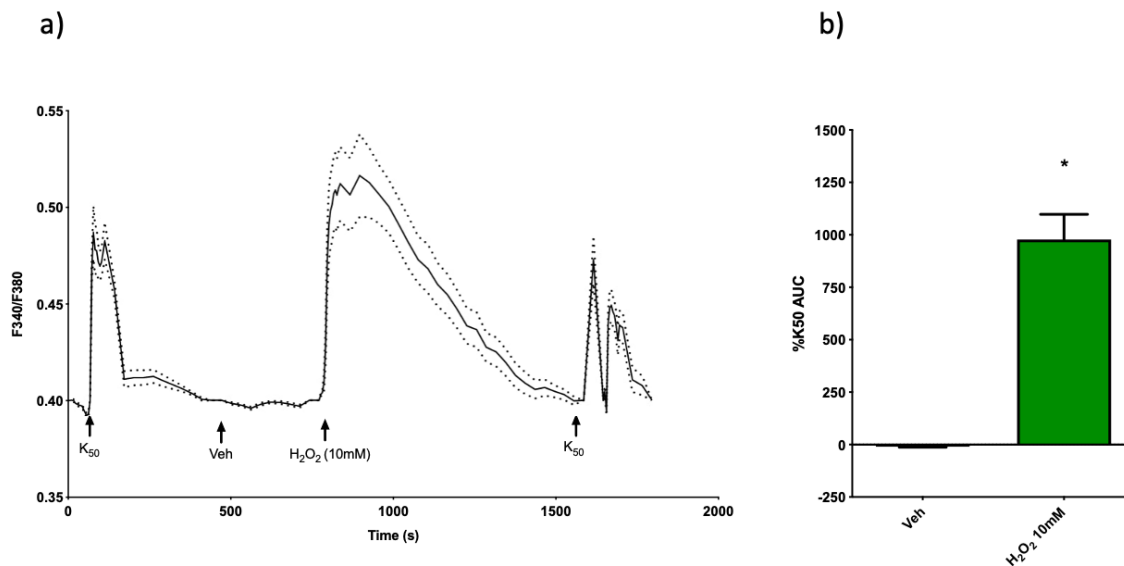


Figure 5-6 Changes in [Ca<sup>2+</sup>]<sub>i</sub> in guinea pig vagal ganglia upon stimulation with H<sub>2</sub>O<sub>2</sub>.

a) An average trace showing intracellular calcium concentration ([Ca<sup>2+</sup>]<sub>i</sub>) levels within guinea pig vagal ganglia neurons when exposed to K<sub>50</sub>, vehicle and the oxidant H<sub>2</sub>O<sub>2</sub>. b) A histogram to show the increase in [Ca<sup>2+</sup>]<sub>i</sub> in guinea pig vagal ganglia neurons induced by the oxidant H<sub>2</sub>O<sub>2</sub> (10mM). Data shown as mean % K<sub>50</sub> Area Under Curve (AUC) ± S.E.M. of GP=3, n=30. \* indicates statistical significance (p < 0.05), paired t-test comparing responses to vehicle.

### 5.3.3 Effect of H<sub>2</sub>O<sub>2</sub> on depolarisation of isolated guinea pig vagus nerves

The effect of the oxidant H<sub>2</sub>O<sub>2</sub> on guinea pig vagus nerve depolarisation was assessed. H<sub>2</sub>O<sub>2</sub> caused a concentration dependent increase in depolarisation. H<sub>2</sub>O<sub>2</sub> (100mM) caused a significant, maximum depolarisation of 0.160mV±0.02 (Figure 5-7). 10mM was taken forward for antagonist studies as this was a submaximal concentration that caused a significant depolarisation compared to vehicle (0.085mV±0.010).

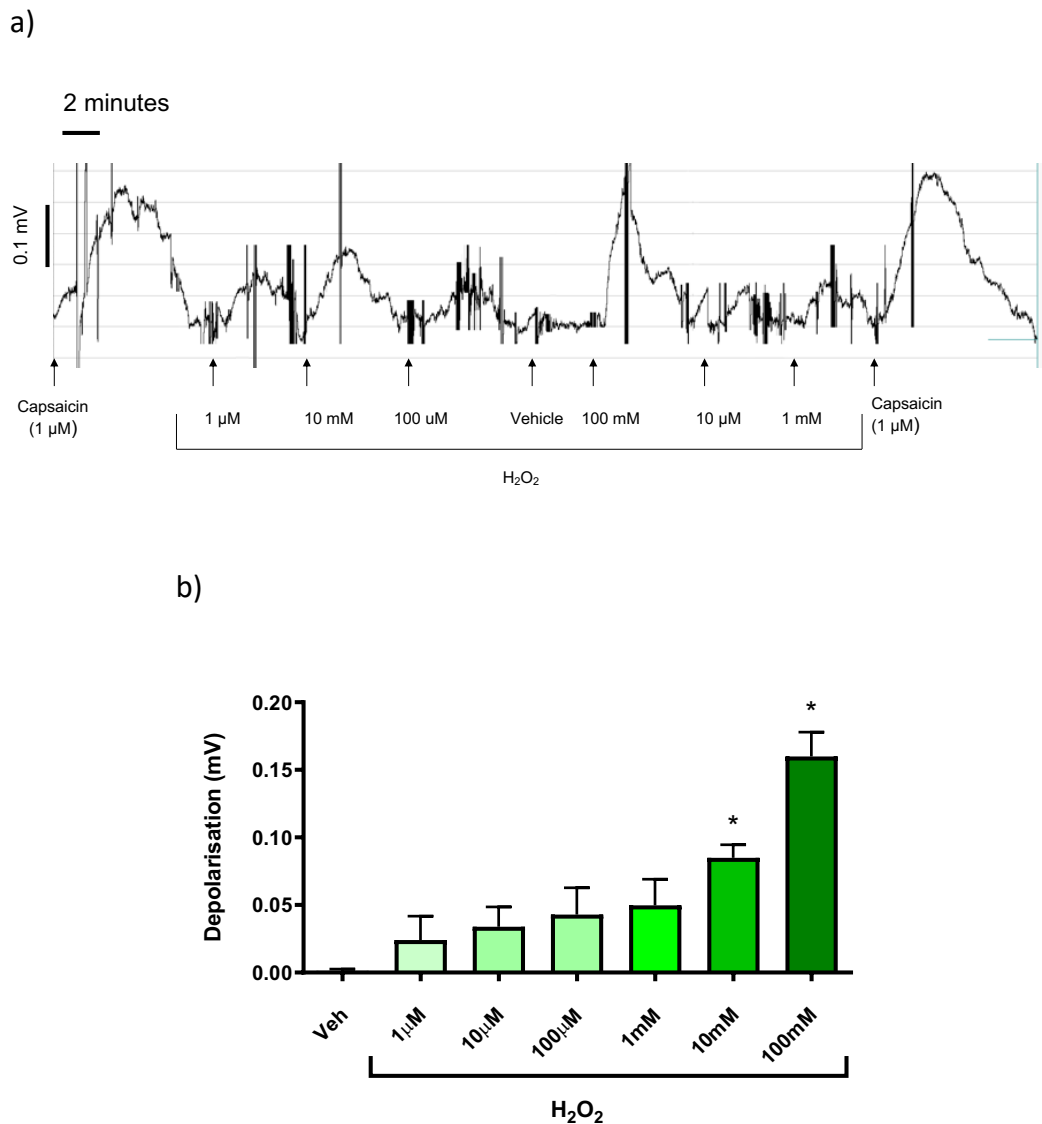


Figure 5-7 A concentration response to the oxidant H<sub>2</sub>O<sub>2</sub> in the isolated vagus nerve model, using guinea pig tissue

A concentration response to the oxidant H<sub>2</sub>O<sub>2</sub> in the 'grease-gap' vagus nerve model, performed on segments of guinea pig vagus nerve trunk. Capsaicin (1μM) was used before and after the experiment to assess nerve viability. **a)** Example trace. **b)** Histogram of combined data.

The nerves were exposed to non-cumulative concentrations of H<sub>2</sub>O<sub>2</sub>, as well as vehicle (all dissolved in KH solution), for 2 minutes, at an approximate rate of 2 ml/min. After this time had elapsed, the response was washed off with KH solution until the signal had returned to baseline, whereupon the next concentration was introduced. Data shown as mean ± S.E.M., 5≤n≤7. \* indicates statistical significance (p < 0.05) measured by performing a paired t test, where each response from each H<sub>2</sub>O<sub>2</sub> concentration was compared to the vehicle response in the same piece of nerve.

### 5.3.4 Selecting a TRPA1 inhibitor to take forward to inhibit H<sub>2</sub>O<sub>2</sub>-induced vagus nerve depolarisation

Before proving that the ion channel TRPA1 was involved in H<sub>2</sub>O<sub>2</sub>-induced vagus nerve depolarisation, it was first necessary to find a selective TRPA1 antagonist. Shown in Figure 5-8, is an antagonist experiment where guinea pig vagus nerve depolarisation caused by the TRPA1 agonist acrolein ( $0.78 \pm 0.242$  mV) was significantly inhibited by the selective TRPA1 antagonist Janssen 130 (J130;  $0.06 \pm 0.017$  mV).

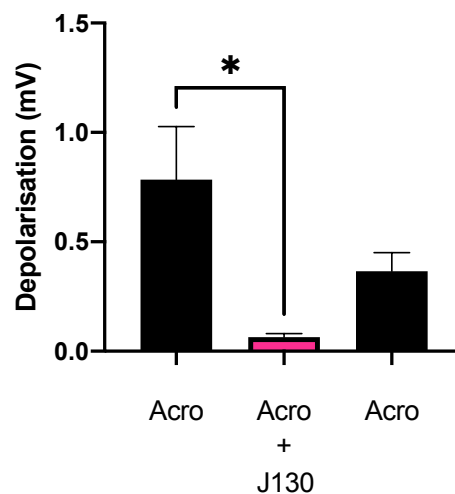


Figure 5-8 Effect of J130 on acrolein induced vagus nerve depolarisation

A histogram to show the mean peak amplitude of the depolarisation (mV) of guinea pig vagus nerve when exposed to TRPA1 agonist Acrolein (Acro;  $300 \mu\text{M}$ ), with or without the selective TRPA1 antagonist Janssen 130 (J130;  $10 \mu\text{M}$ ).

Data shown as mean  $\pm$  S.E.M.,  $n=5$ . \* indicates statistical significance ( $p \leq 0.05$ ) by way of a paired t test comparing responses in the same piece of nerve with and without J130.

For this antagonist experiment, the nerves were first stimulated with Acrolein for 2 minutes, up to 3 times, to obtain at least 2 reproducible responses. Following each of these 2-minute periods, any response was washed off with KH solution until the signal returned to baseline. The nerve was then 'blocked' with J130 for 10 minutes. Once this time had elapsed, the nerve was then immediately exposed to both acrolein and the blocking compound for 2 minutes. This response was then washed off before a final stimulation took place with acrolein, to ensure the nerve was still viable. All drugs were dissolved in KH solution and suffused the nerve at a rate of 2 ml/min.



### 5.3.5 Effect of N-Acetylcysteine and a selective TRPA1 antagonist on H<sub>2</sub>O<sub>2</sub>-induced vagus nerve depolarisation

The ability of the antioxidant N-Acetylcysteine (NAC) and the selective TRPA1 antagonist J130, to inhibit H<sub>2</sub>O<sub>2</sub>-induced vagus nerve depolarisation was investigated. NAC (1mM) was able to significantly inhibit H<sub>2</sub>O<sub>2</sub> (10mM) induced responses by 97.7% ± 2.3, in guinea pig tissue. J130 was also able to significantly inhibit H<sub>2</sub>O<sub>2</sub>-induced vagus nerve responses in guinea pigs by 95.5% ± 4.5 (Figure 5-10a).

In human tissue, although so far *n* of 2, both NAC (1mM) and J130 (10µM) appeared to inhibit H<sub>2</sub>O<sub>2</sub> (10mM) induced vagus nerve depolarisation, whereas vehicle did not (Figure 5-10b, c & d).

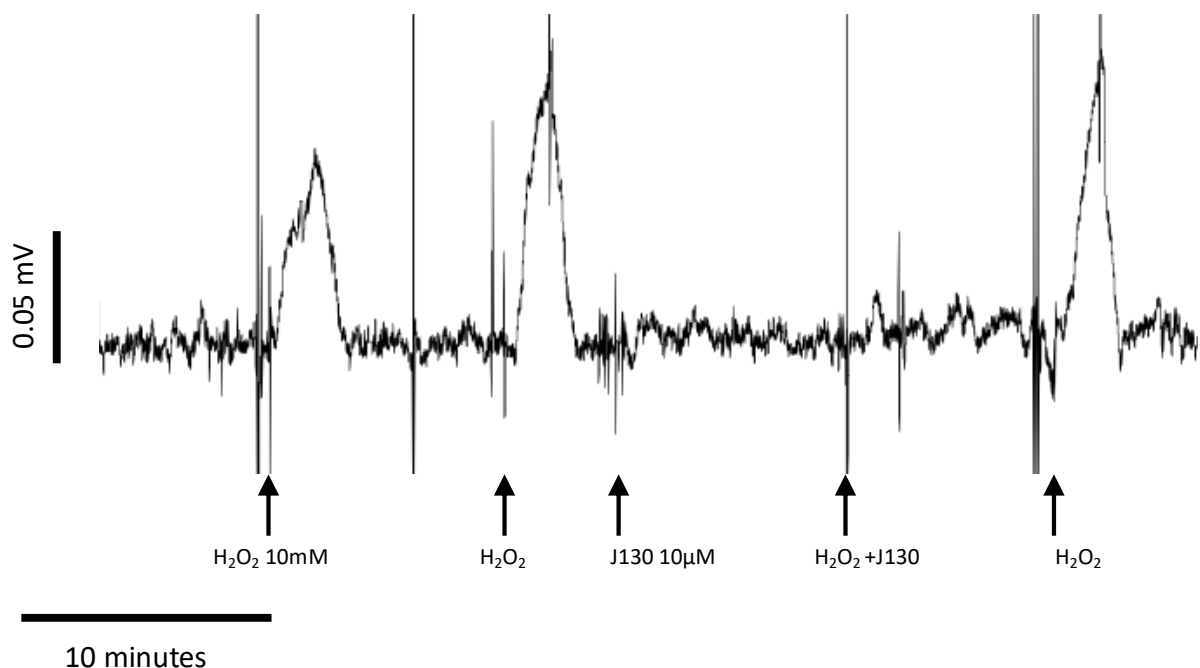
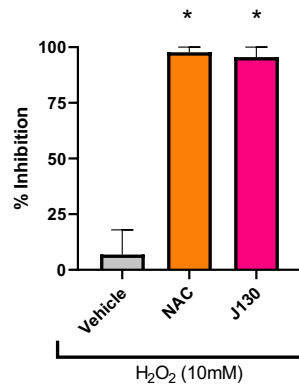


Figure 5-9 Inhibition of H<sub>2</sub>O<sub>2</sub>-induced vagus nerve depolarisation by TRPA1-selective antagonist J130

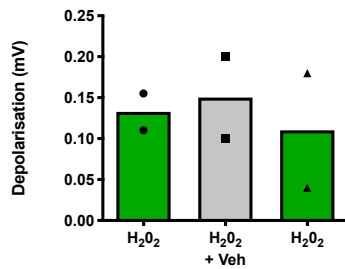
An example isolated vagus nerve model trace using guinea pig tissue, showing the TRPA1-selective antagonist J130 (10µM) inhibiting vagus nerve depolarisation caused by the oxidant H<sub>2</sub>O<sub>2</sub> (10mM)

For each of these antagonist experiments, the nerve was first stimulated with the H<sub>2</sub>O<sub>2</sub> for 2 minutes, up to 3 times, to obtain at least 2 reproducible responses. Following each of these 2-minute periods, any response was washed off with KH solution until the signal returned to baseline. The nerve was then 'blocked' with either J130 or vehicle, for 10 minutes. Once this time had elapsed, the nerve was then immediately exposed to both H<sub>2</sub>O<sub>2</sub> and the blocking compound for 2 minutes. This response was then washed off before a final stimulation took place with H<sub>2</sub>O<sub>2</sub>, to ensure the nerve was still viable. All drugs were dissolved in KH solution and suffused the nerve at a rate of 2 ml/min.

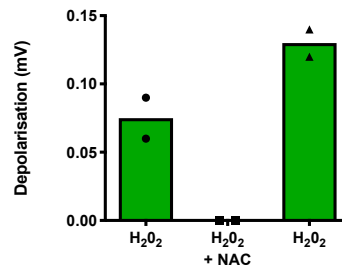
a) Guinea Pig



b) Human



c) Human



d) Human

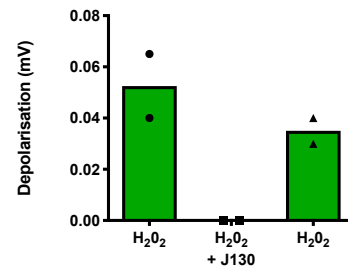


Figure 5-10 Inhibition of H<sub>2</sub>O<sub>2</sub>-induced vagus nerve depolarisation using NAC and J130.

**a)** a histogram to indicate the inhibitory effect of vehicle (0.1% DMSO), N-Acetylcysteine (NAC; 1mM) and selective TRPA1 antagonist Janssen 130 (J130; 10 $\mu$ M) on H<sub>2</sub>O<sub>2</sub> (10mM) induced vagus nerve depolarisation, in guinea pigs. Data shown as mean  $\pm$  S.E.M, 4 $\leq$ n $\leq$ 5. \* indicates statistical significance ( $p \leq 0.05$ ) by way of a paired t-test comparing responses in the same piece of nerve with and without antagonist.

**b), c) & d)** are histograms to show the mean peak amplitude of the depolarisation (mV) of human vagus nerve when exposed to H<sub>2</sub>O<sub>2</sub> (10mM) with or without vehicle (0.1%DMSO), NAC (1mM) or J130(10 $\mu$ M), respectively. Data shown is mean, with dots to denote individual values, n=2 (the first bar is an average of the two initial H<sub>2</sub>O<sub>2</sub> responses).

For each of these antagonist experiments, the nerve was first stimulated with H<sub>2</sub>O<sub>2</sub> for 2 minutes, up to 3 times, to obtain at least 2 reproducible responses. Following each of these 2-minute periods, any response was washed off with KH solution until the signal returned to baseline. The nerve was then 'blocked' with either NAC, J130 or vehicle, for 10 minutes. Once this time had elapsed, the nerve was then immediately exposed to both H<sub>2</sub>O<sub>2</sub> and the blocking compound for 2 minutes. This response was then washed off before a final stimulation took place with H<sub>2</sub>O<sub>2</sub>, to ensure the nerve was still viable. All drugs were dissolved in KH solution and suffused the nerve at a rate of 2 ml/min.

## 5.4 Discussion

The aim of this chapter was to investigate whether naturally occurring oxidants such as  $\text{H}_2\text{O}_2$  were capable of activating airway sensory nerves, which therefore might suggest that they have a protussive effect. Oxidative stress is an abnormal redox state within a cell where its antioxidants are overcome by an excessive presence of oxidants (Sies, 1997). Cellular oxidants include Reactive Oxygen Species (ROS), such as the superoxide radical ( $\text{O}_2^-$ ) and the hydroxyl radical ( $^*\text{OH}$ ), these species are highly reactive due them both having at least one unpaired electron, however, there also exist non-radical ROS such as Ozone ( $\text{O}_3$ ) and  $\text{H}_2\text{O}_2$ , which are readily converted into the former, respectively (Bayr, 2005). Small amounts of ROS are sometimes generated as a by-product of cellular respiration, they also have important roles in cell signalling and homeostasis (Devasagayam et al., 2004). In a healthy cell, radicals are stabilised by free radical scavenging enzymes (*e.g.* superoxide dismutase) and antioxidants (*e.g.* glutathione) (Weydert and Cullen, 2010). It is crucial for the cell to manage its level of ROS as they readily react with and degrade key components of the cell including DNA (Cadet et al., 2012), proteins (Berlett and Stadtman, 1997) and lipids (Mylonas and Kouretas, 1999), and as such, are implicated in a wide range of diseases such as: atherosclerosis, diabetes, cancer, neurodegeneration, and aging (Ray et al., 2012). Oxidative stress is involved in several chronic lung diseases including asthma and COPD (Anderson and Macnee, 2009, Riedl and Nel, 2008), as well as IPF (Malli et al., 2013). Oxidative stress was first discovered to be a feature of IPF in 1998 (then referred to as ‘cryptogenic fibrosis alveolitis’), when Montushi *et al* discovered sufferers had a higher concentration of 8-isoprostane (a biomarker of lipid peroxidation) in their bronchoalveolar lavage when compared to healthy subjects.

Given the above, and the fact chronic cough is a frequent feature of IPF (Hope-Gill et al., 2003, Key et al., 2010) we sought to explore whether ROS could be contributing to cough in the IPF lung by investigating whether they could activate airway sensory neurons and nerves. We chose  $\text{H}_2\text{O}_2$  as our ROS because of its relative safety and ease of application. Before a functional role for  $\text{H}_2\text{O}_2$  could be established with calcium imaging of airway terminating neurons, it first had to be shown that  $\text{H}_2\text{O}_2$  did indeed generate intracellular oxidative stress within the neurons of this model. This was accomplished using the fluorescent, oxidative stress-sensitive dye DHE, and it was found  $\text{H}_2\text{O}_2$  did cause concentration dependent oxidative stress within guinea pig vagal neurons (Figure 5-5).

Next, using a concentration of  $\text{H}_2\text{O}_2$  (10mM) that was found to cause significant oxidative stress, it was shown that  $\text{H}_2\text{O}_2$  also caused a significant increase in the  $[\text{Ca}^{2+}]_i$  of guinea pig airway terminating vagal neurons (Figure 5-6). Calcium imaging is a useful model for ascertaining the protussive properties of a compound because stimuli that are capable of causing cough *in vivo* (*e.g.* capsaicin, bradykinin and TRPV4 ligands) are also capable of causing increases in  $[\text{Ca}^{2+}]_i$  of vagal ganglionic

neurons, the location where the nerve cell bodies that mediate the cough reflex are situated (Bonvini et al., 2016, Grace et al., 2012, Birrell et al., 2014); therefore the finding that H<sub>2</sub>O<sub>2</sub> causes increases in [Ca<sup>2+</sup>]<sub>i</sub> likely means it has protussive activity.

To further characterise H<sub>2</sub>O<sub>2</sub> as a protussive agent, it was used in the *in vitro* isolated vagus nerve model. As described previously, the isolated vagus nerve model is another useful pharmacologically amenable method to assess a compound's propensity to cause cough. Like with [Ca<sup>2+</sup>]<sub>i</sub>, H<sub>2</sub>O<sub>2</sub> was also capable of generating concentration dependent depolarisation of guinea pig vagus nerves (Figure 5-7). A submaximal concentration of 10mM was taken forward for antagonist studies as it was the lowest concentration of H<sub>2</sub>O<sub>2</sub> able to cause a significant depolarisation.

Finally, we attempted to inhibit H<sub>2</sub>O<sub>2</sub> induced vagus nerve depolarisation with the antioxidant N-acetylcysteine (NAC) (Samuni et al., 2013) and the selective TRPA1 antagonist J130 (Berthelot Didier et al., 2010). NAC is a medication used to treat paracetamol overdose and loosen mucus build up in some bronchopulmonary disorders, it has also shown recent potential in the treatment for a range of psychiatric disorders (Millea, 2009, Ooi et al., 2018). It is a prodrug to L-cysteine, which is itself a precursor to the antioxidant glutathione (GSH) (Holdiness, 1991). NAC was able to significantly inhibit H<sub>2</sub>O<sub>2</sub>-induced vagus nerve depolarisation in the guinea pig, and although not yet repeated enough times in human tissue to achieve statistical power, it so far appears to have the same effect on human donor vagus nerves too (Figure 5-10).

NAC has been trialled multiple times as a treatment for IPF, either solely, or in combination with other therapies, and these studies have generated conflicting results as to whether it can slow a patient's progressive decline in lung function; also and albeit unfortunately, none of these studies included objective cough frequency as a clinical endpoint (Demedts et al., 2005, Homma et al., 2012, Martinez et al., 2014, Raghu et al., 2012). A recent meta-analysis found that while there is some evidence that NAC could be beneficial to slowing disease progression when used in combination (*e.g.* with pirfenidone), when used as a monotherapy however, it did not slow lung function decline significantly, unlike the currently approved treatments Pirfenidone and Nintedanib, which did (Rogliani et al., 2016). More worryingly, NAC appeared to increase the likelihood of adverse events, although not significantly, which could disqualify NAC as an antitussive candidate for IPF patients. NAC also has a less than ideal pharmacokinetic profile, since it is rapidly metabolised by the liver, thus resulting in an approximate bioavailability of only 10% for the original molecule (Dekhuijzen, 2004). Recent evidence has however come to light, which indicates that NAC may be an efficacious therapy for IPF patients with a particular variant of the *TOLLIP* gene (Oldham et al., 2015); this has led to the commencement of the first clinical trial to utilise precision medicine in the treatment of

IPF (ClinicalTrials.gov, 2020). Whilst this study will unfortunately not be assessing patients' objective cough rates, it will, however, be using the LCQ as a secondary outcome measure.

As mentioned above, we are not aware of any clinical studies that have investigated if NAC has any effect on objective cough rates in IPF. Interestingly however, pirfenidone (one of only two anti-fibrotic drugs currently prescribed to IPF patients) has been shown to reduce cough rate by 34% (van Manen et al., 2017). Whilst this study should be interpreted somewhat cautiously due to it lacking any placebo control and it having been conducted with a cough monitor lacking FDA approval or CE marking, it is nonetheless curious that pirfenidone has shown antioxidant capabilities *in vitro* through the inhibition of NADPH oxidase (Misra and Rabideau, 2000, Giri et al., 1999).

Like NAC, TRPA1 antagonist J130 was also capable of significantly inhibiting H<sub>2</sub>O<sub>2</sub>-induced vagus nerve depolarisation in guinea pigs, and appeared to have the same effect on the two human donor nerves that were tested (Figure 5-10). Whilst these results with the isolated vagus nerve model cannot definitively prove that oxidants like H<sub>2</sub>O<sub>2</sub> trigger cough, due to the vagus nerve trunk innervating other organs besides the airways and it possibly expressing receptors that mediate cough differently to the sensory nerve endings, these results do however provide a foundation for TRPA1 antagonists to be taken forward for future study. Indeed, we aim in the near future to test TRPA1 antagonists against H<sub>2</sub>O<sub>2</sub>-induced nerve activation in more airway relevant models *e.g.* eTRec and the *in vivo* single fibre model.

As mentioned in the introduction, it would appear possible that TRPA1 could indeed mediate IPF-associated cough when considering that cromoglycate, a drug that inhibits TRPA1 via GPR35 agonism (Maher et al., 2015), is capable of reducing IPF patient cough frequency (Birring et al., 2017). Interestingly the team that conducted the aforementioned clinical trial also tested the drug in a parallel cohort of patients with chronic idiopathic cough, but found it to have no treatment benefit for this set of patients; this therefore indicates that IPF-associated chronic cough is likely underpinned by a different aetiology. Cromoglycate has a notoriously poor PK profile, which is why it is now rarely used as an asthma medication (Taburet and Schmit, 1994), however modulating one of its downstream signalling targets – such as TPRA1 – could provide a more effective means of treating asthma and IPF-associated chronic cough, alike. A TRPA1 antagonist has been trialled in the treatment of cough in patients with idiopathic chronic cough to limited success, but there was no target engagement demonstrated in this study and therefore it cannot be ruled out that the drug failed due to lack of an appropriate pharmacokinetic programme, which resulted in insufficient lung exposure (Morice, 2017). It is also not clear whether TRPA1 antagonists would be effective

antitussives for IPF patients, but given cromoglycate's encouraging results, they are certainly worth considering.

In summary, the oxidant H<sub>2</sub>O<sub>2</sub> has been shown to not only cause intracellular oxidative stress in airway terminating vagal ganglia-derived neurons from guinea pigs, but also cause an increase in [Ca<sup>2+</sup>]<sub>i</sub>, thereby suggesting a role in airway sensory nerve activation and possibly cough. Next, this H<sub>2</sub>O<sub>2</sub>-induced oxidative stress was shown to cause depolarisation of both guinea pig and human vagus nerves. Finally, through the use of pharmacological tools, this activation of vagus nerves was inhibited by application of NAC and a TRPA1 antagonist.

The findings above support this chapter's hypothesis that there is indeed a role for oxidative stress in airway sensory nerve activation, and that TRPA1 likely mediates this. TRPA1 will no doubt be an interesting target to explore in the *in vivo* model of fibrosis-induced spontaneous cough (described in Chapter 3), and could be a novel target in the treatment of IPF-associated chronic cough.

## 6 Investigating a role for PAR2 in airway sensory nerves

### 6.1 Rationale

Protein Activated Receptor 2 (PAR2) is one of four members of the Protease Activated Receptors, a subfamily of G protein coupled receptors. The PARs are known for their unique activation mechanism whereby their n-terminus is proteolytically cleaved, which unmask a tethered ligand, that then activates the receptor (Al-Ani et al., 2002). The PARs are involved in blood clotting and maintaining vascular tone (Coughlin, 2000), but are also implicated in a range of diseases including cancer and inflammation (Steinhoff et al., 2000, Das et al., 2018).

One protease capable of activating PAR2 is tryptase (Molino et al., 1997), which has been shown to be increased in the BALF of IPF patients and has been associated with poorer prognoses (Kawatani et al., 2007, Compton et al., 2001). PAR2 has been shown to be expressed on nociceptive neurons (Steinhoff et al., 2000, Vergnolle et al., 2001), and there is some evidence already that PAR2 can activate the TRPV4 channel (Grace et al., 2014, Poole et al., 2013). It therefore stands to reason that PAR2 could be an upstream actor involved in the TRPV4-ATP-P2X3 axis (Bonvini et al., 2016), a protussive signalling pathway that could be implicated in chronic cough (Abdulqawi et al., 2015). This is not the first time PAR2 has been linked to cough, a study by Gatti *et al.* in 2006 did not find that PAR2 agonists could elicit cough, but rather, that PAR2 agonists potentiated coughs elicited by aerosolised citric acid and resiniferatoxin (a functional homologue of capsaicin), in guinea pigs. Whether PAR2 agonists themselves can activate airway sensory nerves and if such a response is mediated by the TRPV4-ATP-P2X3 axis remains to be seen.

#### 6.1.1 Chapter Hypotheses

PAR2 agonists activate airway sensory nerves through the TRPV4-ATP-P2X3 axis.

#### 6.1.2 Aims

- To evaluate the effect of four PAR2 agonists on airway sensory nerves *in vitro*: AC-55541, a nonpeptidic small molecule (Seitzberg et al., 2008); Ser-Leu-Ile-Gly-Lys-Val-NH<sub>2</sub> (SLIGKV) and 2-furoyl-Leu-Ile-Gly-Arg-Leu-Orn-NH<sub>2</sub> (2-furoyl-LIGRLO), two agonists derived from PAR2's endogenous tethered peptide ligand (McGuire et al., 2004); and trypsin, a proteolytic enzyme that activates PAR2 endogenously (Nystedt et al., 1994). These pharmacological tools used will be assessed in isolated murine, guinea pig and donor human tissue.
- Further prove that these depolarisation events in vagal nerves are the result of PAR2-specific activation by:

- Inhibiting them with palmitate-RSSAMDENSEKKRKSIAK-NH<sub>2</sub> (P2Pal-18s), a cell-penetrating lipopeptide “pepducin” antagonist of PAR2 (Sevigny et al., 2011), in guinea pig and donor human tissues
- Abrogating them through the use of PAR2 knockout mice
- To take the most selective ligand forward *ex vivo*, to test whether it is able to induce compound action potential firing of the Recurrent Laryngeal Nerve (RLN) in an electrophysiological tracheal recording (eTRec).
- Assess this PAR2 activating ligand *in vivo*, to ascertain whether it is able to instigate an action potential in guinea pig isolated single fibres
- Determine if PAR2 airway nerve activation is mediated through the TRPV4-ATP-P2X3 axis by
  - Using TRPV4 channel blocker GSK2193874 (GSK219) (Thorneloe et al., 2012) to determine if TRPV4 plays a role in PAR2-induced vagus nerve depolarisation.
  - Using AF-353 a P2X3 channel blocker (Gever et al., 2010) to determine if P2X3 plays a role in PAR2-induced vagus nerve depolarisation.

## 6.2 Methods

### 6.2.1 Isolated Vagal Nerve Recordings

Vagus nerves dissected and cleaned from male Dunkin Hartley Guinea pigs, WT C57/Bl6 mice or PAR2<sup>-/-</sup> mice were placed into the grease-gap recording chamber (Section 2.4). Key experiments were also repeated using human vagus nerves from deceased donors.

#### 6.2.1.1 Agonist concentration response experiments

To determine if PAR2 activation caused vagus nerve depolarisation, the following experimental protocol was executed. Non-cumulative concentrations of PAR2 agonists were applied to the vagus nerve on one side of the grease gap as outlined in Section 2.4.4. The PAR2 agonists and (concentrations used) were: AC-55541 (10nM-10µM); SLIGKV (10nM-10µM), 2-furoyl-LIGRLO (1nM-1µM), and trypsin (30U-1000U). In addition to the agonist, the nerve was also exposed to capsaicin and the agonist’s vehicle, as a positive and negative control, respectively. The tested concentration ranges for each agonist were selected by taking into account their activity data from the literature (*e.g.* AC-55541 has a published pEC<sub>50</sub> of 6.7 (Seitzberg et al., 2008)).

A submaximal concentration was selected for each agonist and taken forward for knockout mouse and antagonist studies.



#### 6.2.1.2 Agonist experiments in PAR2 knockout mice

The selectivity of the available tools was then tested by utilising vagal nerves from F2LR1<sup>-/-</sup> mice and aged matched wild type controls. How PAR2 was confirmed inoperative is described in Section 2.3.2.

Vagus nerves from WT C57Bl/6 mice or F2LR1<sup>-/-</sup> mice were exposed to the previously selected submaximal concentrations of the PAR2 agonists: AC-55541, SLIGKV and 2-furoyl-LIGRLO.

To ensure that vagus nerve depolarisation was not altered for TRPV4, TRPV1 or TRPA1 (calcium channels capable of eliciting cough) responses to GSK101 (300nM), Capsaicin (1μM) and Acrolein (300μM), were also assessed, respectively.

#### 6.2.1.3 Antagonist experiments using human donor and guinea pig vagus nerves

We deployed a classical pharmacological approach to further ensure that the vagus nerve depolarisations above were induced by PAR2 (outlined in Section 2.4.4). We selected a PAR2 agonist of choice based on its biological relevance, specificity and efficacy, and then tested it in the presence of P2Pal-18s (10μM), a cell-penetrating lipopeptide “pepducin” antagonist of PAR2 (Sevigny et al., 2011). We used a concentration of 10μM because studies performed at other research institutes had determined this concentration to be efficacious *in vitro* (Bagher et al., 2018, Lin et al., 2015b). As a negative control, a scrambled version of the peptide sequence of P2Pal-18s was also tested (scr-P2Pal-18s).

Later, we probed whether these PAR2-mediated vagus nerve depolarisations could be mediated through the TRPV4-ATP-P2X3 axis (Bonvini et al., 2016). This was achieved by stimulating vagal nerves with a PAR2 agonist whilst in the presence of AF-353 (10μM) or GSK219 (10μM), a P2X3 antagonist and TRPV4 antagonist, respectively. The concentrations used for these antagonists was approximately 100-fold that of the ligand’s affinity (pA<sub>2</sub>) to its target receptor (7.4 for both) (Thorneloe et al., 2012, Gever et al., 2010), and these had previously been found to be sufficient in this model (Bonvini et al., 2016). As a negative control, PAR2-mediated responses were also tested in the presence of the antagonists’ vehicle, DMSO.

#### 6.2.1.4 Analysis

Individual nerve depolarisations were assessed by measuring the peak amplitude of the response (in mV); and antagonist inhibitions were calculated (see Section 2.4.4).

Statistical analysis for agonist concentration responses was carried out using a paired, two-tailed t test, where each response generated by each PAR2 agonist was compared to the response generated by the vehicle in the same piece of nerve.

For antagonist studies, a paired, two-tailed t test was used comparing the magnitude of depolarisation by the agonist with and without the presence of antagonist in the same piece of nerve.

All data is presented as mean  $\pm$  S.E.M., with statistical significance set at  $P < 0.05$ .

### 6.2.2 eTRec of the recurrent laryngeal nerve (RLN)

Dunkin Hartley guinea pig tracheas and their attached RLNs were prepared as described in Section 2.5.1.

Compounds were administered by perfusing them through the trachea at a rate of 2 ml per minute. Prior to each administration, a time-matched baseline recording was taken. Capsaicin (10 $\mu$ M) was administered for 3 minutes, vehicle (0.1% DMSO) was administered for 3 minutes, and 2-Furoyl-LIGLRO was administered for 10 minutes.

Example data are presented in neurograms with RLN firing events in the y axis and time (s) in the x axis. Summarised data is presented as  $\Delta$  mean max firing rate, where the mean max firing rate of the RLN during baseline is subtracted from the mean max firing rate of the RLN during administration of the compound, for the same amount of time.

### 6.2.3 *In Vivo* Single Fibre Recording

#### 6.2.3.1 *Agonist concentration response*

The following experimental protocol was undertaken to examine the affect PAR2 agonist 2-furoyl-LIGRLO had on airway terminating A $\delta$ -fibres, as these nerve fibres mediate the protussive TRPV4-ATP-P2X3 axis. A future aim of this work will be to determine whether C-fibres are also receptive to PAR2 agonists, through a separate mechanism (Section 8.4).

Male Dunkin Hartley guinea pigs were prepared and the single fibre was characterised as described in Section 2.6.1. Following surgery, the animals were left to stabilise for 30 minutes, after which a baseline recording was made for 2 minutes. Next, vehicle (0.1%) was aerosolised into the airways for 1 minute, during which any changes in nerve fibre activity, intratracheal pressure or blood pressure were monitored, these were then allowed to return to baseline or to achieve a steady state. After 20 minutes, citric acid (0.3M) was aerosolised into the airways and the response was monitored. This process whereby a compound was aerosolised into the lungs and the resulting response was monitored and allowed to return to baseline for 20 minutes, was repeated with noncumulative concentrations of PAR2 agonist 2-Furoyl-LIGLO (ranging between 1nM and 1 $\mu$ M). A final citric acid response was undertaken to ensure that the fibre in question was an A $\delta$ -fibre. After this had taken place a conduction velocity measurement was made to further confirm it was an A $\delta$ -fibre.

### 6.2.3.2 Data analysis

Data are expressed as neurograms with impulses per second in y axis and time in the x axis.

## 6.3 Results

### 6.3.1 Effect of PAR2 agonists and antagonists on depolarisation of isolated vagus nerves

#### 6.3.1.1 Effect of selective and nonselective PAR2 agonists in the guinea pig

The isolated vagus nerve technique provides a useful, airway relevant model to determine the effect of PAR2 agonists on depolarisation.

PAR2 specific ligands AC-55541, SLIGKV and 2-Furoyl-LIGRLO caused a concentration dependent depolarisation of guinea pig vagus nerves. Trypsin, a nonspecific PAR2 agonist was also capable of causing a dose dependent depolarisation of guinea pig. 2-Furoyl-LIGRLO (1 $\mu$ M) and SLIGKV (10 $\mu$ M), both agonists based on PAR2's endogenous tethered ligand, caused a maximum depolarisation of 0.10mV $\pm$ 0.016mV and 0.10mV $\pm$ 0.024mV, respectively. Small molecule PAR2 agonist AC-55541 (10 $\mu$ M) and trypsin (300 Units/ml), a proteolytic enzyme capable of unmasking PAR2's tethered ligand, caused a maximum depolarisation of 0.09mV $\pm$ 0.028mV and 0.11mV $\pm$ 0.026mV, respectively.

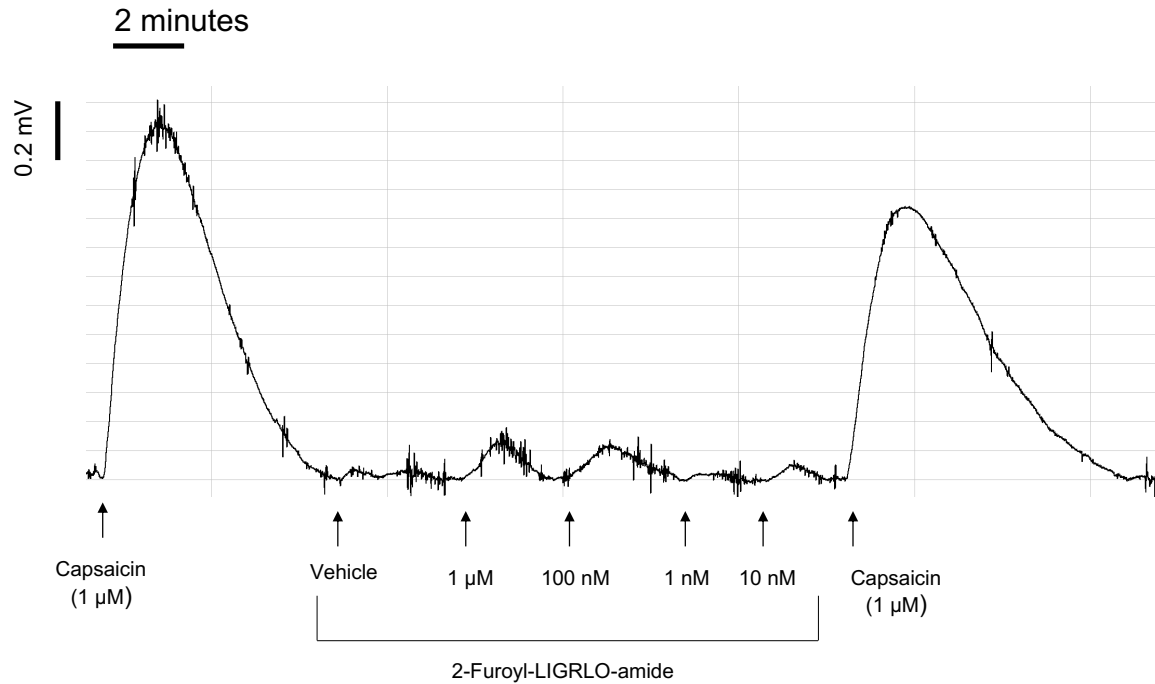


Figure 6-1 Trace of vagus nerve depolarisations during a concentration response to a PAR2 agonist.

An example trace showing a concentration response to PAR2-agonist 2-Furoyl-LIGRLO-amide and capsaicin in the 'grease-gap' vagus nerve model, performed on a segment of guinea pig vagus nerve trunk. The nerve was exposed to non-cumulative concentrations of 2-Furoyl-LIGRLO-amide as well as vehicle. To ensure nerve viability, all nerves were exposed to capsaicin before and after each concentration response experiment. The nerve was exposed to each stimulant (all dissolved in KH solution) for 2 minutes, at an approximate rate of 2 ml/min. After this time had elapsed, the response was washed off with KH solution until it had returned to baseline.

NB It is common for the nerve to partially lose its excitability by the time of the second capsaicin-induced depolarisation in a vagus nerve concentration response experiment, to account for this: 1) all experiments are repeated, and 2) the order of application of each of the different concentrations for the test compound is randomised every time, thereby helping to ensure that the data produced in a concentration response is more reliable

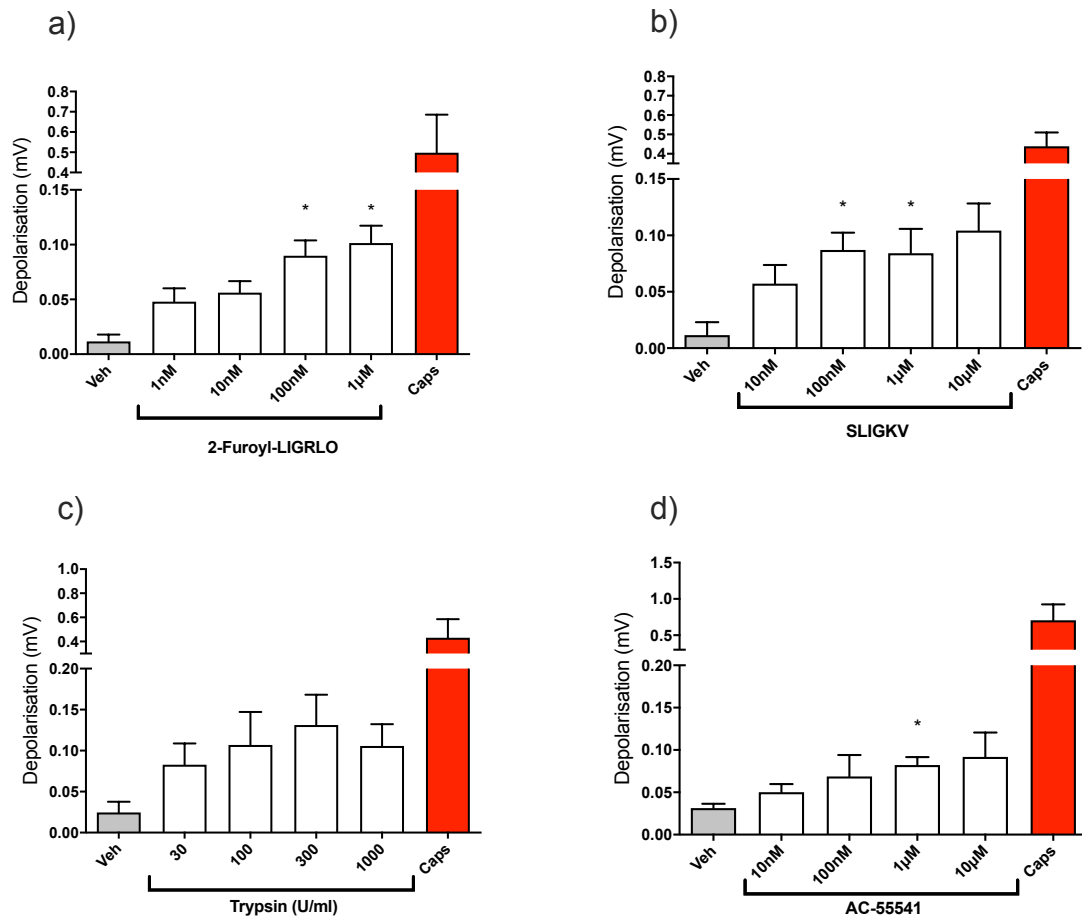


Figure 6-2 A selection of concentration responses to PAR2 agonists in guinea pig vagus nerves.

2-Furoyl-LIGRLO-Amide (a), SLIGKV (b), Trypsin (c) and AC-55514 (d), were tested on guinea pig vagus nerves in the grease-gap model. Vehicle (Veh) and capsaicin (Caps), used as negative and positive control, respectively.

The nerves were exposed to non-cumulative concentrations of the PAR2 agonists as well as vehicle. To ensure nerve viability, all nerves were exposed to capsaicin before and after each concentration response experiment. The nerves were exposed to each stimulant (all dissolved in KH solution) for 2 minutes, at an approximate rate of 2 ml/min. After this time had elapsed, the response was washed off with KH solution until the signal had returned to baseline. Following this, the nerve was exposed to the next concentration, etc.

Data shown as mean  $\pm$  S.E.M., n=4. \* indicates statistical significance ( $p < 0.05$ ) measured by performing a paired t test, where each response from each PAR2 agonist concentration was compared to the vehicle response in the same piece of nerve.

### 6.3.1.2 Effect of selective and nonselective PAR2 agonists in WT and *F2LR1*<sup>-/-</sup> KO mice

The next step in assessing the specificity of the PAR2 tools, was to test them on the vagus nerves of mice that had their gene for the PAR2 protein (*F2LR1*) disrupted and compare these responses to WT mice. These PAR2 agonists were tested alongside GSK101, capsaicin and acrolein, which are ligands for the TRPV4, TRPV1 and TRPA1 ion channel, respectively; each of these is capable of depolarising vagus nerves and has a protussive effect *in vivo*. Knockout of *F2LR1* was determined using standard genotyping techniques, and an example gel is shown in Figure 6-3.

In knockout mice, responses to all PAR2 agonists were significantly reduced, and in 2-Furoyl-LIGRLO and SLIGKV were virtually abolished (Figure 6-4). Responses to the TRP channel agonists GSK101 (300nM), capsaicin (1 $\mu$ M) and acrolein (300 $\mu$ M) were not significantly altered in knockout mouse tissue compared to WT tissue.

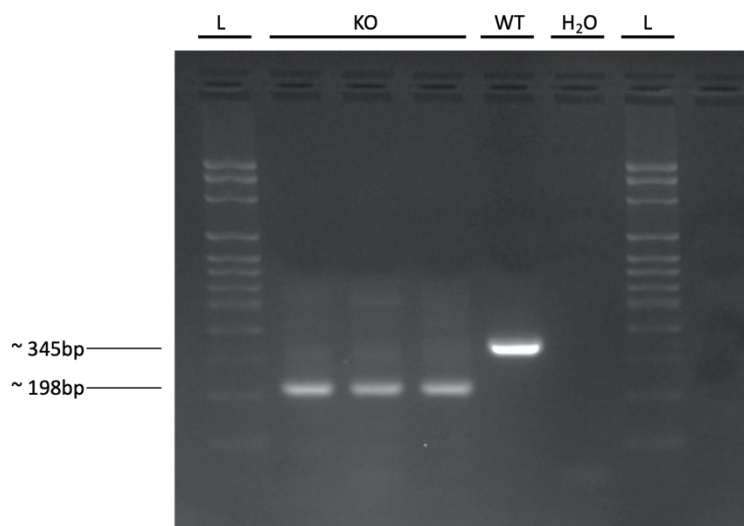


Figure 6-3 Confirming PAR2 knockout in gene edited mice.

An example scan from an electrophoretic gel used to confirm knockout of the gene for PAR2 (*F2LR1*) in mice. The DNA products ran through the gel were amplified through PCR. Wild Type (WT) mice produced a band at ~345bp whilst *F2LR1*<sup>-/-</sup> (KO) mice produced a band at ~198bp. A 50-2000bp ladder was used in lane 'L' and a water control in lane 'H<sub>2</sub>O'

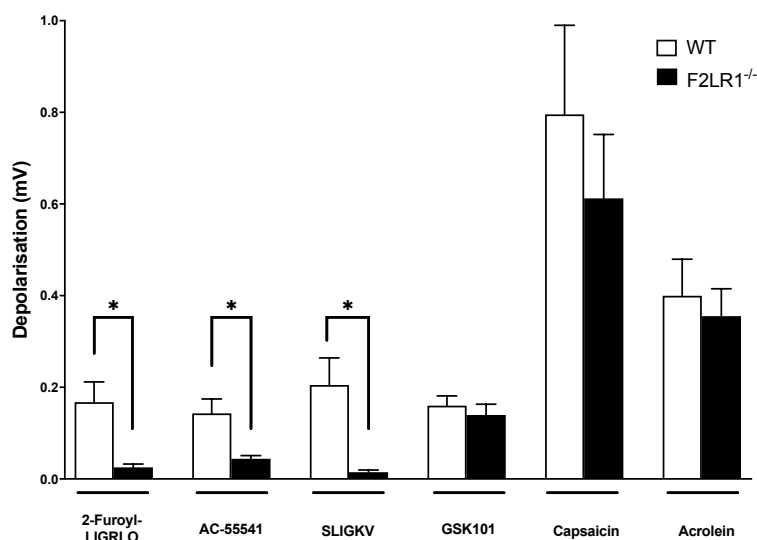


Figure 6-4 The effect of various PAR2 agonists and other protussive stimuli on vagus nerve depolarisation in PAR2 knockout (F2LR1<sup>-/-</sup>) mice.

Responses to the selective PAR2 agonists 2-Furoyl-LIGRLO (10nM), AC-55541 (1 $\mu$ M) and SLIGKV-amide (100nM) were abolished in F2LR1<sup>-/-</sup> mice. Responses to the TRPV4 ligand GSK101 (300nM), the TRPV1 ligand capsaicin (1 $\mu$ M) and the TRPA1 ligand acrolein (300 $\mu$ M) were not significantly altered.

The nerves were exposed to each stimulant (all dissolved in KH solution) for 2 minutes, at an approximate rate of 2 ml/min. After this time had elapsed, any response was washed off with KH solution until it had returned to baseline.

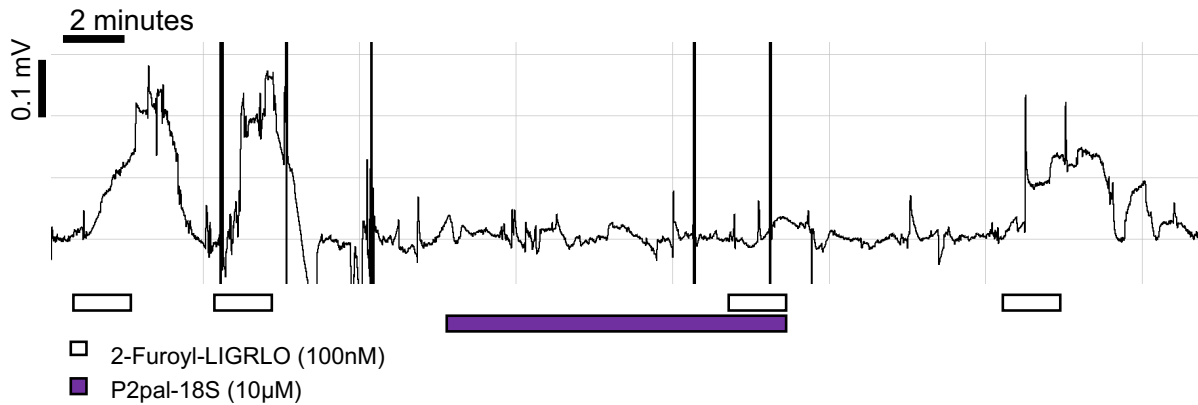
The data is presented as mean  $\pm$  S.E.M. of 5  $\leq$  n  $\leq$  6. \* indicates statistical significance ( $p < 0.05$ ), using a nonparametric (Mann Whitney) test comparing responses in PAR2<sup>-/-</sup> tissue with wild-type (WT) control.

### 6.3.1.3 Effect of selective PAR2 antagonist P2Pal-18s

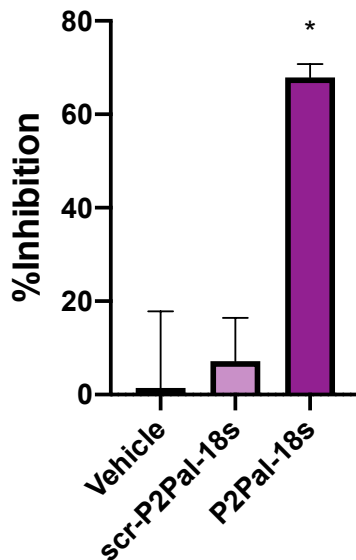
The ability of P2Pal-18s (10 $\mu$ M), a cell-penetrating lipopeptide “pepducin”, to antagonise PAR2 was then investigated. To test this, we selected 2-Furoyl-LIGRLO to take forward as our PAR2 agonist of choice, at a concentration of 100nM, due to its physiological relevancy and relative efficacy. To ensure that any observed inhibitory effect was due to the specific order of P2Pal-18s’ peptide sequence, a scrambled version of this sequence (scr-P2Pal-18s) was also tested alongside P2Pal-18s.

P2Pal-18s was able to significantly inhibit 2-Furoyl-LIGRLO induced depolarisation in guinea pig vagus nerves (67.9% $\pm$ 2.8), whilst scr-P2Pal-18s did not (Figure 6-5b). Although not yet replicated due to the lack of human donor tissue availability, P2Pal-18s also inhibited 2-Furoyl-LIGRLO induced human vagus nerve depolarisation (Figure 6-5c).

a) Example human vagus nerve trace



b) Guinea Pig



c) Human

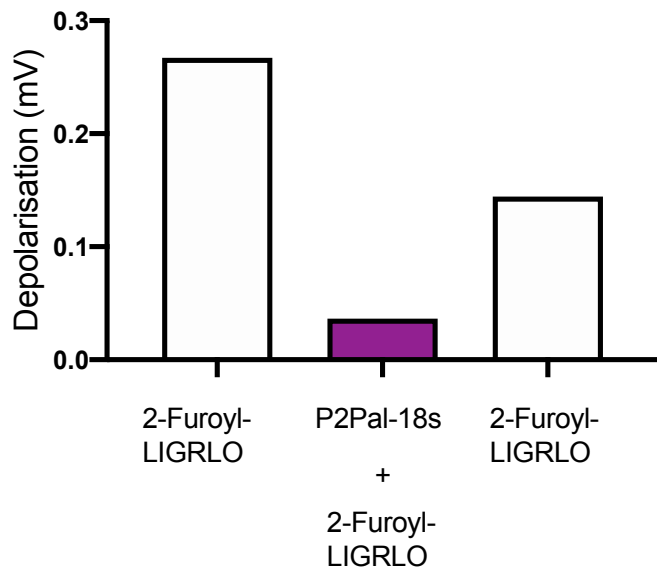


Figure 6-5 Inhibition of PAR2 agonist-induced vagus nerve depolarisation with PAR2-selective antagonist P2Pal-18s.

a) an example isolated vagus nerve model trace using human tissue, showing the PAR2-specific peptide antagonist P2Pal-18s inhibiting the PAR2 agonist 2-Furoyl-LIGRLO induced depolarisation. b) The % inhibition of P2Pal-18s (10µM) and a scrambled version of P2Pal-18s' sequence (scr-P2Pal-18s; 10µM) on 2-Furoyl-LIGRLO induced depolarisation. The data is presented as mean  $\pm$  S.E.M. of n=5 observations. \* indicates statistical significance (p < 0.05) by way of a paired t test comparing responses in the same piece of nerve with and without antagonist. c) a histogram to show the depolarisation of human vagus nerve from (a) (the first bar is an average of the two initial 2-Furoyl-LIGRLO induced responses).

For each of these antagonist experiments, the nerve was first stimulated with the PAR2 agonist 2-Furoyl-LIGRLO (100nM) for 2 minutes, up to 3 times, to obtain at least 2 reproducible responses. Following each of these 2-minute periods, any response was washed off with KH solution until the signal returned to baseline. The nerve was then 'blocked' with either PAR2 antagonist P2Pal-18s (10µM), scr-P2Pal-18s (10µM) or vehicle, for 10 minutes. Once this time had elapsed, the nerve was then immediately exposed to both 2-Furoyl-LIGRLO and the blocking compound for 2 minutes. This response was then washed off before a final stimulation took place with 2-Furoyl-LIGRLO, to ensure the nerve was still viable. All drugs were dissolved in KH solution and suffused the nerve at a rate of 2 ml/min.



### 6.3.2 Effect of PAR2 agonist 2-Furoyl-LIGRLO on RLN firing

We deployed an *ex vivo* electrophysiological tracheal recording (eTRec) system to measure the change in firing rate of a guinea pig's recurrent laryngeal nerve (RLN) when PAR2 agonist 2-Furoyl-LIGRLO was perfused through the trachea it was innervating. This is a more airway relevant technique than isolated vagus nerve recording, as it measures firing events of the RLN caused by activation of nerve endings within the tracheal wall, rather than depolarisation caused by activation of receptors expressed along the vagus nerve trunk.

We found that 2-Furoyl-LIGRLO amide was capable of instigating a higher rate of RLN firing events (signal – baseline) within the eTRec system when compared to vehicle (21.5 versus -4.5 impulses per second, respectively) (Figure 6-6). Capsaicin had a mean max firing rate of 52.5 impulses per second.

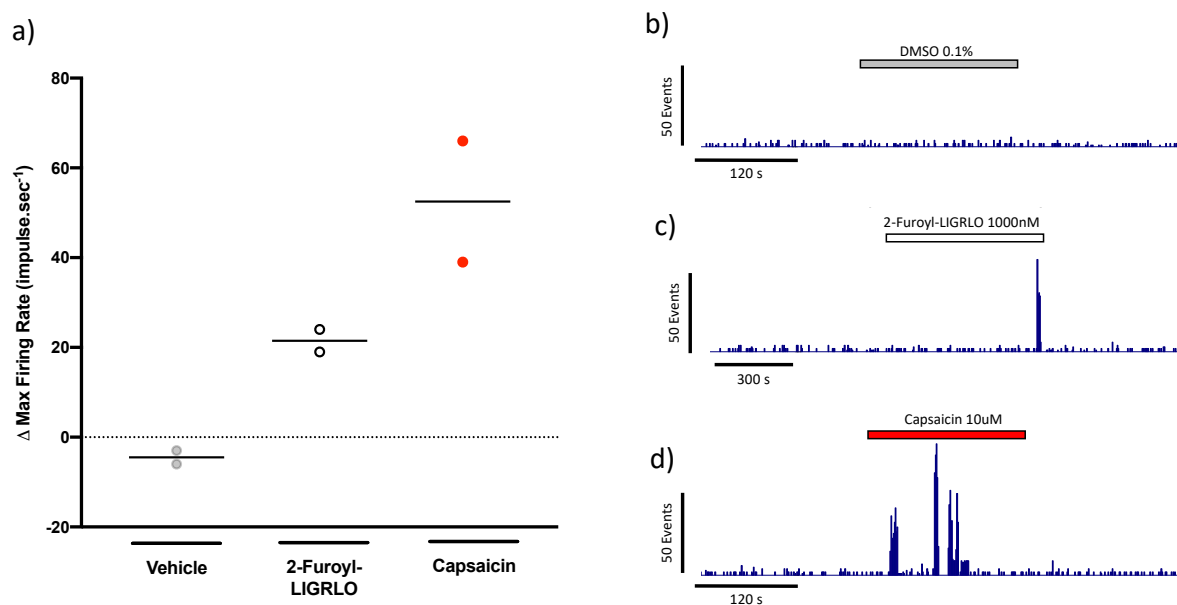


Figure 6-6 Measuring guinea pig recurrent laryngeal nerve (RLN) firing in response to PAR2 agonist 2-Furoyl-LIGRLO.

**a)** mean max firing rate (signal – baseline) of the RLN within the eTRec system when perfusing the trachea with vehicle (0.1% DMSO), 2-Furoyl-LIGRLO (1000nM) or capsaicin (10 $\mu$ M). Vehicle and capsaicin were administered for 3 minutes, whilst 2-Furoyl-LIGRLO was administered for 10 minutes. n=2

Right side: example neurograms showing the firing events of the RLN by time (seconds) when the trachea is perfused with DMSO vehicle (**b**), 2-Furoyl-LIGRLO (**c**), or capsaicin (**d**).

### 6.3.3 Effect of PAR2 agonists on firing of airway terminating vagus nerve single fibres *in vivo*

In addition to eTRec, the airway single fibre model is another more airway relevant model that measures action potential firing, it can also indicate which nerve fibre subtypes mediate a tussive response. We used the *in vivo* single fibre recording model to see the effect of intratracheally aerosolised 2-Furoyl-LIGRLO, at a range of concentrations, on an airway terminating A $\delta$ -fibre from within an anaesthetised guinea pig.

The A $\delta$ -fibre was distinguished from other fibre subtypes (*e.g.* C-fibres) by confirming its response to citric acid, as well as using the other techniques mentioned in Section 2.6.2. The A $\delta$ -fibre investigated had a conduction velocity of 6 m/s and was capsaicin sensitive.

Although not yet replicated, the PAR2 agonist 2-Furoyl-LIGRLO increased the firing rate of the A $\delta$ -fibre that was tested (Figure 6-7). The onset of Covid-19 limited the number of experiments that could be completed using this model, future plans (see Section 8.4) will include additional replicates, testing 2-Furoyl-LIGRLO on C-fibres and attempting to inhibit these action potential firings with pharmacological antagonists.

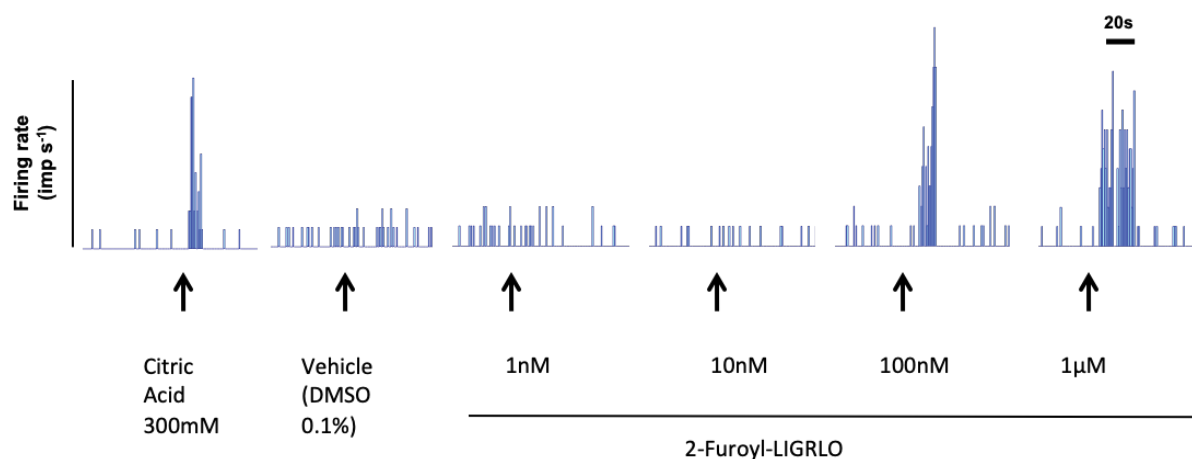


Figure 6-7 *In vivo* A $\delta$ -fibre firing in response to different concentrations of PAR2 agonist 2-Furoyl-LIGRLO in a guinea pig.

Pictured is a neurogram to demonstrate the effect of citric acid and various concentrations of PAR2 agonist 2-Furoyl-LIGRLO on the firing rate (impulses per second) of a guinea pig airway A $\delta$ -fibre  $n=1$ .

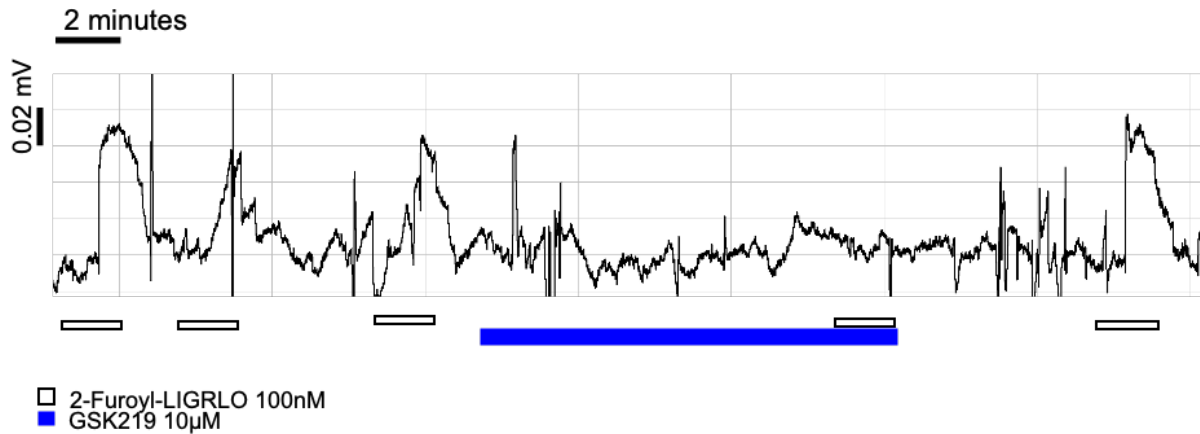
An anaesthetised, paralysed and mechanically ventilated guinea pig was exposed to citric acid or different doses of 2-Furoyl-LIGRLO by having them nebulised into its lungs. Each dose was nebulised into the airways for 1 minute, the firing rate of the airway terminating A $\delta$ -fibre was then electrophysiologically monitored for a further 20 minutes and allowed to return to baseline before the next dose was administered.

#### 6.3.4 Determining a role for the TRPV4-ATP-P2X3 axis in PAR2-agonist induced vagus nerve depolarisation

We sought to investigate whether PAR2 agonist induced vagus nerve depolarisation was at all mediated by the TRPV4-ATP-P2X3 axis, a protussive signalling pathway that could be involved in chronic cough (Bonvini et al., 2016, Abdulqawi et al., 2015). To investigate this, we used TRPV4 channel blocker GSK2193874 (GSK219; 10 $\mu$ M) (Thorneloe et al., 2012) and P2X3 channel blocker AF-353 (10 $\mu$ M) (Gever et al., 2010) to determine whether they could inhibit 2-Furoyl-LIGRLO induced depolarisation in the isolated vagus nerve model. The concentrations used for these antagonists were previously found to be sufficient in the isolated vagus nerve model (Bonvini et al., 2016).

GSK219 (10 $\mu$ M) and AF-353 (10 $\mu$ M) were able to inhibit 2-Furoyl-LIGRLO induced vagus nerve depolarisation by 42%  $\pm$  9.0% and 46%  $\pm$  8.0%, respectively, in guinea pig tissue, whilst vehicle did not (Figure 6-8b). Although not yet replicated due to the lack of human donor tissue availability, GSK219 also inhibited 2-Furoyl-LIGRLO induced human vagus nerve depolarisation whereas vehicle did not (Figure 6-9).

a) Guinea pig



b) Guinea pig

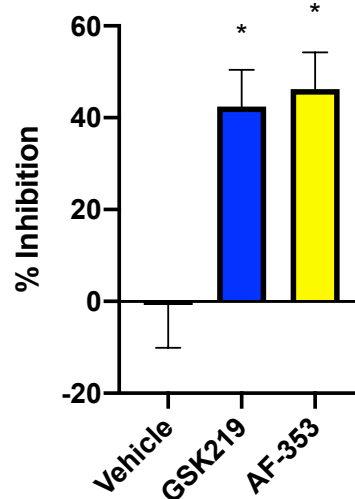


Figure 6-8 Inhibition of PAR2 agonist-induced vagus nerve depolarisation with TRPV4 and P2X3 antagonists in guinea pigs.

a) an example trace from an isolated vagus nerve recording to demonstrate the inhibitory effect TRPV4 antagonist GSK219 has on PAR2 agonist 2-Furoyl-LIGRLO induced depolarisation. b) a histogram to summarise the inhibitory effect TRPV4 antagonist GSK219 (10µM) and P2X3 antagonist AF-353 (10µM) have on PAR2 agonist 2-Furoyl-LIGRLO (100nM) induced depolarisation compared to vehicle (0.1% DMSO). Data shown as mean  $\pm$  S.E.M,  $5 \leq n \leq 7$ . \* indicates statistical significance ( $p \leq 0.05$ ) by way of a paired t-test comparing responses in the same piece of nerve with and without antagonist.

For each of these antagonist experiments, the nerve was first stimulated with the PAR2 agonist 2-Furoyl-LIGRLO (100nM) for 2 minutes, up to 3 times, to obtain at least 2 reproducible responses. Following each of these 2-minute periods, any response was washed off with KH solution until the signal returned to baseline. The nerve was then 'blocked' with either GSK219 (10µM), AF-353 (10µM) or vehicle, for 10 minutes. Once this time had elapsed, the nerve was then immediately exposed to both 2-Furoyl-LIGRLO and the blocking compound for 2 minutes. This response was then washed off before a final stimulation took place with 2-Furoyl-LIGRLO, to ensure the nerve was still viable. All drugs were dissolved in KH solution and suffused the nerve at a rate of 2 ml/min.

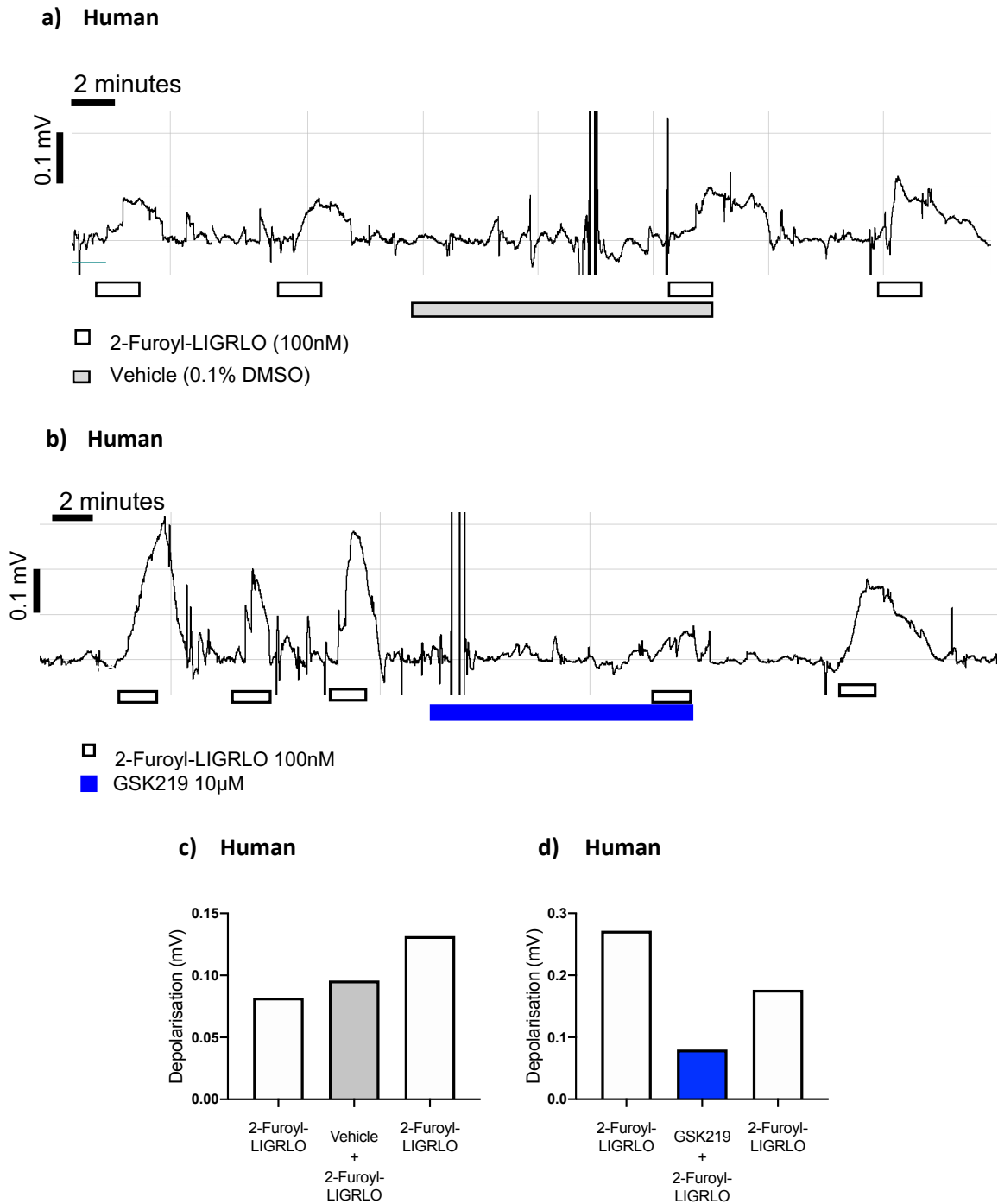


Figure 6-9 Inhibition of PAR2 agonist-induced vagus nerve depolarisation with a TRPV4 antagonist in donor human tissue.

Example traces to show the effect of vehicle **(a)** and TRPV4 antagonist GSK219 **(b)** on PAR2 agonist 2-Furoyl-LIGRLO induced vagus nerve depolarisation in human tissue. **(c)** and **(d)** are histograms to show the peak amplitude of the depolarisation (mV) of human vagus nerve from **(a)** and **(b)**, respectively. Data shown is mean,  $n=1$  (the first bar is an average of the two initial 2-Furoyl-LIGRLO induced responses)

For both of these antagonist experiments, the nerve was first stimulated with 2-Furoyl-LIGRLO (100nM) for 2 minutes, up to 3 times, to obtain at least 2 reproducible responses. Following each of these 2-minute periods, any response was washed off with KH solution until the signal returned to baseline. The nerve was then 'blocked' with either GSK219 or vehicle, for 10 minutes. Once this time had elapsed, the nerve was then immediately exposed to both 2-Furoyl-LIGRLO and the blocking compound for 2 minutes. This response was then washed off before a final stimulation took place with 2-Furoyl-LIGRLO, to ensure the nerve was still viable. All drugs were dissolved in KH solution and suffused the nerve at a rate of 2 ml/min.

## 6.4 Discussion

The aim of this chapter was to investigate whether agonists for PAR2 were capable of activating airway sensory nerves, such a finding would suggest that they might be able to elicit cough. With chronic cough being a common symptom of IPF (Key et al., 2010), it is interesting to note the increasing evidence that PAR2 contributes to the pathophysiology of the disease. This includes: the discovery that there is increased PAR2 expression in the IPF lung (Wygrecka et al., 2011), and that this correlates with the 'honeycombing' of the lung architecture (Park et al., 2013); the finding that the PAR2 agonist tryptase stimulates the growth of human lung fibroblasts, thus potentiating the production of extracellular matrix (Wygrecka et al., 2013); and a study confirming that mice without a functioning gene for PAR2 are more resistant to bleomycin-induced lung injury (Borensztajn et al., 2010). Also, pertinent to this chapter and the next, is that P2Pal-18s (the PAR2 specific antagonist we used) was found to reduce the severity of fibrosis in bleomycin-treated mice (Lin et al., 2015a).

Despite the study by Gatti *et al* finding that PAR2 activation could not cause cough *per se*, we nevertheless sought to investigate a role for PAR2 in airway sensory nerve activation. This was due to the above evidence of PAR2's involvement in IPF and due to PAR2's purported ability to trigger neurogenic inflammation and pain through TRPV4 (Grace et al., 2014, Poole et al., 2013), an ion channel capable of causing cough when activated (Bonvini et al., 2016).

The effect of PAR2 agonists was pharmacologically evaluated *in vitro* in the isolated vagus nerve model; this is a useful model to infer whether a compound might have a protussive effect, because stimuli such as capsaicin, and endogenous stimuli such as the prostanoid PGE<sub>2</sub> and bradykinin, all elicit depolarisation of isolated vagus nerves and also cause cough when inhaled by human subjects (Bonvini et al., 2016, Grace et al., 2012, Birrell et al., 2009, Belvisi et al., 2017). To complete this work, we used donated human vagus nerves when possible, as well guinea pig and mouse vagus tissue. Guinea pigs are a useful species for assessing the effect of tussive agents because they are the smallest rodents that have a cough response similar to our own (Maher et al., 2009). Whether or not mice cough is a source of much debate (Mackenzie et al., 2004), and although there are claims that the species are capable of this reflex (Chen et al., 2013), many in respiratory field are yet to be convinced. There is, however, ample evidence that the afferent sensory arm of the mouse cough reflex is fully functional and similar to man (Maher and Belvisi, 2010), which means that the tissues of transgenic mice can still be used to probe tussive mechanisms. The PAR2 agonists 2-Furoyl-LIGRLO, SLIGKV, AC-55541 and trypsin were all shown to cause concentration dependent increases in depolarisation in guinea pig vagus nerves (Figure 6-2). To further check their specificity for PAR2, these tools were then carried forward for studies in mice with a disrupted PAR2 gene (F2LR1<sup>-/-</sup> mice), apart from trypsin, as this nonspecific enzyme hydrolyses a near-infinite amount of peptide-based

substrates. We found that responses to PAR2 agonist 2-Furoyl-LIGLRO, SLIGKV and AC-55541 were abrogated, whilst responses to GSK101, capsaicin and acrolein (agonists of the TRPV4, TRPV1 and TRPA1 ion channels, respectively) remained unchanged. This was important as it meant that these compounds were acting solely through the PAR2 receptor and not through an off-target effect on any ion channels that typically mediate chemosensitive cough reflexes.

We took the 2-Furoyl-LIGRLO (at a submaximal concentration of 100nM) forward for antagonist studies, because this appeared to be one of the most efficacious compounds (Figure 6-2), and, since it was designed to mimic the tethered ligand that activates PAR2 endogenously, it was also highly physiologically relevant. We attempted to block this depolarisation with P2Pal-18s, a cell-penetrating lipopeptide antagonist of PAR2. P2Pal-18s was used in the isolated vagus nerve model at a concentration of 10 $\mu$ M, this concentration was chosen due to two *in vitro* studies conducted elsewhere that had determined it to be efficacious at reducing the migratory capacity of murine and human lung fibroblasts (Bagher et al., 2018, Lin et al., 2015b). The selective PAR2 antagonist P2Pal-18s was able to inhibit 2-Furoyl-LIGRLO induced vagus nerve depolarisation in the guinea pig (Figure 6-5b) and although so far only tested on one human vagus nerve, it appears to have the same effect (Figure 6-5a,c). These data furthered our belief that 2-Furoyl-LIGRLO induced vagus nerve depolarisation was as a result of PAR2 specific agonism.

Whilst the isolated vagus nerve technique allows for a pharmacological evaluation of agonists and antagonists *in vitro*, one should be cautious when drawing conclusions relating to pro or antitussive effects. This is because the vagus nerve also innervates other organs besides the trachea (Gray et al., 2005), and the expression of receptors on the nerve trunk may differ from the nerve endings (Patel et al., 2003). Therefore, to more accurately predict the tussive potential of a compound, it is important to utilise more airway relevant techniques *e.g.* RLN eTRec and *in vivo* single fibre recordings.

We used eTRec to discern whether 2-Furoyl-LIGRLO was capable of causing compound action potential firing of the recurrent laryngeal nerve (RLN) when perfused through a guinea pig's trachea, *ex vivo*. The RLN is known for being one of the few nerves that follows a recurrent course *i.e.* it moves in the opposite direction (along the trachea) to the nerve from which it branches (the vagus nerve). Whilst the RLN controls all but one of the laryngeal muscles and carries sensory information from the oesophagus (Balakrishnan and Verma, 2013), it also innervates the trachea, and is responsible for afferent limb of the cough reflex (Canning et al., 2004). Although so far only *n* of 2, 2-Furoyl-LIGLRO appears capable of activating the airway sensory nerve endings that innervate the

trachea, thus causing them to fire. This further indicates that activating PAR2 could have a protussive effect.

The final method by which we confirmed a role for PAR2 in sensory airway nerve activation was through the *in vivo* single fibre model. As outlined in the introduction (Section 1.3.6), there are several types of nerve fibre thought to be involved in the afferent limb of the cough reflex including: A $\delta$ -fibre (*e.g.* RARs and cough receptors) and C-fibres. Although not yet tested on a C-fibre due to time limitations, we were able to test 2-Furoyl-LIGRLO on a single A $\delta$ -fibre (Figure 6-7), the other chemosensitive afferent fibre able to cause cough. 2-Furoyl-LIGRLO appeared to cause firing similar in magnitude to citric acid, at concentrations of 100nM and 1 $\mu$ M. That PAR2-induced airway nerve activation might be mediated through faster, myelinated A $\delta$ -fibres is interesting, given that this is the case for TRPV4 agonists in the protussive TRPV4-ATP-P2X3 signalling pathway (Bonvini et al., 2016). Due to this, we aimed to determine whether TRPV4 and P2X3 might be involved in PAR2 agonist-induced airway nerve activation, by using antagonists for these ion channels in the isolated vagus nerve model.

Unfortunately, we were not able to test P2X3 antagonist AF-353 on 2-Furoyl-LIGRLO responses in human vagus nerves, however TRPV4 antagonist GSK219 was tested, and appears to so far inhibit them (Figure 6-9). In the guinea pig, both GSK219 and AF-353 were each able to significantly inhibit PAR2 agonist 2-Furoyl-LIGRLO induced vagus nerve depolarisation, by approximately 45% (Figure 6-8). These findings suggests that these two ion channels are involved in the response, and that the TRPV4-ATP-P2X3 pathway is a mechanism by which PAR2 agonists can activate airway sensory nerves. However, as these average inhibitions were less than the inhibition of PAR2 specific antagonist P2Pal-18s (68%), it leaves the possibility for at least one other parallel signalling pathway, working in concert, to also be mediating PAR2 agonist-induced airway nerve activation. To determine if this is the case, further work will need to be undertaken (Section 8.4), with one unexplored avenue being whether PAR2 agonists can also elicit the firing of airway terminating C-fibres.

In summary, PAR2 ligands have been shown to activate airway sensory nerves *in vitro* through causing depolarisation of human, guinea pig and mouse vagus nerves. These depolarisations were shown to be PAR2 specific, firstly through the use of a pharmacological antagonist in the case of human and guinea pig nerves, and secondly, through the use of genetic disruption in mice vagus nerves. PAR2 agonists were then shown to cause firing in guinea pig airway sensory nerves *ex vivo* and *in vivo*, using the eTRec and airway single fibre models, respectively, when they made contact



with the animals' tracheas. Finally, PAR2 agonists were shown to activate airway sensory nerves *in vitro* through activation of TRPV4 and P2X3.

The findings above show that there is indeed a role for PAR2 in airway sensory nerve activation, and that the TRPV4-ATP-P2X3 axis may at least be partly involved, thereby lending support to this chapter's hypothesis. Indeed, the finding that extracellular ATP is present at greater concentrations in the lungs of IPF patients, suggests that this pathway may be overactive (Riteau et al., 2010). In addition, knowing that the presence of agonists for PAR2 are elevated within the IPF lung (Kawatani et al., 2007), it remains feasible that this could be contributing to the distressing chronic cough symptom that most IPF patients suffer from (Key et al., 2010). Whilst the study by Gatti *et al* did not find PAR2 agonists capable of eliciting cough in guinea pigs, *per se*, it is important to note that these guinea pigs were naïve animals and were not modelling IPF. It thus remains possible that established pulmonary fibrosis generates a disease phenotype that renders the tussive reflex more vulnerable to PAR2 agonists. Indeed, one thing to evaluate in a guinea pig fibrosis model would be whether the tussive response could be altered by modulating PAR2 activation; this is why it was important for this PhD project to establish a bleomycin-induced fibrosis model in guinea pigs, where spontaneous cough could be monitored. To conclude, PAR2 appears to be a justifiable target to further investigate with regards to IPF-associated chronic cough, and further, modulating PAR2 may have a therapeutic benefit, not only on fibrosis proliferation, but on patient chronic cough, and therefore quality of life, too.

## 7 Characterising tools to be used in the fibrosis-induced spontaneous cough model

### 7.1 Rationale

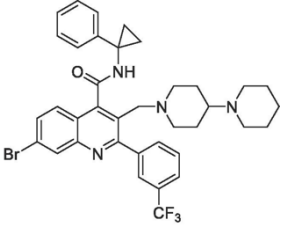
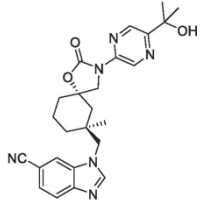
IPF-associated chronic cough is a deeply distressing symptom for IPF patients, that has proven largely refractory to treatment, and there are currently no approved antitussive therapies for it (Birring et al., 2017, Key et al., 2010). Identifying efficacious, novel antitussives using the *in vivo* model of fibrosis associated spontaneous cough outlined in Chapter 3 of this thesis, a model more akin to the objective cough frequencies measured in the clinic, may help in the development of efficacious new therapeutic targets.

The aim of my thesis was to investigate the mechanism behind cough in IPF and results have so far suggested that the TRPV4-ATP-P2X3 axis may be involved in the increased spontaneous cough frequencies seen in the model outlined in Chapter 3. In order to fully test this hypothesis, a potent and selective TRPV4 antagonist will be required.

This chapter outlines the work that has been undertaken to characterise GSK2798745 (henceforth referred to as GSK279) *in vitro* and *in vivo*. GSK279 (Table 7-1) is a recently discovered small molecule antagonist of TRPV4 (Brooks et al., 2019) that is reported to have a greater antagonist affinity, and thereby a lower half maximal inhibitory concentration ( $IC_{50}$ ) than HC-067047 and GSK219 (Lawhorn et al., 2020), two antagonists previously used within the lab. In addition, this compound has been shown to be highly selective and efficacious in human, rat and guinea pig cells and tissue, with it also having a good pharmacokinetic and safety profile in the clinic, and a systemic half-life of around 13 hours (Goyal et al., 2019) (Figure 7-1). This is therefore a clinically relevant, potent and efficacious molecule that, once profiled, could be taken forward into the bleomycin spontaneous cough model in the guinea pig.

Table 7-1 The structure and potency of TRPV4 antagonists GSK219 compared with GSK279

Antagonist affinity data generated internally at AstraZeneca and displayed with permission here. FLIPR – Fluorescent Imaging Plate Reader; CHO – Chinese Hamster Ovary; ASMC – Airway Smooth Muscle Cell. Each CHO cell has been transfected in order to overexpress the relevant species' TRPV4 ion channel, whereas ASMCs already express native TRPV4 ion channels.

TRPV4 antagonist	Molecular Structure	Human ASMC FLIPR pIC <sub>50</sub>	Human CHO FLIPR pIC <sub>50</sub>	GP CHO pIC <sub>50</sub>
GSK2193874 (GSK219)		7.81	7.71	7.28
GSK2798745 (GSK279)		9.4	8.4	7.97

In order for the effect of an antagonist to be seen in the model outlined in Chapter 3, we would ideally want the drug to have a robust duration of action, that lasts at least 24-hours. Having a compound with a duration of effect this long would therefore mean that it would only need to be dosed once, over the course of a 24-hour spontaneous cough recording. Multiple dosing of guinea pigs should ideally be avoided, as it would negatively impact the animals from a welfare standpoint, and further, any disruption would likely also affect the cough responsiveness of the animals, thereby increasing the variability of the results. Therefore, one aim of this chapter is to determine the duration of action of GSK279.

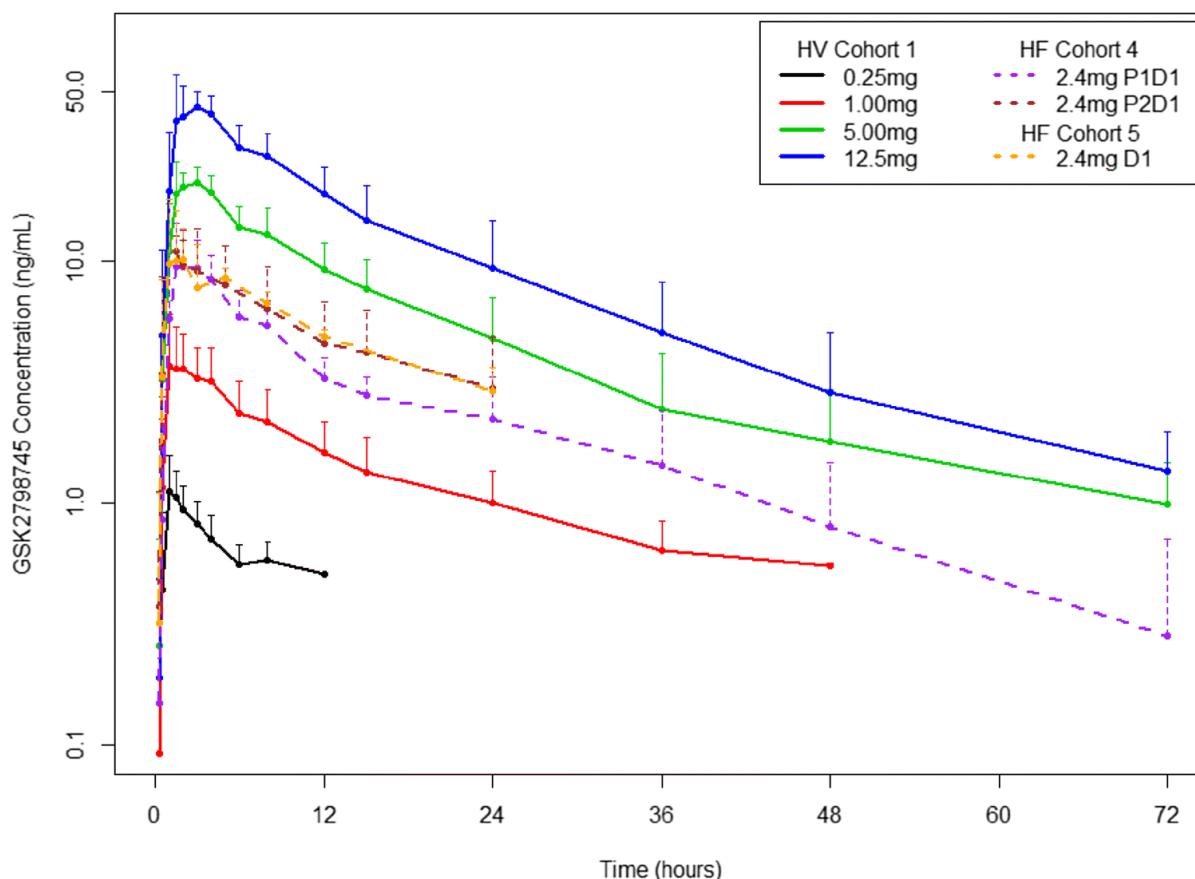


Figure 7-1 Pharmacokinetic performance of GSK279 in a Phase 1 clinical trial

A Phase 1 human volunteer study illustrating the dose dependent pharmacokinetic profile of GSK279 as assessed by plasma concentrations at various time points, conducted in healthy volunteers and stable heart failure patients, adapted from Goyal et al. (2019). GSK279 was administered once at a range of doses. GSK279 demonstrated dose proportionality throughout the doses tested in healthy volunteers. The mean systemic half-life of the compound was approximately 13 hours. HF: patients with heart failure, HV: healthy volunteers.

### 7.1.1 Chapter Hypothesis

GSK279 is a potent and selective antagonist of TRPV4, with a 24-hour long duration of action *in vivo*

Aims:

- Evaluate the potency and efficacy of GSK279 (Brooks et al., 2019) *in vitro*, against GSK1016790a-induced depolarisation of isolated guinea pig and donor human vagal nerve tissue
- Evaluate the antitussive efficacy of GSK279 in a conscious guinea pig cough model, induced by the TRPV4 antagonist GSK1016790a (henceforth referred to as GSK101)
- Determine the duration of efficacy of GSK279 in a functional time course cough experiment over 24 hours in order to decide a dosing regimen for the IPF cough model

## 7.2 Methods

### 7.2.1 Isolated Vagal Nerve Recordings

#### 7.2.1.1 Assessing TRPV4 antagonism by GSK279 and GSK219

To evaluate GSK279's ability to block GSK101 responses *in vitro*, the isolated vagus nerve model was used (described in detail in Section 2.4). Guinea pig nerves were perfused with GSK279 or GSK219, at a range of concentrations, in order to block GSK101-induced vagus nerve depolarisation, according to the antagonist protocol previously outlined (2.4.4). A suitable concentration of the new antagonist GSK279 was then taken forward for use in antagonist studies involving vagus nerves from human donors.

#### 7.2.1.2 Statistical Analysis

Individual nerve depolarisations were assessed by measuring the peak amplitude of the response (in mV); and antagonist inhibitions were calculated (see Section 2.4.4).

For the antagonist studies, a paired two tailed t-test was used comparing the magnitude of depolarisation by the agonist with and without the presence of antagonist in the same piece of nerve. The data is presented as mean  $\pm$  S.E.M., with statistical significance set at  $P < 0.05$ .

### 7.2.2 TRPV4 agonist-induced cough

#### 7.2.2.1 GSK279 Dose Response Study

An *in vivo* provoked cough study (protocol described in Section 2.6.4) was undertaken to assess whether the selective TRPV4 antagonist GSK279 could inhibit cough elicited by the TRPV4 agonist GSK101 in guinea pigs.

Prior to cough provocation, male Dunkin Hartley guinea pigs weighing 350g, were dosed *per os* with vehicle (2% DSPE-PEG in 5% mannitol) or a range of doses of GSK279 (determined from a separate pilot study), at a volume of 2 ml/kg. After 2 hours, the animals were placed within plethysmography cough chambers and allowed to acclimatise to their new environment for 3 minutes. Following acclimatisation, basal levels of cough were recorded for 2 minutes. Next, cough was further recorded for a 10-minute challenge period, the first 5 minutes of which TRPV4 agonist GSK101 (30  $\mu$ g/ml) was aerosolised into the plethysmography chamber. After the challenge period was over, the animals were euthanised through an overdose of pentobarbitone (Section 2.2).

To help characterise the therapeutic effect of GSK279 for the specified dosage, plasma concentrations of the compound were measured in each group to determine GSK279 exposure levels. Following euthanasia, a blood sample was collected from each guinea pig by performing cardiac puncture with a heparinised needle and syringe. The sample was then centrifuged at 4000 g

for 10 minutes, to separate the blood cells from the plasma, whereupon the latter was stored at -20°C for future analysis.

GSK279 levels in the plasma were then quantified through mass spectroscopy by our collaborators in the *Drug Metabolism and Pharmacokinetics* department at AstraZeneca.

Following analysis, a suitable and effective dose was taken forward for future *in vivo* studies.

#### 7.2.2.2 GSK279 Time Course Study

A time course study was undertaken in order to determine how long a single administration of GSK279 remained effective at inhibiting GSK101-induced cough *i.e.* GSK279's duration of action. Such pharmacodynamic insight will be required before testing GSK279 in the *in vivo* model of fibrosis-induced spontaneous cough (outlined in Chapter 3), as it may be necessary to dose GSK279 multiple times over the course of a 24-hour spontaneous cough assessment if its duration of action is short.

Guinea pigs weighing approximately 350g were dosed with vehicle (2% DSPE-PEG in 5% mannitol) or GSK279 (1 mg/kg), *per os*, at a volume of 2 ml/kg. Following dosing, guinea pigs then underwent GSK101-induced cough challenge 2, 4, 6, 8, 12 or 24 hours later, as described in the previous section (7.2.2.1). Finally, guinea pigs were euthanised through an overdose of pentobarbitone (Section 2.2).

To help characterise the therapeutic effect of GSK279 for the specified dosage over time, plasma concentrations of the compound were measured at each time point to determine GSK279 exposure levels. Plasma was collected, prepared and analysed identically to the prior study (7.2.2.1).

#### 7.2.2.3 Statistical Analysis

For the GSK279 dose response study, statistical significance of cough inhibition was assessed by using the Kruskal-Wallis test, accompanied by a Dunn's multiple comparison post-test, where total coughs from antagonist-treated animals were compared to that of vehicle-treated animals.

For the 24-hour time course study, a Mann-Whitney test was used to compare cough counts, at each time point, of GSK279-treated animals to that of vehicle-treated animals.

## 7.3 Results

### 7.3.1 Effect of selective TRPV4 antagonist GSK279 on TRPV4 agonist GSK101-induced vagus nerve depolarisation

The *in vitro* isolated vagus nerve model was used to assess the effect of the new TRPV4 antagonist GSK279 on TRPV4 agonist GSK101-induced responses; for comparison the inhibitory effect of TRPV4 antagonist GSK219 was also tested (Figure 7-2).

At doses 1, 10, 100 and 1000 nM, GSK279 was able to significantly inhibit GSK101-induced vagus nerve depolarisation by  $44.0 \pm 7.35\%$ ,  $61.7 \pm 10.06\%$ ,  $75.6 \pm 7.78\%$  and  $74.1 \pm 3.85\%$ , respectively. GSK219 however, had lower efficacy, and significantly inhibited GSK101 at concentrations 1, 3 and 10  $\mu\text{M}$  by  $57.86 \pm 4.60\%$ ,  $68.19 \pm 1.94\%$  and  $93.3 \pm 6.67\%$ . Together, these results yielded an approximate  $\text{pIC}_{50}$  of 6.1 for GSK219 and a more potent  $\text{pIC}_{50}$  of 9.3 for GSK279, equivalent to 794 nM and 0.5 nM, respectively. Although the potency of GSK279 seems to line up well with the data in Table 7.1, this is a dramatic loss of potency in the isolated GP vagus compared to the data seen in the CHO cells for GSK219. This would suggest that the data with overexpressed cells may not always be indicative of what happens with the native ion channel in the vagus nerve.

In the one human donor vagus nerve that was tested on prior to the Covid-19 pandemic, GSK279 successfully blocked GSK101-induced depolarisation (Figure 7-2c). This human vagus nerve derived from a deceased 65-year-old female donor, who was diagnosed with COPD.

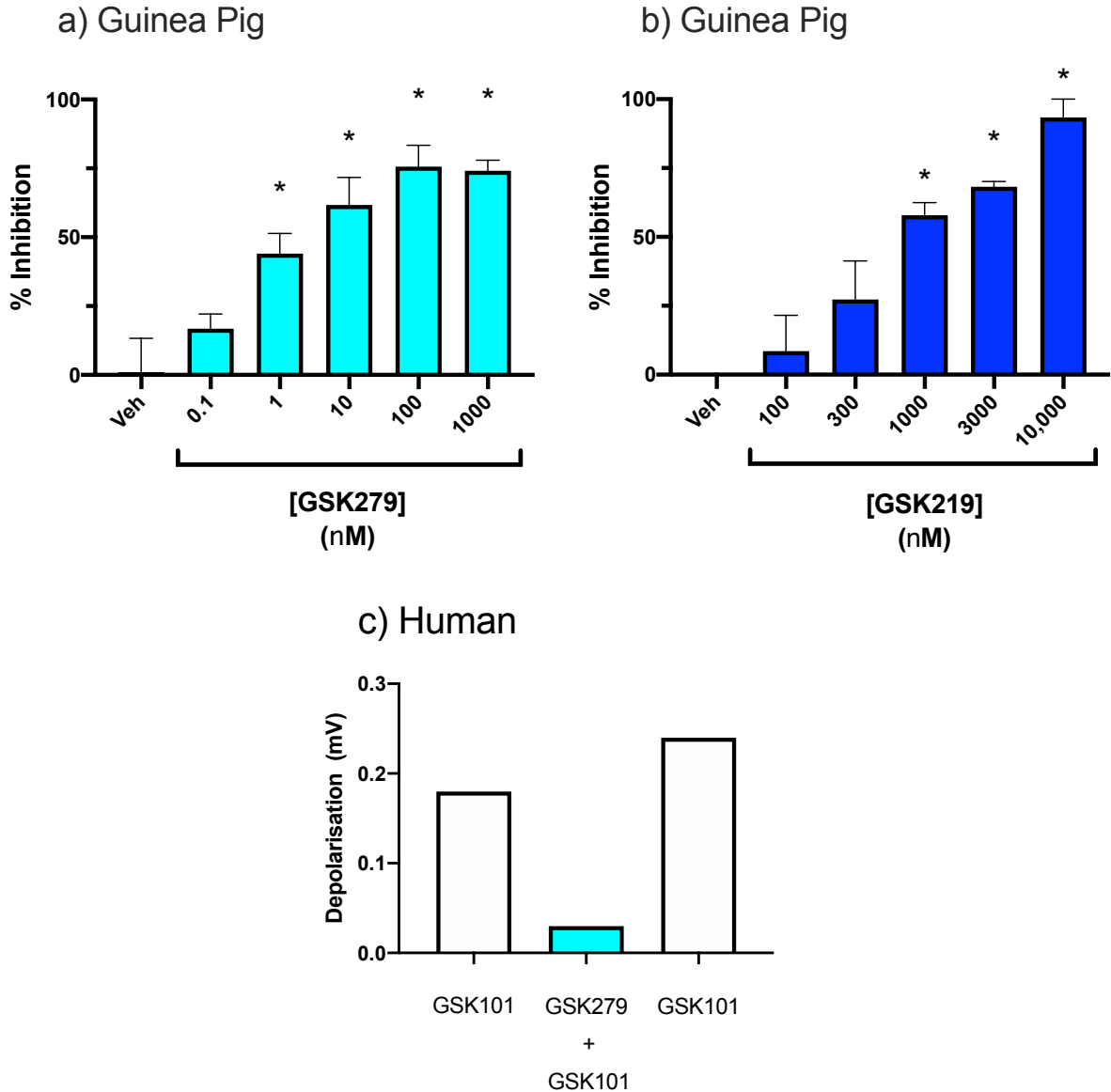


Figure 7-2 Effect of selective TRPV4 antagonists on TRPV4 agonist GSK101 (300nM) induced vagus nerve depolarisation.

**a)** Inhibitory effect of GSK279 in guinea pigs,  $3 \leq n \leq 5$ . **b)** Inhibitory effect of GSK219 in guinea pigs,  $3 \leq n \leq 5$ . For both a & b, data is shown as mean inhibition  $\pm$  S.E.M. \* indicates statistical significance ( $p \leq 0.05$ ) by way of a paired t-test comparing responses in the same piece of nerve with and without antagonist. **c)** a histogram to show GSK101 (300nM) induced depolarisation of human vagus with and without the presence of GSK279 (10nM),  $n=1$ .

For each of these antagonist experiments, the nerve was first stimulated with the TRPV4 agonist GSK101 (300nM) for 2 minutes, up to 3 times, to obtain at least 2 reproducible responses. Following each of these 2-minute periods, any response was washed off with KH solution until the signal returned to baseline. The nerve was then 'blocked' with either one of the TRPV4 antagonists GSK279 or GSK219, at a range of concentrations, for 10 minutes. Once this time had elapsed, the nerve was then immediately exposed to both GSK101 and the TRPV4 antagonist for 2 minutes. This response was then washed off before a final stimulation took place with GSK101, to ensure the nerve was still viable. All drugs were dissolved in KH solution and suffused the nerve at a rate of 2 ml/min. Only one concentration of antagonist was tested for each nerve piece.



## 7.3.2 Effect of TRPV4 antagonist GSK279 on the cough response to TRPV4 agonist GSK101 in naïve guinea pigs

### 7.3.2.1 GSK279 dose response

To initially characterise TRPV4 antagonist GSK279's antitussive properties *in vivo*, two dose response experiments were undertaken to block GSK101-induced cough in guinea pigs. The first study (Figure 7-3a) had a dose range of between 0.005 and 30 mg/kg and showed that a suitable submaximal dose lay between 0.05 and 2 mg/kg; the second study, which had a narrower concentration range of GSK279 in order to determine a more precise ED<sub>50</sub>, is presented in Figure 7-3b. Animals pre-treated with vehicle coughed an average of 21.9±5.26 times, the cough response however was completely abrogated (p<0.05) for animals pre-treated with 0.3 or 1 mg/kg of GSK279, and significantly reduced for animals pre-treated with 0.1 mg/kg of GSK279 (6.9±4.46 coughs). TRPV4 antagonist GSK219 has previously been shown by this lab to inhibit GSK101-induced cough in guinea pigs (Bonvini et al., 2016), and it demonstrated a similar biological (although not significant) effect in this study (Figure 7-3c). Plasma levels suggested that free levels of GSK219 in this study (373 ± 36.6 nM) were not at a level high enough to inhibit the vagus IC<sub>50</sub> of 794 nM, which would explain the lack of significance.

To quantify the exposure to GSK279, plasma levels for the antagonist were measured in each of the animals from the dose response study. Total free plasma levels of GSK279 were found to be 0, 1, 35, 26, 105, 308 and 761 nM, in animals treated with vehicle, 0.003, 0.01, 0.03, 0.1, 0.3 and 1 mg/kg of GSK279, respectively (Figure 7-4).

As the next stage of investigating GSK279 was administering it as part of a 24-hour time course study, it was therefore required of us to select a dose that would remain in the plasma at a high concentration, for as long a time as possible. Two hours following administration, a dose of 1 mg/kg abrogated GSK101-induced cough and further yielded a total free plasma concentration of 761±166.3 nM, which vastly exceeded the IC<sub>50</sub> generated using the isolated vagus nerve model: 0.5 nM. It was because of this that a dose of 1 mg/kg of GSK279 was taken forward into the next study.

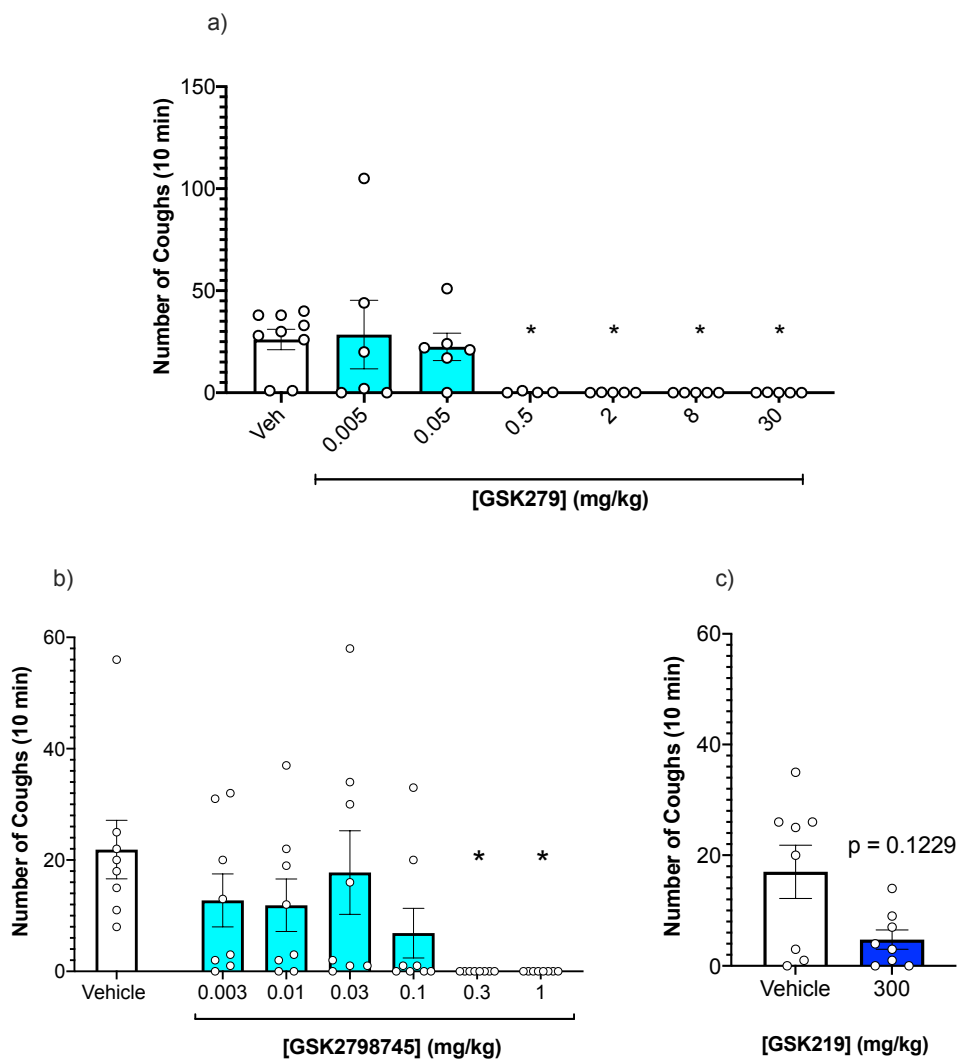


Figure 7-3 The effect of TRPV4 selective antagonists on guinea pig coughs elicited by aerosolised TRPV4 agonist GSK101.

**a) & b)** The effect of different concentrations of TRPV4 antagonist GSK279 on GSK101-induced cough,  $5 \leq n \leq 8$ . Guinea pigs were dosed with vehicle or GSK279 (p.o.) 2 hours prior to exposure to TRPV4 agonist GSK101 (30  $\mu\text{g/ml}$ , aerosolised for 5 minutes). **c)** Data from this lab showing the effect of TRPV4 antagonist GSK219 on GSK101-induced cough,  $n=8$ . Guinea pigs were dosed with GSK219 (i.p.) 1 hour prior to exposure to TRPV4 agonist GSK101 (30  $\mu\text{g/ml}$ , aerosolised for 5 minutes).

Data is shown as mean inhibition  $\pm$  S.E.M. \* indicates statistical significance ( $p < 0.05$ ), measured by performing Kruskal-Wallis test with Dunn's post-test, whereby coughs in the antagonist-treated groups were compared to that of the vehicle-treated group. For (c), a Mann-whitney test was used to determine statistical significance.

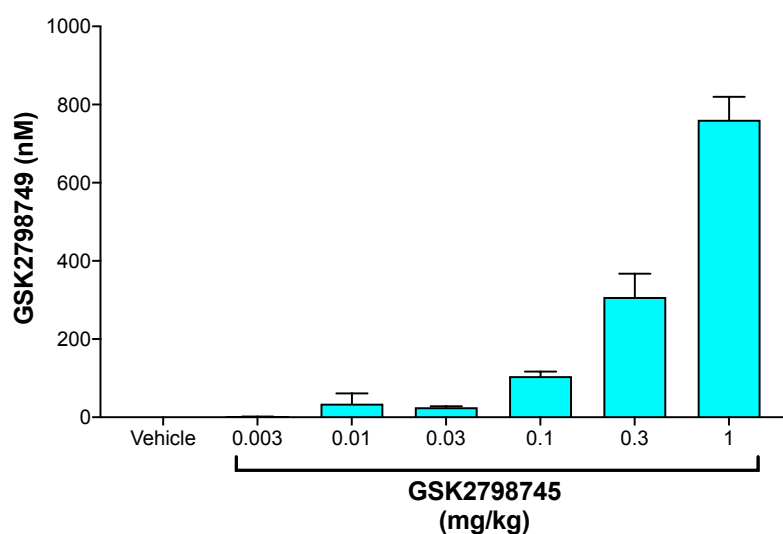


Figure 7-4 Total free plasma levels of GSK279 in guinea pigs treated with this compound in the second dose response study

A histogram to show the total free plasma levels of TRPV4 antagonist GSK279 in guinea pigs 2 hours after having been dosed (p.o.) with different amounts of this compound.

### 7.3.2.2 GSK279 time course experiment

To determine the duration of action of GSK279's inhibition of TRPV4 agonist-induced cough, a time course study was undertaken. Knowing the duration of GSK279's TRPV4 blocking action will help inform the dosing regimen for this compound when it is eventually trialled in the fibrosis-induced spontaneous cough model (outlined in Chapter 3).

Oral application of GSK279 was found to be significantly effective ( $p < 0.05$ ) at blocking TRPV4 agonist GSK101-induced cough 2, 8, 24 hours after dosing (Figure 7-5). Whilst the number of GSK101-induced coughs were reduced 4, 6 and 12 hours after GSK279 dosing, these reductions were not significant ( $p = 0.1429, 0.1429$  and  $0.0571$ , respectively).

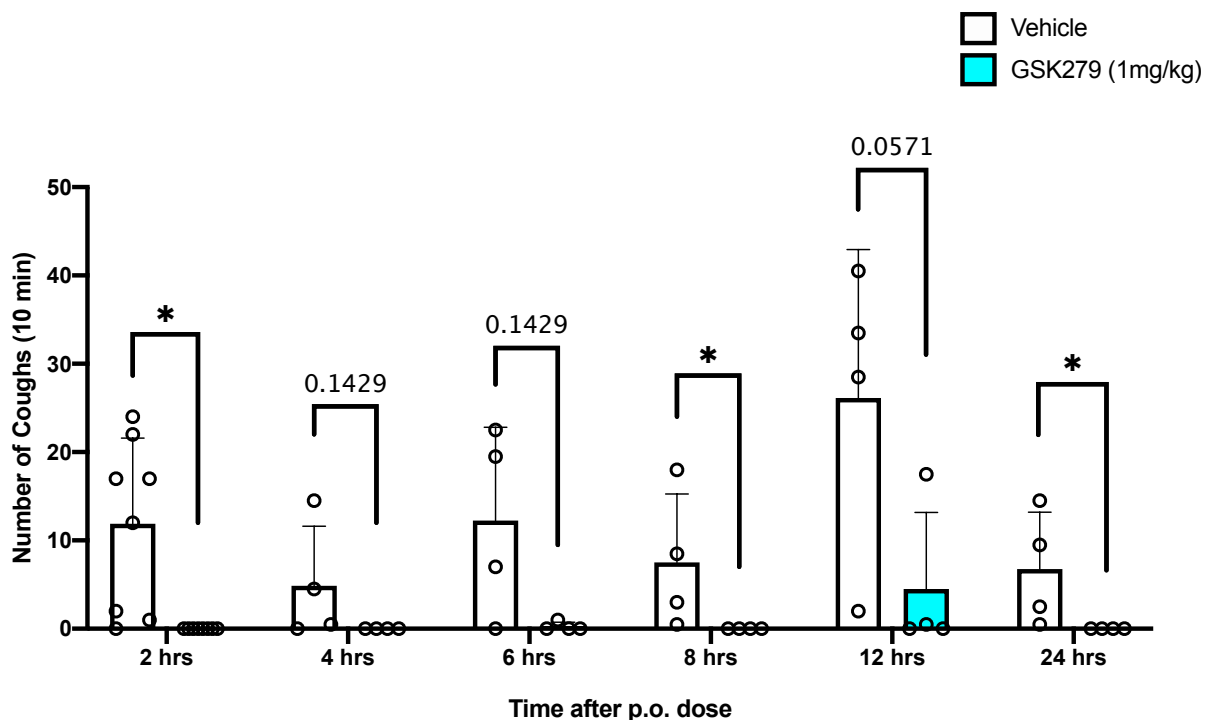


Figure 7-5 A time course effect of selective TRPV4 antagonist GSK279 on GSK101-induced cough in guinea pigs.

Guinea pigs were dosed with vehicle or GSK279 (p.o.) 2, 4, 6, 8, 12 or 24 hours prior to exposure to TRPV4 agonist GSK101 (30 µg/ml, aerosolised for 5 minutes).

Data is shown as mean inhibition ± S.E.M. \* indicates statistical significance ( $p < 0.05$ ), through using a Mann Whitney test where responses from the antagonist group were compared to the vehicle control.

To determine whether GSK279 was present in the animals systemically throughout the time course, and in enough of a concentration to inhibit GSK101-induced vagus nerve activation, plasma levels for the antagonist were measured at each time point. GSK279 plasma concentration was  $5081 \pm 547.5$  nM 2 hours after dosing, and it was still present at a concentration of  $519 \pm 278.5$  nM at 24 hours post dose (Figure 7-6). Importantly, the latter concentration was still above the  $IC_{50}$  that was generated for this compound using the isolated vagus nerve model, thereby indicating that levels of GSK279 found in the plasma were still high enough to inhibit TRPV4, and thus confirming the cough inhibition to be an on-target effect.

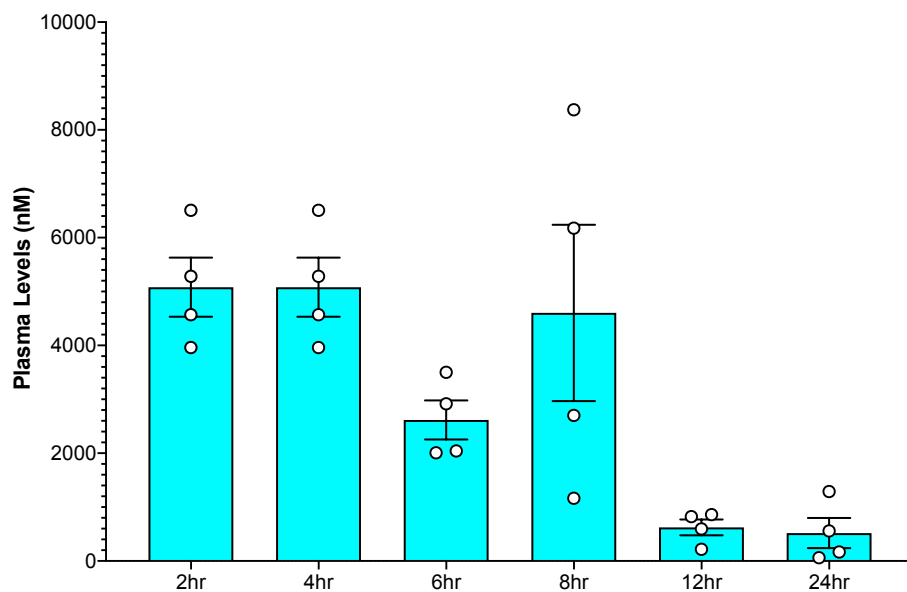


Figure 7-6 Total free plasma levels of GSK279 in guinea pigs treated with this compound in the time course study

A histogram to show the total free plasma levels of TRPV4 antagonist GSK279 in guinea pigs 2, 4, 6, 8, 12, 16, or 24 hours after p.o. dosing with this compound. NB at 24-hours post dose, compound levels were above the  $pIC_{50}$  (9.3) generated using GSK279 against GSK101-induced depolarisation in the isolated vagus nerve model. This therefore indicates that there was enough compound present systemically to inhibit TRPV4-induced activation of the vagus nerve and therefore also cough.

## 7.4 Discussion

One of the aims of this thesis is to determine if TRPV4 is involved in IPF-associated cough. To confirm this hypothesis, we aim to test a selective TRPV4 antagonist in the fibrosis-induced spontaneous cough model detailed in Chapter 3, but doing so will require an appropriate pharmacological tool that is efficacious and long lasting. We sought to characterise a new TRPV4 antagonist, GSK279 (Brooks et al., 2019), using the isolated vagus nerve model and a provoked guinea pig cough model, in the hopes that this would be a more suitable compound than the other TRPV4 antagonists that have preceded it.

GSK219 and HC-067047, the TRPV4 antagonists used by this lab prior to GSK279 (Bonvini et al., 2020, Bonvini et al., 2016), are part of a group of more historical agents that have proven useful in probing the biological effects of TRPV4 inhibition *in vivo* and *in vitro* (Lawhorn et al., 2020). Indeed, GSK219 was the first TRPV4 antagonist found to be capable of preventing and resolving pulmonary oedema in rodent heart failure models (Thorneloe et al., 2012). Despite their usefulness however, these older TRPV4 antagonists have suboptimal pharmacokinetics, are subject to selectivity concerns (e.g. P450 inhibition), and have been accompanied by negative safety findings, that have prevented them from reaching the clinic (Lawhorn et al., 2020). Further high-throughput screening performed by GlaxoSmithKline found compounds based on spirocarbamate (as opposed to GSK219's quinoline-based structure) (Cheung et al., 2017) to have a higher potency and lower lipophilicity, which eventually led to the discovery of GSK279 (Brooks et al., 2019). Subsequently, GSK279 became the first TRPV4 ion channel inhibitor to undergo phase I clinical testing, where it was found to be well tolerated in healthy volunteers and in patients with stable heart failure (Goyal et al., 2019).

Using guinea pig tissue in the *in vitro* isolated vagus nerve model, GSK279 was found to be a more potent inhibitor of TRPV4 agonist GSK101-induced depolarisation, when compared to GSK219, the previously used TRPV4 antagonist. Similarly, in the one human donor vagus nerve tested before the Covid-19 pandemic, GSK279 was also able to inhibit GSK101-induced depolarisation. Importantly, the human vagus nerve used was derived from a 65-year-old female diagnosed with COPD, thereby suggesting that this antagonist might be able to inhibit vagal nerve depolarisation in patients with respiratory disease.

The TRPV4 antagonist GSK279 was then tested *in vivo* using a provoked cough model, whereby Guinea pigs treated orally with this compound were then exposed to aerosolised TRPV4 agonist GSK101, two hours later. The relative potency of GSK279 compared to the previously used TRPV4 antagonist GSK219, was illustrated clearly by it being able to abrogate GSK101-induced cough at a

dose of 0.3 mg/kg, a feat that GSK219 failed to do significantly at a dose 1000-fold higher in this particular study.

Before being able to investigate whether GSK279 functions as an antitussive in the *in vivo* model of fibrosis-induced spontaneous cough, a time course experiment was performed to determine GSK279's duration of action. Due to the variability and sporadic nature of spontaneous cough rates in the *in vivo* model of fibrosis-induced spontaneous cough, the longer the period of time bleomycin-treated guinea pigs can be observed for coughing, the more statistically powerful any antitussive study would be. For example, watching back an uneventful recording of an animal from 10:00am to 4:00pm would be less reliable than watching that same animal from 10:00am to 10:00pm if that animal was then to go on and have two large coughing peals later at 5:00pm. A longer duration of action (*e.g.* 24 hours) would be advantageous, as it would mean the animals could be observed for longer periods without needing to be re-dosed with the antitussive compound, which could itself pose welfare issues and also impact the reliability of such a behavioural study.

Our results indicate that GSK279 maintains its ability to inhibit GSK101-induced coughing at 24 hours post dose, although GSK279 did not significantly inhibit GSK101-induced cough at all of the timepoints leading up to 24 hours. We believe this can be explained by the low power of the study ( $n=4$ ), as it is common for some vehicle-treated guinea pigs to not respond to an aerosolised tussive stimulus (Belvisi et al., 2017). Increasing  $n$  to 8 would likely have yielded significant cough inhibitions at each time point, however, doubling the animals used in the study would not be in the interests of the 3R principles for animal welfare.

Whilst the above results regarding GSK279's *in vitro* and *in vivo* antitussive potency are encouraging, one potentially worrying development relating to this compound is the recent termination of the GlaxoSmithKline-sponsored phase 2a clinical trial in patients with chronic idiopathic cough, due to a lack of efficacy (ClinicalTrials.gov, 2017). Although the results have not been published in full, the median objective cough counts (with 95% confidence interval) for a 10-hour day-time period during placebo treatment were 181 (138 to 235) compared to 241 (181 to 320) during GSK279 treatment (Ludbrook et al., 2019). Whilst these findings do make for pessimistic reading with regards to the utility of TRPV4 antagonism in the treatment of chronic cough, it should be pointed out that GlaxoSmithKline never showed target engagement with the daily dose of 2.4 mg that they were administering to the trial participants. Seeing as hypo-osmotic solutions can elicit cough through the TRPV4 channel (Bonvini et al., 2016, Fuller and Collier, 1984), a suitable way of proving target engagement could have been through conducting an inhaled cough challenge with distilled water vapour to ensure that the GSK279 dose was sufficient. A similar method was used to rule out TRPV1

involvement in chronic cough because whilst a twice daily 4mg dose of TRPV1 antagonist XEN-D0501 was proven to have a superior efficacy and potency in inhibiting a capsaicin cough challenge, it was not capable of reducing the patients' spontaneous cough frequency (Belvisi et al., 2017).

Conversely, supposing that the GSK279 was administered at a sufficient dose to inhibit the TRPV4 ion channel in this trial, it would only rule TRPV4 antagonism out as a treatment for idiopathic chronic cough, and not IPF-associated chronic cough, which could theoretically be underpinned by a different mechanism. Indeed, evidence implicating TRPV4 involvement in IPF fibrogenesis is compelling, so it is not unreasonable to posit that it could also be involved in the dry chronic cough that IPF patients frequently suffer from. A transcriptional profiling study performed by Yang et al. (2013) comparing lung tissue from IPF and UIP (usual interstitial pneumonia) patients to non-diseased controls, found that the TRPV4 transcript was within the most significantly upregulated network of genes and exhibited a 1.62-fold increase in expression. Rahaman et al. (2014) presented several intriguing findings regarding TRPV4 including: that it is expressed and functional in human lung fibroblasts, that TRPV4-deficient mice are resistant to bleomycin-induced fibrosis, that TRPV4 is required for TGF- $\beta$ 1-induced differentiation of human lung myofibroblasts, and importantly, that TRPV4-mediated  $Ca^{2+}$  influx is greater in lung fibroblasts derived from patients with IPF than when compared to normal controls. And finally, pertinent to the work performed by this lab that discovered the tussigenic TRPV4-ATP-P2X3 signalling pathway (Bonvini et al., 2016), a study by Rahman et al. (2018) found that human pulmonary fibroblasts when stimulated with the TRPV4 agonist 4 $\alpha$ PDD, began a delayed release of ATP into the extracellular space via pannexin channels. Besides TRPV4, there remain other targets we seek to pharmacologically probe in our guinea pig model of fibrosis-induced spontaneous cough *e.g.* TRPA1 (Section 8.4.2).

Whether or not TRPV4 antagonism would prove effective in alleviating IPF-associated chronic cough remains to be seen. This chapter has, however, shown GSK279 to be a potent and efficacious inhibitor of TRPV4 agonist-induced vagus nerve depolarisation and cough, with it further having a duration of action of 24 hours in the latter; all of which is in support of this chapter's hypothesis. We look forward to testing this compound in the *in vivo* model of fibrosis-induced spontaneous cough outlined in Chapter 3 of this thesis. For this future experiment, we plan to treat pulmonary fibrotic guinea pigs that spontaneously cough, with GSK279, and then immediately film them for 24 hours using the CCTV system. After these 24 hours of recording have elapsed, we then intend to confirm target engagement by immediately performing the same provoked cough challenge experiment with GSK101, as used in this chapter. Determining GSK279 to have an antitussive effect on *in vivo* spontaneous cough, would provide strong evidence that TRPV4 is a valid target to take forward into



clinical trials with IPF patients. Conversely, if TRPV4 is still being engaged after 24 hours of cough recording, but spontaneous cough rate does not decrease in GSK279-treated animals, then TRPV4 can be ruled out as a driver of cough in the model and perhaps in IPF too.

## 8 Conclusions and future work

### 8.1 Thesis Summary

IPF is a poorly understood disease characterised by a progressive build-up of scar tissue within the lung parenchyma. In Europe and North America, the disease is estimated to have an incidence range of between 3 to 9 cases per 100,000 per year (Hutchinson et al., 2015). The clinical features of IPF include a dry chronic cough, dyspnoea, digital clubbing, restrictive spirometry, and inspiratory crackles on auscultation (Raghu et al., 2018).

Cough is a common and very distressing symptom for IPF patients, with patients coughing a median of 9.4 times an hour, and therefore hundreds of times per day (Key et al., 2010). Indeed, it is often the first symptom that patients present to a clinician with before a diagnosis, and it is frequently described by patients to be one of the most troublesome aspects of the disease (Swigris et al., 2005, Vigeland et al., 2017).

The aetiology behind IPF-associated cough remains speculative at best, with several different proposed explanations. These hypotheses, that are not necessarily mutually exclusive include: common comorbidities in IPF such as GERD stimulating cough; the disease's architectural distortion of the lungs causing cough by inflicting mechanical stress on airway sensory nerves; airway nerves in the IPF lung adopting a neurophenotype with heightened cough reflex sensitivity to percussive or chemical stimuli; elevated expressions of neurotrophins within the IPF lung promoting the survival and development of airway sensory nerves which may also cause them to be more sensitive (van Manen et al., 2016).

The aims of this thesis were to investigate what the underlying mechanism behind cough in IPF could be. To facilitate this, we first sought to establish a preclinical model of spontaneous cough in guinea pigs with pulmonary fibrosis. Of all the laboratory rodents, guinea pigs are the most frequently used in provoked models of cough to investigate novel antitussives, as they have a tussive response most similar to humans (Maher and Belvisi, 2010). Measuring cough reflex sensitivity is a useful tool to assess target validation, however its reliability in predicting the effectiveness of novel antitussives has recently been called into question following the failure of some to reduce spontaneous cough frequency in chronic cough patients (Belvisi et al., 2017). In clinical trials there has been a relatively recent move towards trial design to count spontaneous coughs over a 24-hour period (objective cough counting) in order to evaluate the effect of potential therapeutics on the cough experienced by patients, rather than cough induced by a specific stimulus. This has resulted in some success, notably the emergence of the P2X3 antagonist Gefapixant, where target engagement was demonstrated against ATP-provoked cough (Morice et al., 2019), and therapeutic relevance and

efficacy were demonstrated from objective cough counts (Abdulqawi et al., 2015). Therefore, one of the aims of this thesis was to establish a more clinically translatable preclinical model of spontaneous cough (as opposed to provoked cough) to enable both identification of new disease mechanisms, and evaluation of future novel antitussives.

We began our investigation by performing a dose response in guinea pigs to an intratracheal instillation of bleomycin; animals were dosed twice with bleomycin before being culled 3 weeks later. Bleomycin is a chemotherapeutic antibiotic that, when used as a challenge agent, is the most well characterised model of pulmonary fibrosis (Peng et al., 2013). Whilst other research groups have described an increase in tussive sensitivity in bleomycin-treated guinea pigs (Fernandez-Blanco et al., 2015, Guo et al., 2019), it was not known whether these animals also cough spontaneously, similarly to IPF patients.

Our bleomycin model was initially validated using a number of assessments to ensure that the animals in our model had indeed developed pulmonary fibrosis. Animal body weights were recorded daily throughout the bleomycin dose-response study, this indicated a trend for animals that had been administered a higher bleomycin dose to exhibit slower weight gain. On visual inspection of the lungs following dissection, higher doses of bleomycin tended to cause more lobe malformation and led to the lungs becoming more rigid and paler, which could be attributed to the increased presence of scar tissue and inflammation. The weights of the animals' lungs also increased according to the dose of bleomycin the animal received, with the top two doses of bleomycin causing a significant increase in lung weight. Microscopic assessment of lung histology told a similar story, as whilst the guinea pig group treated with saline exhibited normal alveolar architecture, the distortion present in bleomycin-treated animal alveoli increased according to bleomycin dose, with the two highest doses exhibiting large fibrotic masses that took over much of the microscopic field. The fibrosis of this model was further assessed by three trained assessors (blinded to treatment) using the Ashcroft score, a blinded semi-quantitative scoring system, which also revealed a dose dependent increase in fibrosis; the two highest doses exhibited a significant increase in Ashcroft score. Two automated fibrosis scoring systems were also piloted that were developed as apps running in the Visiopharm software package: one measured the proportion of the lobe section that was occupied by fibrosis, whilst the other measured the proportion of the section that was occupied by collagen. Both apps showed a dose dependent increase in the area occupied by fibrosis or collagen, with the former app showing a steeper rise in occupied area as bleomycin dose increased and a significant increase (compared to saline-treated animals) in percentage area occupied by fibrosis at the highest dose of bleomycin. Taken together, these assessments provide a validation that the bleomycin administration did indeed induce fibrotic lung pathophysiological changes.

Having determined that fibrotic changes had occurred in the lungs of bleomycin challenged guinea pigs, we next sought to examine whether animals with bleomycin-induced fibrosis cough spontaneously. To achieve this, we began by building a CCTV system that utilised compact, night vision capable cameras, typically used in birdwatching. After confirming that this CCTV system could record capsaicin-induced coughs in sufficient quality, it was then used to film the animals in the above bleomycin dose response study. Excitingly, and in a preclinical first, spontaneous coughs in pulmonary fibrotic animals were indeed recorded using the CCTV system that had been developed. Due to the immense time it would take to watch all of the footage recorded of every animal's cage throughout the three week study, spontaneous cough assessment was originally conducted for  $n=2$  animals, and by only watching back approximately 4 hours of footage from each day. These four hours were further divided, with two hours being assessed at what equated to the animals' dawn, and the other two hours being at the animals' dusk (relative to the artificially maintained day/night cycle in the animal facility). Dawn and dusk were selected as guinea pigs are known to be most active at these times, on account of their crepuscular nature (Terril et al., 1998). After quantifying spontaneous coughs in this  $n$  of 2 pilot assessment and interpreting the preceding fibrosis data, 6 USP/kg of bleomycin was selected as a submaximal dose to take forward for cough assessment with  $n=6$  animals per saline or bleomycin treated group. In doing so, it was then revealed that bleomycin-challenged guinea pigs coughed significantly more than vehicle controls over the course of the three-week study. Next, two days with high coughing rates were selected to further quantify coughs over the course of a 24-hour period, instead of the two 2-hour periods at dawn and dusk. This further revealed that cough rates were highest between 06:00 and 09:00 at 8 days following initial bleomycin administration and between 06:00 and 12:00 at 16 days following bleomycin.

To better characterise the fibrosis and inflammation in our model, a time course study was undertaken, where endpoints were assessed at 1, 2, 3 or 4 weeks, in guinea pigs challenged with bleomycin or saline. As before, weight gain was initially stalled in bleomycin-treated animals before rising at a similar rate to the saline treated group. To check for an altered sensory nerve phenotype, vagus nerves harvested from these animals were exposed to a range of protussive stimuli using the *ex vivo* isolated vagus nerve model. Unlike in nerves derived from smoke exposed guinea pigs (or human smokers), that demonstrate an altered neurophenotype of heightened response to capsaicin but a reduced response to PGE<sub>2</sub> (Belvisi et al., 2016), nerves from animals with pulmonary fibrosis did not seem to exhibit any significant differences in their response to tussigenic stimuli. As with the prior dose response study, the lungs were assessed microscopically using the Ashcroft score and the automated methods that utilise Visiopharm software, all three methods showed that bleomycin-treated lungs were significantly more fibrotic than vehicle treated lungs across the 4-week study.

Furthermore, immunofluorescence was utilised to visualise  $\alpha$ -SMA in the histological lung slides, a protein that is commonly used as a biomarker for myofibroblasts (Nagamoto et al., 2000); nuclear DNA was also fluorescently stained with DAPI. These fluorescent immunostains revealed that, in contrast to vehicle treated animals where  $\alpha$ -SMA was expressed only in smooth muscle cells of the bronchioli and associated blood vessels, in bleomycin-treated animals,  $\alpha$ -SMA was also highly expressed in focal fibrotic parenchymal regions. When viewing these immunostains and Azan Mallory-stained lung slices together, it became abundantly clear that fibroblastic foci were being recapitulated in this model; a common criticism of bleomycin animal models is that they are not capable of this (Degryse and Lawson, 2011). Further weight was added to these observations with gene expression data generated using qRT-PCR, which revealed a significant increase in the expression of the gene for  $\alpha$ -SMA (*ACTA2*), that began two weeks after bleomycin-instillation; the expression of other fibrosis-related genes were similarly elevated. Automated and differential cell counting of leukocytes within the BALF of this animal model revealed an initial increase in inflammatory cells following i.t. administration of both saline and bleomycin. This increase in inflammatory BAL cell count fell rapidly after the first week in vehicle treated animals, however it decreased more gradually in bleomycin treated animals; these results were also confirmed visually on inspection of the lung histology.

The above results allowed us to conclude that this was a robust preclinical model of pulmonary fibrosis, which mimicked several key aspects of IPF, most importantly: spontaneous cough.

Next, BALF from this model was analysed to identify possible protussive biomarkers. For comparison, these biomarkers were also assayed in a small pool of BALF samples kindly donated by IPF patients (as part of the PROFILE study) and healthy controls, from Royal Brompton Hospital. The biomarkers selected for measurement were ATP, tryptase and 8-isoprostane; with all three having previously been found to be elevated in the IPF lung (Chow et al., 2012, Hunt et al., 1992, Kawatani et al., 2007, Montuschi et al., 1998, Müller et al., 2017, Psathakis et al., 2006, Riteau et al., 2010). Airway extracellular ATP had already been shown to have a role in cough through purinergic signalling (Abdulqawi et al., 2015, Bonvini et al., 2016), whilst the link between 8-isoprostane and tryptase with cough was more speculative. 8-isoprostane is a commonly used biomarker for oxidative stress (Catalán et al., 2018, Montuschi et al., 1998), which itself is a widely accepted and well characterised feature of the IPF lung (Kinnula et al., 2005, Kliment and Oury, 2010). As oxidants like  $H_2O_2$  have previously been shown to activate sensory neurons (Andersson et al., 2008, Sawada et al., 2008), we hypothesised that oxidants in the airways of IPF patients could be activating their airway sensory nerves too, thereby causing them to cough or contributing to their chronic cough. Tryptase was selected because of its ability to activate PAR2 (Molino et al., 1997), a G-protein coupled receptor

expressed on nociceptive neurons (Steinhoff et al., 2000, Vergnolle et al., 2001). Furthermore, there is evidence that PAR2 may be able to activate TRPV4 (Grace et al., 2014, Poole et al., 2013). TRPV4 is an ion channel that (as previously shown by this lab) when activated, can cause cough in guinea pigs through the TRPV4-ATP-P2X3 axis via the release of ATP, which activates P2X3 on airway sensory nerves (Bonvini et al., 2016).

Airway oxidative stress appeared to be elevated in guinea pigs with bleomycin-induced fibrosis, as 8-isoprostane concentrations in BALF were significantly higher in those animals than in nonfibrotic animals. In the limited number of human BALF samples obtained for this PhD project, 8-isoprostane was also significantly higher in IPF patients when compared to healthy controls. Tryptase levels in BALF, which were measured through a colourimetric assay of its enzymatic activity, were consistently and significantly higher in animals with bleomycin-induced fibrosis than in saline-treated animals. This increase, however, was not seen so clearly in IPF patient samples, as only one patient appeared to have a much higher tryptase activity in their BALF when compared to the BALF samples donated by the healthy controls. ATP, which proved more difficult to measure likely due to it being quickly catabolised by extracellular ATPases (Kaczmarek et al., 1996, Picher et al., 2003), appeared to be elevated in bleomycin-treated animals ( $p=0.0628$ ), but only at one week post instillation; this was however consistent with the clinical BALF samples where no significant increase in ATP was observed in IPF patient when compared to healthy control BALF samples. It is important to note that  $n$  numbers were low for these IPF patient BAL sample assays, and unbiased bioinformatic analysis with larger patient populations, will be required to understand any associations between these biomarkers and IPF disease pathophysiology or symptoms like cough (Section 8.4.5).

Next, we began to investigate a role for possible tussigenic targets that related to these biomarkers in airway sensory nerves. Seeing as though biomarkers for oxidative stress are increased in the IPF lung and also within the lungs of guinea pigs from this thesis' fibrosis-induced spontaneous cough model, we investigated whether oxidants such as  $H_2O_2$  could activate airway sensory nerves. Further to this, we wanted to investigate whether any such activation was mediated through the TRPA1 ion channel. TRPA1 is activated by  $H_2O_2$  in other sensory neurons (Sawada et al., 2008, Andersson et al., 2008), and is also widely considered to be a protussive receptor in guinea pigs and humans, since it has been shown to evoke cough by activation with acrolein and cinemaldehyde (Andre et al., 2009, Birrell et al., 2009).

Vagal ganglionic neurons (*i.e.* jugular and nodose neurons) were isolated from guinea pigs that, two weeks prior, had been intranasally dosed with the retrograde tracer dye Dil (Dubuis et al., 2013). Once plated onto a FluoroDish™, airway terminating neurons were selected for imaging if they

exhibited Dil staining. A dose response to the oxidant H<sub>2</sub>O<sub>2</sub> was conducted on these neurons to first confirm that it was indeed capable of causing intracellular oxidative stress in airway terminating neurons, with oxidative stress being visualised using DHE, a superoxide-sensitive fluorescent dye (Bindokas et al., 1996). Following this confirmation, airway terminating vagal ganglionic neurons from guinea pigs were again exposed to H<sub>2</sub>O<sub>2</sub>, however this time their intracellular calcium concentrations were monitored using Fura2-AM, the ratiometric calcium sensitive dye (Roe et al., 1990). This experiment established that the concentration of H<sub>2</sub>O<sub>2</sub> that caused the highest increase in oxidative stress, also led to a significant increase in intracellular calcium concentration within these neurons. As increases in intracellular calcium within neurons are indicative of activation, these results thereby suggest that oxidizing agents may have a protussive effect.

To further characterise H<sub>2</sub>O<sub>2</sub> as a protussive agent, a concentration response was conducted in the *in vitro* isolated vagus nerve model, using guinea pig tissue. A submaximal dose of this oxidant capable of causing significant depolarisation compared to vehicle was then taken forward for antagonist studies. Next, using guinea pig tissue, this H<sub>2</sub>O<sub>2</sub>-induced vagus nerve depolarisation was shown to be significantly inhibited by the antioxidant NAC, and more importantly, by the TRPA1 antagonist Janssen 130 also, thereby implicating that calcium channel in the response. Moreover, these results also appeared to be replicated in human donor vagus nerves, although only *n* of 2. Together, these results suggest that oxidative stress can cause activation of airway sensory nerves, which is likely mediated by TRPA1. When considering the above results and the unusually high levels of oxidative stress in the IPF lung, TRPA1 would appear to an antitussive target in IPF patients worthy of future investigation.

In the next chapter of this thesis, we sought to investigate a role for PAR2 in airway sensory nerves. We began by performing concentration responses to a range of different PAR2 stimuli: one of which was trypsin, an endogenous enzyme that activates PAR2 through proteolytically cleaving the receptor's n-terminus to reveal PAR2's hidden tethered ligand (Nystedt et al., 1994); two were small peptides that mimic said tethered ligand, SLIGKV and 2-furoyl-LIGRLO (McGuire et al., 2004); and lastly, the final ligand was AC-55541, a nonpeptidic small molecule agonist of PAR2 (Seitzberg et al., 2008). Using the isolated vagus nerve model, it was shown that all four of these PAR2 agonists caused a concentration dependent depolarisation of guinea pig vagus nerves. Following this, vagus nerves were obtained from mice that were deficient for the PAR2 gene (*F2LR1*). Whilst most in the respiratory field are unconvinced that mice can cough (Mackenzie et al., 2004), their afferent arm for this reflex appears to be fully functioning (Maher and Belvisi, 2010), thereby making experiments with vagus nerve tissue derived from genetically edited mice, a viable strategy for confirming receptors activated by ligands. Using these nerves, it was shown that the PAR2 agonists SLIGKV,

AC55541 and 2-Furoyl-LIGRLO were specific, as vagus nerve depolarisation to these agonists in F2LR1<sup>-/-</sup> mice was virtually abolished. However, depolarisation responses to TRPV4, TRPA1 or TRPV1 agonists were not significantly altered in F2LR1<sup>-/-</sup> mice. To further confirm the specificity of these PAR2 ligands, we tested the effect of a selective PAR2 antagonist on PAR2-mediated vagus nerve depolarisation in both human and guinea pig tissue. P2Pal-18s, a cell-penetrating lipopeptide “pepducin” antagonist of PAR2, significantly inhibited 2-Furoyl-LIGRLO-induced vagus nerve depolarisation in guinea pigs. As a negative control, a lipopeptide with a scrambled version of P2Pal-18s’ residue sequence was also tested and found to be no more effective at inhibiting PAR2-induced responses than vehicle. In the final set of human donor lungs received before the pandemic struck, P2Pal-18s appeared to be capable of inhibiting a 2-Furoyl-LIGRLO-induced vagus nerve response.

To further characterise PAR2 agonist-induced airway nerve responses, the *ex vivo* eTRec system was deployed. This is a more airway relevant way of assessing the afferent arm of the cough reflex than the isolated vagus nerve method, because it enables one to measure recurrent laryngeal nerve (RLN) firing that comes as a result of tussigenic stimuli activating airway sensory nerve termini, connected to the RLN branch of the vagus nerve. Using this method, it appeared that the PAR2 agonist 2-Furoyl-LIGLRO was capable of increasing the nerve firing rate when compared to baseline; this result was more than vehicle, which did not increase RLN firing rate, but still less than capsaicin, which did ( $n=2$ ). Following this, the guinea pig *in vivo* single fibre model was also deployed, to further characterise the mechanics of PAR2 mediated airway sensory nerve activation (Adcock et al., 2014). After having identified an airway terminating A $\delta$ -fibre by confirming its pattern of spontaneous activity, response to hyperinflation and deflation, and its response to citric acid aerosol, a concentration response was then performed to intratracheally aerosolised 2-Furoyl-LIGLRO. At the two highest concentrations (100nM and 1 $\mu$ M), 2-Furoyl-LIGLRO increased the firing rate of the A $\delta$ -fibre that was tested.

To conclude Chapter 6, 2-Furoyl-LIGLRO-induced vagus nerve depolarisation was again measured, this time with the addition of pharmacological antagonists for P2X3 and TRPV4, in order to determine whether the TRPV4-ATP-P2X3 axis might be involved in PAR2-mediated airway nerve activation. Both antagonists that were tested significantly reduced 2-Furoyl-LIGLRO-induced vagus nerve depolarisation by approximately 40% in guinea pigs, suggesting that the TRPV4-ATP-P2X3 axis may at least partly be involved in PAR2-induced airway nerve responses. When taking into consideration the reportedly high levels of endogenous PAR2 agonists (*e.g.* tryptase) in some IPF patients’ lungs (Kawatani et al., 2007, Compton et al., 2001), the above results provide a possible explanation for how such mediators may contribute to the disease’s chronic cough symptom.



With our end goal being to eventually test novel antitussives in this thesis' *in vivo* model of fibrosis-induced spontaneous cough, the final chapter of this thesis aimed to characterise one such compound in preparation for this. GSK2798745 (GSK279) is a recently developed TRPV4 antagonist, that is reported to have a higher potency than any of those that have preceded it (Brooks et al., 2019). We began by once again returning to the *in vitro* isolated vagus nerve model, where it was shown that GSK279 was capable of significantly inhibiting TRPV4 agonist GSK1016790A (GSK101)-induced vagus nerve depolarisation in guinea pigs; this compound appeared to be 1000-fold more potent than the previously used TRPV4 antagonist, GSK2193874 (GSK219). In the one human vagus nerve tested, GSK279 also appeared to be capable of inhibiting the TRPV4-induced response.

To determine if GSK279's TRPV4 blocking capacity was as effective *in vivo*, it was then deployed in a TRPV4 agonist-evoked cough model. A dose response to GSK279 was performed by exposing naïve guinea pigs to nebulised TRPV4 agonist GSK101. At 0.1 mg/kg, GSK279 was capable of significantly inhibiting GSK101-induced cough; and at higher doses (0.3 and 1 mg/kg) this cough was abolished.

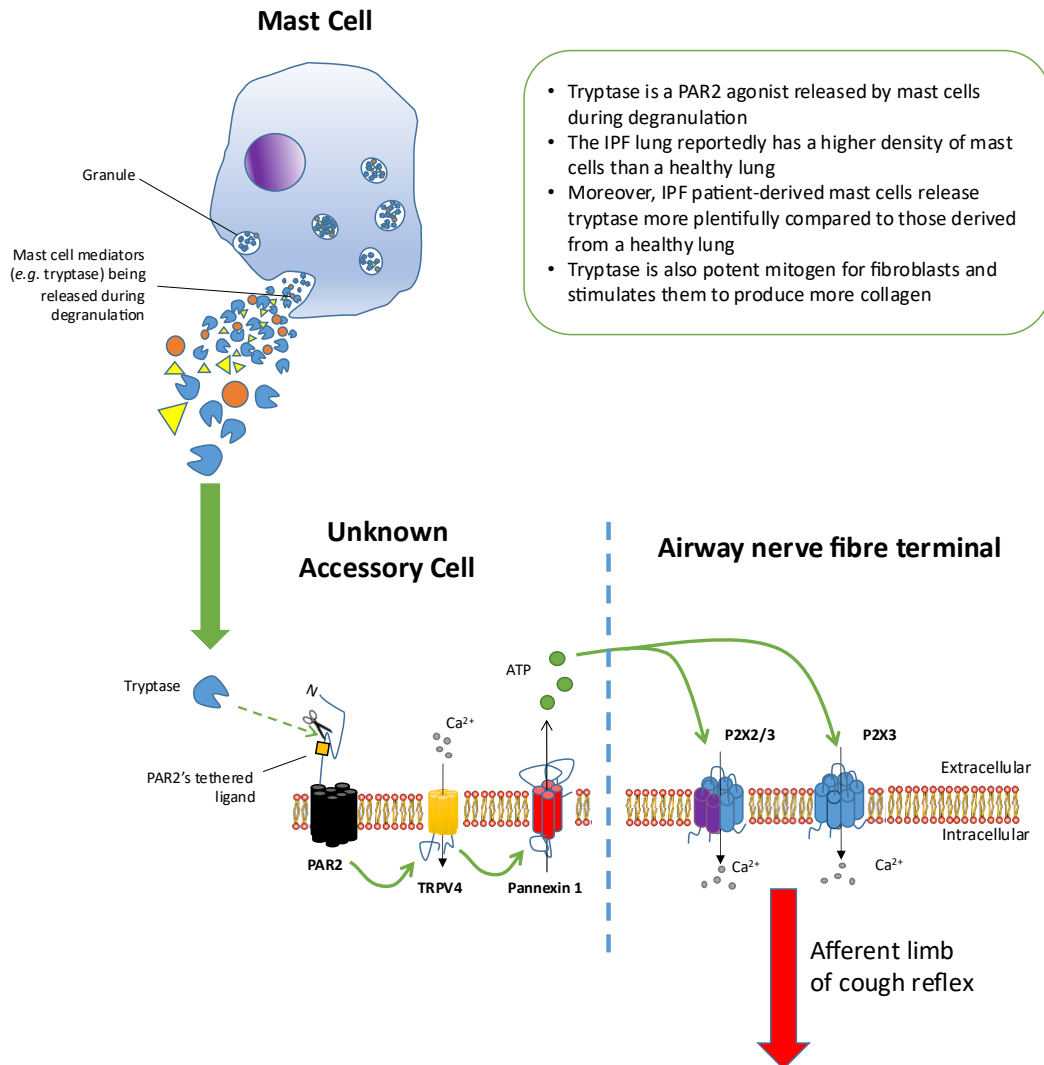
Finally, prior to administering GSK279 in this thesis' *in vivo* model of fibrosis-induced spontaneous cough, we sought to determine the compound's duration of action; knowing how long GSK279 engages the TRPV4 ion channel in guinea pigs would allow us to determine how often it would need to be administered to prevent fibrosis-induced coughing over a 24-hour recording period. In this final experiment, a time course cough study was executed whereby guinea pigs were incubated with GSK279 for 2, 4, 6, 8, 12 or 24 hours, prior to being challenged with GSK101. Variability in cough counts was high, likely due to the small *n* number, however GSK101-induced cough appeared to be reduced 4, 6, and 12 hours after GSK279 administration ( $p=0.1429$ ,  $0.1429$  and  $0.0571$ , respectively), and was significantly inhibited 2, 8 and 24 hours after GSK279 administration. Systemic free plasma levels of GSK279 were also tested at each of these timepoints, and it was shown that GSK279 was present at a concentration above the  $IC_{50}$  generated in vagus nerve experiments with GSK101, throughout the 24-hour study. Having now characterised GSK279 antitussive action in GSK101-induced cough, the compound will be taken forward to the *in vivo* model of fibrosis-induced spontaneous cough. Determining GSK279 to have an antitussive effect in this thesis' novel model would provide strong evidence that TRPV4 is a valid target to take forward into clinical trials with IPF patients.

To conclude, this thesis has presented evidence for the novel finding that guinea pigs with bleomycin-induced fibrosis spontaneously cough. Moreover, this finding was accompanied by a wealth of data that characterised the fibrosis and inflammation within this newly presented model of fibrosis-induced spontaneous cough; such a model will no doubt be a useful tool in the future

search for novel antitussives. Next in this thesis, prospective and previously identified, endogenous tussive stimuli were measured in this thesis' model and in samples donated by IPF patients and healthy controls. Subsequently, a role for protussive receptors (relating to the above stimuli) in airway sensory nerve activation was investigated, using a variety of *in vitro*, *ex vivo* and *in vivo* methods. Together, this revealed evidence for the possible involvement of oxidative stress and the TRPV4-ATP-P2X3 axis in IPF-associated cough; with the latter mechanism possibly being instigated by PAR2 activation. Finally, this thesis has produced data to show that GSK279 is a highly potent inhibitor of TRPV4-agonist induced coughing, which, if shown to be capable of inhibiting fibrosis-induced spontaneous cough in guinea pigs, will be a target worth taking forward to clinical trials with IPF patients.

Schematics for the proposed involvement of oxidative stress and a PAR2-TRPV4-ATP-P2X3 axis in IPF-associated cough, can be found in Figure 8-1 and Figure 8-2. Both proposed mechanisms are, however, subject to the caveat that there remain limitations to the methods used in this thesis, and further, that additional work will be required to prove or disprove these hypotheses; this is elaborated on in the next sections.

## Proposed Mechanism 1



- Tryptase is a PAR2 agonist released by mast cells during degranulation
- The IPF lung reportedly has a higher density of mast cells than a healthy lung
- Moreover, IPF patient-derived mast cells release tryptase more plentifully compared to those derived from a healthy lung
- Tryptase is also potent mitogen for fibroblasts and stimulates them to produce more collagen

Figure 8-1 This thesis' first proposed mechanism for IPF-associated cough

- 1) Mast cells, which are more present and active within the IPF lung (Hunt et al., 1992), degranulate and release mediators e.g. tryptase (a PAR2 agonist)
- 2) Tryptase proteolytically cleaves the N-terminus of PAR2 present on the surface of an as yet unknown cell, thereby revealing the PAR2 receptor's tethered ligand, which subsequently activates the receptor
- 3) Through a yet to be defined signalling mechanism, the activated PAR2 receptor causes the TRPV4 channel to open, thereby facilitating the influx of calcium ions into the accessory cell
- 4) Through another intracellular signalling mechanism, the TRPV4-mediated influx of calcium causes pannexin 1 pores to open, thereby releasing ATP into the extracellular space
- 5) The extracellular ATP in the airways activates P2X3 and P2X2/3 receptors that are present on the termini of airway nerve fibres. This causes an influx of calcium through the P2X channels' pores and into the nerve ending, which depolarises it. If the magnitude of this depolarisation exceeds the threshold potential, an action potential will be formed, and the nerve impulse will be carried up towards the brain stem along the vagus nerve, thereby forming the afferent limb of the cough reflex

## Proposed Mechanism 2

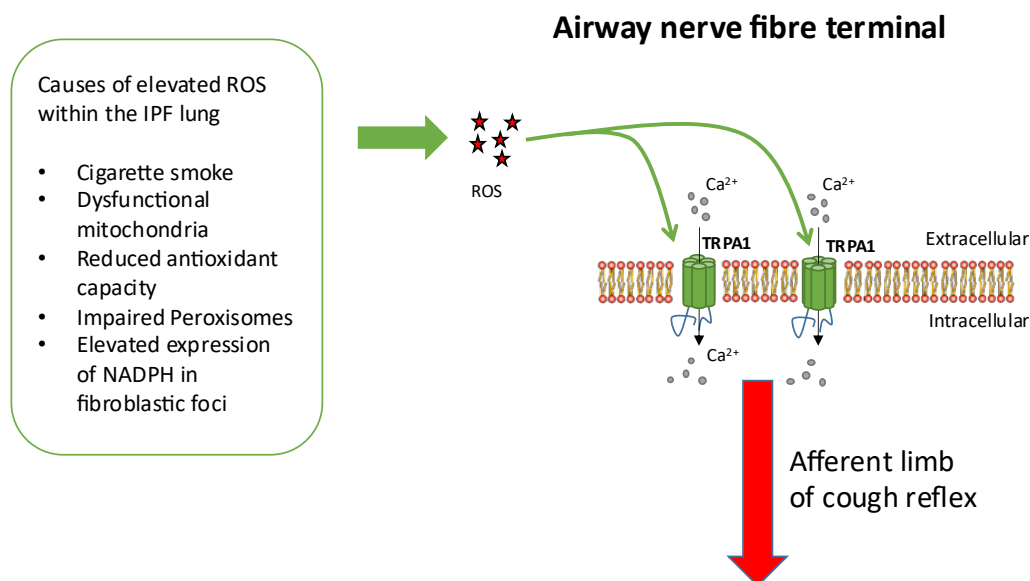


Figure 8-2 The second proposed mechanism for IPF-associated cough

Reactive oxygen species (ROS), such as  $H_2O_2$ , are more present in the airways of IPF patients than in healthy individuals (Montuschi et al., 1998); possible reasons for this include cigarette smoke exposure, and mitochondrial or peroxisomal dysfunction (Baumgartner et al., 1997, Oruqaj et al., 2015, Zank et al., 2018). These ROS cause the activation of TRPA1 channels that are present on airway C-fibre termini (Robinson et al., 2018). The activated TRPA1 channels are gated open which leads to an influx of calcium ions that depolarises the nerve termini. If this depolarisation exceeds the threshold potential, an action potential will be formed, and the nerve impulse will be carried up towards the brain stem along the vagus nerve, thereby forming the afferent limb of the cough reflex.

## 8.2 Limitations of thesis

There remain a number of limitations to the models and techniques used in this thesis. With regards to the *in vivo* model of fibrosis-induced cough, bleomycin and indeed other animal models of IPF are often criticised for their inability to mimic the progressive scarring nature of the disease. To mimic this somewhat, a two-dose regimen of bleomycin was used, but this is still unrepresentative of the onslaught of repetitive microinjuries that are said to instigate the clinical disease (Degryse et al., 2010, Baily et al., 2019). Similarly, due to IPF being a disease of the aging lung, some research groups have begun to use aged mice or mice with accelerated senescence to recapitulate this phenotype (Huang et al., 2015, Xu et al., 2009). Due to guinea pigs being the smallest rodents capable of the cough reflex (Maher et al., 2009), using such mice would not have been an option for developing this model, furthermore, senescence accelerated guinea pigs (to our knowledge) do not exist, and aged guinea pigs were not available from our supplier. Another limitation of our model could be that spontaneous cough quantification did not occur in a blinded fashion, unlike the phenotypic scoring used to assess fibrosis. This was originally so that animals could be more easily recognised during the

dose response study through the CCTV system. Since a tolerable submaximal dose of bleomycin has been found, new experiments undertaken in this model will utilise blinded spontaneous cough assessment.

Another limitation of this thesis is that biomarker analysis of IPF patient or healthy volunteer BAL was limited in sample size, further patient samples from additional patients and volunteers will be required to confirm findings. ATP is especially difficult to assay due to it being quickly broken down by extracellular ATPases, therefore it would be prudent to investigate other methods of quantifying it besides the luciferase assay used in this thesis (*e.g.* by using mass-spectrometry to identify ATP and its breakdown products). We also recognise the benefit correlating the levels of these BAL biomarkers with physiological parameters, as this may yield significant observations that have not yet been seen; this is something we are currently attempting to do (see Section 8.4.5).

As has already been described, there are limitations to some of the *in vitro* methods used in this thesis. The isolated vagus nerve technique for instance, whilst being relatively high throughput, measures the depolarisation of the entire nerve trunk, not just the fibres within it that innervate the airways. Additionally, the method only measures the response of receptors that are expressed along the vagus nerve trunk, and not the receptors at the nerve termini. Both of these disadvantages can be overcome through the use of more complicated and laborious techniques, such as eTRec and the *in vivo* single fibre model, although we have not yet attempted to replicate the antagonist studies that were conducted in the vagus nerve model using these more airway specific electrophysiology methods. Another issue is that the receptors present on guinea pig or mouse airway nerves could be different to those of humans. To overcome this, key experiments were also completed using vagus nerves from human donors too, but additional repeats of key experiments will be required to generate statistically meaningful results; human tissue is difficult to acquire and this has only been made worse by the global pandemic. Finally, whilst it is possible to image changes in intracellular calcium in airway terminating neurons due to them being stained with DiI, a stimulus causing a significant increase in intracellular calcium does not necessarily mean the same stimulus would cause a nerve impulse (and cough) if it made contact with airway nerve termini.

### 8.3 Thesis hypotheses

Providing that one is satisfied by the premisses that, firstly, Chapter 3's guinea pig bleomycin model recapitulates IPF, and secondly, that these animals do indeed cough spontaneously, then one can begin to judge whether or not the findings in this thesis support its main hypotheses (see Section 1.6), which were:

## Spontaneous cough in a guinea pig model of IPF is caused by:

### 1) Oxidative stress which activates airway sensory nerves via the TRPA1 channel

and/or

### 2) PAR2-induced activation of the TRPV4-ATP-P2X3 axis

Naturally, to ultimately prove whether either one of the above hypotheses are true, it would be required that this thesis show that antioxidants and pharmacological antagonists for TRPA1; or pharmacological antagonists for PAR2, TRPV4 or P2X3; respectively; could inhibit the spontaneous cough of guinea pigs with bleomycin-induced lung fibrosis. Unfortunately, however, due to the disruption caused by the coronavirus pandemic, it was not possible to conduct and fully analyse *in vivo* studies that used such tools.

Whilst not confirming this thesis' hypotheses per se, this thesis' findings that oxidative stress, the PAR2 agonist tryptase, and ATP, all appear elevated in the BALF of bleomycin-treated guinea pigs that spontaneously cough, does give support to our hypotheses. Giving further support to them, are the findings that both oxidative stress (via TRPA1) and PAR2 (via the TRPV4-ATP-P2X3) axis, can cause airway sensory nerve activation in guinea pigs and humans. To determine if the main hypotheses are correct will require future work (see next section), but importantly, the results thus far have not disproven them.

## 8.4 Future work

### 8.4.1 Increasing replicates, using more airway relevant techniques and power analyses

Firstly, it will be required that we increase the number of replicates for *in vitro* studies with human tissue, and repeat antagonist experiments performed in the vagus nerve model in more airway relevant models (*e.g.* eTRec and *in vivo* single fibre).

By assessing the current *n* numbers and variance from the studies described in this thesis and inputting the data into G\*Power (Düsseldorf, Germany), a software package capable of computing statistical power analyses, we will ensure that future *in vitro* and *in vivo* experiments have enough replicates to yield statistically significant results.

### 8.4.2 Test novel antitussives in the *in vivo* model of fibrosis-induced spontaneous cough

This thesis has described a new technique that uses bleomycin-treated guinea pigs to model IPF-associated chronic cough (Chapter 3). We look forward to conducting future studies with this model to probe the tussigenic targets proposed in this thesis (*e.g.* TRPA1, PAR2, *etc*), or indeed other novel targets proposed elsewhere.

Currently underway, is an investigation into the effect of TRPV4 antagonist GSK279, on spontaneous cough frequency, in bleomycin-treated guinea pigs. This study required that bleomycin treated guinea pigs (used at a time point where fibrotic lesions had been established) be orally dosed with either vehicle or GSK279, before being returned to their cages for 24-hour CCTV cough monitoring. Once these 24 hours had elapsed, the animals underwent a provoked cough challenge with aerosolised TRPV4 agonist GSK101 (much like the experiments in Section 7.2.2), to confirm target engagement. Preliminary results so far appear promising, with GSK279 causing a significant reduction in TRPV4 agonist-induced cough, 24 hours post dose, in both animals with and without pulmonary fibrosis (Figure 8-3). Although not significant, there was a trend for vehicle-treated animals with fibrosis to cough more in response to aerosolised GSK101 than vehicle-treated animals without fibrosis, suggesting the former may have an enhanced cough reflex to this stimulus. The spontaneous cough footage generated by this study is still being analysed, but we await the results with eager anticipation.

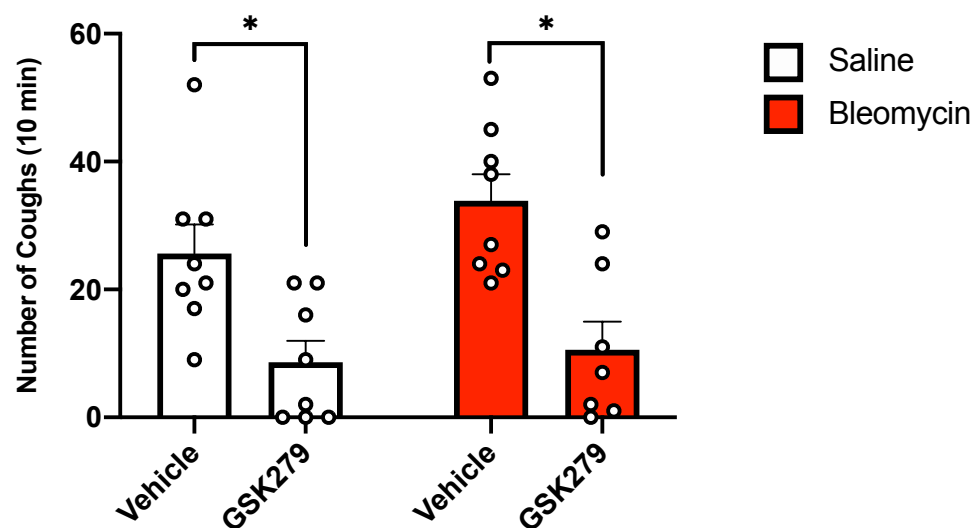


Figure 8-3 The effect of TRPV4 antagonist GSK279 on GSK101-induced cough in bleomycin-treated guinea pigs

We are currently analysing data from a study that sought to investigate whether TRPV4 antagonist GSK279 inhibits spontaneous cough in animals with bleomycin-induced pulmonary fibrosis. Animals were intratracheally instilled with either bleomycin (3 USP/kg) or saline, twice, 3 days apart. 16 days after the first instillation, guinea pigs were orally dosed with either vehicle or TRPV4 antagonist GSK279 (1 mg/kg). The animals were then returned to their cages where they were recorded using a CCTV system for 24-hours to monitor spontaneous cough frequency (data not yet available). To confirm target engagement of GSK279, once the 24 hours had elapsed, guinea pigs were challenged with TRPV4 agonist GSK101 (30 µg/ml, aerosolised for 5 minutes).

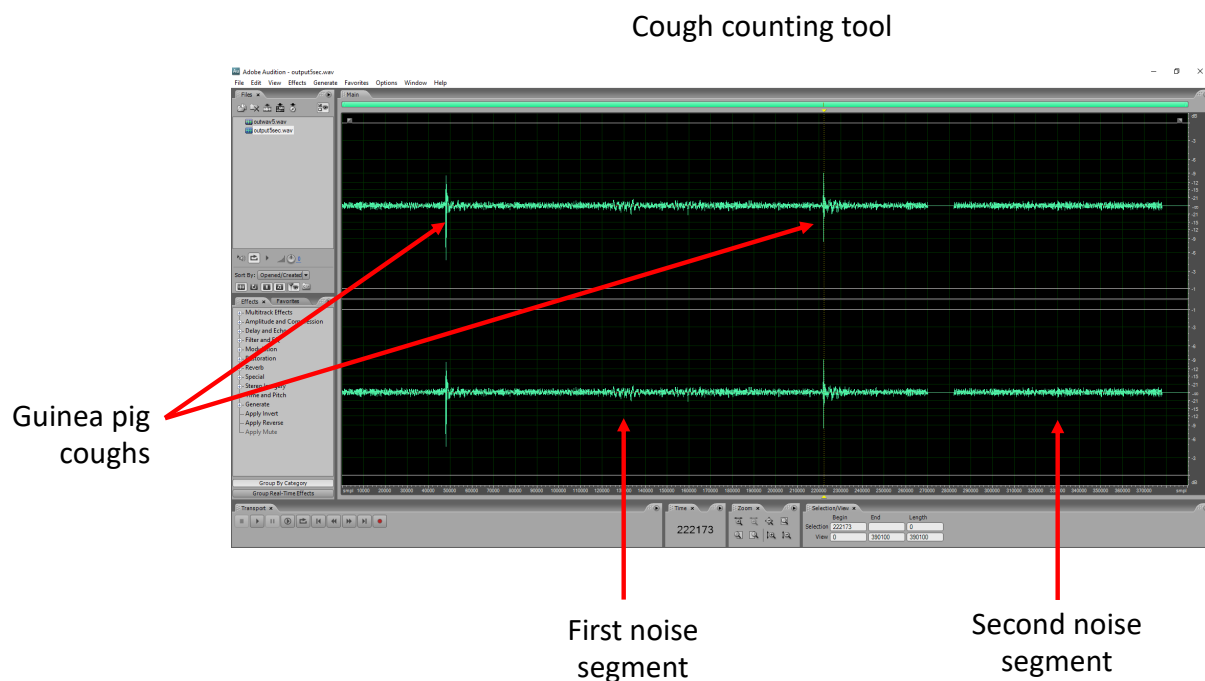
Data is shown as mean inhibition ± S.E.M. \* indicates statistical significance ( $p < 0.05$ ), through using a Mann Whitney test where responses from the antagonist group were compared to their relevant vehicle control.

#### 8.4.3 Optimise data acquisition in the *in vivo* model of fibrosis-induced spontaneous cough

Presently, cough frequency data in the *in vivo* model of fibrosis-induced spontaneous cough is acquired by manually watching CCTV footage of the animals in their cages. As we are aiming to

assess 24 hour recordings to be in keeping with clinical ambulatory cough monitoring (Sunger et al., 2013), we are actively seeking out methods that will make this a less laborious process.

One method to reduce the operator input, that we are currently pursuing with our collaborators at the University of Manchester, is to reengineer the algorithm used to truncate VitaloJAK™ recordings of human subjects (Barton et al., 2012). By eliminating periods of relative silence from each cage's recording, it is hoped that a 24-hour recording would instead be compressed to approximately two hours, thereby dramatically reducing operator input.



*Figure 8-4 Reengineering the VitaloJAK™ algorithm to optimise spontaneous cough quantification in guinea pigs*

*Shown above is a screenshot of a sound file's stereo waveform within the audio processing software Adobe Audition. The sound file has been ripped from video taken of a guinea pig's cage, that was recorded during the development of the in vivo model of fibrosis-induced spontaneous cough (Chapter 3). The file has been truncated using VitaloJAK™ software, to eliminate periods of relatively low noise, much like how a 24-hour sound recording of an individual wearing a VitaloJAK™ cough monitor would be processed. Highlighted are 2 segments of audio, with relatively higher noise, that were recognised by the algorithm, and cut out of the original recording; only the first segment actually contains coughs.*

We further hope that if enough video and audio of spontaneous cough is compiled from this model, then it will soon be possible to utilise machine learning to quantify coughs with virtually no operator input at all. Indeed, due to the ubiquity of smart devices in one's home, interest in applying neural networks to the detection of cough and diagnosis of respiratory disease has grown dramatically over recent years, not only from academic research groups (Kvapilova et al., 2019), but also the technology industry (Bridge, 2018); unsurprisingly the rate of research in this field has only accelerated under the Covid-19 pandemic (Brown et al., 2020, Whitehill et al., 2020).



#### 8.4.4 Determine if aerosolised PAR2 agonists cause C-fibre activation, or elicit cough in guinea pigs or exaggerate the cough response

Having determined that PAR2 agonists are capable of causing airway A $\delta$ -fibre activation in guinea pigs using the *in vivo* single fibre model in Chapter 6, we further aim to determine whether they might also be able to activate airway C-fibres too.

As previously discussed, research conducted by Gatti et al. (2006) found that PAR2 agonists were not capable of eliciting cough in guinea pigs *per se*. The authors instead provided evidence that PAR2 stimulation of airway sensory nerves exaggerated the TRPV1-mediated cough response, through a mechanism involving Protein Kinase A, C and the release of prostanoids. Both of these are findings that we would like to verify, not just in naïve guinea pigs, but in bleomycin-treated animals too. We feel further investigation is warranted because this thesis has shown that exogenous PAR2 agonists are capable of causing airway sensory nerve impulses (Chapter 6), whilst endogenous PAR2 agonists are elevated in the lungs of guinea pigs from our *in vivo* model of fibrosis-induced chronic cough and in the lungs of some IPF patients too (Chapter 4).

#### 8.4.5 Correlation of BAL biomarkers

As has been previously mentioned in the discussion section of Chapter 4, one of our intentions for this PhD had been to correlate the biomarkers measured in patient BAL (8-isoprostane, eATP and tryptase levels) with outcome measures from the PROFILE study (*e.g.* lung function parameters, cough-related quality of life questionnaire scores, and objective cough measurements), in a larger set of IPF patient samples. Unfortunately, there were delays to our procurement of this wider sample set and our access to this patient data, due to the onset of the COVID-19 pandemic. Nonetheless, work towards this objective is ongoing and we hope it generates new insights into how these BAL biomarkers relate to IPF disease progression, subjective cough severity, and objective cough frequency.

## 8.5 Concluding remarks

IPF is a devastating and invariably fatal disease, compounded by exasperating symptoms, one of which is very often a chronic, non-productive cough (Key et al., 2010, Swigris et al., 2005). As there are currently no approved antitussive therapies for IPF associated cough, nor chronic idiopathic cough in general, there is a clear and present need for effective therapies for these patients. Preclinical and clinical modelling of cough thus far has focussed on finding therapies that modulate cough reflex sensitivity to inhaled stimuli, however recent studies have called into question the effectiveness of this approach (Belvisi et al., 2017). It was therefore hoped that a preclinical model of spontaneous cough might be a more reliable platform to evaluate novel antitussives.

The work carried out in this thesis has shown that, in a preclinical first, guinea pigs with bleomycin-induced pulmonary fibrosis cough spontaneously. This novel finding was made by constructing a first-of-its-kind CCTV system capable of not only recording footage of the animals in light and darkness, but also of capturing high fidelity audio from within the animals' cages themselves; this was then followed by painstakingly reviewing hundreds of hours of CCTV footage.

This *in vivo* model of fibrosis-induced spontaneous cough was further validated and characterised through gene expression analysis, histological scoring, measuring animal whole body and organ weights, immunohistochemical staining, leukocyte quantification in BALF and further BALF biomarker analysis.

As a result of data generated using a variety of *in vitro*, *ex vivo*, and *in vivo* techniques, we have also been able to propose two new possible mechanisms for the aetiology of IPF-associated chronic cough, these are: oxidative stress-induced activation of the TRPA1 channel, and a PAR2-TRPV4-ATP-P2X3 axis. Whether these two mechanisms are involved in IPF associated cough remains to be seen, but by developing the model outlined in Chapter 3, this thesis has provided a means to help solve this question.

Finally, we characterised the antitussive efficacy of GSK279 in guinea pigs, a highly potent TRPV4 antagonist with a duration of action in excess of 24-hours. We eagerly await the testing of this compound and other novel antitussives in our *in vivo* model of fibrosis-induced spontaneous cough, and hope that one day the work in this thesis will help in identifying an effective treatment for chronic cough in IPF patients.

## 9 Bibliography

- ABDULQAWI, R., DOCKRY, R., HOLT, K., LAYTON, G., MCCARTHY, B. G., FORD, A. P. & SMITH, J. A. 2015. P2X3 receptor antagonist (AF-219) in refractory chronic cough: a randomised, double-blind, placebo-controlled phase 2 study. *Lancet*, 385, 1198-205.
- ADAMSON, I. Y. & BOWDEN, D. H. 1974. The pathogenesis of bleomycin-induced pulmonary fibrosis in mice. *Am J Pathol*, 77, 185-97.
- ADCOCK, J. J., BIRRELL, M. A., MAHER, S. A., BONVINI, S. J., DUBUIS, E., WORTLEY, M. A., BAKER, K. E. & BELVISI, M. G. 2014. Making Sense Of Sensory Nerves: An In Vivo Characterisation Of A $\delta$ -And C-Fibres Innervating Guinea-Pig Airways. C19. *NEW SENSATIONS IN THE LUNG: THE GOOD, THE BAD, AND THE NERVE*.
- ADCOCK, J. J., DOUGLAS, G. J., GARABETTE, M., GASCOIGNE, M., BEATCH, G., WALKER, M. & PAGE, C. P. 2003. RSD931, a novel anti-tussive agent acting on airway sensory nerves. *Br J Pharmacol*, 138, 407-16.
- AL-ANI, B., WIJESURIYA, S. J. & HOLLENBERG, M. D. 2002. Proteinase-activated receptor 2: differential activation of the receptor by tethered ligand and soluble peptide analogs. *J Pharmacol Exp Ther*, 302, 1046-54.
- ALDER, J. K., CHEN, J. J., LANCASTER, L., DANOFF, S., SU, S. C., COGAN, J. D., VULTO, I., XIE, M., QI, X., TUDER, R. M., PHILLIPS, J. A., 3RD, LANSDORP, P. M., LOYD, J. E. & ARMANIOS, M. Y. 2008. Short telomeres are a risk factor for idiopathic pulmonary fibrosis. *Proc Natl Acad Sci U S A*, 105, 13051-6.
- ALLAWZI, A., ELAJAILI, H., REDENTE, E. F. & NOZIK-GRAYCK, E. 2019. Oxidative Toxicology of Bleomycin: Role of the Extracellular Redox Environment. *Curr Opin Toxicol*, 13, 68-73.
- ALLEN, R. J., PORTE, J., BRAYBROOKE, R., FLORES, C., FINGERLIN, T. E., OLDHAM, J. M., GUILLEN-GUIO, B., MA, S.-F., OKAMOTO, T., JOHN, A. E., OBEIDAT, M. E., YANG, I. V., HENRY, A., HUBBARD, R. B., NAVARATNAM, V., SAINI, G., THOMPSON, N., BOOTH, H. L., HART, S. P., HILL, M. R., HIRANI, N., MAHER, T. M., MCANULTY, R. J., MILLAR, A. B., MOLYNEAUX, P. L., PARFREY, H., RASSL, D. M., WHYTE, M. K. B., FAHY, W. A., MARSHALL, R. P., OBALLA, E., BOSSÉ, Y., NICKLE, D. C., SIN, D. D., TIMENS, W., SHRINE, N., SAYERS, I., HALL, I. P., NOTH, I., SCHWARTZ, D. A., TOBIN, M. D., WAIN, L. V. & JENKINS, R. G. 2017. Genetic variants associated with susceptibility to idiopathic pulmonary fibrosis in people of European ancestry: a genome-wide association study. *The Lancet. Respiratory medicine*, 5, 869-880.
- AMARA, N., GOVEN, D., PROST, F., MULOWAY, R., CRESTANI, B. & BOCZKOWSKI, J. 2010. NOX4/NADPH oxidase expression is increased in pulmonary fibroblasts from patients with idiopathic pulmonary fibrosis and mediates TGFbeta1-induced fibroblast differentiation into myofibroblasts. *Thorax*, 65, 733-8.
- ANDERSON, D. & MACNEE, W. 2009. Targeted treatment in COPD: a multi-system approach for a multi-system disease. *Int J Chron Obstruct Pulmon Dis*, 4, 321-35.
- ANDERSSON, D. A., GENTRY, C., MOSS, S. & BEVAN, S. 2008. Transient receptor potential A1 is a sensory receptor for multiple products of oxidative stress. *J Neurosci*, 28, 2485-94.
- ANDO, A., FARRELL, M. J. & MAZZONE, S. B. 2014. Cough-related neural processing in the brain: a roadmap for cough dysfunction? *Neurosci Biobehav Rev*, 47, 457-68.
- ANDRE, E., GATTI, R., TREVISANI, M., PRETI, D., BARALDI, P. G., PATACCHINI, R. & GEPPETTI, P. 2009. Transient receptor potential ankyrin receptor 1 is a novel target for pro-tussive agents. *Br J Pharmacol*, 158, 1621-8.
- ANTONIADES, H. N., BRAVO, M. A., AVILA, R. E., GALANOPOULOS, T., NEVILLE-GOLDEN, J., MAXWELL, M. & SELMAN, M. 1990. Platelet-derived growth factor in idiopathic pulmonary fibrosis. *The Journal of Clinical Investigation*, 86, 1055-1064.
- ANTONIOU, K. M., MARGARITOPOULOS, G. A., TOMASSETTI, S., BONELLA, F., COSTABEL, U. & POLETTI, V. 2014. Interstitial lung disease. *European Respiratory Review*, 23, 40-54.

- ARAKAWA, H. & HONMA, K. 2011. Honeycomb lung: history and current concepts. *AJR. American journal of roentgenology*, 196 4, 773-82.
- ARMANIOS, M. Y., CHEN, J. J., COGAN, J. D., ALDER, J. K., INGERSOLL, R. G., MARKIN, C., LAWSON, W. E., XIE, M., VULTO, I., PHILLIPS, J. A., 3RD, LANSDORP, P. M., GREIDER, C. W. & LOYD, J. E. 2007. Telomerase mutations in families with idiopathic pulmonary fibrosis. *N Engl J Med*, 356, 1317-26.
- ASHCROFT, T., SIMPSON, J. M. & TIMBRELL, V. 1988. Simple method of estimating severity of pulmonary fibrosis on a numerical scale. *J Clin Pathol*, 41, 467-70.
- ATS & ERS 2002. American Thoracic Society/European Respiratory Society International Multidisciplinary Consensus Classification of the Idiopathic Interstitial Pneumonias. This joint statement of the American Thoracic Society (ATS), and the European Respiratory Society (ERS) was adopted by the ATS board of directors, June 2001 and by the ERS Executive Committee, June 2001. *Am J Respir Crit Care Med*, 165, 277-304.
- AZUMA, A., TAGUCHI, Y., OGURA, T., EBINA, M., TANIGUCHI, H., KONDOH, Y., SUGA, M., TAKAHASHI, H., NAKATA, K., SATO, A., KUDOH, S., NUKIWA, T. & PIRFENIDONE CLINICAL STUDY GROUP IN, J. 2011. Exploratory analysis of a phase III trial of pirfenidone identifies a subpopulation of patients with idiopathic pulmonary fibrosis as benefiting from treatment. *Respir Res*, 12, 143.
- BAGHER, M., LARSSON-CALLERFELT, A. K., ROSMARK, O., HALLGREN, O., BJERMER, L. & WESTERGREN-THORSSON, G. 2018. Mast cells and mast cell tryptase enhance migration of human lung fibroblasts through protease-activated receptor 2. *Cell Commun Signal*, 16, 59.
- BAILY, J., SERRANO, O. P., MARSDEN, A., BRIGGS, M., LOVE, I., MADDEN, S., GANDI, S., WHITMARSH, M. & YOUNG, A. 2019. Pharmacokinetics and Efficacy of Nintedanib in a Repetitive Bleomycin Challenge Model of Rat Lung Fibrosis. *C65. DIFFUSE PARENCHYMAL LUNG DISEASES: BASIC AND CLINICAL STUDIES*.
- BALAKRISHNAN, V. & VERMA, S. P. 2013. *Laryngeal Nerve Anatomy* [Online]. Medscape: Medscape Publishers' Circle®. Available: <https://emedicine.medscape.com/article/1923100-overview> [Accessed May 13 2020].
- BARGAGLI, E., BIGLIAZZI, C., LEONINI, A., NIKIFORAKIS, N., PERARI, M. G. & ROTTOLI, P. 2005. Tryptase concentrations in bronchoalveolar lavage from patients with chronic eosinophilic pneumonia. *Clin Sci (Lond)*, 108, 273-6.
- BARGAGLI, E., PENZA, F., VAGAGGINI, C., MAGI, B., PERARI, M. G. & ROTTOLI, P. 2007. Analysis of carbonylated proteins in bronchoalveolar lavage of patients with diffuse lung diseases. *Lung*, 185, 139-44.
- BARNETT, M. W. & LARKMAN, P. M. 2007. The action potential. *Pract Neurol*, 7, 192-7.
- BARRATT, S. L., CREAMER, A., HAYTON, C. & CHAUDHURI, N. 2018. Idiopathic Pulmonary Fibrosis (IPF): An Overview. *J Clin Med*, 7.
- BARRY, S. J., DANE, A. D., MORICE, A. H. & WALMSLEY, A. D. 2006. The automatic recognition and counting of cough. *Cough*, 2, 8.
- BARTLETT, D., JR., JEFFERY, P., SANT'AMBROGIO, G. & WISE, J. C. 1976. Location of stretch receptors in the trachea and bronchi of the dog. *J Physiol*, 258, 409-20.
- BARTON, A., GAYDECKI, P., HOLT, K. & SMITH, J. A. 2012. Data reduction for cough studies using distribution of audio frequency content. *Cough*, 8, 12.
- BASOGLU, O. K., BARNES, P. J., KHARITONOV, S. A. & PELLEGG, A. 2015. Effects of Aerosolized Adenosine 5'-Triphosphate in Smokers and Patients With COPD. *Chest*, 148, 430-435.
- BASOGLU, O. K., PELLEGG, A., ESSILFIE-QUAYE, S., BRINDICCI, C., BARNES, P. J. & KHARITONOV, S. A. 2005. Effects of aerosolized adenosine 5'-triphosphate vs adenosine 5'-monophosphate on dyspnea and airway caliber in healthy nonsmokers and patients with asthma. *Chest*, 128, 1905-9.

- BAUMGARTNER, K. B., SAMET, J. M., STIDLEY, C. A., COLBY, T. V. & WALDRON, J. A. 1997. Cigarette smoking: a risk factor for idiopathic pulmonary fibrosis. *Am J Respir Crit Care Med*, 155, 242-8.
- BAUTISTA, D. M., JORDT, S. E., NIKAI, T., TSURUDA, P. R., READ, A. J., POBLETE, J., YAMOAH, E. N., BASBAUM, A. I. & JULIUS, D. 2006. TRPA1 mediates the inflammatory actions of environmental irritants and proalgesic agents. *Cell*, 124, 1269-82.
- BAXTER, M., ELTOM, S., DEKKAK, B., YEW-BOOTH, L., DUBUIS, E. D., MAHER, S. A., BELVISI, M. G. & BIRRELL, M. A. 2014. Role of transient receptor potential and pannexin channels in cigarette smoke-triggered ATP release in the lung. *Thorax*, 69, 1080-9.
- BAYR, H. 2005. Reactive oxygen species. *Critical Care Medicine*, 33, S498-S501.
- BELLOU, V., BELBASIS, L., KONSTANTINIDIS, A. & EVANGELOU, E. 2017. Tobacco smoking and risk for idiopathic pulmonary fibrosis: a prospective cohort study in UK Biobank. *European Respiratory Journal*, 50, PA4887.
- BELVISI, M. G. 2002. Overview of the innervation of the lung. *Curr Opin Pharmacol*, 2, 211-5.
- BELVISI, M. G. 2003. Sensory nerves and airway inflammation: role of A delta and C-fibres. *Pulm Pharmacol Ther*, 16, 1-7.
- BELVISI, M. G., BIRRELL, M. A., KHALID, S., WORTLEY, M. A., DOCKRY, R., COOTE, J., HOLT, K., DUBUIS, E., KELSALL, A., MAHER, S. A., BONVINI, S., WOODCOCK, A. & SMITH, J. A. 2016. Neurophenotypes in Airway Diseases. Insights from Translational Cough Studies. *Am J Respir Crit Care Med*, 193, 1364-72.
- BELVISI, M. G., BIRRELL, M. A., WORTLEY, M. A., MAHER, S. A., SATIA, I., BADRI, H., HOLT, K., ROUND, P., MCGARVEY, L., FORD, J. & SMITH, J. A. 2017. XEN-D0501, a Novel Transient Receptor Potential Vanilloid 1 Antagonist, Does Not Reduce Cough in Patients with Refractory Cough. *Am J Respir Crit Care Med*, 196, 1255-1263.
- BELVISI, M. G., DUBUIS, E. & BIRRELL, M. A. 2011. Transient receptor potential A1 channels: insights into cough and airway inflammatory disease. *Chest*, 140, 1040-7.
- BELVISI, M. G. & GEPPETTI, P. 2004. Cough. 7: Current and future drugs for the treatment of chronic cough. *Thorax*, 59, 438-40.
- BELVISI, M. G. & HELE, D. J. 2003. Soft steroids: a new approach to the treatment of inflammatory airways diseases. *Pulm Pharmacol Ther*, 16, 321-5.
- BENNETT, J. M. & REICH, S. D. 1979. Drugs five years later: Bleomycin. *Annals of Internal Medicine*, 90, 945-948.
- BEREND, N. 1985. Inhibition of bleomycin lung toxicity by N-acetyl cysteine in the rat. *Pathology*, 17, 108-10.
- BERGERON, A., SOLER, P., KAMBOUCHNER, M., LOISEAU, P., MILLERON, B., VALEYRE, D., HANCE, A. J. & TAZI, A. 2003. Cytokine profiles in idiopathic pulmonary fibrosis suggest an important role for TGF-beta and IL-10. *Eur Respir J*, 22, 69-76.
- BERLETT, B. S. & STADTMAN, E. R. 1997. Protein oxidation in aging, disease, and oxidative stress. *J Biol Chem*, 272, 20313-6.
- BERTHELOT DIDIER, J.-C., GIJSEN HENRICUS JACOBUS, M., ZAJA, M., RECH, J., LEBSACK, A., XIAO, W. E. I., BRANSTETTER, B. & BREITENBUCHER GUY, J. 2010. *HETEROCYCLIC AMIDES AS MODULATORS OF TRPA1*. US201013375833.
- BIGATTO, V., MANNI, E., POMPILIO, D., BRANA', M., CHALIDOU, A., VELDEN, J., CORSI, M., RUSSELL, V. & ANDREETTA, F. 2019. Quantitation of hydroxyproline in a mouse model of bleomycin-induced lung fibrosis: comparison with histological analysis. *European Respiratory Journal*, 54, PA2419.
- BINDOKAS, V., JORDAN, J., LEE, C. & MILLER, R. 1996. Superoxide production in rat hippocampal neurons: selective imaging with hydroethidine. *The Journal of Neuroscience*, 16, 1324-1336.
- BIRRELL, M. A., BELVISI, M. G., GRACE, M., SADOFSKY, L., FARUQI, S., HELE, D. J., MAHER, S. A., FREUND-MICHEL, V. & MORICE, A. H. 2009. TRPA1 agonists evoke coughing in guinea pig and human volunteers. *Am J Respir Crit Care Med*, 180, 1042-7.

- BIRRELL, M. A., BONVINI, S. J., DUBUIS, E., MAHER, S. A., WORTLEY, M. A., GRACE, M. S., RAEMDONCK, K., ADCOCK, J. J. & BELVISI, M. G. 2014. Tiotropium modulates transient receptor potential V1 (TRPV1) in airway sensory nerves: A beneficial off-target effect? *J Allergy Clin Immunol*, 133, 679-87 e9.
- BIRRELL, M. A., CRISPINO, N., HELE, D. J., PATEL, H. J., YACOUB, M. H., BARNES, P. J. & BELVISI, M. G. 2002. Effect of dopamine receptor agonists on sensory nerve activity: possible therapeutic targets for the treatment of asthma and COPD. *Br J Pharmacol*, 136, 620-8.
- BIRRING, S. S., FLEMING, T., MATOS, S., RAJ, A. A., EVANS, D. H. & PAVORD, I. D. 2008. The Leicester Cough Monitor: preliminary validation of an automated cough detection system in chronic cough. *Eur Respir J*, 31, 1013-8.
- BIRRING, S. S., MATOS, S., PATEL, R. B., PRUDON, B., EVANS, D. H. & PAVORD, I. D. 2006. Cough frequency, cough sensitivity and health status in patients with chronic cough. *Respir Med*, 100, 1105-9.
- BIRRING, S. S., PRUDON, B., CARR, A. J., SINGH, S. J., MORGAN, M. D. & PAVORD, I. D. 2003. Development of a symptom specific health status measure for patients with chronic cough: Leicester Cough Questionnaire (LCQ). *Thorax*, 58, 339-43.
- BIRRING, S. S., WIJSENBECK, M. S., AGRAWAL, S., VAN DEN BERG, J. W. K., STONE, H., MAHER, T. M., TUTUNCU, A. & MORICE, A. H. 2017. A novel formulation of inhaled sodium cromoglicate (PA101) in idiopathic pulmonary fibrosis and chronic cough: a randomised, double-blind, proof-of-concept, phase 2 trial. *Lancet Respir Med*, 5, 806-815.
- BJORAKER, J. A., RYU, J. H., EDWIN, M. K., MYERS, J. L., TAZELAAR, H. D., SCHROEDER, D. R. & OFFORD, K. P. 1998. Prognostic Significance of Histopathologic Subsets in Idiopathic Pulmonary Fibrosis. *American Journal of Respiratory and Critical Care Medicine*, 157, 199-203.
- BLANC, P. D., ANNESI-MAESANO, I., BALMES, J. R., CUMMINGS, K. J., FISHWICK, D., MIEDINGER, D., MURGIA, N., NAIDOO, R. N., REYNOLDS, C. J., SIGSGAARD, T., TORÉN, K., VINNIKOV, D. & REDLICH, C. A. 2019. The Occupational Burden of Nonmalignant Respiratory Diseases. An Official American Thoracic Society and European Respiratory Society Statement. *American Journal of Respiratory and Critical Care Medicine*, 199, 1312-1334.
- BONGIANNI, F., MUTOLO, D., FONTANA, G. A. & PANTALEO, T. 1998. Discharge patterns of Botzinger complex neurons during cough in the cat. *Am J Physiol*, 274, R1015-24.
- BONVINI, S. J. & BELVISI, M. G. 2017. Cough and airway disease: The role of ion channels. *Pulmonary Pharmacology & Therapeutics*, 47, 21-28.
- BONVINI, S. J., BIRRELL, M. A., DUBUIS, E., ADCOCK, J. J., WORTLEY, M. A., FLAJOLET, P., BRADDING, P. & BELVISI, M. G. 2020. Novel airway smooth muscle-mast cell interactions and a role for the TRPV4-ATP axis in non-atopic asthma. *Eur Respir J*, 56.
- BONVINI, S. J., BIRRELL, M. A., GRACE, M. S., MAHER, S. A., ADCOCK, J. J., WORTLEY, M. A., DUBUIS, E., CHING, Y. M., FORD, A. P., SHALA, F., MIRALPEIX, M., TARRASON, G., SMITH, J. A. & BELVISI, M. G. 2016. Transient receptor potential cation channel, subfamily V, member 4 and airway sensory afferent activation: Role of adenosine triphosphate. *J Allergy Clin Immunol*, 138, 249-261 e12.
- BONVINI, S. J., BIRRELL, M. A., SMITH, J. A. & BELVISI, M. G. 2015. Targeting TRP channels for chronic cough: from bench to bedside. *Naunyn Schmiedebergs Arch Pharmacol*, 388, 401-20.
- BOOMARS, K. A., WAGENAAR, S. S., MULDER, P. G., VAN VELZEN-BLAD, H. & VAN DEN BOSCH, J. M. 1995. Relationship between cells obtained by bronchoalveolar lavage and survival in idiopathic pulmonary fibrosis. *Thorax*, 50, 1087-92.
- BOOTH, A. J., HADLEY, R., CORNETT, A. M., DREFFS, A. A., MATTHES, S. A., TSUI, J. L., WEISS, K., HOROWITZ, J. C., FIORE, V. F., BARKER, T. H., MOORE, B. B., MARTINEZ, F. J., NIKLASON, L. E. & WHITE, E. S. 2012. Acellular normal and fibrotic human lung matrices as a culture system for in vitro investigation. *American journal of respiratory and critical care medicine*, 186, 866-876.

- BORENSZTAJN, K., BRESSER, P., VAN DER LOOS, C., BOT, I., VAN DEN BLINK, B., DEN BAKKER, M. A., DAALHUISEN, J., GROOT, A. P., PEPPELENBOSCH, M. P., VON DER THUSEN, J. H. & SPEK, C. A. 2010. Protease-activated receptor-2 induces myofibroblast differentiation and tissue factor up-regulation during bleomycin-induced lung injury: potential role in pulmonary fibrosis. *Am J Pathol*, 177, 2753-64.
- BORIE, R., CRESTANI, B., DIEUDE, P., NUNES, H., ALLANORE, Y., KANNENGIESSER, C., AIRO, P., MATUCCI-CERINIC, M., WALLAERT, B., ISRAEL-BIET, D., CADRANEL, J., COTTIN, V., GAZAL, S., PELJTO, A. L., VARGA, J., SCHWARTZ, D. A., VALEYRE, D. & GRANDCHAMP, B. 2013. The MUC5B variant is associated with idiopathic pulmonary fibrosis but not with systemic sclerosis interstitial lung disease in the European Caucasian population. *PLoS One*, 8, e70621.
- BORIE, R., LE GUEN, P., GHANEM, M., TAILLÉ, C., DUPIN, C., DIEUDÉ, P., KANNENGIESSER, C. & CRESTANI, B. 2019. The genetics of interstitial lung diseases. *European Respiratory Review*, 28, 190053.
- BOS, A., WEVER, R. & ROOS, D. 1978. Characterization and quantification of the peroxidase in human monocytes. *Biochim Biophys Acta*, 525, 37-44.
- BOURKE, S. J. 2006. Interstitial lung disease: progress and problems. *Postgraduate medical journal*, 82, 494-499.
- BOURS, M. J., SWENNEN, E. L., DI VIRGILIO, F., CRONSTEIN, B. N. & DAGNELIE, P. C. 2006. Adenosine 5'-triphosphate and adenosine as endogenous signaling molecules in immunity and inflammation. *Pharmacol Ther*, 112, 358-404.
- BRIDGE, M. 2018. Dr Alexa wants you to cough up for medicine. *The Times of London*.
- BRIDGES, J. P., WERT, S. E., NOGEE, L. M. & WEAVER, T. E. 2003. Expression of a human surfactant protein C mutation associated with interstitial lung disease disrupts lung development in transgenic mice. *J Biol Chem*, 278, 52739-46.
- BRIGNALL, K., JAYARAMAN, B. & BIRRING, S. S. 2008. Quality of life and psychosocial aspects of cough. *Lung*, 186 Suppl 1, S55-8.
- BROOKS, C. A., BARTON, L. S., BEHM, D. J., EIDAM, H. S., FOX, R. M., HAMMOND, M., HOANG, T. H., HOLT, D. A., HILFIKER, M. A., LAWHORN, B. G., PATTERSON, J. R., STOY, P., ROETHKE, T. J., YE, G., ZHAO, S., THORNELOE, K. S., GOODMAN, K. B. & CHEUNG, M. 2019. Discovery of GSK2798745: A Clinical Candidate for Inhibition of Transient Receptor Potential Vanilloid 4 (TRPV4). *ACS Med Chem Lett*, 10, 1228-1233.
- BROUNS, I., PINTELON, I., TIMMERMANS, J. P. & ADRIAENSEN, D. 2012. Novel insights in the neurochemistry and function of pulmonary sensory receptors. *Adv Anat Embryol Cell Biol*, 211, 1-115, vii.
- BROWN, C., CHAUHAN, J., GRAMMENOS, A., HAN, J., HASTHANASOMBAT, A., SPATHIS, D., XIA, T., CICUTA, P. & MASCOLO, C. 2020. Exploring Automatic Diagnosis of COVID-19 from Crowdsourced Respiratory Sound Data. *arXiv preprint arXiv:2006.05919*.
- BROZMANOVA, M., HANACEK, J., TATAR, M. & SZEPE, P. 2004. The influence of hyperoxia on cough reflex intensity in guinea pigs treated with bleomycin. *Bratisl Lek Listy*, 105, 65-71.
- BURNSTOCK, G. 2006. Pathophysiology and therapeutic potential of purinergic signaling. *Pharmacol Rev*, 58, 58-86.
- CADET, J., RAVANAT, J. L., TAVERNAPORRO, M., MENONI, H. & ANGELOV, D. 2012. Oxidatively generated complex DNA damage: tandem and clustered lesions. *Cancer Lett*, 327, 5-15.
- CAIRNS, J. A. & WALLS, A. F. 1997. Mast cell tryptase stimulates the synthesis of type I collagen in human lung fibroblasts. *J Clin Invest*, 99, 1313-21.
- CANNING, B. J. 2006. Anatomy and neurophysiology of the cough reflex: ACCP evidence-based clinical practice guidelines. *Chest*, 129, 335-475.
- CANNING, B. J., MAZZONE, S. B., MEEKER, S. N., MORI, N., REYNOLDS, S. M. & UNDEM, B. J. 2004. Identification of the tracheal and laryngeal afferent neurones mediating cough in anaesthetized guinea-pigs. *J Physiol*, 557, 543-58.

- CANNING, B. J. & MORI, N. 2010. An essential component to brainstem cough gating identified in anesthetized guinea pigs. *FASEB J*, 24, 3916-26.
- CANNING, B. J. & MORI, N. 2011. Encoding of the cough reflex in anesthetized guinea pigs. *Am J Physiol Regul Integr Comp Physiol*, 300, R369-77.
- CANNING, B. J., MORI, N. & MAZZONE, S. B. 2006. Vagal afferent nerves regulating the cough reflex. *Respir Physiol Neurobiol*, 152, 223-42.
- CANTIN, A. M., NORTH, S. L., FELLS, G. A., HUBBARD, R. C. & CRYSTAL, R. G. 1987. Oxidant-mediated epithelial cell injury in idiopathic pulmonary fibrosis. *J Clin Invest*, 79, 1665-73.
- CARR, M. J. & UNDEM, B. J. 2003. Pharmacology of vagal afferent nerve activity in guinea pig airways. *Pulm Pharmacol Ther*, 16, 45-52.
- CATALÁN, V., FRÜHBECK, G. & GÓMEZ-AMBROSI, J. 2018. Chapter 8 - Inflammatory and Oxidative Stress Markers in Skeletal Muscle of Obese Subjects. In: DEL MORAL, A. M. & AGUILERA GARCÍA, C. M. (eds.) *Obesity*. Academic Press.
- CATERINA, M. J. 2007. Chemical biology: sticky spices. *Nature*, 445, 491-2.
- CHAMBERLAIN, S. A. F., GARROD, R., DOUIRI, A., MASEFIELD, S., POWELL, P., BÜCHER, C., PANDYAN, A., MORICE, A. H. & BIRRING, S. S. 2015. The Impact of Chronic Cough: A Cross-Sectional European Survey. *Lung*, 193, 401-408.
- CHANG, A. B., LASSERSON, T. J., GAFFNEY, J., CONNOR, F. L. & GARSKE, L. A. 2011. Gastro-oesophageal reflux treatment for prolonged non-specific cough in children and adults. *Cochrane Database Syst Rev*, 2011, Cd004823.
- CHAUDHARY, N. I., ROTH, G. J., HILBERG, F., MÜLLER-QUERNHEIM, J., PRASSE, A., ZISSEL, G., SCHNAPP, A. & PARK, J. E. 2007. Inhibition of PDGF, VEGF and FGF signalling attenuates fibrosis. *Eur Respir J*, 29, 976-85.
- CHEN, H., QU, J., HUANG, X., KURUNDKAR, A., ZHU, L., YANG, N., VENADO, A., DING, Q., LIU, G., ANTONY, V. B., THANNICKAL, V. J. & ZHOU, Y. 2016. Mechanosensing by the  $\alpha 6$ -integrin confers an invasive fibroblast phenotype and mediates lung fibrosis. *Nature Communications*, 7, 12564.
- CHEN, L., LAI, K., LOMASK, J. M., JIANG, B. & ZHONG, N. 2013. Detection of mouse cough based on sound monitoring and respiratory airflow waveforms. *PLoS One*, 8, e59263.
- CHEUNG, M., BAO, W., BEHM, D. J., BROOKS, C. A., BURY, M. J., DOWDELL, S. E., EIDAM, H. S., FOX, R. M., GOODMAN, K. B., HOLT, D. A., LEE, D., ROETHKE, T. J., WILLETTE, R. N., XU, X., YE, G. & THORNELOE, K. S. 2017. Discovery of GSK2193874: An Orally Active, Potent, and Selective Blocker of Transient Receptor Potential Vanilloid 4. *ACS Med Chem Lett*, 8, 549-554.
- CHILOSI, M., POLETTI, V., ZAMÒ, A., LESTANI, M., MONTAGNA, L., PICCOLI, P., PEDRON, S., BERTASO, M., SCARPA, A., MURER, B., CANCELLIERI, A., MAESTRO, R., SEMENZATO, G. & DOGLIONI, C. 2003. Aberrant Wnt/ $\beta$ -Catenin Pathway Activation in Idiopathic Pulmonary Fibrosis. *The American Journal of Pathology*, 162, 1495-1502.
- CHO, P. S. P., FLETCHER, H. V., TURNER, R. D., PATEL, I. S., JOLLEY, C. J. & BIRRING, S. S. 2020. The Relationship Between Cough Reflex Sensitivity and Exacerbation Frequency in Chronic Obstructive Pulmonary Disease. *Lung*, 198, 617-628.
- CHOMCZYNSKI, P. & SACCHI, N. 1987. Single-step method of RNA isolation by acid guanidinium thiocyanate-phenol-chloroform extraction. *Anal Biochem*, 162, 156-9.
- CHOU, Y. L., SCARUPA, M. D., MORI, N. & CANNING, B. J. 2008. Differential effects of airway afferent nerve subtypes on cough and respiration in anesthetized guinea pigs. *Am J Physiol Regul Integr Comp Physiol*, 295, R1572-84.
- CHOUDRY, N. & FULLER, R. 1992. Sensitivity of the cough reflex in patients with chronic cough. *European Respiratory Journal*, 5, 296-300.
- CHOW, S., THOMAS, P. S., MALOUF, M. & YATES, D. H. 2012. Exhaled breath condensate (EBC) biomarkers in pulmonary fibrosis. *J Breath Res*, 6, 016004.
- CHUNG, K. F. & PAVORD, I. D. 2008. Prevalence, pathogenesis, and causes of chronic cough. *Lancet*, 371, 1364-74.



- CICKO, S., KOHLER, T. C., AYATA, C. K., MULLER, T., EHRAT, N., MEYER, A., HOSSFELD, M., ZECH, A., DI VIRGILIO, F. & IDZKO, M. 2018. Extracellular ATP is a danger signal activating P2X7 receptor in a LPS mediated inflammation (ARDS/ALI). *Oncotarget*, 9, 30635-30648.
- CISNEROS-LIRA, J., GAXIOLA, M., RAMOS, C., SELMAN, M. & PARDO, A. 2003. Cigarette smoke exposure potentiates bleomycin-induced lung fibrosis in guinea pigs. *Am J Physiol Lung Cell Mol Physiol*, 285, L949-56.
- CLAUSSEN, C. A. & LONG, E. C. 1999. Nucleic Acid recognition by metal complexes of bleomycin. *Chem Rev*, 99, 2797-816.
- CLINICALTRIALS.GOV. 2017. *A Study to Assess the Effectiveness and Side Effects of GSK2798745 in Participants With Chronic Cough* [Online]. Available: <https://clinicaltrials.gov/ct2/show/study/NCT03372603> [Accessed October 2020].
- CLINICALTRIALS.GOV. 2019. *A Dose Escalation Study of BLU-5937 in Unexplained or Refractory Chronic Cough (RELIEF)* [Online]. Available: <https://clinicaltrials.gov/ct2/show/study/NCT03979638> [Accessed January 2021].
- CLINICALTRIALS.GOV. 2020. *Prospective Treatment Efficacy in IPF Using Genotype for Nac Selection (PRECISIONS) Trial (PRECISIONS)* [Online]. Available: <https://www.clinicaltrials.gov/ct2/show/NCT04300920> [Accessed January 2021].
- COLERIDGE, J. C. & COLERIDGE, H. M. 1984. Afferent vagal C fibre innervation of the lungs and airways and its functional significance. *Rev Physiol Biochem Pharmacol*, 99, 1-110.
- COMPTON, S. J., RENAUX, B., WIJESURIYA, S. J. & HOLLENBERG, M. D. 2001. Glycosylation and the activation of proteinase-activated receptor 2 (PAR(2)) by human mast cell tryptase. *Br J Pharmacol*, 134, 705-18.
- COSTELLO, J. F., DUNLOP, L. S. & GARDINER, P. J. 1985. Characteristics of prostaglandin induced cough in man. *British journal of clinical pharmacology*, 20, 355-359.
- COUGHLIN, S. R. 2000. Thrombin signalling and protease-activated receptors. *Nature*, 407, 258-64.
- COYLE, M. A., KEENAN, D. B., HENDERSON, L. S., WATKINS, M. L., HAUMANN, B. K., MAYLEBEN, D. W. & WILSON, M. G. 2005. Evaluation of an ambulatory system for the quantification of cough frequency in patients with chronic obstructive pulmonary disease. *Cough*, 1, 3.
- CRYSTAL, R. G., FULMER, J. D., ROBERTS, W. C., MOSS, M. L., LINE, B. R. & REYNOLDS, H. Y. 1976. Idiopathic pulmonary fibrosis. Clinical, histologic, radiographic, physiologic, scintigraphic, cytologic, and biochemical aspects. *Ann Intern Med*, 85, 769-88.
- CULLINAN, P. 1992. Persistent cough and sputum: prevalence and clinical characteristics in south east England. *Respir Med*, 86, 143-9.
- DAKHLALLAH, D., BATTE, K., WANG, Y., CANTEMIR-STONE, C. Z., YAN, P., NUOVO, G., MIKHAIL, A., HITCHCOCK, C. L., WRIGHT, V. P., NANA-SINKAM, S. P., PIPER, M. G. & MARSH, C. B. 2013. Epigenetic regulation of miR-17~92 contributes to the pathogenesis of pulmonary fibrosis. *Am J Respir Crit Care Med*, 187, 397-405.
- DALLE-DONNE, I., ROSSI, R., GIUSTARINI, D., MILZANI, A. & COLOMBO, R. 2003. Protein carbonyl groups as biomarkers of oxidative stress. *Clinica Chimica Acta*, 329, 23-38.
- DANIIL, Z. D., PAPAGEORGIOU, E., KOUTSOKERA, A., KOSTIKAS, K., KIROPOULOS, T., PAPAIOANNOU, A. I. & GOURGOULIANIS, K. I. 2008. Serum levels of oxidative stress as a marker of disease severity in idiopathic pulmonary fibrosis. *Pulm Pharmacol Ther*, 21, 26-31.
- DAS, K., PRASAD, R., SINGH, A., BHATTACHARYA, A., ROY, A., MALLIK, S., MUKHERJEE, A. & SEN, P. 2018. Protease-activated receptor 2 promotes actomyosin dependent transforming microvesicles generation from human breast cancer. *Mol Carcinog*, 57, 1707-1722.
- DAVENPORT, P. W. & VOVK, A. 2009. Cortical and subcortical central neural pathways in respiratory sensations. *Respir Physiol Neurobiol*, 167, 72-86.
- DECALMER, S. C., WEBSTER, D., KELSALL, A. A., MCGUINNESS, K., WOODCOCK, A. A. & SMITH, J. A. 2007. Chronic cough: how do cough reflex sensitivity and subjective assessments correlate with objective cough counts during ambulatory monitoring? *Thorax*, 62, 329-34.

- DEGRYSE, A. L. & LAWSON, W. E. 2011. Progress toward improving animal models for idiopathic pulmonary fibrosis. *Am J Med Sci*, 341, 444-9.
- DEGRYSE, A. L., TANJORE, H., XU, X. C., POLOSUKHIN, V. V., JONES, B. R., MCMAHON, F. B., GLEAVES, L. A., BLACKWELL, T. S. & LAWSON, W. E. 2010. Repetitive intratracheal bleomycin models several features of idiopathic pulmonary fibrosis. *American Journal of Physiology-Lung Cellular and Molecular Physiology*, 299, L442-L452.
- DEKHUIJZEN, P. N. 2004. Antioxidant properties of N-acetylcysteine: their relevance in relation to chronic obstructive pulmonary disease. *Eur Respir J*, 23, 629-36.
- DEMEDTS, M., BEHR, J., BUHL, R., COSTABEL, U., DEKHUIJZEN, R., JANSEN, H. M., MACNEE, W., THOMEER, M., WALLAERT, B., LAURENT, F., NICHOLSON, A. G., VERBEKEN, E. K., VERSCHAKELEN, J., FLOWER, C. D., CAPRON, F., PETRUZZELLI, S., DE VUYST, P., VAN DEN BOSCH, J. M., RODRIGUEZ-BECERRA, E., CORVASCE, G., LANKHORST, I., SARDINA, M., MONTANARI, M. & GROUP, I. S. 2005. High-dose acetylcysteine in idiopathic pulmonary fibrosis. *N Engl J Med*, 353, 2229-42.
- DENKER, S. P. & BARBER, D. L. 2002. Ion transport proteins anchor and regulate the cytoskeleton. *Curr Opin Cell Biol*, 14, 214-20.
- DESAI, T. J., BROWNFIELD, D. G. & KRASNOW, M. A. 2014. Alveolar progenitor and stem cells in lung development, renewal and cancer. *Nature*, 507, 190-4.
- DEVASAGAYAM, T. P., TILAK, J. C., BOLOOR, K. K., SANE, K. S., GHASKADBI, S. S. & LELE, R. D. 2004. Free radicals and antioxidants in human health: current status and future prospects. *J Assoc Physicians India*, 52, 794-804.
- DI FILIPPO, P., SCAPAROTTA, A., PETROSINO, M. I., ATTANASI, M., DI PILLO, S., CHIARELLI, F. & MOHN, A. 2018. An underestimated cause of chronic cough: The Protracted Bacterial Bronchitis. *Annals of thoracic medicine*, 13, 7-13.
- DICPINIGAITIS, P. V. & ALVA, R. V. 2005. Safety of capsaicin cough challenge testing. *Chest*, 128, 196-202.
- DICPINIGAITIS, P. V., MCGARVEY, L. P. & CANNING, B. J. 2020. P2X3-Receptor Antagonists as Potential Antitussives: Summary of Current Clinical Trials in Chronic Cough. *Lung*, 198, 609-616.
- DICPINIGAITIS, P. V., MORICE, A. H., BIRRING, S. S., MCGARVEY, L., SMITH, J. A., CANNING, B. J. & PAGE, C. P. 2014. Antitussive drugs--past, present, and future. *Pharmacol Rev*, 66, 468-512.
- DIXON, J. R., JR. 1998. The International Conference on Harmonization Good Clinical Practice guideline. *Qual Assur*, 6, 65-74.
- DOHERTY, M. J., MISTER, R., PEARSON, M. G. & CALVERLEY, P. M. 2000. Capsaicin induced cough in cryptogenic fibrosing alveolitis. *Thorax*, 55, 1028-32.
- DUBUIS, E., GRACE, M., WORTLEY, M. A., BIRELL, M. A. & BELVISI, M. G. 2013. Harvesting, isolation, and functional assessment of primary vagal ganglia cells. *Curr Protoc Pharmacol*, 62, Unit 12 15.
- DUTTA, P., FUNSTON, W., MOSSOP, H., RYAN, V., JONES, R., FORBES, R., SEN, S., PEARSON, J., GRIFFIN, S. M., SMITH, J. A., WARD, C., FORREST, I. A. & SIMPSON, A. J. 2019. Randomised, double-blind, placebo-controlled pilot trial of omeprazole in idiopathic pulmonary fibrosis. *Thorax*, 74, 346-353.
- ECCLES, R., MORRIS, S. & JAWAD, M. 1992. Lack of effect of codeine in the treatment of cough associated with acute upper respiratory tract infection. *J Clin Pharm Ther*, 17, 175-80.
- FABBRETTI, E. & NISTRÌ, A. 2012. Regulation of P2X3 receptor structure and function. *CNS Neurol Disord Drug Targets*, 11, 687-98.
- FANG, Z., HUANG, C., ZHANG, J. J., XIE, J., DAI, S., GE, E., XIANG, J., YAO, H., HUANG, R., BI, X., WANG, B., ZHONG, N. & LAI, K. 2019. Traffic-related air pollution induces non-allergic eosinophilic airway inflammation and cough hypersensitivity in guinea-pigs. *Clin Exp Allergy*, 49, 366-377.
- FENSKE, M. 1992. Body weight and water intake of guinea pigs: influence of single caging and an unfamiliar new room. *J Exp Anim Sci*, 35, 71-9.

- FERNANDEZ, I. E. & EICKELBERG, O. 2012. The impact of TGF-beta on lung fibrosis: from targeting to biomarkers. *Proc Am Thorac Soc*, 9, 111-6.
- FERNANDEZ PEREZ, E. R., DANIELS, C. E., SCHROEDER, D. R., ST SAUVER, J., HARTMAN, T. E., BARTHOLMAI, B. J., YI, E. S. & RYU, J. H. 2010. Incidence, prevalence, and clinical course of idiopathic pulmonary fibrosis: a population-based study. *Chest*, 137, 129-37.
- FERNANDEZ-BLANCO, J. A., AGUILERA, M., DOMENECH, A., TARRASON, G., PRATS, N., MIRALPEIX, M. & DE ALBA, J. 2015. Enhanced cough reflex in a model of bleomycin-induced lung fibrosis in guinea pigs. *Clin Sci (Lond)*, 129, 1001-10.
- FERRARI, D., CHIOZZI, P., FALZONI, S., DAL SUSINO, M., MELCHIORRI, L., BARICORDI, O. R. & DI VIRGILIO, F. 1997. Extracellular ATP triggers IL-1 beta release by activating the purinergic P2Z receptor of human macrophages. *J Immunol*, 159, 1451-8.
- FINGERLIN, T. E., MURPHY, E., ZHANG, W., PELJO, A. L., BROWN, K. K., STEELE, M. P., LOYD, J. E., COSGROVE, G. P., LYNCH, D., GROSHONG, S., COLLARD, H. R., WOLTERS, P. J., BRADFORD, W. Z., KOSSEN, K., SEIWERT, S. D., DU BOIS, R. M., GARCIA, C. K., DEVINE, M. S., GUDMUNDSSON, G., ISAKSSON, H. J., KAMINSKI, N., ZHANG, Y., GIBSON, K. F., LANCASTER, L. H., COGAN, J. D., MASON, W. R., MAHER, T. M., MOLYNEAUX, P. L., WELLS, A. U., MOFFATT, M. F., SELMAN, M., PARDO, A., KIM, D. S., CRAPO, J. D., MAKE, B. J., REGAN, E. A., WALEK, D. S., DANIEL, J. J., KAMATANI, Y., ZELENKA, D., SMITH, K., MCKEAN, D., PEDERSEN, B. S., TALBERT, J., KIDD, R. N., MARKIN, C. R., BECKMAN, K. B., LATHROP, M., SCHWARZ, M. I. & SCHWARTZ, D. A. 2013. Genome-wide association study identifies multiple susceptibility loci for pulmonary fibrosis. *Nat Genet*, 45, 613-20.
- FOIS, A. G., PALIOGIANNIS, P., SOTGIA, S., MANGONI, A. A., ZINELLU, E., PIRINA, P., CARRU, C. & ZINELLU, A. 2018. Evaluation of oxidative stress biomarkers in idiopathic pulmonary fibrosis and therapeutic applications: a systematic review. *Respir Res*, 19, 51.
- FONG, J., SANDHU, G., ELLAWAY, P., DAVEY, N., STRUTTON, P., MURPHY, K. & GUZ, A. 2004. What do we know about how humans cough? *Pulm Pharmacol Ther*, 17, 431-4.
- FONTANA, G. A., PANTALEO, T., LAVORINI, F., MALUCCIO, N. M., MUTOLO, D. & PISTOLESI, M. 1999. Repeatability of cough-related variables during fog challenges at threshold and suprathreshold stimulus intensity in humans. *Eur Respir J*, 13, 1447-50.
- FORD, A. C., FORMAN, D., MOAYYEDI, P. & MORICE, A. H. 2006. Cough in the community: a cross sectional survey and the relationship to gastrointestinal symptoms. *Thorax*, 61, 975-9.
- FORSBERG, K. & KARLSSON, J. A. 1986. Cough induced by stimulation of capsaicin-sensitive sensory neurons in conscious guinea-pigs. *Acta Physiol Scand*, 128, 319-20.
- FOX, A. J., BARNES, P. J., URBAN, L. & DRAY, A. 1993. An in vitro study of the properties of single vagal afferents innervating guinea-pig airways. *J Physiol*, 469, 21-35.
- FRANTZ, C., STEWART, K. M. & WEAVER, V. M. 2010. The extracellular matrix at a glance. *Journal of Cell Science*, 123, 4195-4200.
- FRENCH, C. L., IRWIN, R. S., CURLEY, F. J. & KRICKORIAN, C. J. 1998. Impact of chronic cough on quality of life. *Arch Intern Med*, 158, 1657-61.
- FRIEDRICH, C., FRANCKE, K., BIRRING, S. S., VAN DEN BERG, J. W. K., MARSDEN, P., MCGARVEY, L., TURNER, A., WIELDERS, P., GASHAW, I., KLEIN, S. & MORICE, A. 2020. Safety and efficacy of P2X3 antagonist BAY 1902607 in refractory chronic cough. *European Respiratory Journal*, 56, 4566.
- FULLER, R. & CHOUDRY, N. 1987. Increased cough reflex associated with angiotensin converting enzyme inhibitor cough. *British Medical Journal (Clinical research ed.)*, 295, 1025 - 1026.
- FULLER, R. W. & COLLIER, J. G. 1984. Sodium cromoglycate and atropine block the fall in FEV1 but not the cough induced by hypotonic mist. *Thorax*, 39, 766-770.
- GAO, X., WU, L. & O'NEIL, R. G. 2003. Temperature-modulated diversity of TRPV4 channel gating: activation by physical stresses and phorbol ester derivatives through protein kinase C-dependent and -independent pathways. *J Biol Chem*, 278, 27129-37.

- GARCEAU, D. & CHAURET, N. 2019. BLU-5937: A selective P2X3 antagonist with potent anti-tussive effect and no taste alteration. *Pulm Pharmacol Ther*, 56, 56-62.
- GARCEAU, D., CHAURET, N. & HARVEY, L. 2019. BLU-5937 a highly selective P2X3 homotrimeric receptor antagonist with improved taste safety profile in healthy subjects. *C37. SYMPTOMS, PLEURAL DISEASE, BEHAVIORAL SCIENCE, AND OTHER TOPICS*. American Thoracic Society.
- GARDINER, P. J. & BROWNE, J. L. 1984. Tussive activity of inhaled PGD2 in the cat and characterisation of the receptor(s) involved. *Prostaglandins Leukot Med*, 14, 153-9.
- GASSER, H. 1941. The classification of nerve fibers. *Ohio Journal of Science*.
- GATTI, R., ANDRE, E., AMADESI, S., DINH, T. Q., FISCHER, A., BUNNETT, N. W., HARRISON, S., GEPPETTI, P. & TREVISANI, M. 2006. Protease-activated receptor-2 activation exaggerates TRPV1-mediated cough in guinea pigs. *Journal of Applied Physiology*, 101, 506-511.
- GESTREAU, C., BIANCHI, A. L. & GRELOT, L. 1997. Differential brainstem Fos-like immunoreactivity after laryngeal-induced coughing and its reduction by codeine. *J Neurosci*, 17, 9340-52.
- GEVER, J. R., SOTO, R., HENNINGSEN, R. A., MARTIN, R. S., HACKOS, D. H., PANICKER, S., RUBAS, W., OGLESBY, I. B., DILLON, M. P., MILLA, M. E., BURNSTOCK, G. & FORD, A. P. 2010. AF-353, a novel, potent and orally bioavailable P2X3/P2X2/3 receptor antagonist. *Br J Pharmacol*, 160, 1387-98.
- GIRI, S. N., LEONARD, S., SHI, X., MARGOLIN, S. B. & VALLYATHAN, V. 1999. Effects of pirfenidone on the generation of reactive oxygen species in vitro. *J Environ Pathol Toxicol Oncol*, 18, 169-77.
- GODLEWSKI, A., BRZEZINSKI, P. M. & LITWIN, J. A. 1999. The effects of tetrachloroplatinum (II) ions on guinea pig peritoneal exudate neutrophil (heterophil) granulocytes. *Folia Histochem Cytobiol*, 37, 115-6.
- GOYAL, N., SKRDLA, P., SCHROYER, R., KUMAR, S., FERNANDO, D., OUGHTON, A., NORTON, N., SPRECHER, D. L. & CHERIYAN, J. 2019. Clinical Pharmacokinetics, Safety, and Tolerability of a Novel, First-in-Class TRPV4 Ion Channel Inhibitor, GSK2798745, in Healthy and Heart Failure Subjects. *Am J Cardiovasc Drugs*, 19, 335-342.
- GRACE, M., BIRRELL, M. A., DUBUIS, E., MAHER, S. A. & BELVISI, M. G. 2012. Transient receptor potential channels mediate the tussive response to prostaglandin E2 and bradykinin. *Thorax*, 67, 891-900.
- GRACE, M. S. & BELVISI, M. G. 2011. TRPA1 receptors in cough. *Pulm Pharmacol Ther*, 24, 286-8.
- GRACE, M. S., LIEU, T., DARBY, B., ABOGADIE, F. C., VELDHIJ, N., BUNNETT, N. W. & MCINTYRE, P. 2014. The tyrosine kinase inhibitor bafetinib inhibits PAR2-induced activation of TRPV4 channels in vitro and pain in vivo. *Br J Pharmacol*, 171, 3881-94.
- GRAY, H., STANDRING, S., ELLIS, H. & BERKOVITZ, B. K. B. 2005. *Gray's anatomy : the anatomical basis of clinical practice*.
- GRAZIOLI, S., DUNN-SIEGRIST, I., PAUCHARD, L.-A., BLOT, M., CHARLES, P.-E. & PUGIN, J. 2019. Mitochondrial alarmins are tissue mediators of ventilator-induced lung injury and ARDS. *PLOS ONE*, 14, e0225468.
- GRUBER, B. L., KEW, R. R., JELASKA, A., MARCHESE, M. J., GARLICK, J., REN, S., SCHWARTZ, L. B. & KORN, J. H. 1997. Human mast cells activate fibroblasts: tryptase is a fibrogenic factor stimulating collagen messenger ribonucleic acid synthesis and fibroblast chemotaxis. *The Journal of Immunology*, 158, 2310-2317.
- GUENTHER, A., KRAUSS, E., TELLO, S., WAGNER, J., PAUL, B., KUHN, S., MAURER, O., HEINEMANN, S., COSTABEL, U., BARBERO, M. A. N., MULLER, V., BONNIAUD, P., VANCHERI, C., WELLS, A., VASAKOVA, M., PESCI, A., SOFIA, M., KLEPETKO, W., SEEGER, W., DRAKOPANAGIOTAKIS, F. & CRESTANI, B. 2018. The European IPF registry (eurIPFreg): baseline characteristics and survival of patients with idiopathic pulmonary fibrosis. *Respir Res*, 19, 141.
- GUENTHER, F. & MELZIG, M. F. 2015. Protease-activated receptors and their biological role - focused on skin inflammation. *J Pharm Pharmacol*, 67, 1623-33.

- GUO, Y., YING, S., ZHAO, X., LIU, J. & WANG, Y. 2019. Increased expression of lung TRPV1/TRPA1 in a cough model of bleomycin-induced pulmonary fibrosis in Guinea pigs. *BMC Pulmonary Medicine*, 19, 27.
- HAGIWARA, S. I., ISHII, Y. & KITAMURA, S. 2000. Aerosolized administration of N-acetylcysteine attenuates lung fibrosis induced by bleomycin in mice. *Am J Respir Crit Care Med*, 162, 225-31.
- HAJI, A., OHI, Y. & TSUNEKAWA, S. 2008. N-methyl-D-aspartate mechanisms in depolarization of augmenting expiratory neurons during the expulsive phase of fictive cough in decerebrate cats. *Neuropharmacology*, 54, 1120-7.
- HALL, J. I., LOZANO, M., ESTRADA-PETROCELLI, L., BIRRING, S. & TURNER, R. 2020. The present and future of cough counting tools. *Journal of thoracic disease*, 12, 5207-5223.
- HALLGREN, J., ESTRADA, S., KARLSON, U., ALVING, K. & PEJLER, G. 2001. Heparin antagonists are potent inhibitors of mast cell tryptase. *Biochemistry*, 40, 7342-9.
- HAMANAKA, K., JIAN, M. Y., TOWNSLEY, M. I., KING, J. A., LIEDTKE, W., WEBER, D. S., EYAL, F. G., CLAPP, M. M. & PARKER, J. C. 2010. TRPV4 channels augment macrophage activation and ventilator-induced lung injury. *Am J Physiol Lung Cell Mol Physiol*, 299, L353-62.
- HAN, M. K., ZHOU, Y., MURRAY, S., TAYOB, N., NOTH, I., LAMA, V. N., MOORE, B. B., WHITE, E. S., FLAHERTY, K. R., HUFFNAGLE, G. B. & MARTINEZ, F. J. 2014. Lung microbiome and disease progression in idiopathic pulmonary fibrosis: an analysis of the COMET study. *Lancet Respir Med*, 2, 548-56.
- HANACEK, J., DAVIES, A. & WIDDICOMBE, J. G. 1984. Influence of lung stretch receptors on the cough reflex in rabbits. *Respiration*, 45, 161-8.
- HARRISON, N. K. 2004. Idiopathic pulmonary fibrosis: a nervous cough? *Pulm Pharmacol Ther*, 17, 347-50.
- HARRISON, N. K. 2013. Cough, sarcoidosis and idiopathic pulmonary fibrosis: raw nerves and bad vibrations. *Cough*, 9, 1-6.
- HASKELL, C. M., WONG, M., WILLIAMS, A. & LEE, L. Y. 1996. Phase I trial of extracellular adenosine 5'-triphosphate in patients with advanced cancer. *Med Pediatr Oncol*, 27, 165-73.
- HAY, J., SHAHZEIDI, S. & LAURENT, G. 1991. Mechanisms of bleomycin-induced lung damage. *Arch Toxicol*, 65, 81-94.
- HE, C., MURTHY, S., MCCORMICK, M. L., SPITZ, D. R., RYAN, A. J. & CARTER, A. B. 2011. Mitochondrial Cu,Zn-superoxide dismutase mediates pulmonary fibrosis by augmenting H<sub>2</sub>O<sub>2</sub> generation. *J Biol Chem*, 286, 15597-607.
- HE, S., GACA, M. D. & WALLS, A. F. 1998. A role for tryptase in the activation of human mast cells: modulation of histamine release by tryptase and inhibitors of tryptase. *J Pharmacol Exp Ther*, 286, 289-97.
- HE, S. H. & XIE, H. 2004. Modulation of tryptase secretion from human colon mast cells by histamine. *World J Gastroenterol*, 10, 323-6.
- HEIDENHAIN, M. 1915. Über die Mallorysche Bindegewebsfärbung mit Karmin und Azokarmin als Vorfarben. *Z. Wiss. Mikrosk.*, 32, 361-372.
- HENGSTERMANN, A. & MULLER, T. 2008. Endoplasmic reticulum stress induced by aqueous extracts of cigarette smoke in 3T3 cells activates the unfolded-protein-response-dependent PERK pathway of cell survival. *Free Radic Biol Med*, 44, 1097-107.
- HERTZ, M. I., WOODWARD, M. E., GROSS, C. R., SWART, M., MARCY, T. W. & BITTERMAN, P. B. 1991. Safety of bronchoalveolar lavage in the critically ill, mechanically ventilated patient. *Crit Care Med*, 19, 1526-32.
- HEUBERGER, D. M. & SCHUEPBACH, R. A. 2019. Protease-activated receptors (PARs): mechanisms of action and potential therapeutic modulators in PAR-driven inflammatory diseases. *Thromb J*, 17, 4.

- HIGASHIYAMA, H., YOSHIMOTO, D., KAISE, T., MATSUBARA, S., FUJIWARA, M., KIKKAWA, H., ASANO, S. & KINOSHITA, M. 2007. Inhibition of activin receptor-like kinase 5 attenuates bleomycin-induced pulmonary fibrosis. *Exp Mol Pathol*, 83, 39-46.
- HILTON, E., MARSDEN, P., THURSTON, A., KENNEDY, S., DECALMER, S. & SMITH, J. A. 2015. Clinical features of the urge-to-cough in patients with chronic cough. *Respir Med*, 109, 701-7.
- HILTON, E. C., BAVEREL, P. G., WOODCOCK, A., VAN DER GRAAF, P. H. & SMITH, J. A. 2013. Pharmacodynamic modeling of cough responses to capsaicin inhalation calls into question the utility of the C5 end point. *J Allergy Clin Immunol*, 132, 847-55 e1-5.
- HIRATA, R., NABE, T. & KOHNO, S. 2003. Augmentation of spontaneous cough by enalapril through up-regulation of bradykinin B1 receptors in guinea pigs. *Eur J Pharmacol*, 474, 255-60.
- HOLDINESS, M. R. 1991. Clinical pharmacokinetics of N-acetylcysteine. *Clin Pharmacokinet*, 20, 123-34.
- HOMMA, S., AZUMA, A., TANIGUCHI, H., OGURA, T., MOCHIDUKI, Y., SUGIYAMA, Y., NAKATA, K., YOSHIMURA, K., TAKEUCHI, M., KUDOH, S. & JAPAN, N. A. C. C. S. G. 2012. Efficacy of inhaled N-acetylcysteine monotherapy in patients with early stage idiopathic pulmonary fibrosis. *Respirology*, 17, 467-77.
- HOPE-GILL, B. D., HILLDRUP, S., DAVIES, C., NEWTON, R. P. & HARRISON, N. K. 2003. A study of the cough reflex in idiopathic pulmonary fibrosis. *Am J Respir Crit Care Med*, 168, 995-1002.
- HUANG, W.-T., AKHTER, H., JIANG, C., MACEWEN, M., DING, Q., ANTONY, V., THANNICKAL, V. J. & LIU, R.-M. 2015. Plasminogen activator inhibitor 1, fibroblast apoptosis resistance, and aging-related susceptibility to lung fibrosis. *Experimental gerontology*, 61, 62-75.
- HUBNER, R. H., GITTER, W., EL MOKHTARI, N. E., MATHIAK, M., BOTH, M., BOLTE, H., FREITAG-WOLF, S. & BEWIG, B. 2008. Standardized quantification of pulmonary fibrosis in histological samples. *Biotechniques*, 44, 507-11, 514-7.
- HUNG, C., LINN, G., CHOW, Y. H., KOBAYASHI, A., MITTELSTADT, K., ALTEMEIER, W. A., GHARIB, S. A., SCHNAPP, L. M. & DUFFIELD, J. S. 2013. Role of lung pericytes and resident fibroblasts in the pathogenesis of pulmonary fibrosis. *Am J Respir Crit Care Med*, 188, 820-30.
- HUNT, L. W., COLBY, T. V., WEILER, D. A., SUR, S. & BUTTERFIELD, J. H. 1992. Immunofluorescent staining for mast cells in idiopathic pulmonary fibrosis: quantification and evidence for extracellular release of mast cell tryptase. *Mayo Clin Proc*, 67, 941-8.
- HUTCHINSON, J., FOGARTY, A., HUBBARD, R. & MCKEEVER, T. 2015. Global incidence and mortality of idiopathic pulmonary fibrosis: a systematic review. *Eur Respir J*, 46, 795-806.
- IDZKO, M., HAMMAD, H., VAN NIMWEGEN, M., KOOL, M., WILLART, M. A., MUSKENS, F., HOOGSTEDEN, H. C., LUTTMANN, W., FERRARI, D., DI VIRGILIO, F., VIRCHOW, J. C., JR. & LAMBRECHT, B. N. 2007. Extracellular ATP triggers and maintains asthmatic airway inflammation by activating dendritic cells. *Nat Med*, 13, 913-9.
- IRVING, W. L., DAY, S. & JOHNSTON, I. D. 1993. Idiopathic pulmonary fibrosis and hepatitis C virus infection. *Am Rev Respir Dis*, 148, 1683-4.
- IRWIN, R. S. 2006a. Chronic cough due to gastroesophageal reflux disease: ACCP evidence-based clinical practice guidelines. *Chest*, 129, 80s-94s.
- IRWIN, R. S. 2006b. Introduction to the diagnosis and management of cough: ACCP evidence-based clinical practice guidelines. *Chest*, 129, 25s-27s.
- IRWIN, R. S., BOULET, L. P., CLOUTIER, M. M., FULLER, R., GOLD, P. M., HOFFSTEIN, V., ING, A. J., MCCOOL, F. D., O'BYRNE, P., POE, R. H., PRAKASH, U. B., PRATTER, M. R. & RUBIN, B. K. 1998. Managing cough as a defense mechanism and as a symptom. A consensus panel report of the American College of Chest Physicians. *Chest*, 114, 133S-181S.
- IRWIN, R. S., CORRAO, W. M. & PRATTER, M. R. 1981. Chronic persistent cough in the adult: the spectrum and frequency of causes and successful outcome of specific therapy. *Am Rev Respir Dis*, 123, 413-7.

- IRWIN, R. S., CURLEY, F. J. & FRENCH, C. L. 1990. Chronic cough. The spectrum and frequency of causes, key components of the diagnostic evaluation, and outcome of specific therapy. *Am Rev Respir Dis*, 141, 640-7.
- IRWIN, R. S., ROSEN, M. J. & BRAMAN, S. S. 1977. Cough: A Comprehensive Review. *Archives of Internal Medicine*, 137, 1186-1191.
- ISLER, J. A., SKALET, A. H. & ALWINE, J. C. 2005. Human cytomegalovirus infection activates and regulates the unfolded protein response. *J Virol*, 79, 6890-9.
- JACKSON, R., RAMOS, C., GUPTA, C. & GOMEZ-MARIN, O. 2010. Exercise decreases plasma antioxidant capacity and increases urinary isoprostanes of IPF patients. *Respir Med*, 104, 1919-28.
- JAKUS, J., POLIACEK, I., HALASOVA, E., MURIN, P., KNOCIKOVA, J., TOMORI, Z. & BOLSER, D. C. 2008. Brainstem circuitry of tracheal-bronchial cough: c-fos study in anesthetized cats. *Respir Physiol Neurobiol*, 160, 289-300.
- JANSON, C., CHINN, S., JARVIS, D. & BURNEY, P. 2001. Determinants of cough in young adults participating in the European Community Respiratory Health Survey. *Eur Respir J*, 18, 647-54.
- JIANG, H., JU, Z. & RUDOLPH, K. L. 2007. Telomere shortening and ageing. *Z Gerontol Geriatr*, 40, 314-24.
- JONA, A., MILTENYI, Z., POLISKA, S., BALINT, B. L. & ILLES, A. 2016. Effect of Bleomycin Hydrolase Gene Polymorphism on Late Pulmonary Complications of Treatment for Hodgkin Lymphoma. *PLoS One*, 11, e0157651.
- JONES, R. M., HILLDRUP, S., HOPE-GILL, B. D., ECCLES, R. & HARRISON, N. K. 2011. Mechanical induction of cough in Idiopathic Pulmonary Fibrosis. *Cough*, 7, 2.
- JULES-ELYSEE, K. & WHITE, D. A. 1990. Bleomycin-induced pulmonary toxicity. *Clin Chest Med*, 11, 1-20.
- KACZMAREK, E., KOZIAK, K., SEVIGNY, J., SIEGEL, J. B., ANRATHER, J., BEAUDOIN, A. R., BACH, F. H. & ROBSON, S. C. 1996. Identification and characterization of CD39/vascular ATP diphosphohydrolase. *J Biol Chem*, 271, 33116-22.
- KAHRILAS, P. J., HOWDEN, C. W., HUGHES, N. & MOLLOY-BLAND, M. 2013. Response of chronic cough to acid-suppressive therapy in patients with gastroesophageal reflux disease. *Chest*, 143, 605-612.
- KAJEKAR, R., PROUD, D., MYERS, A. C., MEEKER, S. N. & UNDEM, B. J. 1999. Characterization of vagal afferent subtypes stimulated by bradykinin in guinea pig trachea. *J Pharmacol Exp Ther*, 289, 682-7.
- KALLENBERG, C. G., SCHILIZZI, B. M., BEAUMONT, F., DE LEIJ, L., POPPEMA, S. & THE, T. H. 1987. Expression of class II major histocompatibility complex antigens on alveolar epithelium in interstitial lung disease: relevance to pathogenesis of idiopathic pulmonary fibrosis. *J Clin Pathol*, 40, 725-33.
- KAMEI, J., IWAMOTO, Y., SUZUKI, T., MISAWA, M., NAGASE, H. & KASUYA, Y. 1993. Antitussive effects of naltrindole, a selective delta-opioid receptor antagonist, in mice and rats. *Eur J Pharmacol*, 249, 161-5.
- KANO, S., KOBAYASHI, H. & MOTOYOSHI, K. 2005. Exhaled ethane: an in vivo biomarker of lipid peroxidation in interstitial lung diseases. *Chest*, 128, 2387-92.
- KARLSSON, J. A. & FULLER, R. W. 1999. Pharmacological regulation of the cough reflex--from experimental models to antitussive effects in Man. *Pulm Pharmacol Ther*, 12, 215-28.
- KASPER, M. & HAROSKE, G. 1996. Alterations in the alveolar epithelium after injury leading to pulmonary fibrosis. *Histol Histopathol*, 11, 463-83.
- KAWANAMI, O., FERRANS, V. J. & CRYSTAL, R. G. 1982. Structure of alveolar epithelial cells in patients with fibrotic lung disorders. *Lab Invest*, 46, 39-53.
- KAWATANI, K., KONDO, M., TAMAOKI, J., TAGAYA, E. & NAGAI, A. 2007. [The clinical significance of mast cell tryptase in bronchial alveolar lavage fluid in interstitial lung diseases]. *Nihon Kokyuki Gakkai Zasshi*, 45, 848-55.

- KELSALL, A., DECALMER, S., MCGUINNESS, K., WOODCOCK, A. & SMITH, J. A. 2009. Sex differences and predictors of objective cough frequency in chronic cough. *Thorax*, 64, 393-8.
- KEY, A. L., HOLT, K., HAMILTON, A., SMITH, J. A. & EARIS, J. E. 2010. Objective cough frequency in Idiopathic Pulmonary Fibrosis. *Cough*, 6, 4.
- KILDUFF, C. E., COUNTER, M. J., THOMAS, G. A., HARRISON, N. K. & HOPE-GILL, B. D. 2014. Effect of acid suppression therapy on gastroesophageal reflux and cough in idiopathic pulmonary fibrosis: an intervention study. *Cough*, 10, 4.
- KILKENNY, C., BROWNE, W. J., CUTHILL, I. C., EMERSON, M. & ALTMAN, D. G. 2010. Improving bioscience research reporting: The ARRIVE guidelines for reporting animal research. *J Pharmacol Pharmacother*, 1, 94-9.
- KINDER, B. W., BROWN, K. K., SCHWARZ, M. I., IX, J. H., KERVITSKY, A. & KING, T. E., JR. 2008. Baseline BAL neutrophilia predicts early mortality in idiopathic pulmonary fibrosis. *Chest*, 133, 226-32.
- KINNULA, V. L., FATTMAN, C. L., TAN, R. J. & OURY, T. D. 2005. Oxidative stress in pulmonary fibrosis: a possible role for redox modulatory therapy. *Am J Respir Crit Care Med*, 172, 417-22.
- KINNULA, V. L., HODGSON, U. A., LAKARI, E. K., TAN, R. J., SORMUNEN, R. T., SOINI, Y. M., KAKKO, S. J., LAITINEN, T. H., OURY, T. D. & PAAKKO, P. K. 2006. Extracellular superoxide dismutase has a highly specific localization in idiopathic pulmonary fibrosis/usual interstitial pneumonia. *Histopathology*, 49, 66-74.
- KITSIOS, G. D., ROJAS, M., KASS, D. J., FITCH, A., SEMBRAT, J. C., QIN, S., VERALDI, K. L., GIBSON, K. F., LINDELL, K., PILEWSKI, J. M., METHE, B., LI, K., MCDYER, J., MCVERRY, B. J. & MORRIS, A. 2018. Microbiome in lung explants of idiopathic pulmonary fibrosis: a case-control study in patients with end-stage fibrosis. *Thorax*, 73, 481-484.
- KLIMENT, C. R. & OURY, T. D. 2010. Oxidative stress, extracellular matrix targets, and idiopathic pulmonary fibrosis. *Free Radic Biol Med*, 49, 707-17.
- KOHROGI, H., GRAF, P. D., SEKIZAWA, K., BORSON, D. B. & NADEL, J. A. 1988. Neutral endopeptidase inhibitors potentiate substance P- and capsaicin-induced cough in awake guinea pigs. *J Clin Invest*, 82, 2063-8.
- KÖNIGSHOFF, M., KRAMER, M., BALSARA, N., WILHELM, J., AMARIE, O. V., JAHN, A., ROSE, F., FINK, L., SEEGER, W., SCHAEFER, L., GÜNTHER, A. & EICKELBERG, O. 2009. WNT1-inducible signaling protein-1 mediates pulmonary fibrosis in mice and is upregulated in humans with idiopathic pulmonary fibrosis. *The Journal of Clinical Investigation*, 119, 772-787.
- KORFEI, M., RUPPERT, C., MAHAVADI, P., HENNEKE, I., MARKART, P., KOCH, M., LANG, G., FINK, L., BOHLE, R. M., SEEGER, W., WEAVER, T. E. & GUENTHER, A. 2008. Epithelial endoplasmic reticulum stress and apoptosis in sporadic idiopathic pulmonary fibrosis. *Am J Respir Crit Care Med*, 178, 838-46.
- KOSKELA, H. O., KONTRA, K. M., PUROKIVI, M. K. & RANDELL, J. T. 2005. Interpretation of cough provoked by airway challenges. *Chest*, 128, 3329-35.
- KOSMIDER, B., MESSIER, E. M., CHU, H. W. & MASON, R. J. 2011. Human alveolar epithelial cell injury induced by cigarette smoke. *PLoS One*, 6, e26059.
- KRAUSS, E., FROEHLER, M., DEGEN, M., MAHAVADI, P., DARTSCH, R. C., KORFEI, M., RUPPERT, C., SEEGER, W. & GUENTHER, A. 2019. Exhalative Breath Markers Do Not Offer for Diagnosis of Interstitial Lung Diseases: Data from the European IPF Registry (eurIPFreg) and Biobank. *J Clin Med*, 8.
- KROPSKI, J. A., BLACKWELL, T. S. & LOYD, J. E. 2015a. The genetic basis of idiopathic pulmonary fibrosis. *Eur Respir J*, 45, 1717-27.
- KROPSKI, J. A., PRITCHETT, J. M., ZOZ, D. F., CROSSNO, P. F., MARKIN, C., GARNETT, E. T., DEGRYSE, A. L., MITCHELL, D. B., POLOSUKHIN, V. V., RICKMAN, O. B., CHOI, L., CHENG, D.-S., MCCONAHA, M. E., JONES, B. R., GLEAVES, L. A., MCMAHON, F. B., WORRELL, J. A., SOLUS, J. F., WARE, L. B., LEE, J. W., MASSION, P. P., ZAYNAGETDINOV, R., WHITE, E. S., KURTIS, J. D., JOHNSON, J. E., GROSHONG, S. D., LANCASTER, L. H., YOUNG, L. R., STEELE, M. P., III, J. A. P.,



- COGAN, J. D., LOYD, J. E., LAWSON, W. E. & BLACKWELL, T. S. 2015b. Extensive Phenotyping of Individuals at Risk for Familial Interstitial Pneumonia Reveals Clues to the Pathogenesis of Interstitial Lung Disease. *American Journal of Respiratory and Critical Care Medicine*, 191, 417-426.
- KUWANO, K., NOMOTO, Y., KUNITAKE, R., HAGIMOTO, N., MATSUBA, T., NAKANISHI, Y. & HARA, N. 1997. Detection of adenovirus E1A DNA in pulmonary fibrosis using nested polymerase chain reaction. *Eur Respir J*, 10, 1445-9.
- KVAPILOVA, L., BOZA, V., DUBEC, P., MAJERNIK, M., BOGAR, J., JAMISON, J., GOLDSACK, J. C., KIMMEL, D. J. & KARLIN, D. R. 2019. Continuous Sound Collection Using Smartphones and Machine Learning to Measure Cough. *Digit Biomark*, 3, 166-175.
- KWONG, K., KOLLARIK, M., NASSENSTEIN, C., RU, F. & UNDEM, B. J. 2008. P2X2 receptors differentiate placodal vs. neural crest C-fiber phenotypes innervating guinea pig lungs and esophagus. *Am J Physiol Lung Cell Mol Physiol*, 295, L858-65.
- LALLOO, U. G., FOX, A. J., BELVISI, M. G., CHUNG, K. F. & BARNES, P. J. 1995. Capsazepine inhibits cough induced by capsaicin and citric acid but not by hypertonic saline in guinea pigs. *J Appl Physiol (1985)*, 79, 1082-7.
- LANCASTER, L., CRESTANI, B., HERNANDEZ, P., INOUE, Y., WACHTLIN, D., LOAIZA, L., QUARESMA, M., STOWASSER, S. & RICHELDI, L. 2019. Safety and survival data in patients with idiopathic pulmonary fibrosis treated with nintedanib: pooled data from six clinical trials. *BMJ Open Respir Res*, 6, e000397.
- LARSON, S., COMINA, G., GILMAN, R. H., TRACEY, B. H., BRAVARD, M. & LOPEZ, J. W. 2012. Validation of an automated cough detection algorithm for tracking recovery of pulmonary tuberculosis patients. *PLoS One*, 7, e46229.
- LASITHIOTAKI, I., ANTONIOU, K. M., VLAHAVA, V. M., KARAGIANNIS, K., SPANDIDOS, D. A., SIAFAKAS, N. M. & SOURVINOS, G. 2011. Detection of herpes simplex virus type-1 in patients with fibrotic lung diseases. *PLoS One*, 6, e27800.
- LAUDE, E. A., HIGGINS, K. S. & MORICE, A. H. 1993. A comparative study of the effects of citric acid, capsaicin and resiniferatoxin on the cough challenge in guinea-pig and man. *Pulm Pharmacol*, 6, 171-5.
- LAWHORN, B. G., BRNARDIC, E. J. & BEHM, D. J. 2020. Recent advances in TRPV4 agonists and antagonists. *Bioorg Med Chem Lett*, 30, 127022.
- LAWSON, W. E., CHENG, D.-S., DEGRYSE, A. L., TANJORE, H., POLOSUKHIN, V. V., XU, X. C., NEWCOMB, D. C., JONES, B. R., ROLDAN, J., LANE, K. B., MORRISEY, E. E., BEERS, M. F., YULL, F. E. & BLACKWELL, T. S. 2011. Endoplasmic reticulum stress enhances fibrotic remodeling in the lungs. *Proceedings of the National Academy of Sciences*, 108, 10562-10567.
- LAWSON, W. E., CROSSNO, P. F., POLOSUKHIN, V. V., ROLDAN, J., CHENG, D. S., LANE, K. B., BLACKWELL, T. R., XU, C., MARKIN, C., WARE, L. B., MILLER, G. G., LOYD, J. E. & BLACKWELL, T. S. 2008. Endoplasmic reticulum stress in alveolar epithelial cells is prominent in IPF: association with altered surfactant protein processing and herpesvirus infection. *Am J Physiol Lung Cell Mol Physiol*, 294, L1119-26.
- LAWSON, W. E., GRANT, S. W., AMBROSINI, V., WOMBLE, K. E., DAWSON, E. P., LANE, K. B., MARKIN, C., RENZONI, E., LYMPANY, P., THOMAS, A. Q., ROLDAN, J., SCOTT, T. A., BLACKWELL, T. S., PHILLIPS, J. A., 3RD, LOYD, J. E. & DU BOIS, R. M. 2004. Genetic mutations in surfactant protein C are a rare cause of sporadic cases of IPF. *Thorax*, 59, 977-80.
- LEACH, H. G., CHROBAK, I., HAN, R. & TROJANOWSKA, M. 2013. Endothelial cells recruit macrophages and contribute to a fibrotic milieu in bleomycin lung injury. *Am J Respir Cell Mol Biol*, 49, 1093-101.
- LECHTZIN, N., HILLIARD, M. E. & HORTON, M. R. 2013. Validation of the Cough Quality-of-Life Questionnaire in Patients With Idiopathic Pulmonary Fibrosis. *Chest*, 143, 1745-1749.
- LEDERER, D. J. & MARTINEZ, F. J. 2018. Idiopathic Pulmonary Fibrosis. *N Engl J Med*, 378, 1811-1823.

- LEE, H. L., RYU, J. H., WITTMER, M. H., HARTMAN, T. E., LYMP, J. F., TAZELAAR, H. D. & LIMPER, A. H. 2005. Familial idiopathic pulmonary fibrosis: clinical features and outcome. *Chest*, 127, 2034-41.
- LEE, L. Y. & PISARRI, T. E. 2001. Afferent properties and reflex functions of bronchopulmonary C-fibers. *Respir Physiol*, 125, 47-65.
- LEE, W., CHUNG, W. S., HONG, K.-S. & HUH, J. 2015. Clinical usefulness of bronchoalveolar lavage cellular analysis and lymphocyte subsets in diffuse interstitial lung diseases. *Annals of laboratory medicine*, 35, 220-225.
- LEE, W. C., CHIANG, P. H., TAIN, Y. L., WU, C. C. & CHUANG, Y. C. 2012. Sensory dysfunction of bladder mucosa and bladder oversensitivity in a rat model of metabolic syndrome. *PLoS One*, 7, e45578.
- LEE, Y. J., CHOI, S. M., LEE, Y. J., CHO, Y. J., YOON, H. I., LEE, J. H., LEE, C. T. & PARK, J. S. 2017. Clinical impact of depression and anxiety in patients with idiopathic pulmonary fibrosis. *PLoS One*, 12, e0184300.
- LENZ, A. G., COSTABEL, U. & MAIER, K. L. 1996. Oxidized BAL fluid proteins in patients with interstitial lung diseases. *Eur Respir J*, 9, 307-12.
- LEWIS, C. A., AMBROSE, C., BANNER, K., BATTRAM, C., BUTLER, K., GIDDINGS, J., MOK, J., NASRA, J., WINNY, C. & POLL, C. 2007. Animal models of cough: Literature review and presentation of a novel cigarette smoke-enhanced cough model in the guinea-pig. *Pulmonary Pharmacology & Therapeutics*, 20, 325-333.
- LIANG, J., ZHANG, Y., XIE, T., LIU, N., CHEN, H., GENG, Y., KURKCIYAN, A., MENA, J. M., STRIPP, B. R., JIANG, D. & NOBLE, P. W. 2016. Hyaluronan and TLR4 promote surfactant-protein-C-positive alveolar progenitor cell renewal and prevent severe pulmonary fibrosis in mice. *Nature Medicine*, 22, 1285-1293.
- LIEDTKE, W., CHOE, Y., MARTI-RENOM, M. A., BELL, A. M., DENIS, C. S., SALI, A., HUDSPETH, A. J., FRIEDMAN, J. M. & HELLER, S. 2000. Vanilloid receptor-related osmotically activated channel (VR-OAC), a candidate vertebrate osmoreceptor. *Cell*, 103, 525-35.
- LIENKAMP, A. C., HEINE, T. & TISCHLER, D. 2020. Chapter Five - Glutathione: A powerful but rare cofactor among Actinobacteria. In: GADD, G. M. & SARIASLANI, S. (eds.) *Advances in Applied Microbiology*. Academic Press.
- LIN, C., VON DER THUSEN, J., DAALHUISEN, J., TEN BRINK, M., CRESTANI, B., VAN DER POLL, T., BORENSZTAJN, K. & SPEK, C. A. 2015a. Pharmacological Targeting of Protease-Activated Receptor 2 Affords Protection from Bleomycin-Induced Pulmonary Fibrosis. *Mol Med*, 21, 576-83.
- LIN, C., VON DER THUSEN, J., DAALHUISEN, J., TEN BRINK, M., CRESTANI, B., VAN DER POLL, T., BORENSZTAJN, K. & SPEK, C. A. 2015b. Protease-activated receptor (PAR)-2 is required for PAR-1 signalling in pulmonary fibrosis. *J Cell Mol Med*, 19, 1346-56.
- LIU, F., MIH, J. D., SHEA, B. S., KHO, A. T., SHARIF, A. S., TAGER, A. M. & TSCHUMPERLIN, D. J. 2010. Feedback amplification of fibrosis through matrix stiffening and COX-2 suppression. *Journal of Cell Biology*, 190, 693-706.
- LOMMATZSCH, M., CICKO, S., MULLER, T., LUCATELLI, M., BRATKE, K., STOLL, P., GRIMM, M., DURK, T., ZISSEL, G., FERRARI, D., DI VIRGILIO, F., SORICHTER, S., LUNGARELLA, G., VIRCHOW, J. C. & IDZKO, M. 2010. Extracellular adenosine triphosphate and chronic obstructive pulmonary disease. *Am J Respir Crit Care Med*, 181, 928-34.
- LORENZO, I. M., LIEDTKE, W., SANDERSON, M. J. & VALVERDE, M. A. 2008. TRPV4 channel participates in receptor-operated calcium entry and ciliary beat frequency regulation in mouse airway epithelial cells. *Proc Natl Acad Sci U S A*, 105, 12611-6.
- LOWRY, R. H., WOOD, A. M. & HIGENBOTTAM, T. W. 1988. Effects of pH and osmolarity on aerosol-induced cough in normal volunteers. *Clin Sci (Lond)*, 74, 373-6.
- LUDBROOK, V., HANROTT, K., MARKS-KONCZALIK, J., KREINDLER, J., BIRD, N., HEWENS, D., BEERAHEE, M., BEHM, D., MORICE, A. & MCGARVEY, L. 2019. S27 A placebo-controlled,

- double-blind, randomised, crossover study to assess the efficacy, safety and tolerability of TRPV4 inhibitor GSK2798745 in participants with chronic cough. *Thorax*, 74, A18.
- MACKENZIE, A. J., SPINA, D. & PAGE, C. P. 2004. Models used in the development of antitussive drugs. *Drug Discovery Today: Disease Models*, 1, 297-302.
- MACNEE, W. & RAHMAN, I. 1995. Oxidants/antioxidants in idiopathic pulmonary fibrosis. *Thorax*, 50 Suppl 1, S53-8.
- MADISON, J. M. & IRWIN, R. S. 2005. Chronic cough in adults with interstitial lung disease. *Curr Opin Pulm Med*, 11, 412-6.
- MAHER, S., BIRRELL, M., BAKER, K., RAEMDONCK, K., BONVINI, S., ADCOCK, J., WORTLEY, M., DUBUIS, E., SHALA, F., JONES, V., BARNES, P., THENNATI, R., SAMANTA, B., DESAI, D., KUMBHANI, A. & BELVISI, M. 2015. Cromoglycate: Breathing life into an old asthma drug. *European Respiratory Journal*, 46, PA1017.
- MAHER, S. A. & BELVISI, M. G. 2010. Prostanoids and the cough reflex. *Lung*, 188 Suppl 1, S9-12.
- MAHER, S. A., BIRRELL, M. A. & BELVISI, M. G. 2009. Prostaglandin E2 mediates cough via the EP3 receptor: implications for future disease therapy. *Am J Respir Crit Care Med*, 180, 923-8.
- MAHER, T. M. 2013. PROFILEing idiopathic pulmonary fibrosis: rethinking biomarker discovery. *European Respiratory Review*, 22, 148-152.
- MALLI, F., BARDAKA, F., TSILIONI, I., KARETSI, E., GOURGOULIANIS, K. I. & DANIL, Z. 2013. 8-isoprostane levels in serum and bronchoalveolar lavage in idiopathic pulmonary fibrosis and sarcoidosis. *Food Chem Toxicol*, 61, 160-3.
- MANOURY, B., NENAN, S., LECLERC, O., GUENON, I., BOICHOT, E., PLANQUOIS, J. M., BERTRAND, C. P. & LAGENTE, V. 2005. The absence of reactive oxygen species production protects mice against bleomycin-induced pulmonary fibrosis. *Respir Res*, 6, 11.
- MARKART, P., RUPPERT, C., WYGRECKA, M., SCHMIDT, R., KORFEI, M., HARBACH, H., THERUVATH, I., PISON, U., SEEGER, W., GUENTHER, A. & WITT, H. 2007. Surfactant protein C mutations in sporadic forms of idiopathic interstitial pneumonias. *Eur Respir J*, 29, 134-7.
- MARSDEN, P. A., SATIA, I., IBRAHIM, B., WOODCOCK, A., YATES, L., DONNELLY, I., JOLLY, L., THOMSON, N. C., FOWLER, S. J. & SMITH, J. A. 2016. Objective Cough Frequency, Airway Inflammation, and Disease Control in Asthma. *Chest*, 149, 1460-6.
- MARTINEZ, F. J., AFZAL, A., KITT, M. M., FORD, A., LI, J. J., LI, Y.-P. & SMITH, J. 2019. The Treatment of Chronic Cough in Idiopathic Pulmonary Fibrosis Patients with Gefapixant, a P2x3 Receptor Antagonist. *American Journal of Respiratory and Critical Care Medicine*, 199, A2638-A2638.
- MARTINEZ, F. J., CHISHOLM, A., COLLARD, H. R., FLAHERTY, K. R., MYERS, J., RAGHU, G., WALSH, S. L., WHITE, E. S. & RICHELDI, L. 2017. The diagnosis of idiopathic pulmonary fibrosis: current and future approaches. *Lancet Respir Med*, 5, 61-71.
- MARTINEZ, F. J., DE ANDRADE, J. A., ANSTROM, K. J., KING, T. E., JR. & RAGHU, G. 2014. Randomized trial of acetylcysteine in idiopathic pulmonary fibrosis. *N Engl J Med*, 370, 2093-101.
- MATTHEWS, D. 2020. BELLUS Health Announces Topline Results from its Phase 2 RELIEF Trial of BLU-5937 for the Treatment of Refractory Chronic Cough. BELLUS Health Inc.
- MAZZONE, S. B. 2004. Sensory regulation of the cough reflex. *Pulm Pharmacol Ther*, 17, 361-8.
- MAZZONE, S. B., CANNING, B. J. & WIDDICOMBE, J. G. 2003. Sensory Pathways for the Cough Reflex. *Cough: Causes, Mechanisms and Therapy*.
- MAZZONE, S. B., MCGOVERN, A. E., COLE, L. J. & FARRELL, M. J. 2011. Central nervous system control of cough: pharmacological implications. *Curr Opin Pharmacol*, 11, 265-71.
- MCANULTY, R. J. 2007. Fibroblasts and myofibroblasts: Their source, function and role in disease. *The International Journal of Biochemistry & Cell Biology*, 39, 666-671.
- MCGARVEY, L., BIRRING, S., MORICE, A., DICPINIGAITIS, P., PAVORD, I., SCHELFHOUT, J., MARTIN NGUYEN, A., LI, Q., TZONTCHEVA, A., ISKOLD, B., GREEN, S., LA ROSA, C., MUCCINO, D. & SMITH, J. 2020. Late Breaking Abstract - Two Phase 3 Randomized Clinical Trials of Gefapixant, a P2X3 Receptor Antagonist, in Refractory or Unexplained Chronic Cough (COUGH-1 and COUGH-2). *European Respiratory Journal*, 56, 3800.

- MCGARVEY, L., MCKEAGNEY, P., POLLEY, L., MACMAHON, J. & COSTELLO, R. W. 2009. Are there clinical features of a sensitized cough reflex? *Pulm Pharmacol Ther*, 22, 59-64.
- MCGARVEY, L. P., CARTON, C., GAMBLE, L. A., HEANEY, L. G., SHEPHERD, R., ENNIS, M. & MACMAHON, J. 2006. Prevalence of psych morbidity among patients with chronic cough. *Cough*, 2, 4.
- MCGARVEY, L. P., HEANEY, L. G., LAWSON, J. T., JOHNSTON, B. T., SCALLY, C. M., ENNIS, M., SHEPHERD, D. R. & MACMAHON, J. 1998. Evaluation and outcome of patients with chronic non-productive cough using a comprehensive diagnostic protocol. *Thorax*, 53, 738-43.
- MCGUIRE, J. J., SAIFEDDINE, M., TRIGGLE, C. R., SUN, K. & HOLLENBERG, M. D. 2004. 2-furoyl-LIGRLO-amide: a potent and selective proteinase-activated receptor 2 agonist. *J Pharmacol Exp Ther*, 309, 1124-31.
- MELONI, F., CAPORALI, R., MARONE BIANCO, A., PASCHETTO, E., MOROSINI, M., FIETTA, A. M., PATRIZIO, V., BOBBIO-PALLAVICINI, F., POZZI, E. & MONTECUCCO, C. 2004. BAL cytokine profile in different interstitial lung diseases: a focus on systemic sclerosis. *Sarcoidosis Vasc Diffuse Lung Dis*, 21, 111-8.
- MERCK 2020. Merck's Gefapixant (45 mg Twice Daily) Significantly Decreased Cough Frequency Compared to Placebo at Week 12 and 24 in Patients with Refractory or Unexplained Chronic Cough. Merck.com: Merck.
- MEYER, K. C., RAGHU, G., BAUGHMAN, R. P., BROWN, K. K., COSTABEL, U., DU BOIS, R. M., DRENT, M., HASLAM, P. L., KIM, D. S., NAGAI, S., ROTTOLI, P., SALTINI, C., SELMAN, M., STRANGE, C., WOOD, B. & AMERICAN THORACIC SOCIETY COMMITTEE ON, B. A. L. I. I. L. D. 2012. An official American Thoracic Society clinical practice guideline: the clinical utility of bronchoalveolar lavage cellular analysis in interstitial lung disease. *Am J Respir Crit Care Med*, 185, 1004-14.
- MILES, J. H. A., DUBUIS, E., BONVINI, S. J., WORTLEY, M. A., TREVISANI, M., VILLETTI, G., PATAcCHINI, R., BIRRELL, M. & BELVISI, M. G. 2019. Monitoring Cough in a Preclinical Guinea Pig Model of Idiopathic Pulmonary Fibrosis. *American Journal of Respiratory and Critical Care Medicine*, 199, A5430-A5430.
- MILLEA, P. J. 2009. N-acetylcysteine: multiple clinical applications. *Am Fam Physician*, 80, 265-9.
- MISRA, H. P. & RABIDEAU, C. 2000. Pirfenidone inhibits NADPH-dependent microsomal lipid peroxidation and scavenges hydroxyl radicals. *Mol Cell Biochem*, 204, 119-26.
- MOELLER, A., ASK, K., WARBURTON, D., GAULDIE, J. & KOLB, M. 2008. The bleomycin animal model: a useful tool to investigate treatment options for idiopathic pulmonary fibrosis? *Int J Biochem Cell Biol*, 40, 362-82.
- MOLINO, M., BARNATHAN, E. S., NUMEROF, R., CLARK, J., DREYER, M., CUMASHI, A., HOXIE, J. A., SCHECHTER, N., WOOLKALIS, M. & BRASS, L. F. 1997. Interactions of mast cell tryptase with thrombin receptors and PAR-2. *J Biol Chem*, 272, 4043-9.
- MOLYNEAUX, P. L., COX, M. J., WILLIS-OWEN, S. A., MALLIA, P., RUSSELL, K. E., RUSSELL, A. M., MURPHY, E., JOHNSTON, S. L., SCHWARTZ, D. A., WELLS, A. U., COOKSON, W. O., MAHER, T. M. & MOFFATT, M. F. 2014. The role of bacteria in the pathogenesis and progression of idiopathic pulmonary fibrosis. *Am J Respir Crit Care Med*, 190, 906-13.
- MOLYNEAUX, P. L. & MAHER, T. M. 2013. The role of infection in the pathogenesis of idiopathic pulmonary fibrosis. *European Respiratory Review*, 22, 376-381.
- MOLYNEAUX, P. L., SMITH, J. J., SAUNDERS, P., CHUA, F., WELLS, A. U., RENZONI, E. A., NICHOLSON, A. G., FAHY, W. A., JENKINS, R. G. & MAHER, T. M. 2020. Bronchoalveolar Lavage is Safe and Well Tolerated in Individuals with Idiopathic Pulmonary Fibrosis: An Analysis of the PROFILE Study. *American Journal of Respiratory and Critical Care Medicine*, 0, null.
- MONTELL, C. & RUBIN, G. M. 1989. Molecular characterization of the drosophila trp locus: A putative integral membrane protein required for phototransduction. *Neuron*, 2, 1313-1323.

- MONTUSCHI, P., CIABATTONI, G., PAREDI, P., PANTELIDIS, P., DU BOIS, R. M., KHARITONOV, S. A. & BARNES, P. J. 1998. 8-Isoprostane as a biomarker of oxidative stress in interstitial lung diseases. *Am J Respir Crit Care Med*, 158, 1524-7.
- MOORE, B., LAWSON, W. E., OURY, T. D., SISSON, T. H., RAGHAVENDRAN, K. & HOGABOAM, C. M. 2013. Animal models of fibrotic lung disease. *Am J Respir Cell Mol Biol*, 49, 167-79.
- MOORE, B. B., PAINE, R., 3RD, CHRISTENSEN, P. J., MOORE, T. A., SITTERDING, S., NGAN, R., WILKE, C. A., KUZIEL, W. A. & TOEWS, G. B. 2001. Protection from pulmonary fibrosis in the absence of CCR2 signaling. *J Immunol*, 167, 4368-77.
- MOREAUX, B., NEMMAR, A., VINCKE, G., HALLOY, D., BEERENS, D., ADVENIER, C. & GUSTIN, P. 2000. Role of substance P and tachykinin receptor antagonists in citric acid-induced cough in pigs. *Eur J Pharmacol*, 408, 305-12.
- MORICE, A. H. 2004. Post-nasal drip syndrome—a symptom to be sniffed at? *Pulmonary Pharmacology & Therapeutics*, 17, 343-345.
- MORICE, A. H. 2017. TRPA1 receptors in chronic cough. *Pulm Pharmacol Ther*, 47, 42-44.
- MORICE, A. H., FONTANA, G. A., BELVISI, M. G., BIRRING, S. S., CHUNG, K. F., DICPINIGAITIS, P. V., KASTELIK, J. A., MCGARVEY, L. P., SMITH, J. A., TATAR, M., WIDDICOMBE, J. & EUROPEAN RESPIRATORY, S. 2007. ERS guidelines on the assessment of cough. *Eur Respir J*, 29, 1256-76.
- MORICE, A. H., JAKES, A. D., FARUQI, S., BIRRING, S. S., MCGARVEY, L., CANNING, B., SMITH, J. A., PARKER, S. M., CHUNG, K. F., LAI, K., PAVORD, I. D., VAN DEN BERG, J., SONG, W.-J., MILLQVIST, E., FARRELL, M. J., MAZZONE, S. B. & DICPINIGAITIS, P. 2014a. A worldwide survey of chronic cough: a manifestation of enhanced somatosensory response. *European Respiratory Journal*, 44, 1149-1155.
- MORICE, A. H., KASTELIK, J. A. & THOMPSON, R. 2001. Cough challenge in the assessment of cough reflex. *Br J Clin Pharmacol*, 52, 365-75.
- MORICE, A. H., KITT, M. M., FORD, A. P., TERSHAKOVEC, A. M., WU, W. C., BRINDLE, K., THOMPSON, R., THACKRAY-NOCERA, S. & WRIGHT, C. 2019. The effect of gefapixant, a P2X3 antagonist, on cough reflex sensitivity: a randomised placebo-controlled study. *Eur Respir J*, 54.
- MORICE, A. H., MILLQVIST, E., BELVISI, M. G., BIEKSIENE, K., BIRRING, S. S., CHUNG, K. F., DAL NEGRO, R. W., DICPINIGAITIS, P., KANTAR, A., MCGARVEY, L. P., PACHECO, A., SAKALAUŠKAS, R. & SMITH, J. A. 2014b. Expert opinion on the cough hypersensitivity syndrome in respiratory medicine. *European Respiratory Journal*, 44, 1132-1148.
- MORTOLA, J., SANT'AMBROGIO, G. & CLEMENT, M. G. 1975. Localization of irritant receptors in the airways of the dog. *Respir Physiol*, 24, 107-14.
- MOTULSKY, H. J. & BROWN, R. E. 2006. Detecting outliers when fitting data with nonlinear regression – a new method based on robust nonlinear regression and the false discovery rate. *BMC Bioinformatics*, 7, 123.
- MUKHOPADHYAY, I., KULKARNI, A., ARANAKE, S., KARNIK, P., SHETTY, M., THORAT, S., GHOSH, I., WALE, D., BHOSALE, V. & KHAIRATKAR-JOSHI, N. 2014. Transient receptor potential ankyrin 1 receptor activation in vitro and in vivo by pro-tussive agents: GRC 17536 as a promising anti-tussive therapeutic. *PLoS One*, 9, e97005.
- MÜLLER, T., FAY, S., VIEIRA, R. P., KARMOUTY-QUINTANA, H., CICKO, S., AYATA, K., ZISSEL, G., GOLDMANN, T., LUNGARELLA, G., FERRARI, D., DI VIRGILIO, F., ROBAYE, B., BOEYNAEMS, J. M., BLACKBURN, M. R. & IDZKO, M. 2017. The purinergic receptor subtype P2Y2 mediates chemotaxis of neutrophils and fibroblasts in fibrotic lung disease. *Oncotarget*, 8, 35962-35972.
- MULUGETA, S., MAGUIRE, J. A., NEWITT, J. L., RUSSO, S. J., KOTORASHVILI, A. & BEERS, M. F. 2007. Misfolded BRICHOS SP-C mutant proteins induce apoptosis via caspase-4- and cytochrome c-related mechanisms. *Am J Physiol Lung Cell Mol Physiol*, 293, L720-9.
- MULUGETA, S., NGUYEN, V., RUSSO, S. J., MUNISWAMY, M. & BEERS, M. F. 2005. A surfactant protein C precursor protein BRICHOS domain mutation causes endoplasmic reticulum stress, proteasome dysfunction, and caspase 3 activation. *Am J Respir Cell Mol Biol*, 32, 521-30.

- MYLONAS, C. & KOURETAS, D. 1999. Lipid peroxidation and tissue damage. *In Vivo*, 13, 295-309.
- NAGAMOTO, T., EGUCHI, G. & BEEBE, D. C. 2000. Alpha-smooth muscle actin expression in cultured lens epithelial cells. *Invest Ophthalmol Vis Sci*, 41, 1122-9.
- NASRA, J. & BELVISI, M. G. 2009. Modulation of sensory nerve function and the cough reflex: understanding disease pathogenesis. *Pharmacol Ther*, 124, 354-75.
- NASSENSTEIN, C., KWONG, K., TAYLOR-CLARK, T., KOLLARIK, M., MACGLASHAN, D. M., BRAUN, A. & UNDEM, B. J. 2008. Expression and function of the ion channel TRPA1 in vagal afferent nerves innervating mouse lungs. *J Physiol*, 586, 1595-604.
- NATHAN, S. D., SHLOBIN, O. A., WEIR, N., AHMAD, S., KALDJOB, J. M., BATTLE, E., SHERIDAN, M. J. & DU BOIS, R. M. 2011. Long-term course and prognosis of idiopathic pulmonary fibrosis in the new millennium. *Chest*, 140, 221-229.
- NIIMI, A., ISHIHARA, H., HIDA, H. & MIYAZAKI, S. 2019. Late Breaking Abstract - Phase 2a randomised, double-blind, placebo-controlled, crossover study of a novel P2X3 receptor antagonist S-600918 in patients with refractory chronic cough. *European Respiratory Journal*, 54, RCT452.
- NISHIMURA, K., KITAICHI, M., IZUMI, T., NAGAI, S., KANAOKA, M. & ITOH, H. 1992. Usual interstitial pneumonia: histologic correlation with high-resolution CT. *Radiology*, 182, 337-42.
- NOTH, I., ZHANG, Y., MA, S. F., FLORES, C., BARBER, M., HUANG, Y., BRODERICK, S. M., WADE, M. S., HYSI, P., SCUIRBA, J., RICHARDS, T. J., JUAN-GUARDELA, B. M., VIJ, R., HAN, M. K., MARTINEZ, F. J., KOSSEN, K., SEIWERT, S. D., CHRISTIE, J. D., NICOLAE, D., KAMINSKI, N. & GARCIA, J. G. N. 2013. Genetic variants associated with idiopathic pulmonary fibrosis susceptibility and mortality: a genome-wide association study. *Lancet Respir Med*, 1, 309-317.
- NYSTEDT, S., EMILSSON, K., WAHLESTEDT, C. & SUNDELIN, J. 1994. Molecular cloning of a potential proteinase activated receptor. *Proceedings of the National Academy of Sciences*, 91, 9208-9212.
- O'DWYER, D. N., ARMSTRONG, M. E., TRUJILLO, G., COOKE, G., KEANE, M. P., FALLON, P. G., SIMPSON, A. J., MILLAR, A. B., MCGRATH, E. E., WHYTE, M. K., HIRANI, N., HOGABOAM, C. M. & DONNELLY, S. C. 2013. The Toll-like receptor 3 L412F polymorphism and disease progression in idiopathic pulmonary fibrosis. *Am J Respir Crit Care Med*, 188, 1442-50.
- OLDHAM, J. M., MA, S. F., MARTINEZ, F. J., ANSTROM, K. J., RAGHU, G., SCHWARTZ, D. A., VALENZI, E., WITT, L., LEE, C., VIJ, R., HUANG, Y., STREK, M. E., NOTH, I. & INVESTIGATORS, I. P. 2015. TOLLIP, MUC5B, and the Response to N-Acetylcysteine among Individuals with Idiopathic Pulmonary Fibrosis. *Am J Respir Crit Care Med*, 192, 1475-82.
- OLSON, A. L. & SWIGRIS, J. J. 2012. Idiopathic pulmonary fibrosis: diagnosis and epidemiology. *Clin Chest Med*, 33, 41-50.
- ONO, S., TANAKA, T., ISHIDA, M., KINOSHITA, A., FUKUOKA, J., TAKAKI, M., SAKAMOTO, N., ISHIMATSU, Y., KOHNO, S., HAYASHI, T., SENBA, M., YASUNAMI, M., KUBO, Y., YOSHIDA, L. M., KUBO, H., ARIYOSHI, K., YOSHIURA, K. & MORIMOTO, K. 2011. Surfactant protein C G100S mutation causes familial pulmonary fibrosis in Japanese kindred. *Eur Respir J*, 38, 861-9.
- ONUMA, T., HOLLAND, J. F., MASUDA, H., WALIGUNDA, J. A. & GOLDBERG, G. A. 1974. Microbiological assay of bleomycin: inactivation, tissue distribution, and clearance. *Cancer*, 33, 1230-8.
- OOI, S. L., GREEN, R. & PAK, S. C. 2018. N-Acetylcysteine for the Treatment of Psychiatric Disorders: A Review of Current Evidence. *Biomed Res Int*, 2018, 2469486.
- ORUQAJ, G., KARNATI, S., VIJAYAN, V., KOTARKONDA, L. K., BOATENG, E., ZHANG, W., RUPPERT, C., GUNTHER, A., SHI, W. & BAUMGART-VOGT, E. 2015. Compromised peroxisomes in idiopathic pulmonary fibrosis, a vicious cycle inducing a higher fibrotic response via TGF-beta signaling. *Proc Natl Acad Sci U S A*, 112, E2048-57.
- OTOUPALOVA, E., SMITH, S., CHENG, G. & THANNICKAL, V. J. 2020. Oxidative Stress in Pulmonary Fibrosis. *Compr Physiol*, 10, 509-547.

- OTSUKA, K., NIIMI, A., MATSUMOTO, H., ITO, I., YAMAGUCHI, M., MATSUOKA, H., JINNAI, M., OGUMA, T., TAKEDA, T., NAKAJI, H., CHIN, K., SASAKI, K., AOYAMA, N. & MISHIMA, M. 2011. Plasma substance P levels in patients with persistent cough. *Respiration*, 82, 431-8.
- PACHECO, A. 2014. Chronic cough: from a complex dysfunction of the neurological circuit to the production of persistent cough. *Thorax*, 69, 881-883.
- PAINTAL, A. 1973. Conduction in mammalian nerve fibres. *Pathological conduction in nerve fibers, electromyography of sphincter muscles, automatic analysis of electromyogram with computers*. Karger Publishers.
- PARK, Y. S., PARK, C. M., LEE, H. J., GOO, J. M., CHUNG, D. H., LEE, S. M., YIM, J. J., KIM, Y. W., HAN, S. K. & YOO, C. G. 2013. Clinical implication of protease-activated receptor-2 in idiopathic pulmonary fibrosis. *Respir Med*, 107, 256-62.
- PARKER, M. W., ROSSI, D., PETERSON, M., SMITH, K., SIKSTRÖM, K., WHITE, E. S., CONNETT, J. E., HENKE, C. A., LARSSON, O. & BITTERMAN, P. B. 2014. Fibrotic extracellular matrix activates a profibrotic positive feedback loop. *The Journal of Clinical Investigation*, 124, 1622-1635.
- PATEL, H. J., BIRRELL, M. A., CRISPINO, N., HELE, D. J., VENKATESAN, P., BARNES, P. J., YACOUB, M. H. & BELVISI, M. G. 2003. Inhibition of guinea-pig and human sensory nerve activity and the cough reflex in guinea-pigs by cannabinoid (CB2) receptor activation. *Br J Pharmacol*, 140, 261-8.
- PEAKE, N. 2020. *Trials show new drug can ease symptoms of chronic cough* [Online]. University of Manchester Website. Available: <https://www.manchester.ac.uk/discover/news/trials-show-new-drug-can-ease-symptoms-of-chronic-cough/> [Accessed 2nd January 2021].
- PELJTO, A. L., SELMAN, M., KIM, D. S., MURPHY, E., TUCKER, L., PARDO, A., LEE, J. S., JI, W., SCHWARZ, M. I., YANG, I. V., SCHWARTZ, D. A. & FINGERLIN, T. E. 2015. The MUC5B promoter polymorphism is associated with idiopathic pulmonary fibrosis in a Mexican cohort but is rare among Asian ancestries. *Chest*, 147, 460-464.
- PELJTO, A. L., STEELE, M. P., FINGERLIN, T. E., HINCHCLIFF, M. E., MURPHY, E., PODLUSKY, S., CARNS, M., SCHWARZ, M., VARGA, J. & SCHWARTZ, D. A. 2012. The pulmonary fibrosis-associated MUC5B promoter polymorphism does not influence the development of interstitial pneumonia in systemic sclerosis. *Chest*, 142, 1584-1588.
- PENG, R., SRIDHAR, S., TYAGI, G., PHILLIPS, J. E., GARRIDO, R., HARRIS, P., BURNS, L., RENTERIA, L., WOODS, J., CHEN, L., ALLARD, J., RAVINDRAN, P., BITTER, H., LIANG, Z., HOGABOAM, C. M., KITSON, C., BUDD, D. C., FINE, J. S., BAUER, C. M. & STEVENSON, C. S. 2013. Bleomycin induces molecular changes directly relevant to idiopathic pulmonary fibrosis: a model for "active" disease. *PLoS One*, 8, e59348.
- PHAN, S. H. 2008. Biology of Fibroblasts and Myofibroblasts. *Proceedings of the American Thoracic Society*, 5, 334-337.
- PICHER, M., BURCH, L. H., HIRSH, A. J., SPYCHALA, J. & BOUCHER, R. C. 2003. Ecto 5'-nucleotidase and nonspecific alkaline phosphatase. Two AMP-hydrolyzing ectoenzymes with distinct roles in human airways. *J Biol Chem*, 278, 13468-79.
- PITOZZI, V., CARUSO, P., BONATTI, M., BIGNAMI, F., PITTELLI, M. G., PONTIS, S., FRATI, C., MANGIARACINA, C., QUAINI, F., LAGRASTA, C., CIVELLI, M., VILLETTI, G. & TREVISANI, M. 2018. Time-course analysis of bleomycin-induced lung fibrosis in the rat. *European Respiratory Journal*, 52, PA1001.
- PLANTIER, L., CRESTANI, B., WERT, S. E., DEHOUX, M., ZWEYTICK, B., GUENTHER, A. & WHITSETT, J. A. 2011. Ectopic respiratory epithelial cell differentiation in bronchiolised distal airspaces in idiopathic pulmonary fibrosis. *Thorax*, 66, 651-657.
- POLIACEK, I. 2020. Sensory Pathways and Neural Modulation of Cough. In: ZANASI, A., FONTANA, G. A. & MUTOLO, D. (eds.) *Cough: Pathophysiology, Diagnosis and Treatment*. Cham: Springer International Publishing.

- POLIACEK, I., HALASOVA, E., JAKUS, J., MURIN, P., BARANI, H., STRANSKY, A. & BOLSER, D. C. 2007. Brainstem regions involved in the expiration reflex. A c-fos study in anesthetized cats. *Brain Res*, 1184, 168-77.
- POLLEY, L., YAMAN, N., HEANEY, L., CARDWELL, C., MURTAGH, E., RAMSEY, J., MACMAHON, J., COSTELLO, R. W. & MCGARVEY, L. 2008. Impact of cough across different chronic respiratory diseases: comparison of two cough-specific health-related quality of life questionnaires. *Chest*, 134, 295-302.
- POOLE, D. P., AMADESI, S., VELDHUIS, N. A., ABOGADIE, F. C., LIEU, T., DARBY, W., LIEDTKE, W., LEW, M. J., MCINTYRE, P. & BUNNETT, N. W. 2013. Protease-activated receptor 2 (PAR2) protein and transient receptor potential vanilloid 4 (TRPV4) protein coupling is required for sustained inflammatory signaling. *J Biol Chem*, 288, 5790-802.
- PSATHAKIS, K., MERMIGKIS, D., PAPTAEODOROU, G., LOUKIDES, S., PANAGOY, P., POLYCHRONOPOULOS, V., SIAFAKAS, N. M. & BOUROS, D. 2006. Exhaled markers of oxidative stress in idiopathic pulmonary fibrosis. *Eur J Clin Invest*, 36, 362-7.
- RAGHU, G. 2011. Idiopathic pulmonary fibrosis: guidelines for diagnosis and clinical management have advanced from consensus-based in 2000 to evidence-based in 2011. *European Respiratory Journal*, 37, 743-746.
- RAGHU, G., ANSTROM, K. J., KING, T. E., JR., LASKY, J. A. & MARTINEZ, F. J. 2012. Prednisone, azathioprine, and N-acetylcysteine for pulmonary fibrosis. *N Engl J Med*, 366, 1968-77.
- RAGHU, G., COLLARD, H. R., EGAN, J. J., MARTINEZ, F. J., BEHR, J., BROWN, K. K., COLBY, T. V., CORDIER, J. F., FLAHERTY, K. R., LASKY, J. A., LYNCH, D. A., RYU, J. H., SWIGRIS, J. J., WELLS, A. U., ANCOCHEA, J., BOUROS, D., CARVALHO, C., COSTABEL, U., EBINA, M., HANSELL, D. M., JOHKOH, T., KIM, D. S., KING, T. E., KONDOH, Y., MYERS, J., MULLER, N. L., NICHOLSON, A. G., RICHELDI, L., SELMAN, M., DUDDEN, R. F., GRISS, B. S., PROTZKO, S. L., SCHUNEMANN, H. J. & COMM, A. E. J. A. 2011. An Official ATS/ERS/ALAT Statement: Idiopathic Pulmonary Fibrosis: Evidence-based Guidelines for Diagnosis and Management. *American Journal of Respiratory and Critical Care Medicine*, 183, 788-824.
- RAGHU, G., FREUDENBERGER, T. D., YANG, S., CURTIS, J. R., SPADA, C., HAYES, J., SILLERY, J. K., POPE, C. E., 2ND & PELLEGRINI, C. A. 2006. High prevalence of abnormal acid gastro-oesophageal reflux in idiopathic pulmonary fibrosis. *Eur Respir J*, 27, 136-42.
- RAGHU, G., REMY-JARDIN, M., MYERS, J. L., RICHELDI, L., RYERSON, C. J., LEDERER, D. J., BEHR, J., COTTIN, V., DANOFF, S. K., MORELL, F., FLAHERTY, K. R., WELLS, A., MARTINEZ, F. J., AZUMA, A., BICE, T. J., BOUROS, D., BROWN, K. K., COLLARD, H. R., DUGGAL, A., GALVIN, L., INOUE, Y., JENKINS, R. G., JOHKOH, T., KAZEROONI, E. A., KITAICHI, M., KNIGHT, S. L., MANSOUR, G., NICHOLSON, A. G., PIPAVATH, S. N. J., BUENDIA-ROLDAN, I., SELMAN, M., TRAVIS, W. D., WALSH, S., WILSON, K. C., AMERICAN THORACIC SOCIETY, E. R. S. J. R. S. & LATIN AMERICAN THORACIC, S. 2018. Diagnosis of Idiopathic Pulmonary Fibrosis. An Official ATS/ERS/JRS/ALAT Clinical Practice Guideline. *Am J Respir Crit Care Med*, 198, e44-e68.
- RAHAMAN, S. O., GROVE, L. M., PARUCHURI, S., SOUTHERN, B. D., ABRAHAM, S., NIESE, K. A., SCHERAGA, R. G., GHOSH, S., THODETI, C. K., ZHANG, D. X., MORAN, M. M., SCHILLING, W. P., TSCHUMPERLIN, D. J. & OLMAN, M. A. 2014. TRPV4 mediates myofibroblast differentiation and pulmonary fibrosis in mice. *J Clin Invest*, 124, 5225-38.
- RAHMAN, M., SUN, R., MUKHERJEE, S., NILIUS, B. & JANSSEN, L. J. 2018. TRPV4 Stimulation Releases ATP via Pannexin Channels in Human Pulmonary Fibroblasts. *Am J Respir Cell Mol Biol*, 59, 87-95.
- RAI, Z. L., FOWLES, H. E., WRIGHT, C., HOWARD, J. & MORICE, A. H. 2018. The effect of pH on citric acid cough challenge: A randomised control trial in chronic cough and healthy volunteers. *Respiratory Physiology & Neurobiology*, 257, 51-54.
- RAMACHANDRAN, G. N., BANSAL, M. & BHATNAGAR, R. S. 1973. A hypothesis on the role of hydroxyproline in stabilizing collagen structure. *Biochim Biophys Acta*, 322, 166-71.



- RANA, T., JIANG, C., LIU, G., MIYATA, T., ANTONY, V., THANNICKAL, V. J. & LIU, R. M. 2020. PAI-1 Regulation of TGF- $\beta$ 1-induced Alveolar Type II Cell Senescence, SASP Secretion, and SASP-mediated Activation of Alveolar Macrophages. *Am J Respir Cell Mol Biol*, 62, 319-330.
- RAY, P. D., HUANG, B. W. & TSUJI, Y. 2012. Reactive oxygen species (ROS) homeostasis and redox regulation in cellular signaling. *Cell Signal*, 24, 981-90.
- REGAL, J. F., REGAL, R. R., MEEHAN, J. L. & MOHRMAN, M. E. 2006. Primary prevention of asthma: age and sex influence sensitivity to allergen-induced airway inflammation and contribute to asthma heterogeneity in Guinea pigs. *Int Arch Allergy Immunol*, 141, 241-56.
- RICCI, A., GRAZIANO, P., BRONZETTI, E., SALTINI, C., SCIACCHITANO, S., CHERUBINI, E., RENZONI, E., DU BOIS, R. M., GRUTTERS, J. C. & MARIOTTA, S. 2007. Increased pulmonary neurotrophin protein expression in idiopathic interstitial pneumonias. *Sarcoidosis Vasc Diffuse Lung Dis*, 24, 13-23.
- RICCIO, M. M., KUMMER, W., BIGLARI, B., MYERS, A. C. & UNDEM, B. J. 1996a. Interganglionic segregation of distinct vagal afferent fibre phenotypes in guinea-pig airways. *J Physiol*, 496 ( Pt 2), 521-30.
- RICCIO, M. M., MYERS, A. C. & UNDEM, B. J. 1996b. Immunomodulation of afferent neurons in guinea-pig isolated airway. *J Physiol*, 491 ( Pt 2), 499-509.
- RICHARDS, D., GEVER, J. R., FORD, A. P. & FOUNTAIN, S. J. 2019. Action of MK-7264 (gefapixant) at human P2X3 and P2X2/3 receptors and in vivo efficacy in models of sensitisation. *Br J Pharmacol*, 176, 2279-2291.
- RIEDL, M. A. & NEL, A. E. 2008. Importance of oxidative stress in the pathogenesis and treatment of asthma. *Curr Opin Allergy Clin Immunol*, 8, 49-56.
- RITEAU, N., GASSE, P., FAUCONNIER, L., GOMBAULT, A., COUEGNAT, M., FICK, L., KANELLOPOULOS, J., QUESNIAUX, V. F., MARCHAND-ADAM, S., CRESTANI, B., RYFFEL, B. & COUILLIN, I. 2010. Extracellular ATP is a danger signal activating P2X7 receptor in lung inflammation and fibrosis. *Am J Respir Crit Care Med*, 182, 774-83.
- ROBINSON, R. K., BIRRELL, M. A., ADCOCK, J. J., WORTLEY, M. A., DUBUIS, E. D., CHEN, S., MCGILVER, C. M., HU, S., SHAFFER, M. S. P., BONVINI, S. J., MAHER, S. A., MUDWAY, I. S., PORTER, A. E., CARLSTEN, C., TETLEY, T. D. & BELVISI, M. G. 2018. Mechanistic link between diesel exhaust particles and respiratory reflexes. *Journal of Allergy and Clinical Immunology*, 141, 1074-1084.e9.
- ROCK, J. R., BARKAUSKAS, C. E., CRONCE, M. J., XUE, Y., HARRIS, J. R., LIANG, J., NOBLE, P. W. & HOGAN, B. L. 2011. Multiple stromal populations contribute to pulmonary fibrosis without evidence for epithelial to mesenchymal transition. *Proc Natl Acad Sci U S A*, 108, E1475-83.
- ROE, M. W., LEMASTERS, J. J. & HERMAN, B. 1990. Assessment of Fura-2 for measurements of cytosolic free calcium. *Cell Calcium*, 11, 63-73.
- ROGLIANI, P., CALZETTA, L., CAVALLI, F., MATERA, M. G. & CAZZOLA, M. 2016. Pirfenidone, nintedanib and N-acetylcysteine for the treatment of idiopathic pulmonary fibrosis: A systematic review and meta-analysis. *Pulm Pharmacol Ther*, 40, 95-103.
- ROTTOLI, P., MAGI, B., CIANTI, R., BARGAGLI, E., VAGAGGINI, C., NIKIFORAKIS, N., PALLINI, V. & BINI, L. 2005. Carbonylated proteins in bronchoalveolar lavage of patients with sarcoidosis, pulmonary fibrosis associated with systemic sclerosis and idiopathic pulmonary fibrosis. *Proteomics*, 5, 2612-8.
- ROY, M. G., LIVRAGHI-BUTRICO, A., FLETCHER, A. A., MCELWEE, M. M., EVANS, S. E., BOERNER, R. M., ALEXANDER, S. N., BELLINGHAUSEN, L. K., SONG, A. S., PETROVA, Y. M., TUVIM, M. J., ADACHI, R., ROMO, I., BORDT, A. S., BOWDEN, M. G., SISSON, J. H., WOODRUFF, P. G., THORNTON, D. J., ROUSSEAU, K., DE LA GARZA, M. M., MOGHADDAM, S. J., KARMOUTY-QUINTANA, H., BLACKBURN, M. R., DROUIN, S. M., DAVIS, C. W., TERRELL, K. A., GRUBB, B. R., O'NEAL, W. K., FLORES, S. C., COTA-GOMEZ, A., LOZUPONE, C. A., DONNELLY, J. M., WATSON, A. M., HENNESSY, C. E., KEITH, R. C., YANG, I. V., BARTHEL, L., HENSON, P. M.,

- JANSSEN, W. J., SCHWARTZ, D. A., BOUCHER, R. C., DICKEY, B. F. & EVANS, C. M. 2014. Muc5b is required for airway defence. *Nature*, 505, 412-416.
- RUDD, R. M., HASLAM, P. L. & TURNER-WARWICK, M. 1981. Cryptogenic fibrosing alveolitis. Relationships of pulmonary physiology and bronchoalveolar lavage to response to treatment and prognosis. *Am Rev Respir Dis*, 124, 1-8.
- RUHL, C. R., PASKO, B. L., KHAN, H. S., KINDT, L. M., STAMM, C. E., FRANCO, L. H., HSIA, C. C., ZHOU, M., DAVIS, C. R., QIN, T., GAUTRON, L., BURTON, M. D., MEJIA, G. L., NAIK, D. K., DUSSOR, G., PRICE, T. J. & SHILOH, M. U. 2020. Mycobacterium tuberculosis Sulfolipid-1 Activates Nociceptive Neurons and Induces Cough. *Cell*, 181, 293-305 e11.
- RUOSS, S. J., HARTMANN, T. & CAUGHEY, G. H. 1991. Mast cell tryptase is a mitogen for cultured fibroblasts. *The Journal of Clinical Investigation*, 88, 493-499.
- RYAN, N. M., BIRRING, S. S. & GIBSON, P. G. 2012. Gabapentin for refractory chronic cough: a randomised, double-blind, placebo-controlled trial. *Lancet*, 380, 1583-9.
- RYERSON, C. J., ABBRITTI, M., LEY, B., ELICKER, B. M., JONES, K. D. & COLLARD, H. R. 2011. Cough predicts prognosis in idiopathic pulmonary fibrosis. *Respirology*, 16, 969-75.
- SACHSER, N. & LICK, C. 1991. Social experience, behavior, and stress in guinea pigs. *Physiol Behav*, 50, 83-90.
- SAHAY, A. S., SUNDRANI, D. P. & JOSHI, S. R. 2017. Chapter Ten - Neurotrophins: Role in Placental Growth and Development. In: LITWACK, G. (ed.) *Vitamins and Hormones*. Academic Press.
- SAMUNI, Y., GOLDSTEIN, S., DEAN, O. M. & BERK, M. 2013. The chemistry and biological activities of N-acetylcysteine. *Biochim Biophys Acta*, 1830, 4117-29.
- SANT'AMBROGIO, G., REMMERS, J. E., DE GROOT, W. J., CALLAS, G. & MORTOLA, J. P. 1978. Localization of rapidly adapting receptors in the trachea and main stem bronchus of the dog. *Respir Physiol*, 33, 359-66.
- SANT'AMBROGIO, G. & WIDDICOMBE, J. 2001. Reflexes from airway rapidly adapting receptors. *Respir Physiol*, 125, 33-45.
- SAWADA, Y., HOSOKAWA, H., MATSUMURA, K. & KOBAYASHI, S. 2008. Activation of transient receptor potential ankyrin 1 by hydrogen peroxide. *Eur J Neurosci*, 27, 1131-42.
- SCHAEFER, C. J., RUHRMUND, D. W., PAN, L., SEIWERT, S. D. & KOSSEN, K. 2011. Antifibrotic activities of pirfenidone in animal models. *Eur Respir Rev*, 20, 85-97.
- SCHAFER, M. J., WHITE, T. A., IJIMA, K., HAAK, A. J., LIGRESTI, G., ATKINSON, E. J., OBERG, A. L., BIRCH, J., SALMONOWICZ, H., ZHU, Y., MAZULA, D. L., BROOKS, R. W., FUHRMANN-STROISSNIGG, H., PIRTSKHALAVA, T., PRAKASH, Y. S., TCHKONIA, T., ROBBINS, P. D., AUBRY, M. C., PASSOS, J. F., KIRKLAND, J. L., TSCHUMPERLIN, D. J., KITA, H. & LEBRASSEUR, N. K. 2017. Cellular senescence mediates fibrotic pulmonary disease. *Nat Commun*, 8, 14532.
- SCHEGLE, E. S. & GREEN, J. F. 2001. An overview of the anatomy and physiology of slowly adapting pulmonary stretch receptors. *Respir Physiol*, 125, 17-31.
- SCHWARTZ, D. A., HELMERS, R. A., GALVIN, J. R., VAN FOSSEN, D. S., FREES, K. L., DAYTON, C. S., BURMEISTER, L. F. & HUNNINGHAKE, G. W. 1994. Determinants of survival in idiopathic pulmonary fibrosis. *Am J Respir Crit Care Med*, 149, 450-4.
- SCHWARTZ, L. B. & BRADFORD, T. R. 1986. Regulation of tryptase from human lung mast cells by heparin. Stabilization of the active tetramer. *J Biol Chem*, 261, 7372-9.
- SEDGWICK, S. G. & SMERDON, S. J. 1999. The ankyrin repeat: a diversity of interactions on a common structural framework. *Trends Biochem Sci*, 24, 311-6.
- SEIBOLD, M. A., WISE, A. L., SPEER, M. C., STEELE, M. P., BROWN, K. K., LOYD, J. E., FINGERLIN, T. E., ZHANG, W., GUDMUNDSSON, G., GROSHONG, S. D., EVANS, C. M., GARANTZIOTIS, S., ADLER, K. B., DICKEY, B. F., DU BOIS, R. M., YANG, I. V., HERRON, A., KERVITSKY, D., TALBERT, J. L., MARKIN, C., PARK, J., CREWS, A. L., SLIFER, S. H., AUERBACH, S., ROY, M. G., LIN, J., HENNESSY, C. E., SCHWARZ, M. I. & SCHWARTZ, D. A. 2011. A common MUC5B promoter polymorphism and pulmonary fibrosis. *N Engl J Med*, 364, 1503-12.

- SEITZBERG, J. G., KNAPP, A. E., LUND, B. W., MANDRUP BERTOZZI, S., CURRIER, E. A., MA, J. N., SHERBUKHIN, V., BURSTEIN, E. S. & OLSSON, R. 2008. Discovery of potent and selective small-molecule PAR-2 agonists. *J Med Chem*, 51, 5490-3.
- SELMAN, M. & PARDO, A. 2014. Revealing the pathogenic and aging-related mechanisms of the enigmatic idiopathic pulmonary fibrosis: an integral model. *Am J Respir Crit Care Med*, 189, 1161-72.
- SEVIGNY, L. M., ZHANG, P., BOHM, A., LAZARIDES, K., PERIDES, G., COVIC, L. & KULIOPULOS, A. 2011. Interdicting protease-activated receptor-2-driven inflammation with cell-penetrating pepducins. *Proc Natl Acad Sci U S A*, 108, 8491-6.
- SGALLA, G., IOVENE, B., CALVELLO, M., ORI, M., VARONE, F. & RICHELDI, L. 2018. Idiopathic pulmonary fibrosis: pathogenesis and management. *Respir Res*, 19, 32.
- SHAHZEIDI, S., SARNSTRAND, B., JEFFERY, P. K., MCANULTY, R. J. & LAURENT, G. J. 1991. Oral N-acetylcysteine reduces bleomycin-induced collagen deposition in the lungs of mice. *Eur Respir J*, 4, 845-52.
- SHARMA, S., GOSWAMI, R., ZHANG, D. X. & RAHAMAN, S. O. 2019. TRPV4 regulates matrix stiffness and TGFbeta1-induced epithelial-mesenchymal transition. *J Cell Mol Med*, 23, 761-774.
- SHESTOPALOV, V. I. & PANCHIN, Y. 2008. Pannexins and gap junction protein diversity. *Cell Mol Life Sci*, 65, 376-94.
- SIES, H. 1997. Oxidative stress: oxidants and antioxidants. *Exp Physiol*, 82, 291-5.
- SKALLI, O., ROPRAZ, P., TRZECIAK, A., BENZONANA, G., GILLESSEN, D. & GABBIANI, G. 1986. A monoclonal antibody against alpha-smooth muscle actin: a new probe for smooth muscle differentiation. *J Cell Biol*, 103, 2787-96.
- SMITH, J., ALLMAN, D., BADRI, H., MILLER, R., MORRIS, J., SATIA, I., WOOD, A. & M, K. T. 2020a. The Neurokinin-1 Receptor Antagonist Orvepitant Is a Novel Antitussive Therapy for Chronic Refractory Cough: Results From a Phase 2 Pilot Study (VOLCANO-1). *Chest*, 157, 111-118.
- SMITH, J., OWEN, E., EARIS, J. & WOODCOCK, A. 2006a. Cough in COPD: correlation of objective monitoring with cough challenge and subjective assessments. *Chest*, 130, 379-85.
- SMITH, J. & WOODCOCK, A. 2008. New developments in the objective assessment of cough. *Lung*, 186 Suppl 1, S48-54.
- SMITH, J. A. & BADRI, H. 2019. Cough: New Pharmacology. *J Allergy Clin Immunol Pract*, 7, 1731-1738.
- SMITH, J. A., DECALMER, S., KELSALL, A., MCGUINNESS, K., JONES, H., GALLOWAY, S., WOODCOCK, A. & HOUGHTON, L. A. 2010. Acoustic cough-reflux associations in chronic cough: potential triggers and mechanisms. *Gastroenterology*, 139, 754-62.
- SMITH, J. A., EARIS, J. E. & WOODCOCK, A. A. 2006b. Establishing a gold standard for manual cough counting: video versus digital audio recordings. *Cough*, 2, 6.
- SMITH, J. A., HILTON, E. C. Y., SAULSBERRY, L. & CANNING, B. J. 2012. Antitussive effects of memantine in guinea pigs. *Chest*, 141, 996-1002.
- SMITH, J. A., KITT, M. M., MORICE, A. H., BIRRING, S. S., MCGARVEY, L. P., SHER, M. R., LI, Y.-P., WU, W.-C., XU, Z. J., MUCCINO, D. R., FORD, A. P., SMITH, J., MCGARVEY, L., BIRRING, S., HULL, J., CARR, W. W., GOLDSOBEL, A. B., GROSS, G. N., HOLCOMB, J. R., HUSSAIN, I., SHER, M., SPANGENTHAL, S., STORMS, W., MORICE, A., ELKAYAM, D., STEVEN, G. C., KRAINSON, J., FAKIH, F. A., MATZ, J., BROOKS, G. D., CASALE, T., BERMAN, G. D., CONDEMI, J. J., GREOS, L. S., GOGATE, S. U., SHER, E. R., FRIESEN, J. H., SCHENKEL, E. J., BERNSTEIN, D. I., CORREN, J., SUNDAR, K., GOTFRIED, M. H., MONTANARO, A., LUMRY, W. R., AMAR, N. J., KAPLAN, M. S., PRENNER, B. M., MURPHY, T. R., GOOD, J. S., PARKER, S., HARRISON, T., PAVORD, I., BRIGHTLING, C., DJUKANOVIC, R., MCQUAID, D., DENENBERG, M., ETTINGER, N. A. & IYER, V. 2020b. Gefapixant, a P2X3 receptor antagonist, for the treatment of refractory or unexplained chronic cough: a randomised, double-blind, controlled, parallel-group, phase 2b trial. *The Lancet Respiratory Medicine*, 8, 775-785.

- SMITH, J. A., OWEN, E. C., JONES, A. M., DODD, M. E., WEBB, A. K. & WOODCOCK, A. 2006c. Objective measurement of cough during pulmonary exacerbations in adults with cystic fibrosis. *Thorax*, 61, 425-9.
- SMITH, J. A. & WOODCOCK, A. 2016. Chronic Cough. *New England Journal of Medicine*, 375, 1544-1551.
- SNETSELAAR, R., VAN BATENBURG, A. A., VAN OOSTERHOUT, M. F. M., KAZEMIER, K. M., ROOTHAAN, S. M., PEETERS, T., VAN DER VIS, J. J., GOLDSCHMEDING, R., GRUTTERS, J. C. & VAN MOORSEL, C. H. M. 2017. Short telomere length in IPF lung associates with fibrotic lesions and predicts survival. *PLOS ONE*, 12, e0189467.
- SPINO, A., LEE, K. K., SINHA, A., ELSTON, C., LOEBINGER, M. R., WILSON, R., CHUNG, K. F., YOUSAF, N., PAVORD, I. D., MATOS, S., GARROD, R. & BIRRING, S. S. 2017. The Objective Assessment of Cough Frequency in Bronchiectasis. *Lung*, 195, 575-585.
- SRIVASTAVA, A. K., KHARE, P., NAGAR, H. K., RAGHUWANSHI, N. & SRIVASTAVA, R. 2016. Hydroxyproline: A Potential Biochemical Marker and Its Role in the Pathogenesis of Different Diseases. *Curr Protein Pept Sci*, 17, 596-602.
- STAN, F. G. 2015. Comparative Anatomical Study of Lungs in Domestic Rabbits (*Oryctolagus cuniculus*) and Guinea Pigs (*Cavia porcellus*). *Bulletin of University of Agricultural Sciences and Veterinary Medicine Cluj-Napoca. Veterinary Medicine*, 72, 195-196.
- STEFANO, A. 2001. Not again! *BMJ*, 322, 548.
- STEINHOFF, M., VERGNOLLE, N., YOUNG, S. H., TOGNETTO, M., AMADESI, S., ENNES, H. S., TREVISANI, M., HOLLENBERG, M. D., WALLACE, J. L., CAUGHEY, G. H., MITCHELL, S. E., WILLIAMS, L. M., GEPPETTI, P., MAYER, E. A. & BUNNETT, N. W. 2000. Agonists of proteinase-activated receptor 2 induce inflammation by a neurogenic mechanism. *Nat Med*, 6, 151-8.
- STEWART, G. A., HOYNE, G. F., AHMAD, S. A., JARMAN, E., WALLACE, W. A., HARRISON, D. J., HASLETT, C., LAMB, J. R. & HOWIE, S. E. 2003. Expression of the developmental Sonic hedgehog (Shh) signalling pathway is up-regulated in chronic lung fibrosis and the Shh receptor patched 1 is present in circulating T lymphocytes. *The Journal of Pathology*, 199, 488-495.
- STEWART, J. P., EGAN, J. J., ROSS, A. J., KELLY, B. G., LOK, S. S., HASLETON, P. S. & WOODCOCK, A. A. 1999. The detection of Epstein-Barr virus DNA in lung tissue from patients with idiopathic pulmonary fibrosis. *Am J Respir Crit Care Med*, 159, 1336-41.
- STRAUSZ, J., MULLER-QUERNHEIM, J., STEPPLING, H. & FERLINZ, R. 1990. Oxygen radical production by alveolar inflammatory cells in idiopathic pulmonary fibrosis. *Am Rev Respir Dis*, 141, 124-8.
- SUNGER, K., POWLEY, W., KELSALL, A., SUMNER, H., MURDOCH, R. & SMITH, J. A. 2013. Objective measurement of cough in otherwise healthy volunteers with acute cough. *Eur Respir J*, 41, 277-84.
- SURPRENANT, A. & NORTH, R. A. 2009. Signaling at purinergic P2X receptors. *Annu Rev Physiol*, 71, 333-59.
- SUZUKI, M., MIZUNO, A., KODAIRA, K. & IMAI, M. 2003. Impaired pressure sensation in mice lacking TRPV4. *J Biol Chem*, 278, 22664-8.
- SWIGRIS, J. J., STEWART, A. L., GOULD, M. K. & WILSON, S. R. 2005. Patients' perspectives on how idiopathic pulmonary fibrosis affects the quality of their lives. *Health Qual Life Outcomes*, 3, 61.
- TABURET, A. M. & SCHMIT, B. 1994. Pharmacokinetic optimisation of asthma treatment. *Clin Pharmacokinet*, 26, 396-418.
- TAKEYAMA, M., NAGAI, S., MORI, K., IKAWA, K., SATAKE, N. & IZUMI, T. 1996. Substance P-like immunoreactive substance in bronchoalveolar lavage fluids from patients with idiopathic pulmonary fibrosis and pulmonary sarcoidosis. *Sarcoidosis Vasc Diffuse Lung Dis*, 13, 33-7.

- TASHIRO, J., RUBIO, G. A., LIMPER, A. H., WILLIAMS, K., ELLIOT, S. J., NINO, I., AIDINIS, V., TZOUVELEKIS, A. & GLASSBERG, M. K. 2017. Exploring Animal Models That Resemble Idiopathic Pulmonary Fibrosis. *Frontiers in Medicine*, 4.
- TASKAR, V. & COULTAS, D. 2008. Exposures and idiopathic lung disease. *Semin Respir Crit Care Med*, 29, 670-9.
- TASKAR, V. S. & COULTAS, D. B. 2006. Is Idiopathic Pulmonary Fibrosis an Environmental Disease? *Proceedings of the American Thoracic Society*, 3, 293-298.
- TATAR, M., SANT'AMBROGIO, G. & SANT'AMBROGIO, F. B. 1994. Laryngeal and tracheobronchial cough in anesthetized dogs. *J Appl Physiol (1985)*, 76, 2672-9.
- TERRIL, L. A., CLEMONS, D. J. & SUCKOW, M. A. 1998. *The laboratory guinea pig*.
- THOMAS, D. C. 2017. The phagocyte respiratory burst: Historical perspectives and recent advances. *Immunol Lett*, 192, 88-96.
- THORNELOE, K. S., CHEUNG, M., BAO, W., ALSAID, H., LENHARD, S., JIAN, M. Y., COSTELL, M., MANISCALCO-HAUK, K., KRAWIEC, J. A., OLZINSKI, A., GORDON, E., LOZINSKAYA, I., ELEFANTE, L., QIN, P., MATASIC, D. S., JAMES, C., TUNSTEAD, J., DONOVAN, B., KALLAL, L., WASZKIEWICZ, A., VAIDYA, K., DAVENPORT, E. A., LARKIN, J., BURGERT, M., CASILLAS, L. N., MARQUIS, R. W., YE, G., EIDAM, H. S., GOODMAN, K. B., TOOMEY, J. R., ROETHKE, T. J., JUCKER, B. M., SCHNACKENBERG, C. G., TOWNSLEY, M. I., LEPORE, J. J. & WILLETTE, R. N. 2012. An orally active TRPV4 channel blocker prevents and resolves pulmonary edema induced by heart failure. *Sci Transl Med*, 4, 159ra148.
- THORNTON, D. J., ROUSSEAU, K. & MCGUCKIN, M. A. 2008. Structure and function of the polymeric mucins in airways mucus. *Annu Rev Physiol*, 70, 459-86.
- TOBIN, R. W., POPE, C. E., 2ND, PELLEGRINI, C. A., EMOND, M. J., SILLERY, J. & RAGHU, G. 1998. Increased prevalence of gastroesophageal reflux in patients with idiopathic pulmonary fibrosis. *Am J Respir Crit Care Med*, 158, 1804-8.
- TOBLER, I. 1995. Is sleep fundamentally different between mammalian species? *Behav Brain Res*, 69, 35-41.
- TOBLER, I., FRANKEN, P. & JAGGI, K. 1993. Vigilance states, EEG spectra, and cortical temperature in the guinea pig. *American Journal of Physiology-Regulatory, Integrative and Comparative Physiology*, 264, R1125-R1132.
- TSAKIRI, K. D., CRONKHITE, J. T., KUAN, P. J., XING, C., RAGHU, G., WEISSLER, J. C., ROSENBLATT, R. L., SHAY, J. W. & GARCIA, C. K. 2007. Adult-onset pulmonary fibrosis caused by mutations in telomerase. *Proc Natl Acad Sci U S A*, 104, 7552-7.
- TSCHUMPERLIN, D. J. 2015. Matrix, Mesenchyme, and Mechanotransduction. *Annals of the American Thoracic Society*, 12, S24-S29.
- TURNER, R. D., BIRRING, S. S., DARMALINGAM, M., HOOPER, R. L., KUNST, H., MATOS, S. & BOTHAMLEY, G. H. 2018. Daily cough frequency in tuberculosis and association with household infection. *Int J Tuberc Lung Dis*, 22, 863-870.
- TURNER-WARWICK, M., BURROWS, B. & JOHNSON, A. 1980. Cryptogenic fibrosing alveolitis: clinical features and their influence on survival. *Thorax*, 35, 171-80.
- TZOUVELEKIS, A., KARAMPITSAKOS, T., KOURTIDOU, S., BOUROS, E., TZILAS, V., KATSARAS, M., ANTONOU, C., DASSIOU, M. & BOUROS, D. 2020. Impact of Depression on Patients With Idiopathic Pulmonary Fibrosis. *Front Med (Lausanne)*, 7, 29.
- UHAL, B. D. 1997. Cell cycle kinetics in the alveolar epithelium. *Am J Physiol*, 272, L1031-45.
- UNDEM, B. J., CHUAYCHOO, B., LEE, M. G., WEINREICH, D., MYERS, A. C. & KOLLARIK, M. 2004. Subtypes of vagal afferent C-fibres in guinea-pig lungs. *J Physiol*, 556, 905-17.
- UNDEM, B. J. & KOLLARIK, M. 2002. Characterization of the vanilloid receptor 1 antagonist iodo-resiniferatoxin on the afferent and efferent function of vagal sensory C-fibers. *J Pharmacol Exp Ther*, 303, 716-22.
- UNDEM, B. J., MCALEXANDER, M. & HUNTER, D. D. 1999. Neurobiology of the upper and lower airways. *Allergy*, 54 Suppl 57, 81-93.

- UNDEM, B. J., OH, E. J., LANCASTER, E. & WEINREICH, D. 2003. Effect of extracellular calcium on excitability of guinea pig airway vagal afferent nerves. *J Neurophysiol*, 89, 1196-204.
- VAN MANEN, M. J., BIRRING, S. S., VANCHERI, C., COTTIN, V., RENZONI, E. A., RUSSELL, A. M. & WIJSENBEK, M. S. 2016. Cough in idiopathic pulmonary fibrosis. *Eur Respir Rev*, 25, 278-86.
- VAN MANEN, M. J. G., BIRRING, S. S., VANCHERI, C., VINDIGNI, V., RENZONI, E., RUSSELL, A.-M., WAPENAAR, M., COTTIN, V. & WIJSENBEK, M. S. 2017. Effect of pirfenidone on cough in patients with idiopathic pulmonary fibrosis. *European Respiratory Journal*, 50, 1701157.
- VERGNOLLE, N., BUNNETT, N. W., SHARKEY, K. A., BRUSSEE, V., COMPTON, S. J., GRADY, E. F., CIRINO, G., GERARD, N., BASBAUM, A. I., ANDRADE-GORDON, P., HOLLENBERG, M. D. & WALLACE, J. L. 2001. Proteinase-activated receptor-2 and hyperalgesia: A novel pain pathway. *Nat Med*, 7, 821-6.
- VERGNON, J. M., VINCENT, M., DE THÉ, G., MORNEX, J. F., WEYNANTS, P. & BRUNE, J. 1984. Cryptogenic fibrosing alveolitis and Epstein-Barr virus: an association? *Lancet*, 2, 768-71.
- VERTIGAN, A. E., THEODOROS, D. G., GIBSON, P. G. & WINKWORTH, A. L. 2006. Efficacy of speech pathology management for chronic cough: a randomised placebo controlled trial of treatment efficacy. *Thorax*, 61, 1065-1069.
- VESTBO, J., HURD, S. S., AGUSTI, A. G., JONES, P. W., VOGELMEIER, C., ANZUETO, A., BARNES, P. J., FABBRI, L. M., MARTINEZ, F. J., NISHIMURA, M., STOCKLEY, R. A., SIN, D. D. & RODRIGUEZ-ROISIN, R. 2013. Global strategy for the diagnosis, management, and prevention of chronic obstructive pulmonary disease: GOLD executive summary. *Am J Respir Crit Care Med*, 187, 347-65.
- VIGELAND, C. L., HUGHES, A. H. & HORTON, M. R. 2017. Etiology and treatment of cough in idiopathic pulmonary fibrosis. *Respir Med*, 123, 98-104.
- VIZEL, E., YIGLA, M., GORYACHEV, Y., DEKEL, E., FELIS, V., LEVI, H., KROIN, I., GODFREY, S. & GAVRIELY, N. 2010. Validation of an ambulatory cough detection and counting application using voluntary cough under different conditions. *Cough*, 6, 3.
- WAGHRAY, M., CUI, Z., HOROWITZ, J. C., SUBRAMANIAN, I. M., MARTINEZ, F. J., TOEWS, G. B. & THANNICKAL, V. J. 2005. Hydrogen peroxide is a diffusible paracrine signal for the induction of epithelial cell death by activated myofibroblasts. *FASEB J*, 19, 854-6.
- WALLS, A. F., BENNETT, A. R., GODFREY, R. C., HOLGATE, S. T. & CHURCH, M. K. 1991. Mast cell tryptase and histamine concentrations in bronchoalveolar lavage fluid from patients with interstitial lung disease. *Clin Sci (Lond)*, 81, 183-8.
- WALSH, S. L., CALANDRIELLO, L., SVERZELLATI, N., WELLS, A. U. & HANSELL, D. M. 2016. Interobserver agreement for the ATS/ERS/JRS/ALAT criteria for a UIP pattern on CT. *Thorax*, 71, 45-51.
- WATANABE, H., VRIENS, J., SUH, S. H., BENHAM, C. D., DROOGMANS, G. & NILIUS, B. 2002. Heat-evoked activation of TRPV4 channels in a HEK293 cell expression system and in native mouse aorta endothelial cells. *J Biol Chem*, 277, 47044-51.
- WEI, R., LI, C., ZHANG, M., JONES-HALL, Y. L., MYERS, J. L., NOTH, I. & LIU, W. 2014. Association between MUC5B and TERT polymorphisms and different interstitial lung disease phenotypes. *Transl Res*, 163, 494-502.
- WELLS, A. U. 2010. The clinical utility of bronchoalveolar lavage in diffuse parenchymal lung disease. *Eur Respir Rev*, 19, 237-41.
- WEYDERT, C. J. & CULLEN, J. J. 2010. Measurement of superoxide dismutase, catalase and glutathione peroxidase in cultured cells and tissue. *Nat Protoc*, 5, 51-66.
- WHITEHILL, M., GARRISON, J. & PATEL, S. Whosecough: In-the-Wild Cougher Verification Using Multitask Learning. ICASSP 2020-2020 IEEE International Conference on Acoustics, Speech and Signal Processing (ICASSP), 2020. IEEE, 896-900.
- WIDDICOMBE, J. 2003. Functional morphology and physiology of pulmonary rapidly adapting receptors (RARs). *Anat Rec A Discov Mol Cell Evol Biol*, 270, 2-10.
- WIDDICOMBE, J. G. 1995. Neurophysiology of the cough reflex. *Eur Respir J*, 8, 1193-202.

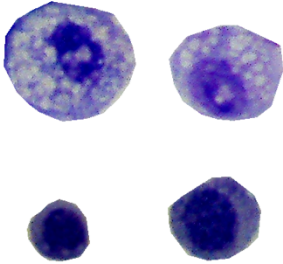

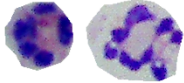
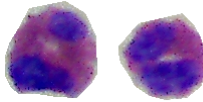
- WIDDICOMBE, J. G. & UNDEM, B. J. 2002. Summary: central nervous pharmacology of cough. *Pulm Pharmacol Ther*, 15, 251-2.
- WIERSINGA, W. J., RHODES, A., CHENG, A. C., PEACOCK, S. J. & PRESCOTT, H. C. 2020. Pathophysiology, Transmission, Diagnosis, and Treatment of Coronavirus Disease 2019 (COVID-19): A Review. *JAMA*, 324, 782-793.
- WINDMON, A., MINAKSHI, M., BHARTI, P., CHELLAPPAN, S., JOHANSSON, M., JENKINS, B. A. & ATHILINGAM, P. R. 2019. TussisWatch: A Smart-Phone System to Identify Cough Episodes as Early Symptoms of Chronic Obstructive Pulmonary Disease and Congestive Heart Failure. *IEEE J Biomed Health Inform*, 23, 1566-1573.
- WONG, C. H., MATAI, R. & MORICE, A. H. 1999. Cough induced by low pH. *Respir Med*, 93, 58-61.
- WUYTS, W. A., CAVAZZA, A., ROSSI, G., BONELLA, F., SVERZELLATI, N. & SPAGNOLO, P. 2014. Differential diagnosis of usual interstitial pneumonia: when is it truly idiopathic? *European Respiratory Review*, 23, 308-319.
- WYGRECKA, M., DAHAL, B. K., KOSANOVIC, D., PETERSEN, F., TABORSKI, B., VON GERLACH, S., DIDIASOVA, M., ZAKRZEWICZ, D., PREISSNER, K. T., SCHERMULY, R. T. & MARKART, P. 2013. Mast cells and fibroblasts work in concert to aggravate pulmonary fibrosis: role of transmembrane SCF and the PAR-2/PKC-alpha/Raf-1/p44/42 signaling pathway. *Am J Pathol*, 182, 2094-108.
- WYGRECKA, M., KWAPISZEWSKA, G., JABLONSKA, E., VON GERLACH, S., HENNEKE, I., ZAKRZEWICZ, D., GUENTHER, A., PREISSNER, K. T. & MARKART, P. 2011. Role of protease-activated receptor-2 in idiopathic pulmonary fibrosis. *Am J Respir Crit Care Med*, 183, 1703-14.
- XAUBET, A., MARIN-ARGUEDAS, A., LARIO, S., ANCOCHEA, J., MORELL, F., RUIZ-MANZANO, J., RODRIGUEZ-BECERRA, E., RODRIGUEZ-ARIAS, J. M., INIGO, P., SANZ, S., CAMPISTOL, J. M., MULLOL, J. & PICADO, C. 2003. Transforming growth factor-beta1 gene polymorphisms are associated with disease progression in idiopathic pulmonary fibrosis. *Am J Respir Crit Care Med*, 168, 431-5.
- XU, J., GONZALEZ, E. T., IYER, S. S., MAC, V., MORA, A. L., SUTLIFF, R. L., REED, A., BRIGHAM, K. L., KELLY, P. & ROJAS, M. 2009. Use of senescence-accelerated mouse model in bleomycin-induced lung injury suggests that bone marrow-derived cells can alter the outcome of lung injury in aged mice. *The journals of gerontology. Series A, Biological sciences and medical sciences*, 64, 731-739.
- XU, Q., CHOKSI, S., QU, J., JANG, J., CHOE, M., BANFI, B., ENGELHARDT, J. F. & LIU, Z. G. 2016. NADPH Oxidases Are Essential for Macrophage Differentiation. *J Biol Chem*, 291, 20030-41.
- YAMAGUCHI, M., HIRAI, S., TANAKA, Y., SUMI, T., MIYAJIMA, M., MISHINA, T., YAMADA, G., OTSUKA, M., HASEGAWA, T., KOJIMA, T., NIKI, T., WATANABE, A., TAKAHASHI, H. & SAKUMA, Y. 2017. Fibroblastic foci, covered with alveolar epithelia exhibiting epithelial-mesenchymal transition, destroy alveolar septa by disrupting blood flow in idiopathic pulmonary fibrosis. *Laboratory Investigation*, 97, 232-242.
- YANG, I. V. 2012. Epigenomics of idiopathic pulmonary fibrosis. *Epigenomics*, 4, 195-203.
- YANG, I. V., COLDREN, C. D., LEACH, S. M., SEIBOLD, M. A., MURPHY, E., LIN, J., ROSEN, R., NEIDERMYER, A. J., MCKEAN, D. F., GROSHONG, S. D., COOL, C., COSGROVE, G. P., LYNCH, D. A., BROWN, K. K., SCHWARZ, M. I., FINGERLIN, T. E. & SCHWARTZ, D. A. 2013. Expression of cilium-associated genes defines novel molecular subtypes of idiopathic pulmonary fibrosis. *Thorax*, 68, 1114-21.
- YANG, I. V., PEDERSEN, B. S., RABINOVICH, E., HENNESSY, C. E., DAVIDSON, E. J., MURPHY, E., GUARDELA, B. J., TEDROW, J. R., ZHANG, Y., SINGH, M. K., CORRELL, M., SCHWARZ, M. I., GERACI, M., SCIURBA, F. C., QUACKENBUSH, J., SPIRA, A., KAMINSKI, N. & SCHWARTZ, D. A. 2014. Relationship of DNA methylation and gene expression in idiopathic pulmonary fibrosis. *American journal of respiratory and critical care medicine*, 190, 1263-1272.

- YOUSAF, N., MONTEIRO, W., PARKER, D., MATOS, S., BIRRING, S. & PAVORD, I. D. 2010. Long-term low-dose erythromycin in patients with unexplained chronic cough: a double-blind placebo controlled trial. *Thorax*, 65, 1107-10.
- YOUSAF, N., MONTINERO, W., BIRRING, S. S. & PAVORD, I. D. 2013. The long term outcome of patients with unexplained chronic cough. *Respir Med*, 107, 408-12.
- YU, S., UNDEM, B. J. & KOLLARIK, M. 2005. Vagal afferent nerves with nociceptive properties in guinea-pig oesophagus. *J Physiol*, 563, 831-42.
- ZANK, D. C., BUENO, M., MORA, A. L. & ROJAS, M. 2018. Idiopathic Pulmonary Fibrosis: Aging, Mitochondrial Dysfunction, and Cellular Bioenergetics. *Front Med (Lausanne)*, 5, 10.
- ZHANG, H., DAVIES, K. J. A. & FORMAN, H. J. 2015. Oxidative stress response and Nrf2 signaling in aging. *Free Radic Biol Med*, 88, 314-336.
- ZHANG, Y., NOTH, I., GARCIA, J. G. & KAMINSKI, N. 2011. A variant in the promoter of MUC5B and idiopathic pulmonary fibrosis. *N Engl J Med*, 364, 1576-7.
- ZHAO, H., YANG, J., SHAN, L. & JORGENSEN, E. D. 2011. Measuring the impact of cigarette smoke on the UPR. *Methods Enzymol*, 489, 147-64.
- ZHOU, Y. H., SUN, L. H., LIU, Z. H., BU, G., PANG, X. P., SUN, S. C., QIAO, G. F., LI, B. Y. & SCHILD, J. H. 2010. Functional impact of the hyperpolarization-activated current on the excitability of myelinated A-type vagal afferent neurons in the rat. *Clin Exp Pharmacol Physiol*, 37, 852-61.



## 10 Appendix

Table 10-1 Criteria for differential leukocyte counting in guinea pig BAL

Cell Type	Description	Example pictures
Macrophages / Monocytes	<ul style="list-style-type: none"> <li>• Largest leukocyte in circulation</li> <li>• Variably shaped nucleus, less condensed chromatin pattern, and moderately abundant blue-grey cytoplasm</li> <li>• Macrophages (activated monocytes; above panel) have a larger, whiter cytoplasm than monocytes (bottom panel)</li> </ul>	
Lymphocytes	<ul style="list-style-type: none"> <li>• Guinea pig lymphocytes have a similar appearance to lymphocytes in other species</li> <li>• Small, well differentiated lymphocytes dominate BAL and are slightly larger than erythrocytes</li> <li>• Typically stain very dark purple and have little to no cytoplasm visible</li> </ul>	
Heterophils (the guinea pig equivalent of neutrophils)	<ul style="list-style-type: none"> <li>• Purple, segmented nucleus with dense chromatic pattern</li> <li>• Cytoplasm contains scattered acidophilic granules that are smaller than those of eosinophils</li> <li>• More cytoplasm is visible in heterophils than in eosinophils</li> <li>• Cytoplasm can be clear in appearance or red</li> </ul>	
Eosinophils	<ul style="list-style-type: none"> <li>• Slightly larger than heterophils</li> <li>• Less segmented nucleus than heterophils</li> <li>• Compared to heterophils, the cytoplasmic granules are larger, more round and bright red</li> <li>• Granules completely fill cytoplasm</li> </ul>	

<b>Drug</b>	<b>Source</b>	<b>Vehicle/Diluent (where applicable)</b>
Acrolein	Sigma-Aldrich	0.1% DMSO in KH solution
AF-353	Afferent Pharmaceuticals	0.1% DMSO in KH solution
Bleomycin	Baxter	Saline
CaCl <sub>2</sub>	VWR	
Capsaicin	Sigma-Aldrich	
Citric Acid		0.9% saline
Collagenase	Worthington	Ca <sup>2+</sup> -free, Mg <sup>2+</sup> - free Hank's balanced salt solution
DHE (Dihydroethidium)	Thermofisher	Extracellular Solution
Dil (DiI C18(3), 1,1'- dioctadecyl-3,3',3'- tetramethylindocarbocyanine perchlorate)	Invitrogen	2% ethanol in 0.9% saline
Dimethyl Sulfoxide (DMSO)	Sigma-Aldrich	
Dispase II	Roche	Ca <sup>2+</sup> -free, Mg <sup>2+</sup> -free Hank's balanced salt solution
Ethanol	VWR	
F12	Invitrogen	
Fura2-AM	Invitrogen	
Glucose	Sigma-Aldrich	
GSK1016790a	Sigma-Aldrich	0.1% DMSO in Krebs (in vitro) 0.1% DMSO in 0.9% saline (in vivo)
GSK2193874	Tocris	0.1% DMSO in Krebs (in vitro) 6% Cavitron 2Hydroxypropyl-β- cyclodextrin in 0.9% saline (in vivo)
GSK279	AstraZeneca	0.1% DMSO in Krebs (in vitro) 6% Cavitron 2Hydroxypropyl-β- cyclodextrin in 0.9% saline (in vivo)
Hydrogen Peroxide (H <sub>2</sub> O <sub>2</sub> )	VWR	KH Solution
Janssen 130	Almirall	0.1% DMSO in Krebs (in vitro). 1% methyl cellulose in saline (in vivo)
KH <sub>2</sub> PO <sub>4</sub>	VWR	
KCl	VWR	
MgSO <sub>4</sub>	VWR	
N-Acetyl-L-cysteine (NAC)	Sigma-Aldrich	
NaCl	VWR	
NaH <sub>2</sub> PO <sub>4</sub>	VWR	
NaHCO <sub>3</sub>	VWR	
Nuclease free water	Promega	
Papain	Sigma-Aldrich	Hanks Balanced Salt Solution
PBS	Sigma-Aldrich	
Percoll	Sigma-Aldrich	
Petroleum Jelly	Vaseline	
PGE <sub>2</sub>	Sigma-Aldrich	0.1% Ethanol in Krebs
Safeview	NBS Biologicals Ltd	